UNIVERSITY OF SOUTHAMPTON

FACULTY OF SOCIAL AND HUMAN SCIENCES

Geography and Environment

Academic Unit

Climate Change and Landslide Risk Assessment in Thailand

by

Shotiros Protong

Thesis for the degree of Doctor of Philosophy

July 2016

UNIVERSITY OF SOUTHAMPTON

ABSTRACT

FACULTY OF SOCIAL AND HUMAN SCIENCES

GEOGRAPHY AND ENVIRONMENT

Doctor of Philosophy

CLIMATE CHANGE AND LANDSLIDE RISK ASSESSMENT IN THAILAND

By Shotiros Protong

The incidents of sudden landslides in Thailand during the past decade have occurred frequently and more severely. It is necessary to focus on the principle parameters used for analysis such as land cover/land use, rainfall values, characteristics of the soil and digital elevation model (DEM). Rainfall has increased in intensity. For example, the rainfall amount in March in 2011 was the highest in the previous 36 years (1974-2011). However, there was only one tropical cyclone that year. This situation was considered unusual compared to other years (TMD, 2011c).

Landslide occurrences occur during intense rainfall especially in the rainy season in Thailand which usually starts around mid-May and ends in the middle of October. The landslide risk analysis is the focus of this research. The combination of geotechnical and hydrological data is used to determine permeability, conductivity, bedding orientation, overburden and presence of loose blocks. The regional landslide hazard mapping is developed using the Slope Stability Index SINMAP model supported by Digital Elevation Model (DEM) in 30 metres. So, the 30 metre pixel size of DEM is used to calculate on the ground.

Geological and land use data are used to define the probability of landslide occurrences in terms of geotechnical data. The geological data can indicate the shear strength and the angle of friction values for soils above given rock types, which leads to the general applicability of the approach for landslide hazard analysis.

To address the research, the following methods are described in this study: the calibration and the sensitivity of the SINMAP model for setup, geotechnical

laboratory, landslide assessment at present calibration and landslide assessment under future climate simulation scenario A2 and B2. A2 simulation scenario delineates a very heterogeneous world and continuous population and economic growth, while B2 storyline is oriented on local solution to economical, social and environmental sustainability (START, 2010).

In terms of hydrological data, the millimetres/twenty-four hours of average rainfall data are used to assess the induced rainfall landslide hazard analysis in slope stability mapping. The period 1954-2012 is used for the baseline of rainfall data for calibration of present-day conditions. Future climate simulation scenarios are downscaled in the local areas. The precipitation trends are needed to predict the future climate. The Statistical Downscaling Model (SDSM), is used to assess the simulation scenario of future change for latitudes 16° 26′ and 18° 37′ and between longitude 98° 52′ and 103° 05′, is about 117,500 km^2, covering Uttaradit province in the northern part of Thailand.

The research allows the mapping of landslide risk, and indicates the spatial and time period of landslide occurrences. Thus, regional landslide hazard mapping under present-day climatic conditions from 1954 to 2012 and simulations of climate change from 2013 to 2099 related to the threshold rainfall values for the selected the study area are presented.

Finally, the zonation of landslide risk will be compared and shown by areas (km^2) in both the present and the future under climate simulation scenarios A2 and B2 in Uttaradit province. The rainfall trend will increase in the future simulation. The zonation of landslide risk is nearly the same between the present and the future simulation, while the failure region will obviously increase in the future, especially in steep slope areas.

Key words: landslide hazard, GIS, Slope Stability Index (SINMAP), landslides, Thailand

Table of Contents

List of Tables

List of Figures

List of Accompanying Materials

A CD-ROM that contains the appendix files

DECLARATION OF AUTHORSHIP

I, **Shotiros Protong**

declare that this thesis and the work presented in it are my own and has been generated by me as the result of my own original research.

Climate Change and Landslide Risk Assessment in Thailand

I confirm that:

1. This work was done wholly or mainly while in candidature for a research degree at this University;
2. Where any part of this thesis has previously been submitted for a degree or any other qualification at this University or any other institution, this has been clearly stated;
3. Where I have consulted the published work of others, this is always clearly attributed;
4. Where I have quoted from the work of others, the source is always given. With the exception of such quotations, this thesis is entirely my own work;
5. I have acknowledged all main sources of help;
6. Where the thesis is based on work done by myself jointly with others, I have made clear exactly what was done by others and what I have contributed myself;

Signed: _____

Date:_____

Acknowledgements

I would like to thank my supervisor Prof. Paul Carling, Dr. Julian Leyland. I finished my research because of their help. The important thing, I learned how to solve the problem for my research during my PhD study. Their experiences in the geography make me to understand and improve my research in academic way. So, I would like to say special thanks for my supervisor team that give me a a PhD experience in the UK.

Thanks to Dr. Suttisuk Sorralum for supporting me in the fieldwork in Thailand, the geotechnical equipment and give me the acknowledge how to use the geotechnical laboratory work. Thanks to staff at Kasetsart University for supporting the geotechnical laboratory.

I would like to say thank for my sponsor for providing funding give me a good consultant. Thanks to my husband for his plenty of help for my life in UK and my parents always support and encourage me everything during my phD.

Finally, I would like to thank all the people who helped me to finish this research.

CHAPTER 1 GENERAL INTRODUCTION AND STUDY AREA

Landslide occurrences have affected and damaged lives, properties and infrastructure, particularly in many elevated and mountainous terrains. Landslides have occurred over the Southeast Asia region, especially in Thailand. Thailand is located in tropical south-east Asia between latitude 5° 37′ and 20° 27′ north and between longitude 97° 22′ and 105° 37′ east. It has a total area of about 513,115 km^2 and is bordered by Myanmar and Laos in the north, and by the Gulf of Thailand, Cambodia and Laos to the east. In the south, it is bordered by Malaysia and in the west, is bordered by Myanmar and the Andaman Sea (TMD, 2007a).

Landslide occurrences have been related to extreme rainfall and monsoons, therefore climate change problems have been affecting global communities, with heavier rainfall causing severe landslides, floods or longer consecutive dry days causing severe drought. Thailand also suffers from the effects of climate change, landslides cause severe damage, including loss of lives, property and economic impacts. Landslides occur in several regions in the southern and the northern parts of Thailand, especially during the rainy season. Evidently, landslides are caused by intense rainfall in the hilly and mountainous terrains (DMR, 2012a).

Rainfall occurrences are also dependent on atmospheric circulation patterns which are driven by the El Niño-Southern Oscillation (ENSO) and other patterns of variability. The relationship between the atmospheric circulation change and climate change can shift the storm tracks and the tropical sea-surface temperature patterns. The El Niño-Southern Oscillation is a coupled ocean- atmosphere phenomenon and involves warming of tropical surface water and ocean circulation. The Southern Oscillation leads to changes in the wind track, which affects tropically circulated precipitation. The global atmospheric circulation depends on the pattern of variability; this circulation is also associated with regional climate in each location in terms of the storm track, the pole-ward fluxes of heat, moisture and momentum. Furthermore, there are seasonal and longer time-scale effects leading to flooding, drought occurrence and other disasters (IPCC, 2007). The interaction between

atmosphere and ocean circulation are linked with the El Niño-Southern Oscillation, leading to anomalies with the circulation and rainfall.

This study seeks to analyse how landsliding in Thailand will respond under different modelled future emissions of greenhouse gases as indexed by both IPCC emission scenario A2 and B2. A series of scenarios for future greenhouse gas emission can be determined by the IPCC Special Report on Emissions Scenarios (SRES) (Nakicenovic et al., 2000) called "SRES scenarios". In this study, the SRES scenario series comprise two scenario storylines: A2 and B2. The SRES scenario of the A2 storyline describes the development of economic growth and technological change on local and regional levels. On the other hand, the scenario of the B2 storyline is in the local situation, in economic, social and environmental sustainability, including environmental protection and social equity (Houghton, 2009). Different precipitation values are evaluated under scenario simulations in both A2 and B2 for landslide analysis in terms of the landslide hazard mapping.

Given past landslide occurrences, Uttaradit province, which lies in the northern part of Thailand, has a high risk of landslides because of the elevated terrain in several regions, hence Uttaradit province is selected as a focus for this research. The Digital Elevation Model (DEM) is described for calculation, including land cover/land use and the characteristics of soil in the Stability Index Mapping (SINMAP) model. The basic theory for stability calculation is presented for landslide stabilization (Veder et, 1981). Moreover, massive mountains and hills, in Uttaradit province, are strongly related to extreme rainfall and monsoons more generally through the severity of the landslide occurrences. According to recorded great landslides in 2006 and in 2011, rainfall volumes have a direct influence, with rain triggering landslides in this province, but this needs quantification and modelling (DMR, 2011a). The inventory landslide hazard analysis is carried out for risk areas in Uttaradit province, consisting of nine districts using landslide occurrences in 2006. Two main districts, Laplea and Thapla, are selected for SINMAP calibration. The Arc map software based on the Arc GIS 10.1 techniques is coupled with the SINMAP model to analyse the hazard landslide mapping and the rain-triggered landslide susceptibility classes.

The study assesses the parameters of landslide dynamics and indicates the trend of landslide occurrences and the regional landslide hazard mapping under simulation of climate change based on scenario A2 and B2, related to the threshold rainfall values and soil and vegetation characteristics. This study should lead to reduced loss of life and property damage by providing early warning of the location of landslide hazard zones.

1.1. Aim and objectives

The aim of this research is to assess the effect of climate change on landslide risk in the northern part of Thailand. The result of this assessment can be used to determine landslide hazard and provide a risk assessment involving rainfall thresholds. Specific objectives of the study are:

a. To investigate the characteristics of meteorology, topography, and soils in landslide risk areas

b. To develop a physically-based hill slope hydrology and slope stability model under local conditions.

c. To appraise the uncertainty of parameters and the calibration of slope stability.

d. To determine the trend of landslide occurrences related to rainfall under climate simulation scenarios A2 and B2.

e. To assess the landslide risk in landslide hazard mapping.

1.2 Study Area

The study area consists of the following location (Fig 1.1). Uttaradit province is located in the northern part of Thailand between latitude 17° 48′ and 18° 12′ north and between longitude 100° 9′ and 101° 5′ east (Fig 1.2). It has a total area of about 7,838.6 km^2. It has borders with Phrea province in the north, and in the east, it is bordered by Laos, while, in the south, it is bordered by Pisanulok province and in the west, by Sukhothai province (DMR, 2011a).

Uttaradit province in the northern part of Thailand, consists of nine districts: Muang, Laplea, Thapla, Nampat, Bankhok, Faktha, Thongsaenkhun, Phichai and Tron. The nine districts in Uttaradit province comprise approximately 7,838.6 km^2 (Fig 1.3).

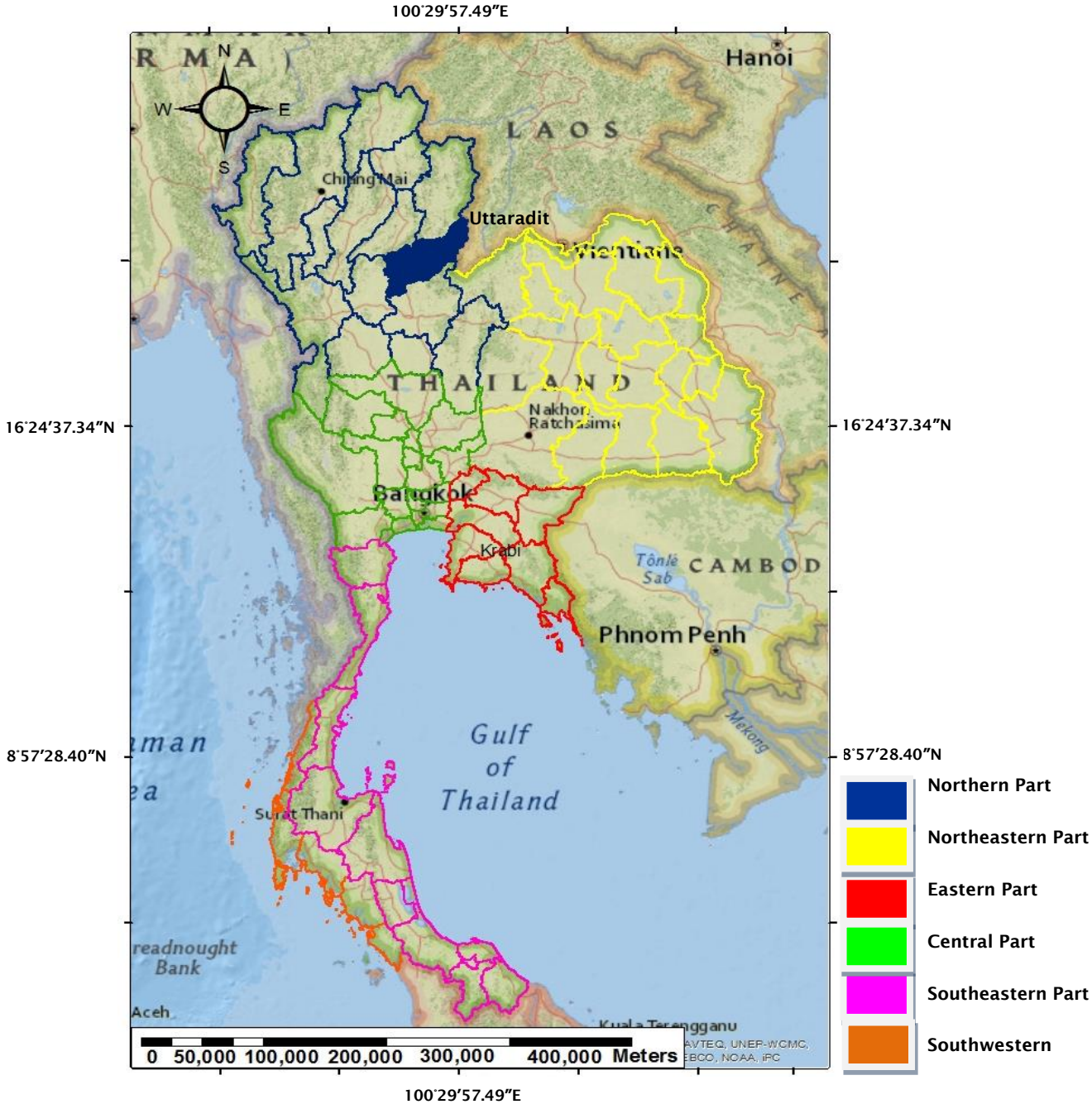

Figure 1.1 Seventy-six provinces in six regions in Thailand (TMD, 2007a)

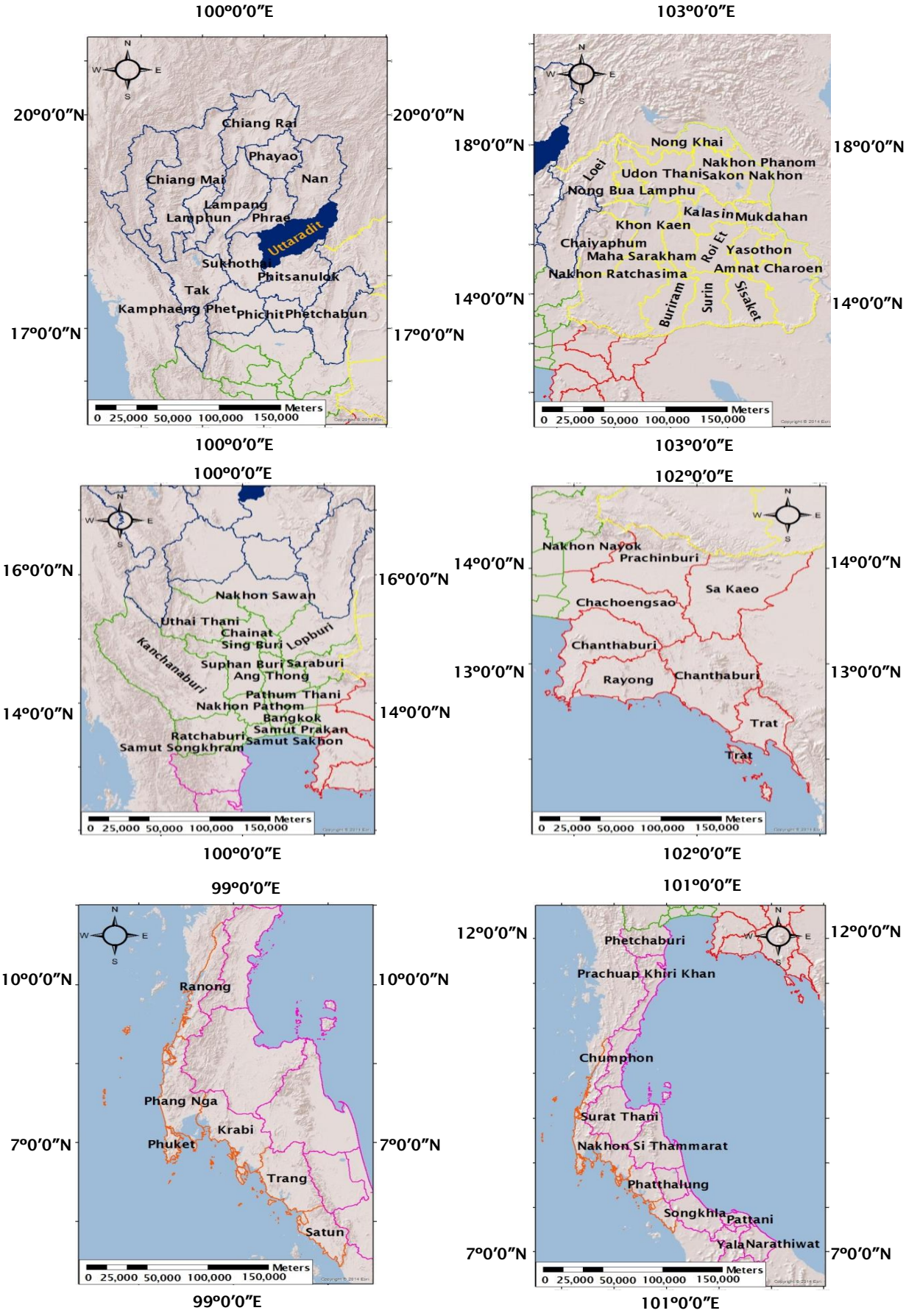

Figure 1.2 Seventy- six provinces in six regions of Thailand, related to the literature review and in Uttaradit province (study site) in the northern part

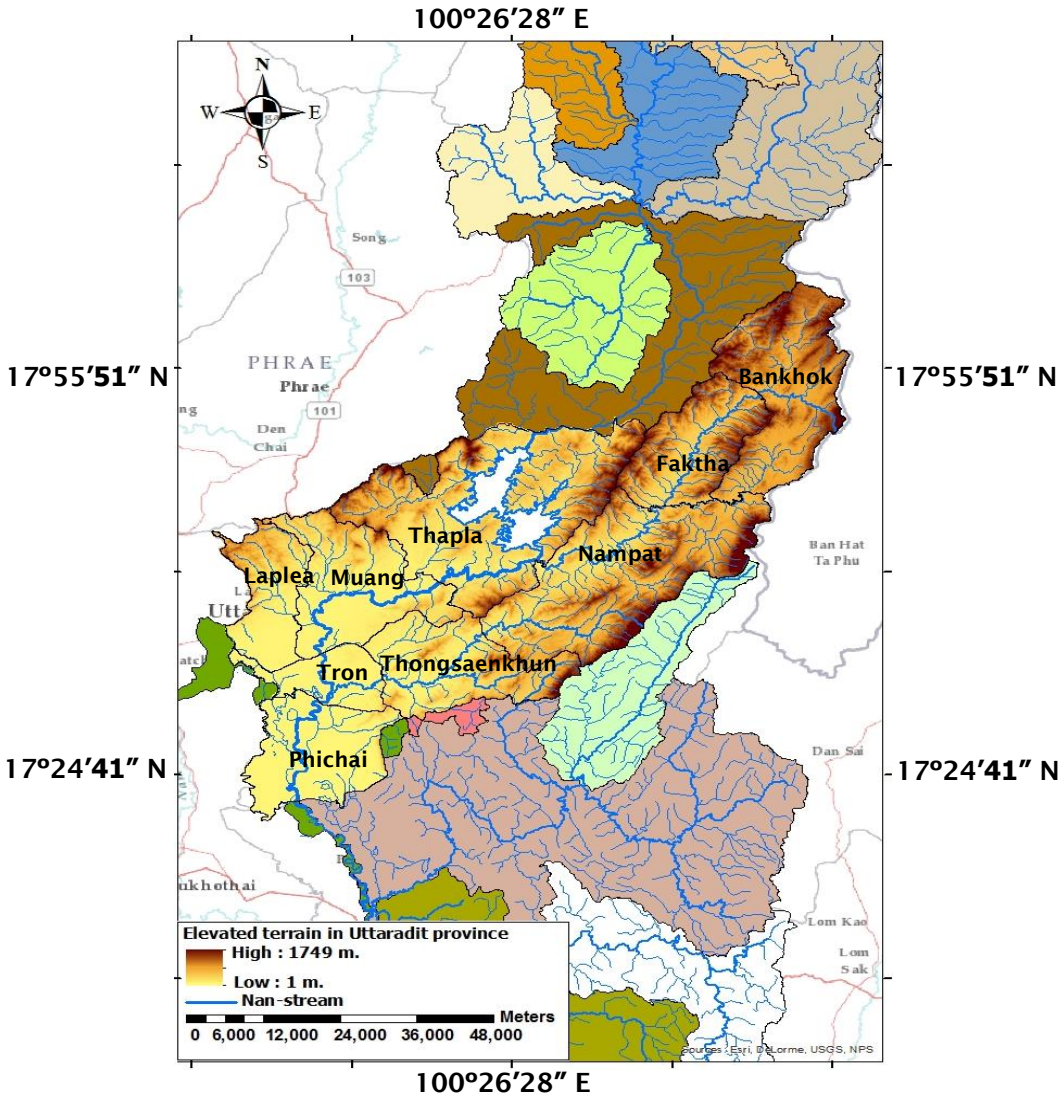

Figure 1.3 The Nan stream boundary of Uttaradit drainage basins in relation to surrounding basins. The locations of specific districts are also noted

1.2.1 General description

Uttaradit province is approximately 7,838.6 km^2, with about 50% of the province composed of hilly and mountainous terrains. Uttaradit consists of nine districts, sixty-seven tambons (3rd-order local government unit) and 562 villages and its population is about 465,277 people. Many people still live around the hilly terrains and mountains (DMR, 2011a).

The Uttaradit terrain can be divided into three types: plains in the river basin, plains in the valleys and surrounding mountains and the high mountainous terrain. The elevation is approximately 50-100 metres above sea level, which lies in three districts: Laplea, Tron and

Thongsaenkhun. About 100-400 metres of elevation lies in the hilly and undulating areas in the northern and the eastern parts of the province in three districts: Laplea, Nampat and Thongsaenkhun, and the high elevated terrain of about 400-1000 metres is also in the northern and eastern parts of the provinces in four districts: Muang, Laplea, Thapla, Nampat, Faktha and Bankhok district (DMR, 2011). The highest point of elevation is about 1,749 metres in four districts: Thapla, Nampat, Faktha and Bankhok. The causes of landslides are usually related to the slopes in elevated terrain. On May 23, 2006, the past landslide occurred and destroyed life and properties. The boundary of landslide scars in a polygon shape was presented around hilly and mountainous areas in both tambon Meaphun in Laplea district and tambon Namman in Thapla district (DMR, 2006).

Uttaradit province is complicated in terms of geology, because the tectonic plates are compressed. They move against each other to form hilly and mountainous terrains in the north-eastern and the south-western parts of the province. There were two geological groups; group 2: Extrusive and Mafic Igneous rocks and group 6: Predominantly Metamorphic rock in Uttaradit province. Only group 2 and group 6 were found deep underground and classified to indicate the shear strength and the angle of friction values in each geological group. Only 4.23% of Extrusive and Mafic Igneous rock and 7.71% of Predominantly Metamorphic rock are obtained for the probability of landslide occurrences (GERD, 2013).

1.2.2 Climate conditions

Climate conditions are dominated by the southwest and the northeast monsoons, the tropical cyclones which usually come during May to October affect rainfall values in several parts of Thailand. When the past landslide occurred in Uttaradit province, the cumulative rainfall values measured approximately 100-300 mm per day by the rain gauge in the hilly terrain. The cumulative rainfall caused pressure and the pore water to increase, it then led to saturated soil and a reduction in the shear strength of the soil. Uttaradit is a tropical climate and mostly mountainous terrain, which leads to heavy rainfall in the rainy season. Approximately 1,500 mm of the average annual rainfall and 35

degrees Celsius of average temperature was reported by the Department of Mineral Resources (2011a).

The tropical cyclone, depression level, moved to cover the Bay of Bengal and the Andaman Sea. In 2006, thirty-four tropical cyclones moved into the western Pacific Ocean, the South China Sea and the Bay of Bengal, but only sixteen tropical cyclones affected Thailand, and only two tropical cyclones directly came into Thailand. The first tropical cyclone was typhoon level, called XangSane, and moved into the upper part, especially in the north-eastern part of Thailand in October. The second, named Durian, was depression level, moving into the southern part in December. Therefore, heavy rainfall occurred in several regions, especially in northern and southern parts (TMD, 2007a).

Rainfall conditions are associated with the southwest monsoon season during April to September. Especially in April, the low pressure area was located in the middle of the country and spread throughout several regions, such as the northern, the north-eastern and the southern parts. It occurred during the warm weather in this month as the season changes from summer to rainy. During the May to September period, the low pressure area covered the northern and the north-eastern parts of Thailand throughout the eastern part and the Gulf of Tonkin. As a result, the wind moved from the Indian Ocean through the Bay of Bengal, the China Sea and the Gulf of Thailand, into the central part of Thailand. This wind moved from the south-western part into the north-eastern part. It is called the southwest wind which originates from the southwest monsoon. Wet days usually dominate by the power of the southwest monsoon and the low pressure area (TMD, 2007a).

The rainfall values in 2006 and in 2011 were greater than the average normal rainfall values in Uttaradit province (TMD, 2012). The rainfall in 2006 and 2011 in Uttaradit province were higher than normal rainfall as shown in Fig 1.4. Three districts were affected by landslides on 23 May 2006; Muang (Fig 1.5), Laplea (Fig 1.6) and Thapla (Fig 1.7) districts, while the mud and timber flowed down into Bantuek, Sisatchanalai district in Sukhothai province around 3 am.

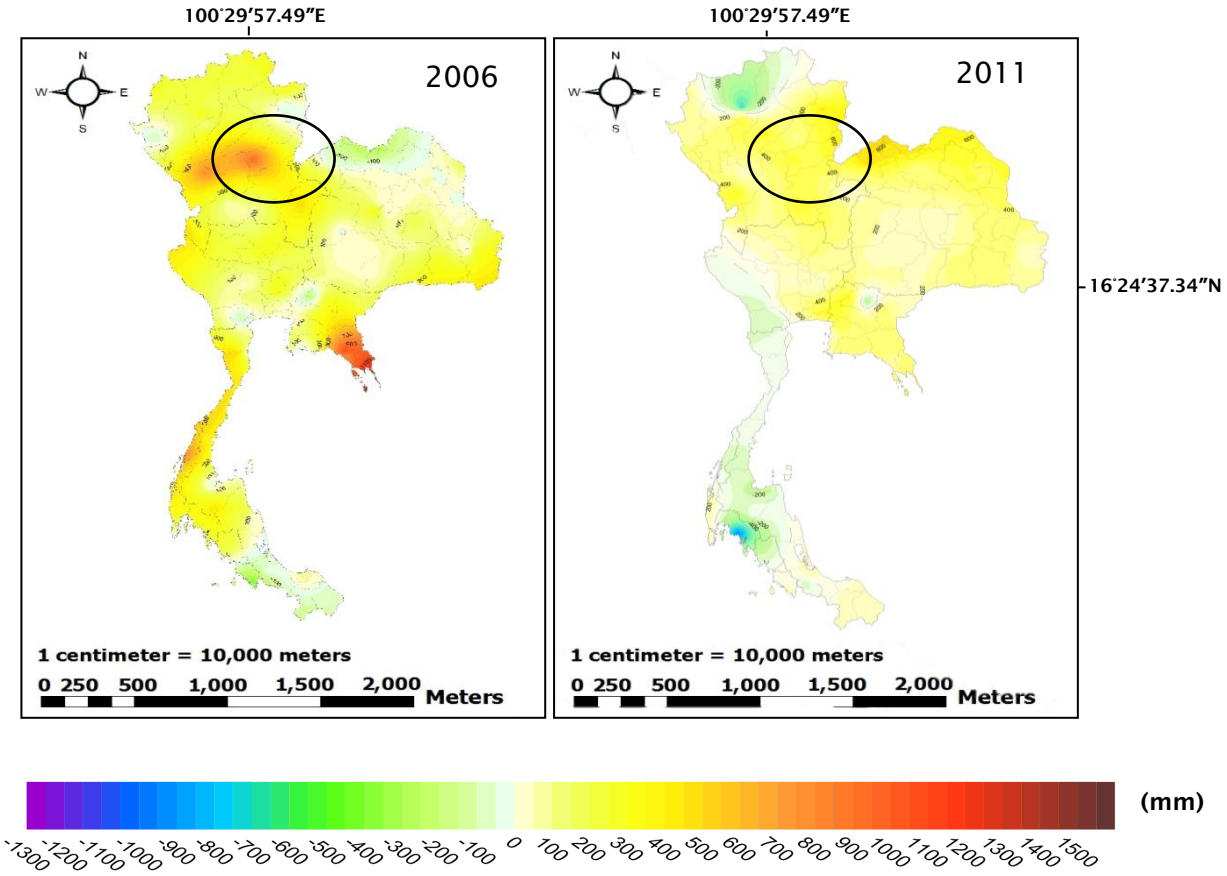

Figure 1.4 The rainfall amount (mm) in the rainy season in 2006 and 2011 (TMD, 2013)

1.2.3 The past landslide

In Uttaradit province, on May 23, 2006 landslides and flash floods occurred in Muang (Fig 1.5), Laplea (Fig 1.6) and Thapla (Fig 1.7) districts. This situation led to 83 people killed, 33 people unaccounted for, 673 houses damaged, including 481,830 hectares (481.803 km^2) of agricultural area damaged, to a total value of £6.17 million (DMR, 2011a). According to the Department of Methodological reports, the Intertropical Convergence Zone moved over the upper part of the northern and north eastern areas on 22 May 2006, so it led to heavy rainfall conditions, approximately 263.7 mm in Muang district and 330 mm in Laplea district in Uttaradit province, especially in tambon Khungtapao in Muang district on 22 May 2006 over 200 mm of rainfall was measured around 3 pm until 11 pm. In Nampat district (Fig 1.8), on 9 September 2011, 242.8 mm of rainfall was measured by the Department of Mineral Resources (DMR, 2011a).

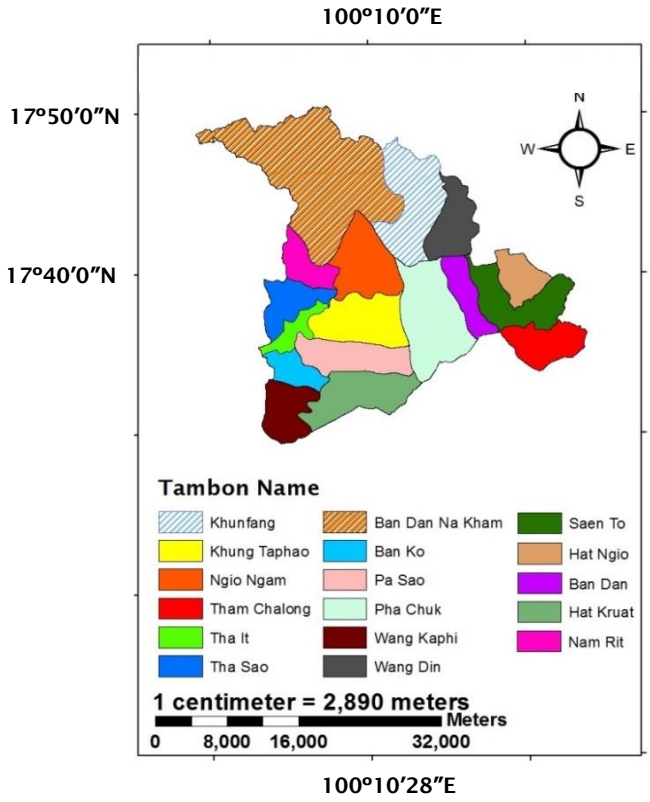

Figure 1.5 The boundary of Tambon in Muang district

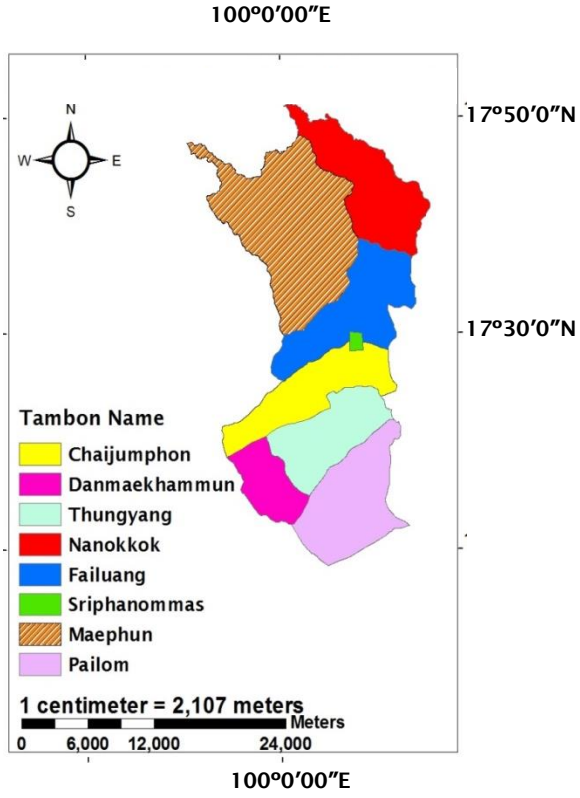

Figure 1.6 The boundary of Tambon in Laplea district

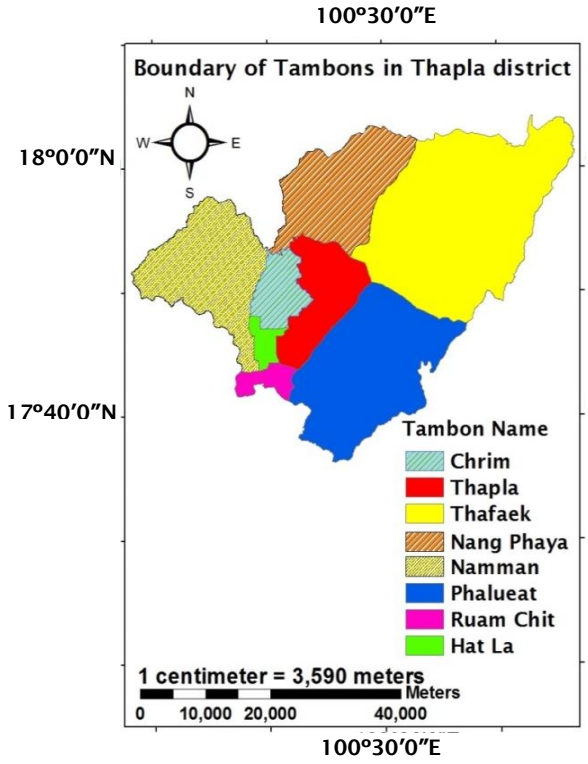

Figure 1.7 The boundary of Tambon In Thapla district

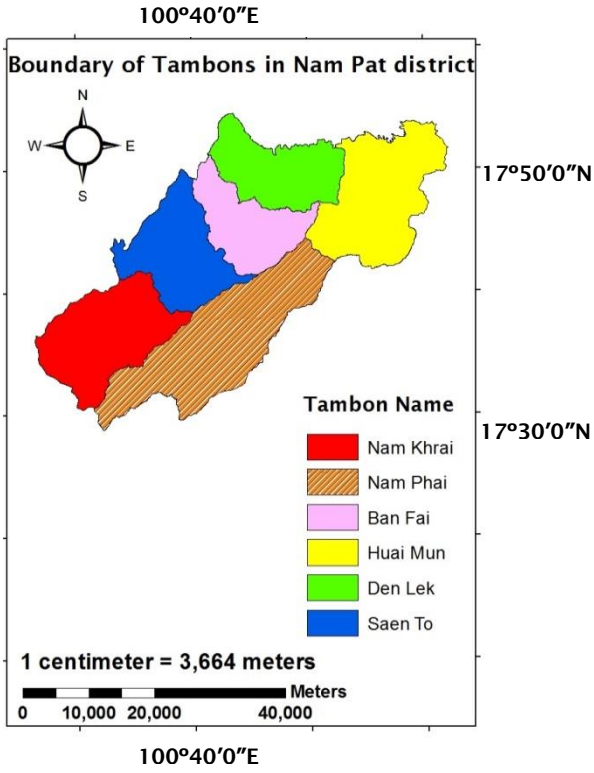

Figure 1.8 The boundary of Tambon in Nampat district

1.3 The conceptual framework

To address the research objectives, this project has been divided into four sections: setup and calibration of the model, sensitivity of the SINMAP model, landslide assessment in the present time and landslide assessment under future climate simulation scenario A2 and B2. First of all, the model is set up and calibrated against the landslide hazard mapping from the past landslide inventory triggered by rainfall values in Thapla and Laplea districts in Uttaradit province in 2006. As a result, the relationship between the output of the SINMAP model and the occurrence of past landslides are compared in terms of the landslide hazard mapping. Secondly, the SINMAP parameters are considered in terms of sensitivity for accuracy, such as trends of rainfall values, soil depth, permeability values, shear strength values, friction angle and slope angles.

Additionally, the SINMAP parameters are calculated using primary data from the geotechnical laboratory at Kasetsart University in Thailand, as well as field data collected as part of this PhD programme.

In the SINMAP model, the average rainfall during 1954 – 2012 is used to assess the rain triggered landslide hazard analysis in the present time, as well as land cover/land use and a digital elevation model (DEM), rock type and geotechnical data including shear strength and the angle of friction values. As a result, a stability class definition is determined for landslide hazard mapping. In addition, the average predicted rainfall during 2013 – 2099 under climate simulation scenarios A2 and B2 is analysed for the landslide hazard mapping in the future.

Finally, the landslide hazard mapping will be compared for both the present-day conditions and the future under climate simulation scenarios A2 and B2. Thailand is located in south-east Asia and in a tropical zone. The Southern Oscillation can shift the storm tracks, which links with tropically circulated precipitation. So climate change problems have been affecting global communities, especially heavier rainfall causing severe landslides. The average predicted rainfall during 2013 – 2099 under climate simulation scenarios A2 and B2 is

downscaled in the study site and is used to analyse the landslide risk in the future.

The literature review consists of distribution of rainfall across Thailand, the extremes of monsoons and typhoons in Thailand, changes in rainfall pattern due to climate change, the threshold value of rainfall for the initiation which causes landslides in Thailand, and landslides and the model of slope failure for landslide analysis.

CHAPTER 2 LITERATURE REVIEW

2.1 Distribution of rainfall across Thailand

2.1.1 Introduction

In Thailand, there are three climate seasons a year, which are the dry season, the rainy season and the winter season. In general, during the middle of February until the middle of May, it is the dry season, lasting three months. In February, the north of Thailand is covered by high pressure from China. Then, it is weakened because of warm air and fog remaining in some areas, thus leading to cool to cold weather in north-eastern and northern parts. In March and April, a hot low pressure cell influences the northern part, moreover, the southeast and the south winds may lie over the north as a result of hot weather in some areas, causing widespread thunder showers and hot weather on some days. In the dry season, the average maximum temperature is around 35 – 40°C (TMD, 2011a). The average rainfall in the dry season from 1981 to 2010 is shown in Fig 2.1.

During the winter season, from mid-October to mid-February, rainfall occurs in the southeast more than the southwest because it is affected by the northeast monsoon. In particular, the rainfall occurrences in November are highest, which is over 4,000 mm of the total annual rainfall in the south-western part, such as in Ranong province, while the least rainfall occurs in the south-eastern part, such as Phetchaburi and Prachuap Khiri Khan provinces (TMD, 2013). The average rainfall in the winter season from 1981 to 2010 is shown in Fig 2.2.

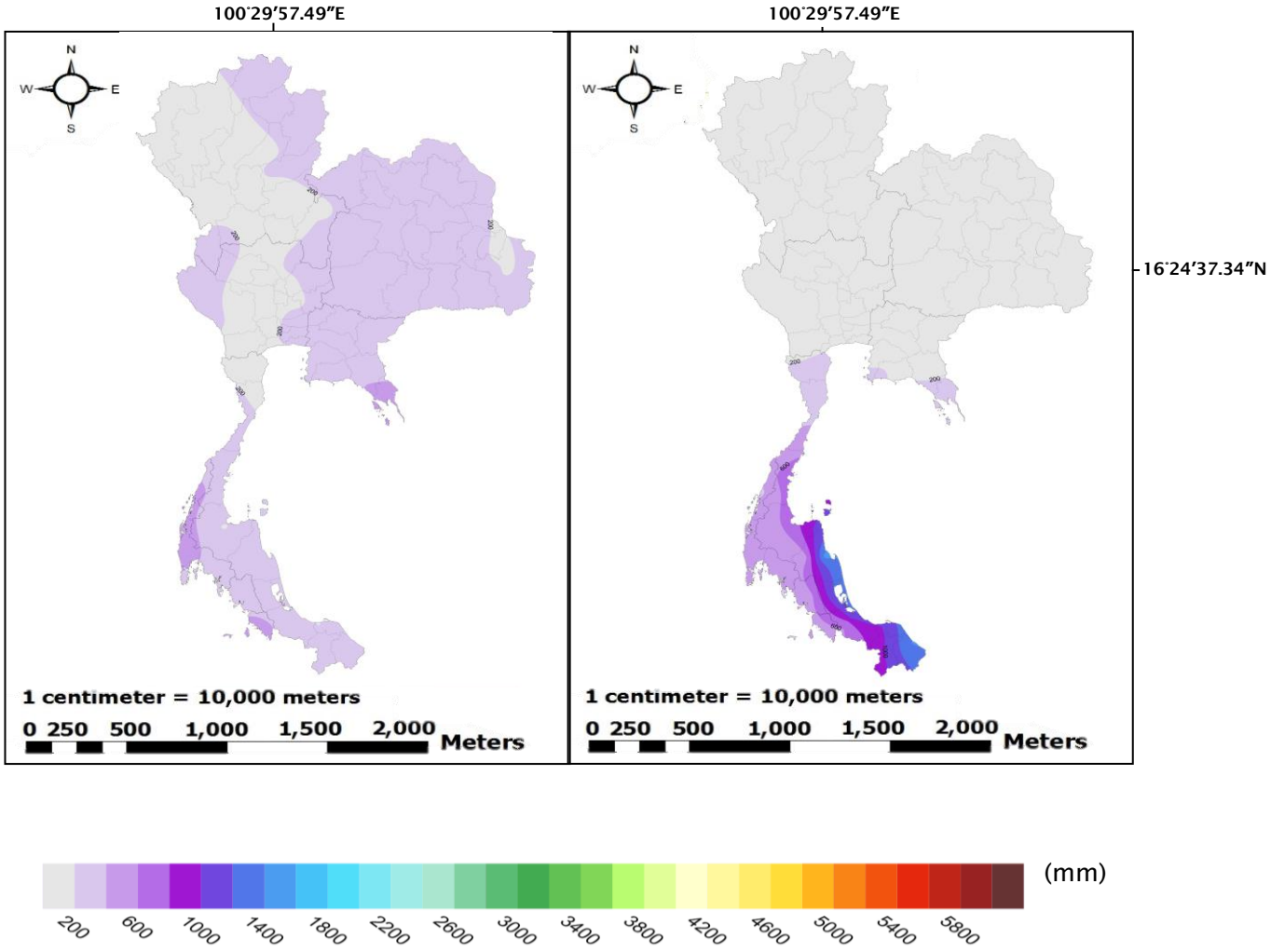

Figure 2.1 The rainfall amount (mm) in the dry season (TMD, 2013)

Figure 2.2 The rainfall amount (mm) in the winter season (TMD, 2013)

The rainy season usually starts around mid-May and ends in the middle of October, which is approximately five months, although in the southern part, rainfall occurrence is still continually widespread until December, especially in the eastern sector, since this area has been influenced by the northeast monsoon affecting the Gulf of Thailand. The southwest monsoon and Intertropical Convergence Zone are the main factors which influence the rainfall, as well as tropical cyclones moving directly into Thailand. The average annual rainfall across Thailand depends on several factors in each area and is about 1,572 mm (TMD, 2007a).

The origin of the monsoon depression in south-east Asia is approximately at the top of the Bay of Bengal and along the Ganges valley, moving across India and Burma. The remaining part of the southwest monsoon moves across the equatorial region from the south, into the eastern part of Africa and over the Indian Ocean. Besides this monsoon, the southwest monsoon, which moves towards the western coast of the Indian peninsula is divided into two parts: the Arabian Sea and the Bay of Bengal, which leads to additional rainfall.

The typical Asian monsoon consists of typhoons or tropical cyclones which circulate wind storms around the China Sea, the northern Arabian Sea and the Bay of Bengal from July to October, and especially in August. Typhoon seasons always start from the Arabian Sea during two periods: May/June and October/November. The force of a typhoon originates from warmth and moisture while the high wind speed of typhoons starts over the ocean in the north and moves westwards across the Philippines through the South China Sea and Vietnam. The period between June and October is the most common time for tropical cyclone occurrences in the Pacific Ocean, travelling from the eastern part of the Philippine Islands and moving into the China Sea through the Gulf of Thailand. Sometimes, tropical cyclones occur in the South China Sea and in the Gulf of Tonkin, leading to heavy rainfall during April to June. Storms reaching the coast and the Gulf of Tonkin contribute to the rainfall occurrences covering the north-eastern, northern and central parts of Thailand (TMD, 2007a) (Fig 2.3).

Normally, the rainy season continuously starts from the end of April because of the south wind and the southeast wind covering the country. The rainy season starts in the first half of May, especially in the north eastern, central and northern parts. Then, the southeast and the south winds move into the Gulf of Thailand, leading to an increase in the amount and distribution of rainfall in the majority of regions during the second half of May, then it leads to the start point of the rainy season.

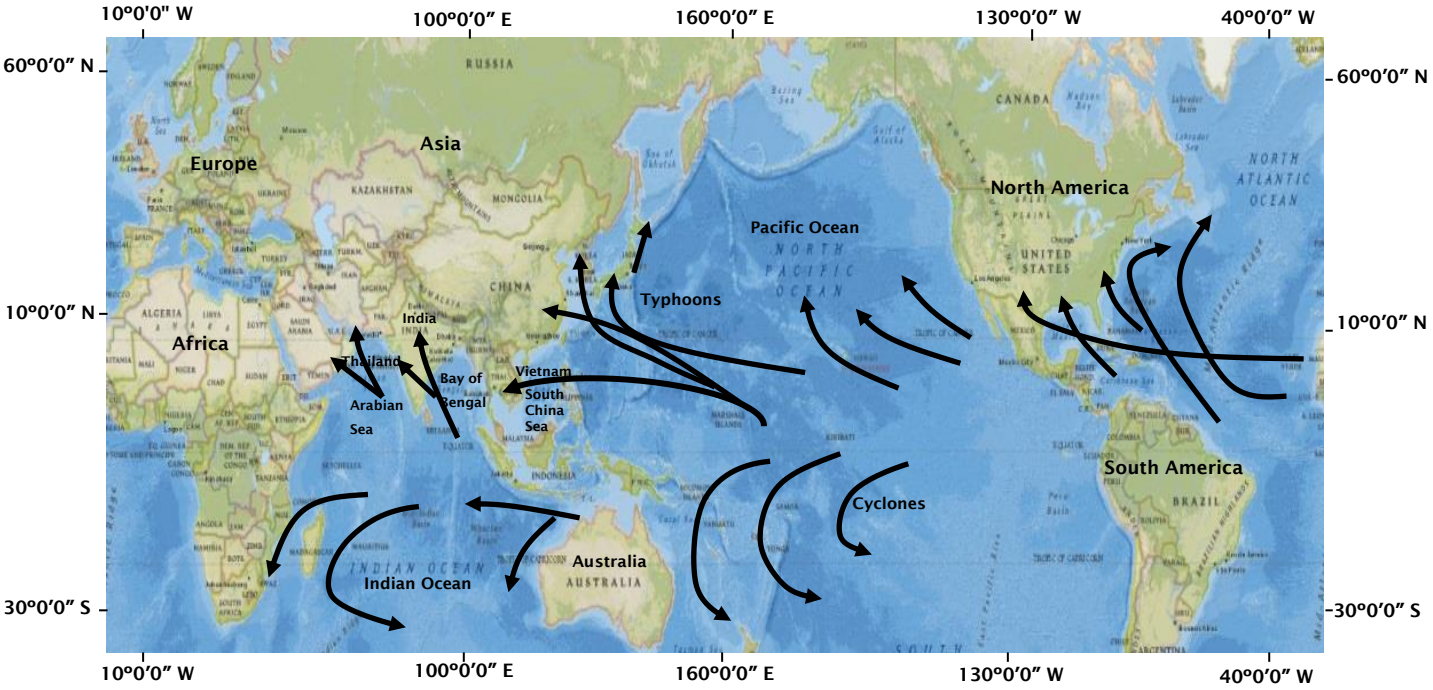

Figure 2.3 The location of south Asia map (TMD, 2007b)

Apart from the phenomenon above, the rainfall occurrences are different in each part of Thailand. In the northern part, it is usually dry and sometimes has rainfall in the winter season. The rainfall trend is highest both in August and in September as sometimes rain showers can be extremely heavy for one or two hours. Moreover, the volumes of rainfall are the most on mountains, which have a total annual rainfall of over 4,000 mm. The wettest areas in the western part are Kanchanaburi province and in the eastern part Chanthaburi and Trat province, since they are influenced by the southwest monsoon. On the other hand, the least volumes of rainfall are in the rain shadows of the mountains, which are the central areas of the northern part: Lamphun province, Lampang province and Phrae province, including parts of Chaiyaphum and Nakhon Ratchasima provinces in the north-eastern part (Fig. 2.4). In the south, rainfall occurs almost all the year except during the summer. In the rainy season, it rains in the southwest more than in the southeast because the effects of the southwest monsoon lead to high volumes of rainfall in September (Prakarnrat et al., 2008).

The total annual average rainfall across Thailand is about 1,500-1,600 mm, being primarily influenced by the southwest monsoon and the northeast monsoon. The southwest monsoon, which occurs from the high pressure area in the southern hemisphere in the Indian Ocean, affects the country from mid-May until mid-

October. This brings moist air from the Indian Ocean to Thailand. Then, cloud cover and rains are abundant, especially along the coast and mountains. During the middle of October until the middle of February, the northeast monsoon leads to cold and dry air covering Thailand. The southwest monsoon brings moisture from the Gulf of Thailand, covering the country, which leads to the rainy season (Prakarnrat et al., 2008).

In this case, four rainfall occurrence cases can produce the landslide as follows:

a. Orographic rain associated with the elevation of mountains when the moist air rises over the mountain, and it rains on the windward side. Furthermore, the cyclonic effects and the upward motion influence the rainfall occurrence on the windward side. On the other hand, the rainfall amounts are less on the leeward side; called “the rain shadow”. In Thailand, orographic rain occurs during May to October because of the southwest monsoon. For example in Ranong province in the south-western part and Chantaburi province in the eastern part, there are many mountains and orographic rainfall is a main factor of landslide occurrence.

b. Monsoon rain is another factor which influences rainfall occurrence. In Thailand, there are two main monsoons: the southwest monsoon and the northeast monsoon which interact as the Intertropical Convergence Zone (ITCZ). The effect of the Intertropical Convergence Zone depends on elevation. When there is upward motion and mixing with cyclonic conditions it leads to very heavy rainfall which occurs for one or two days in wide areas. These conditions often occur in May when it travels from the southern part to the northern part of the country.

c. Convective rain originates from the evaporation of water vapour and the flow of air currents which occur vertically, rising from heating of the radiant sun. The convective rain is heavy and usually occurs for short periods and in narrow areas during the dry season. During the convective rain, thunderstorms originate from the collision between cold air and hot air masses, then the moving hot air will be lifted above the cold air mass quickly. This situation is called a summer storm, and usually occurs in the dry season.

d. Cyclonic rain is mostly caused by the influence of the tropical cyclone. When the tropical cyclones come, low pressure occurs around the vertical density centre and leads to heavy rainfall that continues for several days. The tropical cyclones

and storms are usually formed in the South China Sea or the Pacific Ocean, which move through neighbouring countries such as Vietnam, Cambodia and Laos before Thailand, thus the storms are weakened into a weaker tropical depression.

Based on Prakarnrat et al., (2008) a total monthly rainfall was indicated during 1951-2005. The rainy season begins from mid-May to mid-October due to the southwest monsoon covering, including the Intertropical Convergence Zone (ITCZ). As a result, it rains in the south, the central parts, the east, the north and the northeast respectively. Sometimes, the Intertropical Convergence Zone moves to the south of China leading to rain delay in Thailand. Then, the southwest monsoon over Thailand occurs again during August to November. It leads to extreme rain in the southern parts, especially in the southeast. The results of data obtained the probability of a monthly total and the distribution rainfall of the country. In addition, the results of the spatial rainfall distribution are found by the interpolation of the rainfall amount during the rainy seasons from 2000 to 2013 in Thailand. The annual rainfall amounts are calculated by the monthly rainfall amounts from May to September during 2000 to 2013 (Fig 2.4). The results of the spatial rainfall distributions are shown in terms of average rainfalls. The annual rainfall is calculated by the rainfall values from a total of 140 rain stations throughout Thailand. Therefore, the spatial rainfall distribution maps are shown below for each region in Thailand (TMD, 2013).

As a result of the spatial rainfall distribution, the rainfall amount in the central part was less than other regions in Thailand from 2000 to 2013. There was a large annual rainfall amount in the northern part, from around 1,200-1,300 mm in 2002 and in 2006, whereas the large annual rainfall amount in Uttaradit province was around 2,000 mm in 2006 and in 2011 and the past landslide also recorded in these two years. There was the highest rainfall amount in the southern part, while the annual rainfall amounts in the south-eastern and the south-western parts were almost the same, at approximately 2,500-3,000 mm. On the other hand, the trend of the rainfall amount in the south western part decreased from 2000 to 2010. In the north-eastern part, the pattern of the rainfall amount was almost the same during the 2000 to 2013 period. The volume of rainfall may vary in each region of Thailand and will be presented by the annual map patter.

The result can be shown the spatial rainfall distribution (Fig. 2.4).

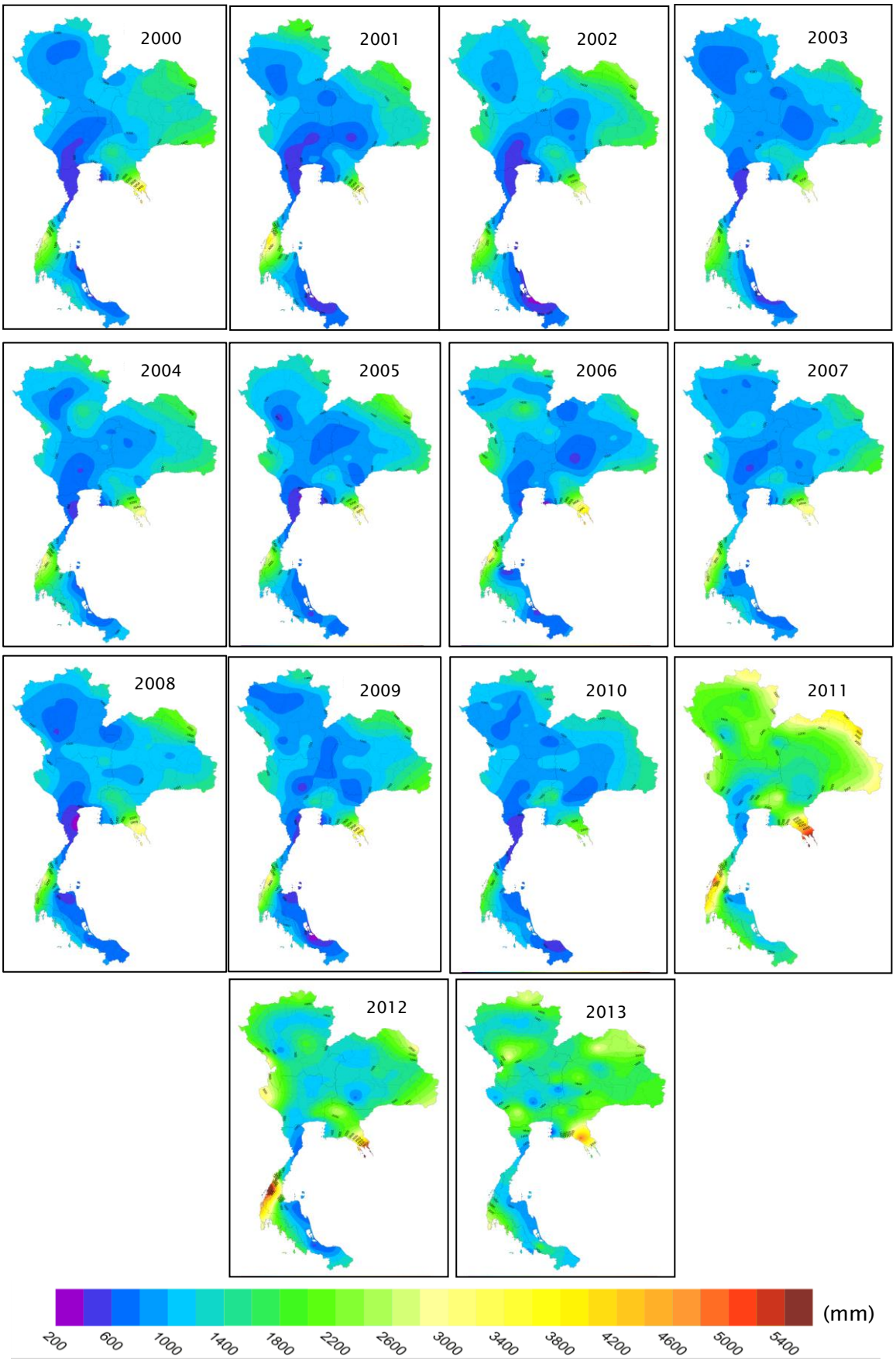

Figure 2.4 The rainfall amount (mm) in the rainy season from 2000 to 2013 (TMD, 2013)

2.1.2 The monsoons in Thailand

There are two monsoons that effect Thailand, the southwest and northeast monsoons. During the May to October period, the southwest monsoon (Fig 2.5) season leads to humid and cloudy skies and heavy rainfall around the country, since the wind direction is influenced by topography in each position. The south westerly winds that blow into Thailand come from the Indian Ocean and the Bay of Bengal. This wind picks up water vapour from the ocean and from the slopes of the mountains. Then, water condenses into clouds leading to rainfall and thunderstorms along the western side of the mountains, where the maximum rainfall is approximately 500 mm. The rainfall amount is almost the same in the eastern part which is near the Gulf of Thailand. When the wind crosses and mixes with the heat from the air above the earth, the water vapour condenses into clouds and heavy rain and storms occur across the country in the low pressure areas (Jutakorn et al., 2010).

The northeast monsoon (Fig 2.5) appears in November, while the high pressure area covers the land. The northeast monsoon blows into the northern, the central and the north-eastern parts which leads to cold and dry weather. Therefore, dry weather occurs in the northern, the north-eastern and central parts respectively. Sometimes, the rainfall occurrences increase in both the south-western and the south-eastern parts, especially the south-western part near the Gulf of Thailand, since the tropical cyclones arrive from the Philippine Islands. The northeast monsoons in December have more power, because of the centre of high pressure area in the southern part of China, which leads to cold and dry weather in several parts of Thailand. Furthermore, during the November to December periods, tropical cyclones in the South China Sea move into the Gulf of Thailand. They originate from the south to the east of the Philippines, which leads to heavy rainfall for one or two days in the eastern part of Thailand. During the northeast monsoon season from January to February, the weather is still cold and dry. At the end of February, the pattern of rainfall remains stable along the coast, since the wind blows from the sea into the central and eastern parts of Thailand. However, the weather is still hot and dry in the northern and north-eastern parts respectively. During March to April, the wind blows from the Gulf of Thailand into the south, since the low pressure area moves up over the equator. In this period, the weather is hot and there are widely scattered rainy showers in some areas. At

the end of April, the rainfall occurrences increase slightly in the southwest, because of the beginning of the southwest monsoon (Jutakorn et al., 2010).

2.1.3 The low pressure area in Thailand

The low pressure area occurs from May to October. Especially in May, the low pressure area (Fig. 2.5) is located at the middle of the country and spreads throughout several regions, such as the northern, the north-eastern and the southern parts. It occurs during the warm weather in May as the season changes from being dry to rainy. During the southwest monsoon, during May to September, the low pressure area covers the central, the northern and the north-eastern parts of Thailand and on throughout the eastern part and the Gulf of Tonkin. As a result, the wind moves from the Indian Ocean through the Bay of Bengal, the South China Sea and the Gulf of Thailand, into the central part of Thailand. This wind moves from the south-western part into the north-eastern part. It is called the southwest wind which originates from the southwest monsoon. From June until September, the low pressure area is located in the northern part, whereas in October the low pressure area is located in the southern part. The southwest monsoon affects the rainfall distribution across Thailand (TMD, 2007a).

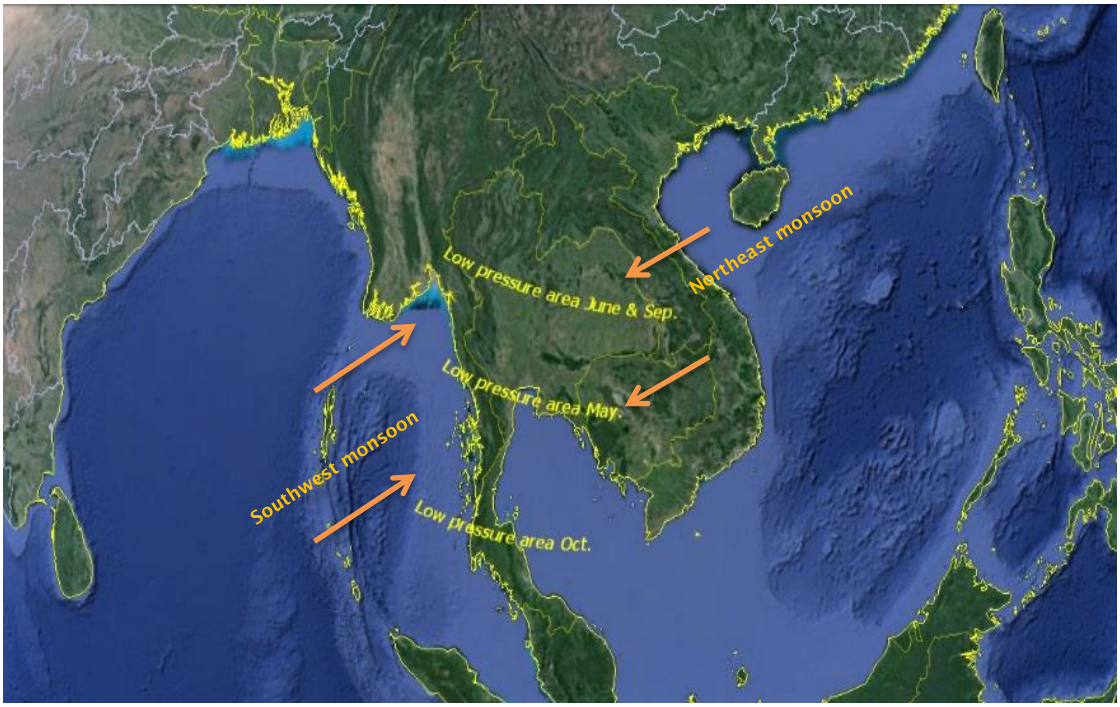

Figure 2.5 The location of low pressure area and southwest and northeast monsoons (TMD, 2007a)

Fig. 2.6 compares the volume of monthly rainfall over Thailand. It averages data for six regions: North, Northeast, Central, East, Southeast and Southwest. As can be seen, it covers the years 1951 to 2011 and describes the average monthly rainfall during 60 years in all regions of Thailand. While the total rainfall from 1951 to 2011 remains steady in the first two months, January and February, there is a steady increase from March to June with a rapid increase at the end of June to peak over 272 mm in September; a dramatic fall follows from October until December.

Fig. 2.7 shows the rainfall from 1951 until 2011. Overall, it can be seen that the trend of rainfall fluctuated from 1951 until 2010, with the highest values in 1953 and in 2011.

At the beginning of the period, the trend in rainfall was downwards from 1951 until 1979. Then, a trend upwards continued through to 1988, when there was another fluctuating rise followed by a further fall to 1992. By the end of the period, the fluctuation climbed to peak at just over 1,900 mm in 2011. Incidentally, the low fluctuation of rainfall amount stood at around 1,500 mm during 1977 to 1991. The exceptional rainfall in 2011 led to the commissioning of the Thai Meteorological Department report in 2012.

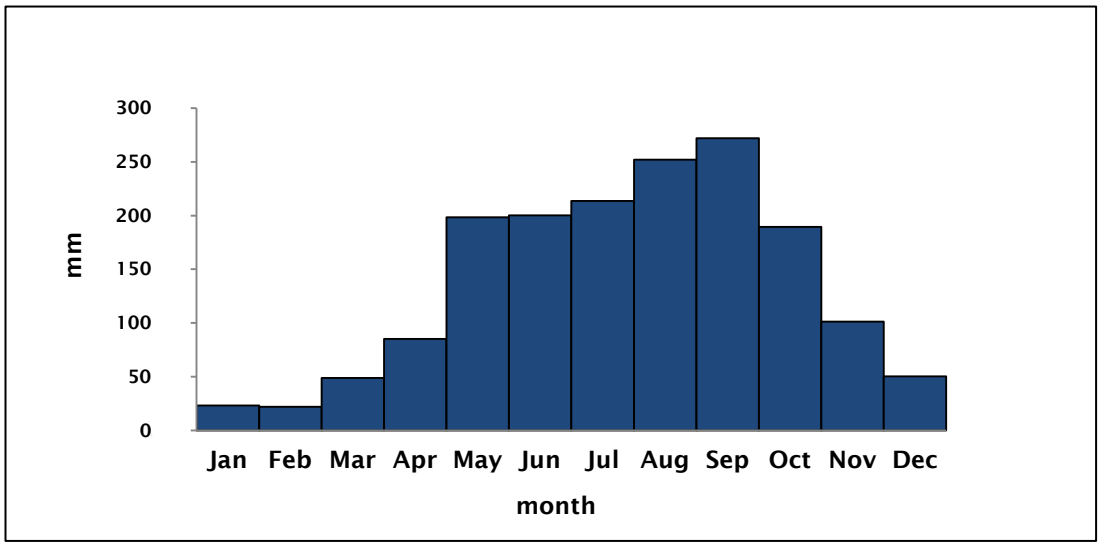

Figure 2.6 Graph (Showing the average rainfall amount in rainy season during 1951 to 2011) (TMD, 2012b)

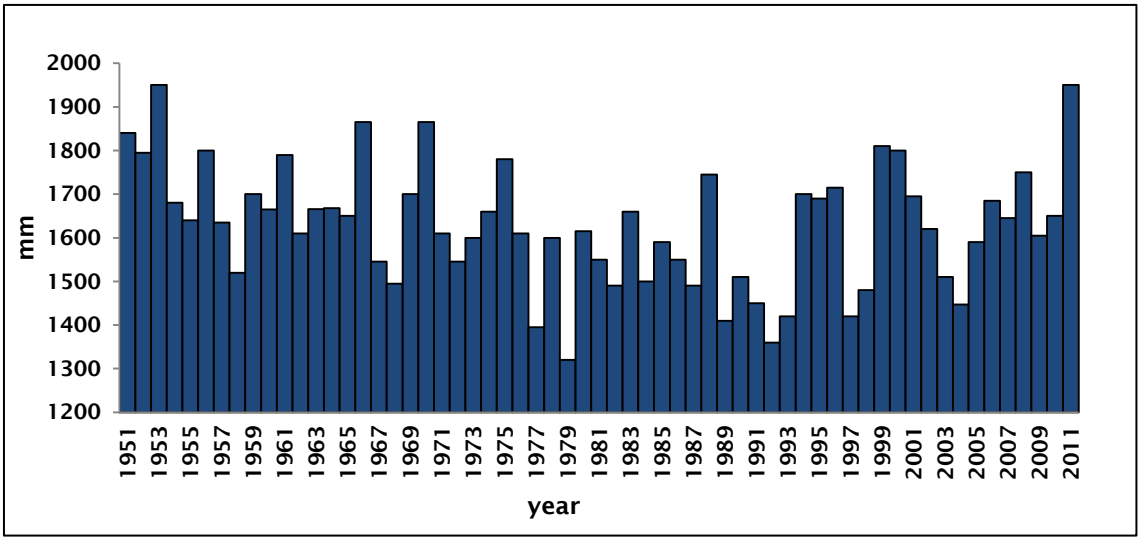

Figure 2.7 The mean annual rainfall in Thailand during 1951 to 2011(TMD, 2012b)

2.1.4 Extreme rainfall distribution

The Thai Meteorological Department report of rainfall distribution across Thailand in 2011 states that it was caused by the conjunction of the southwest monsoon and the tropical cyclone, which lay over the northern part of Thailand.

Normally, the typical weather is to have the dry season in March, but the high pressure areas from China extended to cover the northern region in 2011. This situation caused occasional rainfall occurrences for almost the whole month in this year. An active low pressure cell also covered the southern area, which caused intense and heavy rainfall in several regions in the south in eleven provinces: Chumphon, Surat Thani, Nakhon Si Thammarat, Songkhla, Patthalung, Narathiwat, Yala, Trang, Phang Nga, Krabi and Satun. Due to this phenomenon, both landslides and mudslides were reported in Nakhon Si Thammarat and Krabi provinces. The rainfall amount in March in 2011 was the highest in the previous 36 years (1974-2011). These situations were considered unusual compared with other years (TMD, 2011c).

In the rainy season of this year, scattered rainfall occurred in several regions of Thailand, but excessive rain was reported in the northern and the north-eastern parts. Flash floods started in the middle of May, then the southwest monsoon caused extreme rainfall in several parts of Thailand, especially in the northern and in the upper central parts. On 24th June, the tropical storm named “Huama” caused rainfall in the northern part of Vietnam, which then weakened to be a depression. This storm became an active low pressure cell on 26th June and

moved across Laos. Afterwards, this storm moved above Nan province, which caused heavy rainfall in several regions in the northern area. The daily rainfall amount measured approximately 335.2 mm at that time. Therefore, landslides occurred in some regions in the northern part, in Maehongson and Uttaradit provinces, which damaged agricultural areas and affected families (DMR, 2011b).

In July, landslides occurred in several regions in the northern part because of an acute depression named "Nock Ten" over Thailand via Nan province (Fig 2.8). Then, it became a low pressure area covering Chiang Mai and Mae Hong Son provinces in the north. On July 30th, the highest rainfall amount was reported: approximately 405.9 mm/24hours in Muang district in Nongkhai province in the northeast.

Moreover, the southwest monsoon usually travels into the northern and the north-eastern regions leading to rainfall occurrence and rainfall distribution around the upper and middle parts of Thailand, such as the northern, central and north-eastern parts during August to September. On September 27th the tropical storm "Haitang" caused landslides in Vietnam, which then became a depression before moving to Laos, but this situation did not affect Thailand. Towards the end of the rainy season, during the end of October, the northeast monsoon influence extended across Thailand and brought occasional rainfall (TMD, 2011c).

Another storm, the typhoon named "Nasat" moved through the Gulf of Tonkin (Fig 2.8), causing landslides in Vietnam on September 30th. This tropical cyclone affected the northern part of Thailand because of heavy rainfall, which led to flash floods. The evaluation of economic losses was approximately 600 million dollars, due to the flood period continuing beyond November 2011.

Finally, the amount of rainfall starting from 1 January to 31 October 2011 measured 1,822.4 mm; approximately 28% above the normal average value and also above the normal value in the northern and lower central parts, but in some areas it was below the normal value as evaluated from the accumulative rainfall from several stations of the Meteorological Department (TMD, 2011c).

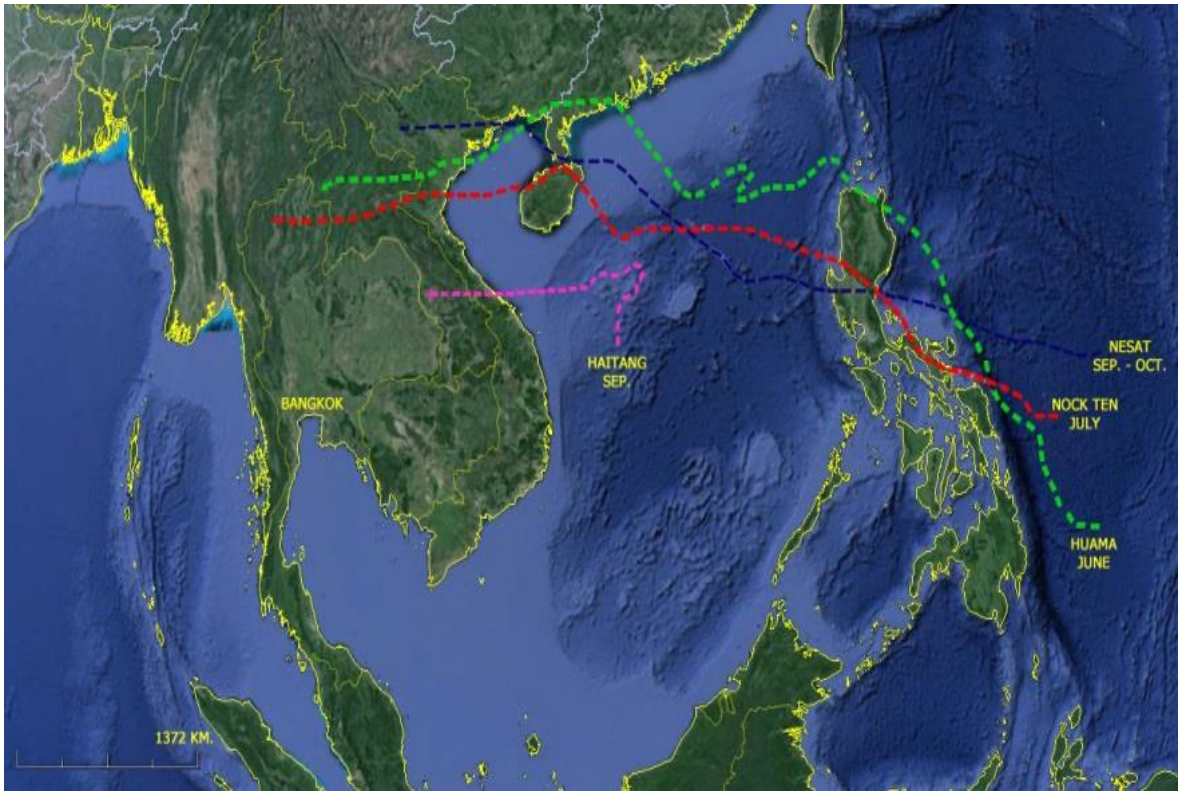

Figure 2.8 The direction of tropical cyclones (TMD, 2012c)

2.2 The extremes of monsoon and typhoon in Thailand

2.2.1 Introduction

The typical Asian monsoon consists of typhoons or tropical cyclones which circulate wind storms around the China Sea, the northern Arabian Sea and the Bay of Bengal during July to October, especially in August. Typhoon seasons always start from the Arabian Sea in two periods: May/June and October/November. The violence of typhoons originate from warm moisture, while the high wind speed of typhoons starts over the ocean in the north and move into westwards across the Philippines through the South China Sea and Vietnam. The period June to October is the best time for tropical cyclone occurrences in the Pacific Ocean, and the east of the Philippine Islands, moving into the China Sea through the Gulf of Thailand. Sometimes, tropical cyclones occur in the South China Sea and the Gulf of Tonkin leading to heavy rainfall during April to June. Storms reaching the coast and the Gulf of Tonkin contribute to the rainfall occurrences covering the north-eastern, northern and central parts of Thailand (TMD, 2007b).

2.2.2 The tropical cyclone in Thailand

Tropical cyclones frequently move westwards at high altitudes, then turn to the east. There are various tropical cyclone categories for the north-west Pacific and the South China Sea as follows (TMD, 2007a).

a. Tropical depression (less than 63 km/hr)

b. Tropical storm (more than 63 km/hr)

c. Typhoon (more than 118 km/hr)

Whatever their category, the tropical cyclones affect large regions of the surrounding countries. In particular, the centre of the cyclone leads to life and property damage caused by heavy rainfall and wind. Normally, there are many tropical cyclones moving into Thailand (Fig 2.9). The tropical cyclones have two sources in the west and the east of the country. The eastern side consists of the Pacific Ocean and the South China Sea, while the west consists of the Bay of Bengal and the Andaman sea. The period from June to October is the best time for tropical cyclone occurrences in the Pacific Ocean, moving from the east of the Philippine Islands into the South China Sea through the Gulf of Thailand. Sometimes, tropical cyclones occur in the South China Sea and the Gulf of Tonkin leading to heavy rainfall from April to June, while, tropical storms reaching the coast and the Gulf of Tonkin contribute to the rainfall occurrences covering the north-eastern, northern and central regions. Sometimes there are more storms, including strong winds, due to the southwest monsoon, which is more intense than usual, and leads to intensive rainfall occurrences that spread widely (TMD, 2007a).

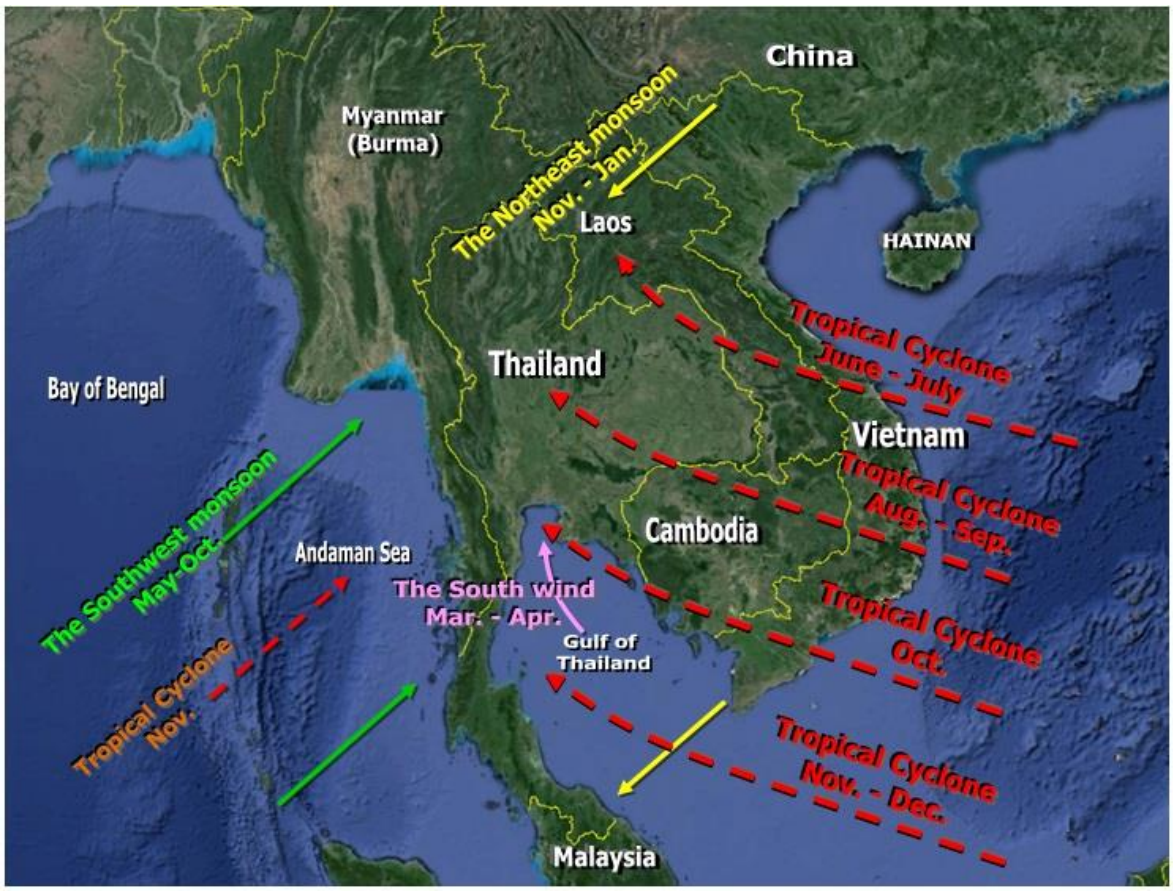

Figure 2.9 The direction of the tropical cyclones (TMD, 2007a)

2.2.3 Case study of extreme monsoons, low pressure areas that led to rain fall occurrences, affecting landslides in Thailand (1999-2008)

In 1999, the southwest monsoons moved through the northern and the north-eastern parts of Thailand during the period from the 20th to the 31st of July. In addition, the low pressure areas moved and increased in power and became a depression storm. Then, on July 30th, heavy rainfall of approximately 430 mm occured causing a landslide in Khao Khitchakut Chanthaburi province. In 2001, the low pressure areas and the southwest monsoon winds covered the northern part of Thailand and increased in their strength, and as a result approximately 300 mm of rainfall values widely spread in the northern part. During the period from May 2nd to 4th, landslides and mud slides occurred in the Wang Chin district, in Phrae province. In 2002, the low pressure area travelled into the northern part of the country in August and linked with the southwest moving monsoon and led to heavy rainfall of approximately 60 mm in September. Thus, during the time from the 15th to the 16th of September, landsliding occurred in the Maechaem district, in Chiangmai province. In 2004, landsliding occurred again in the

Maechaem district, in Chiangmai province, on May 6th, because of the low pressure area and the southwest monsoon moving together. It led to heavy rainfall of approximately 162.4 mm in the northern part. In 2006, the influence of the southwest monsoon was concentrated in the northern part in the beginning of May, and then the low pressure area moved through the north and the north-eastern parts in the middle of May. Approximately 206 - 330 mm of heavy rainfall widely spread from the 23rd to the 24th of May in six provinces in the northern part of Thailand, such as, Uttaradit, Phrae, Nan, Lampang Tak and Sukhothai. On May 23rd, landsliding occurred in three districts in Uttaradit province, and in one district in Sukhothai and in Phrae provinces respectively (DMR, 2011a) (Fig. 2.10).

The southwest monsoon and the low pressure areas are the main factors which have influenced the rainfall, as well as the tropical cyclone moving directly into Thailand (TMD, 2007a). Therefore, the relationship between the southwest monsoon, low pressure and tropical cyclone are linked with the trend of rainfall. In 2002, 2006 and 2011, the rainfall volumes were 1,631mm, 1,684 mm and 1,948 mm respectively. These rainfall values are related to the southwest monsoons, the low pressure areas and the tropical cyclones, which had their movements during the same year, as shown in Fig. 2.11 and Fig. 2.12.

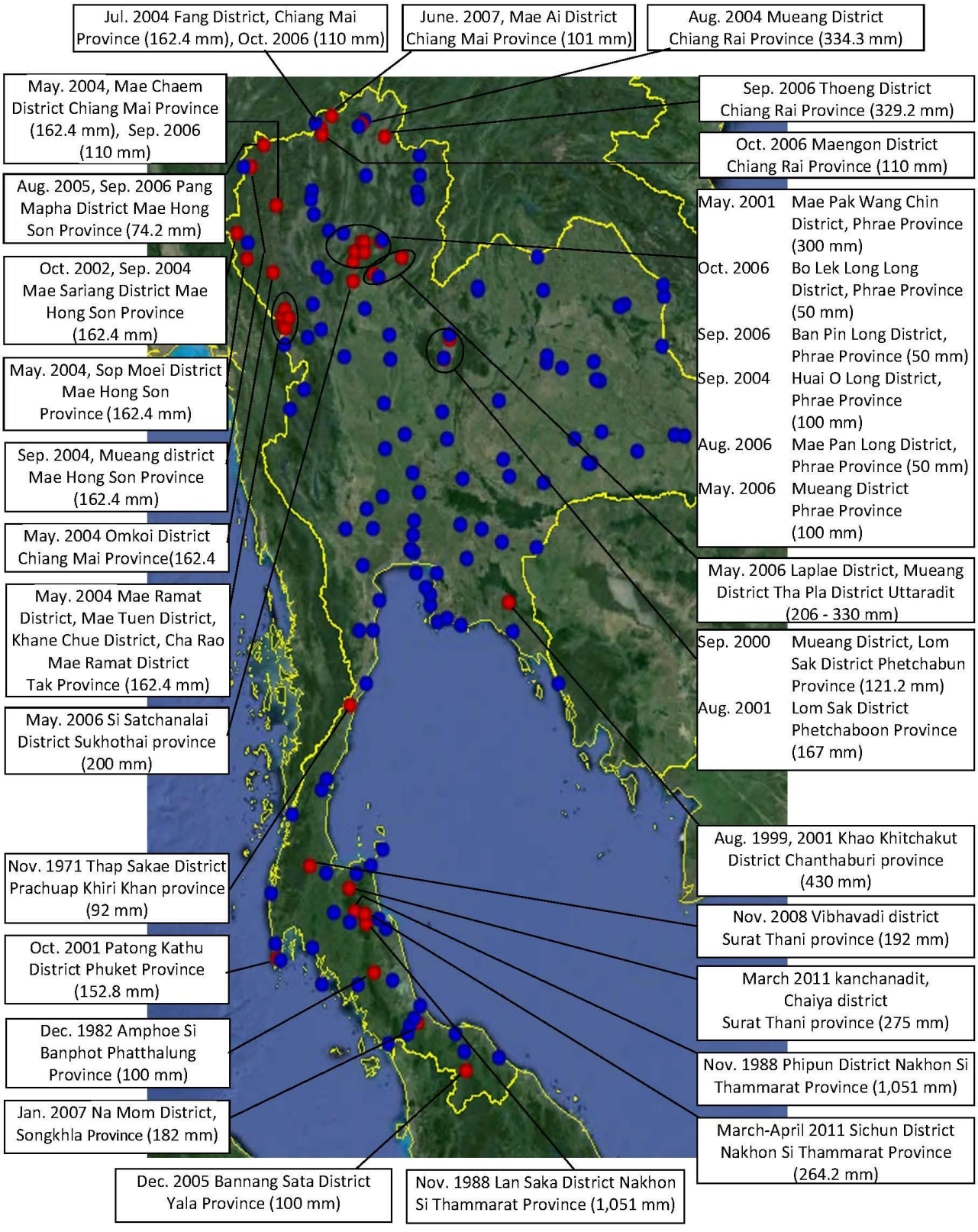

Figure 2.10 The past landslides (DMR, 2011a, b, c, d, e, g) (GERD, 2006) and daily rainfall (TMD, 2012b) from 1988 to 2006 and rain stations in Thailand

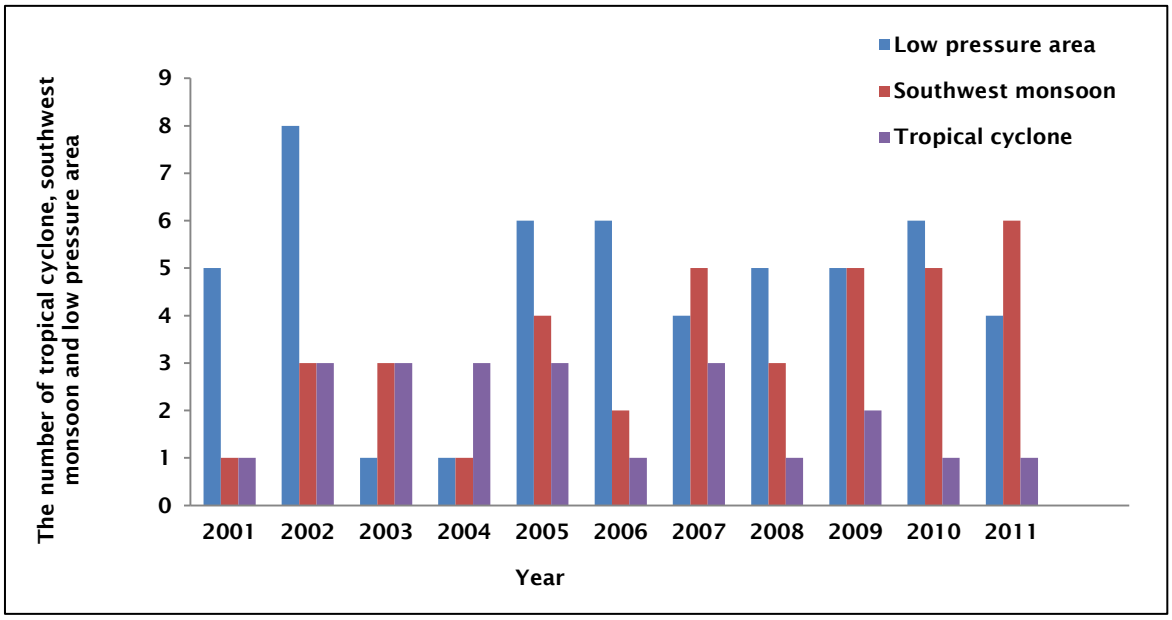

Figure 2.11 The tropical cyclone, the monsoon and the low pressure area moving into Thailand during 2001 to 2011 (TMD, 2012c)

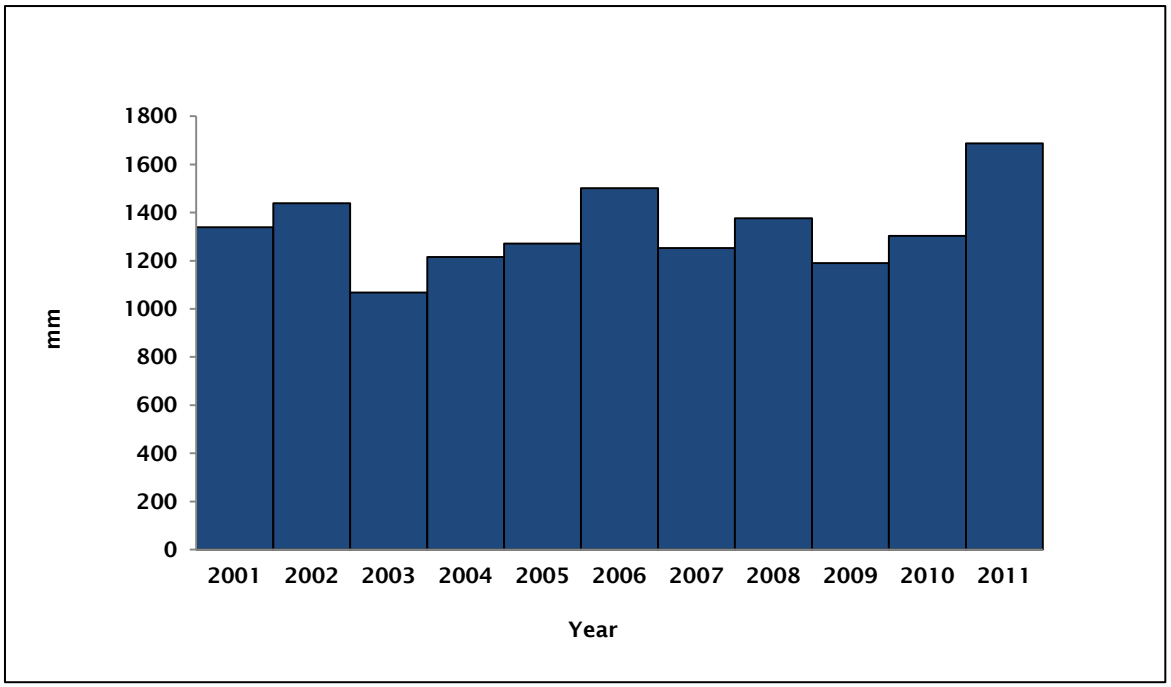

Figure 2.12 The trend of annual rainfall volumes during 2001 to 2011 (TMD, 2012b)

Landslides occur in several regions in the southern and northern parts of Thailand during the rainy season. Evidently, landslides are caused by heavy and intense rainfall in the southern and northern parts of Thailand. In the northern part, landslide risk areas consist of ten provinces: Chiang Mai province; Chiang Raiprovince; Lamphun province; Lampang province; Prae province; Nan province;

Uttaradit province; Maehongson province; Payao province and Tak province. Whereas, in the southern part, there are seven provinces: Krabi province; Suratthani province; Trang province; Ranong province; Phatthalung province; Nakhonsithammarat province and Chumphon province. These are predicted as high risk areas using past landslide events as a guide (DMR, 2011a).

In the southern part, the south west monsoon which originates from the Indian Ocean is influenced by the tropical cyclones. The northeast monsoon winds move into the Gulf of Thailand leading to the rainy season during May until January. For example, Wangwongchai (2005) found that the features of the atmospheric circulation and the maximum of the convergence of moisture near the southern part of Thailand led to the extreme rainfall 550 mm in Songkhla province in November 2000. Moreover, the effect of the Asian winter monsoon originating from Siberia, moving into the southern part of Thailand, correlated with the extreme rainfall in several regions in the southern part. During the winter monsoon, the large rainfall volumes are over the southern part of Thailand.

In addition, the influence of the storm tracks and low pressure areas lead to the severity of landslides. The topography of the southern part consists of high and hilly mountainous areas. Normally, rainfall average is approximately 1,280-3,694 mm throughout the year. There are several more recent landslide occurrences in each region in the southern part of Thailand (DMR, 2011e).

There were five landslide cases in the past, for example in the northern and the southern parts of Thailand.

According to the Meteorological Department, the low pressure area covered the northern and the north eastern parts of Thailand and led to heavy rainfall approximately 330 mm, 206.4 mm and 263.7 mm in the Laplea district, Thapla district and Muang district in Uttaradit province respectively, on May 23, 2006. Mud flows and woody debris engulfed villages and destroyed life and properties (Fig. 2.13). In addition, the boundary of landslide scars in a polygon shape were presented in both tambon Meaphun in Laplea district and tambon Namman in Thapla district. The landslide scars were obtained from satellite images, after landslides occurred and the boundaries of the landslide scars were calculated in terms of square kilometres (DMR, 2006).

Figure 2.13 The impact of landslide occurrences in Uttaradit province (DMR, 2011a)

On 7 August 2006, landslides occurred in Los Mae Fah Luang, Mae Fah Luang, in Chiang Rai province (Fig 2.14). These incidents occurred due to approximately 110 mm of rainfall values because the southwest monsoon extended over the southern part and low air pressure winds dominated the northern part (DMR, 2011b).

Figure 2.14 Road side cutting failure at Mae Fa Luang district, Chiang Rai province (DMR, 2011b)

During 23 March until 5 April 2011, the maximum daily rainfall was approximately 264.2 mm on 25 March 2011 landslides and flash floods flowed into many villages in Nakhon Si Thammarat province (Fig 2.15). It affected 20,000 households and the transportation system was disrupted, causing migration to secure areas (DMR, 2011f).

Figure 2.15 On 25-31 March 2011 The landslide and flash flood in Nakhon Si Thammarat province (DMR, 2011f)

On 9 September 2011, the influence of the low pressure area and the southwest monsoon over the northern part led to approximately 242.8 mm of rainfall values. As a result, landslides and mud slides occurred in Nampat district in Uttaradit province (DMR, 2011a) (Fig 2.16).

Figure 2.16 The impact of landslide and flash flood in September 2011 in Uttaradit province (DMR, 2011a)

2.2.4 Case study of extreme tropical cyclone leading to landsliding in Thailand (2010 - 2011)

In 2010, tropical cyclones formed in the Western North Pacific Ocean, the South China Sea and the Bay of Bengal. There were thirteen cyclones in Thailand, however, only one tropical depression moved into Thailand. It was formed in the

South China Sea and moved through the Gulf of Thailand in November. The influence of this storm was concentrated in many provinces in the southern part of Thailand, such as Chumphon, Surat Thani, Nakhon Si Thammarat, Songkhla, Pattani, Yala, Phatthalung, Trang, Krabi, Satun, and Narathiwat provinces. Afterwards, approximately 206.4 - 330 mm of rainfall values were spatially widely spread for twenty-four hours causing sudden severe flooding and landsliding, on 4th November, in Khanom and Sichon districts in Nakhonsithammarat province which destroyed agricultural areas, houses and lives. In addition, this storm moved into the Andaman Sea, increasing its power to a cyclone, called JAL, and entered the Bay of Bengal (Fig 2.17). At the end of August, another tropical cyclone of depression level moved into the northern and the north eastern parts leading to heavy rainfall and flash floods in several areas, especially in the northern and north eastern parts (TMD, 2011a).

In March 2011, the rainfall occurrences were extreme in several areas. Approximately 264.2 mm of daily rainfall value was due to an active low pressure cell in the middle part of the southern region. In several regions of the southern part, there were landslide occurrences. The total of rainfall in this year was higher than in the past thirty-six years. For example, there was the highest annual rainfall amount of 3,547 mm in Ranong province in the southern part. During the rainy season, the rainfall amount was 40-50% higher than normal. The excess rainfall occurrences were often in the northern and north-eastern parts. The main factors for this situation were the southwest monsoon and low pressure traveling into the country. On the 24th of June 2011, Huama was the tropical cyclone which caused landslide occurrences in Vietnam before becoming a depression and moving into Nan province in the northern part of Thailand. This tropical cyclone led to very heavy rainfall, approximately 242.8 mm in many provinces in the northern part of Thailand. Furthermore, flash floods and landslides were recorded often in Prae, Chiang Rai, Phayao, Nan, Tak, and Sukhothai provinces including the loss of lives and properties (Fig. 2.17) (TMD, 2011b).

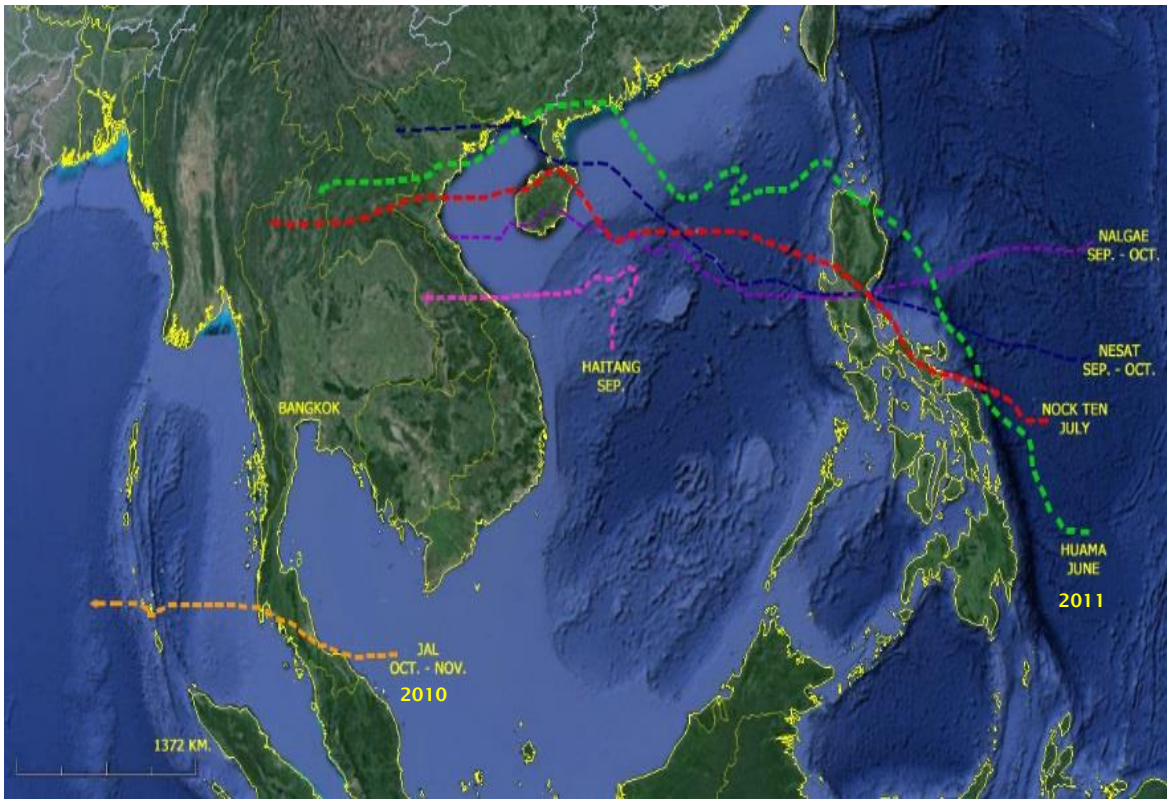

Figure 2.17 Typhoon track moving into Thailand in 2010 and in 2011 (TMD, 2012c)

2.2.5 Tropical cyclones moving into Thailand during 1951-2011

Fig. 2.18 details the number of tropical cyclones classified as depression, tropical storm and typhoon in the past sixty years between 1951 and 2011 in Thailand. Fig. 2.19 shows the monthly tropical cyclones and the relationship between the tropical cyclones and landslide occurrences during 1998 to 2011 (Fig. 2.20). Overall it can be seen that the depressions are more prevalent than tropical storms and typhoons which remained relatively in significant in number.

The number of depressions was nine in 1964. Depressions occurred more than other levels, whereas tropical storms were the second highest. The trend of the tropical storms and typhoons were quite similar. Three decades later, the number of depressions decreased substantially. A comparison of monthly data presented that fewer depressions appear in April. Then the trend of depressions increased steadily from April until October, whereas the depression level and tropical storm level dropped to around eight and two respectively in December. Also, the tropical storms were nearly the same as during August until December. Furthermore, typhoons only occurred in November.

Fig 2.20 shows the number of annual tropical cyclones (TMD, 2012c) and landslide occurrences during 1998-2011(DMR, 2012). A tropical cyclone occurred around two or three times in each year. Then, there were around one or two events of landsliding each year. Whereas, the number of landslide occurrences were high in 2004, 2006, 2010 and 2011, ie. six, four, four and eleven respectively, the number of tropical cyclones were few: ie. as two, two, one and one respectively in the same year. In particular, the number of landslides was eleven in 2011, but there was only one tropical cyclone moving into Thailand. The eleven landslides occurred in several regions of Thailand in 2011. The antecedent precipitation index (API) is one factor in evaluating landslide occurrences in this year. The antecedent rainfall and soil moisture are important for landslides. The basic of API is the moisture of soil at any time that is recorded, as well as the soil moisture related to the accumulated rainfall, which will be reduced at the end of the rainfall (Ohtsu et al., 2012). The critical API affects the shear strength of soil on slope stability. Then, the relationship between the API and the shear strength of soil are used to determine landslides (Soralump et al., 2007). For example, the rainfall amount in March 2011 was the highest in the previous 36 years (1974-2011) (TMD, 2011). Approximately 42.44% of annual rainfall in 2011 in the north and approximately 25.67% in the central region was higher than normal years. It means that these situations led to the occurrence of the critical API and landslides in Thailand (Witthawatchutikul et al., 2011).

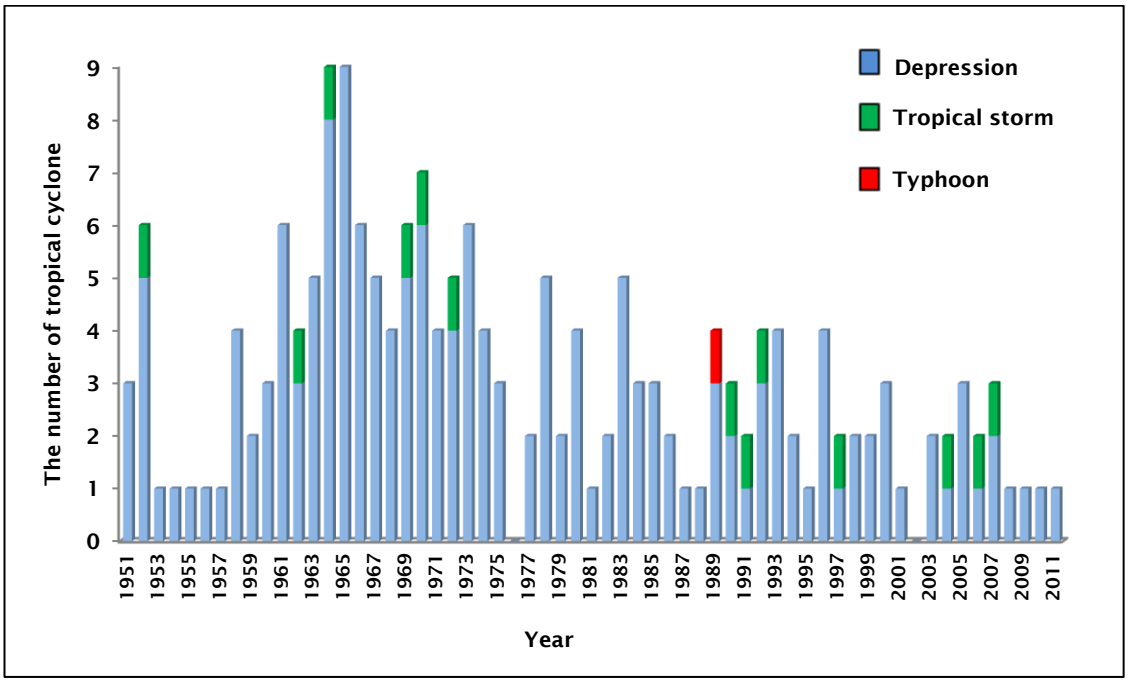

Figure 2.18 Tropical cyclones moving into Thailand during 1951-2011 (TMD, 2012c)

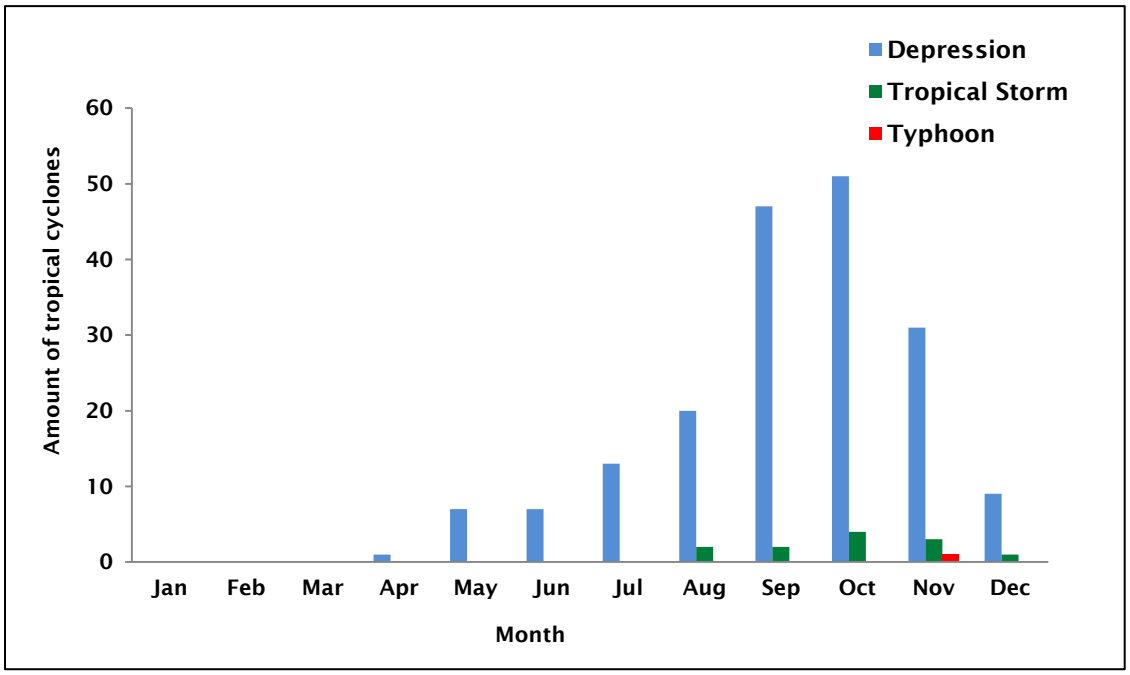

Figure 2.19 Monthly tropical cyclones moving into Thailand during 1951-2011(TMD, 2012c)

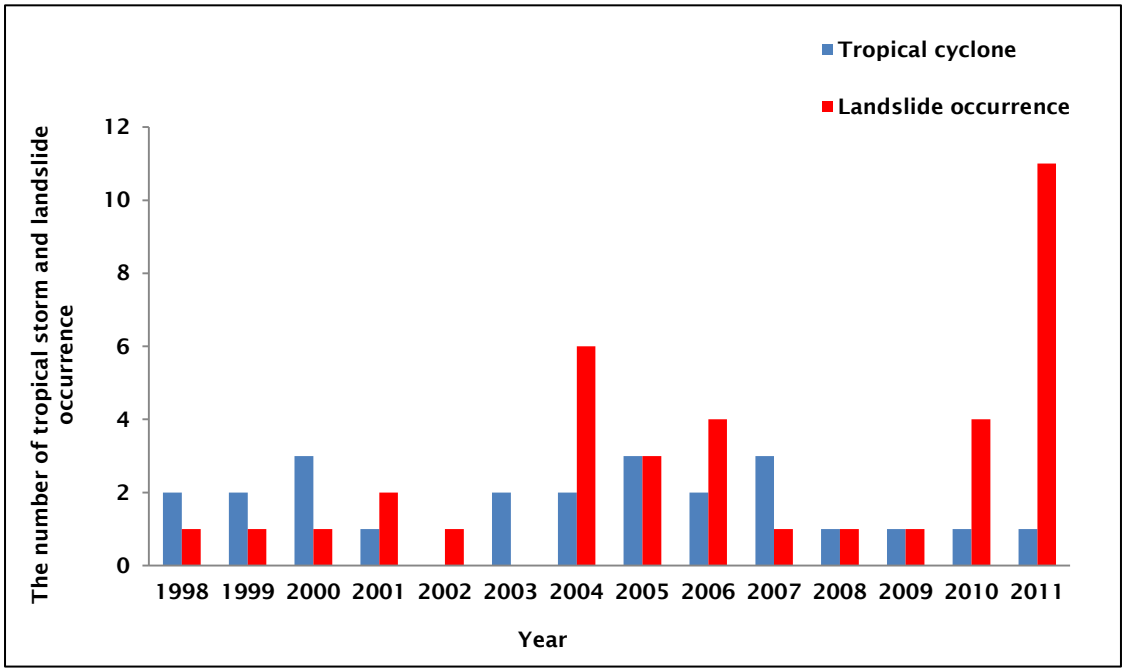

Figure 2.20 Annual tropical cyclones and major landslide occurrences during 1998-2011 (TMD, 2012c), (DMR, 2012)

2.2.6 The relationship between El Niño-southern oscillation (ENSO) and monsoon rainfall

The behaviour of El Niño is linked with the warm phase of the El Niño-Southern Oscillation (ENSO) in the central and the east-central equatorial Pacific. The relationship between ENSO and the monsoon is identified by the Oscillation. The Southern Oscillation (SO) originates from the exchange of air between the south-east Pacific subtropical anti-cyclone and the Indonesian equatorial low (Bhalme and Jadhav, 1984). The air pressure of the SO relates to the Walker circulation zone. The cold phase of ENSO is caused by La Niña, while the warm phase is caused by El Niño. The impact of the Oscillation relates to a strong or weak monsoon summer. The combination between a large enough spatial scale and a long enough timescale of the Southern Oscillation (SO) can define the suitable time of the Asian Summer Monsoon (ASM). The characteristic of the ASM links to the monsoon onset (Webster et al, 1998) and the inverse of the meridional temperature gradient in the upper troposphere in the southern part of the Tibetan Plateau. The existence of the cross-equatorial flow will become the monsoon jet stream which is associated with the contrast in surface friction across both land and sea of the Indian Ocean (Rodwell and Hoskins, 1995). Thus, in May, the cross-equatorial Somali jet stream occurs in the equatorial western Indian Ocean, it brings about a south-westerly flow associated with the monsoon over Southeast Asia (Ju and Slingo, 1995).

The warm phase (El Niño) is linked with a weakening of the Indian monsoon and leads to decreased rainfall, on the other hand the cold phase (La Niña) is linked with a strengthening of the Indian monsoon and leads to increased rainfall (Kripalani et al, 2007). Nounmusig et al., (2006) found that the annual and monthly precipitation decreased during El Niño in 1997 and in 1998, whereas the precipitation was higher than normal during La Niña in 1999, besides which, the rainy season also started early that year. Then, the relationship between the ENSO and rainfall was also studied in the central part of Thailand by Wikarmpapraharn et al., (2010) to analyse the monthly rainfall and the El Niño-Southern Oscillation (ENSO) in terms of the standardized precipitation index (SPI) and the strengths of ENSO by the Multivariate ENSO Index (MEI). In this study, the correlation between rainfall and ENSO focuses on four provinces in the central part: Kanchanaburi, Lop Buri, Nakhon Sawan and Suphan Buri. The regression model was used to analyse the correlation between the SPI and the MEI to show the ENSO condition that had

the effect of insufficient seasonal rainfall during the post rainy to the dry season period from November to April. In another study, the correlation between ENSO and Mekong is shown by Darby et al., (2013); ENSO is strongly associated with the Mekong river basin, which is near the north-eastern part of Thailand. Therefore, studying the relationship between the El Niño and the La Niña phenomena is associated with the observed annual precipitations in the north-eastern part of Thailand during May to October.

Singhrattna et al., (2005) present a statistical forecasting method for the summer monsoon rainfall in both the traditional linear regression and a local polynomial based nonparametric method. The large scale ocean atmospheric circulation variable is part of the El Niño/Southern Oscillation used to analyse this study during the August to October period. The relationship between the Indian summer monsoon and the El Niño/Southern Oscillation (ENSO) was strong during the post 1980 period leading to the prediction of rainfall in a couple of seasons. As a result, the dominant El Niño/Southern Oscillation (ENSO) and Indian summer monsoon are strongly implicated to predict the monsoon rainfall.

Inversely, the ENSO phenomena affects the monsoon variability, so both Indian Monsoon Rainfall (IMR) and ENSO are linked by the Kripalani (2007) study. The linkage between the ENSO phenomena and monsoon behaviour is defined by computing correlation coefficients (CCs) between monthly Sea Surface Temperature (SSTs) over the Nino three regions and summer monsoon rainfall. During the 1961-1980 period the observed CCs is -0.7, thus during the El Niño (La Niña) event, IMR is normal. During the 1981-2000 period, the weakening of the ENSO-monsoon teleconnection shows the peak correlation decrease to -2. The weakening of this relationship occurs during the monsoon period. As a result, the weakening of the ENSO-monsoon linkages in the warm world (Vecchi et al, 2006) present a weakening of the tropical Pacific Walker circulation because of anthropogenic forcing. The ENSO event may not affect the summer monsoon rainfall over south Asia.

2.3 Changes in rainfall pattern due to climate change

2.3.1 Introduction

Global warming, or the greenhouse effect, is linked to an increase in greenhouse gases (GHG) in the atmosphere. Industrial development and urbanization have

direct effects on the environment because of these gases released into the atmosphere i.e. carbon dioxide, carbon monoxide, sulphur dioxide and methane. The activities of humans are considered as the main factors causing global warming in each region of the earth, such as deforestation and fossil fuel burning. In the long term, global warming or greenhouse gases change will impact on a climate change phenomenon. As a result, it can bring about high temperatures in some regions which is divided into three parts: air temperature over land, air temperature over oceans and sea surface temperature. The trend of air temperature over land increased faster than over the ocean from 1860 until 2000 (Archer, 2010). For example, the temperature rose to 40C° in European countries such as France, Italy, The Netherlands, Portugal and Spain in 2003. Many people died in some areas of Europe due to this cause (Houghton, 2009). In terms of high temperature, it leads to the Earth warming and variable weather which impacts on human beings either directly or indirectly.

In the South Asian monsoon, for instance, the El Niño/Southern Oscillation (ENSO) directly affects monsoon rainfall and temperature change. During 1950-1999, the greenhouse gases and aerosols were rapidly released into the atmosphere causing warmer weather and increasing monsoon rainfall. Besides, the thermodynamic forcing leads to increased precipitation in South Asia as the atmospheric moisture content is higher over the Indian Ocean. Therefore, the variable monsoon rainfall is averaged by four models: mpi_echam5, gfdl_cm2_1, gfdl_cm2_0 and ens_mean, which is important for calculating uncertainty values and also to develop quality data and accuracy of modelling. In all India, the trends of monsoon rainfall in the summer period (June-September) are compared with different models over the twentieth century by simulating the pattern of spatial distribution, season and inter-annual monsoon rainfall trends (Turner et al., 2012).

Over the second half of the twentieth century, the change of monsoon rainfall has been linked with increased greenhouse gases and aerosol concentrations leading to the prediction modelled monsoon under equilibrium. The model uncertainty is considered and shows the linkage between temporal and spatial scales. Then, according to series A1B under increasing greenhouse gases concentrations, multi models can enhance rainfall data over some regions of South Asia, the rainfall data are compared to the all Indian Rainfall Index (AIR) during 1871-2008, India Meteorological Department (IMD) in daily data (1951-2004) and Climate Research

Unit (CRU) in monthly-gridded data for the 1901-2009 period. Modelling data shows the trend of rainfall over the western part of the North Pacific into the centre of the broader Asian monsoon eastwards. The result shows the AIR trend of rainfall declines in three-month periods from July until September, for 30 individual rainfall subdivisions over central and north western parts of India, hence the weakening of monsoon rainfall around 1950, as reported by CRU. The intensity of rainfall over the western part of the North Pacific and the centre is widely increased (Turner et al., 2012). The trend of rainfall decreased to moderate rainfall, while the increased intensity of monsoon rainfall under the model projection remains high. The overall annual rainfall is relatively low, while daily rainfall changes are high during the Asian monsoon.

In the middle of 2011, for example, the sea surface water temperature in the equatorial Pacific Ocean was close to normal values except in the west and east of the Pacific Ocean, which exhibited higher than normal values by approximately 0.5 degrees Celsius, while the surface temperature of the sea water from 100 to 300 m depth was higher than normal values. Overall, the temperature of the sea water was determined to be normal. Some adjustments of the climate systems still occurred accordingly with La Niña conditions, since the trade winds at 850 hPa covered the middle of the Southeast and the equatorial Pacific Ocean water.

The east side of the ocean is affected by the westerly wind, which was slightly stronger than normal at 200 hPa level in the central equatorial Pacific Ocean region. Whereas, the convection of mass of water in the tropical Pacific Ocean in the east of Indonesia continuously occurs due to this area accumulating a mass of warm water. Therefore, this area will be higher in temperature. The hot air will rise into the upper atmosphere, including adequately saturated moisture drifting up to be clouds and rain. Therefore, this situation leads to heavy rain during the rainy season. Furthermore, there are still factors that can contribute to tropical cyclones in the Pacific Ocean to the east of the Philippines. Consequently, the storm moves into the South China Sea through Vietnam and becomes the low pressure area over the upper part of northern Thailand. As a result of this storm insertion, heavy rainfall occurs. However, disorders have occurred continuously in both the ocean and the atmosphere since the beginning of 2011 (TMD, 2012a).

Apart from the above, the climate and weather anomalies have been brought about by an increase in rainfall, wind storms and tropical cyclones in several regions in the world leading to natural disasters, such as landslides and mudslides. Landslides and mudslides were reported in several areas in the northern and the north eastern parts in 2011 (TMD, 2011c).

The climate change phenomena requires a climate simulation scenario in forecasts. The prediction of future climate is achieved using General Circulation Models (GCMs), which have been developed by simulating future climate conditions at a global scale. The components of mass and energy flows are simulated under emission scenarios, which vary rainfall data, temperature, volume, volatility, vapour pressure and wind speed as defined by the Intergovernmental Panel on Climate Change (IPCC, 2007).

The regional or local climate change impacts can be downscaled for future climate scenarios at local scale in terms of topographic variables and extreme weather. Future climate scenario features can be based on various sources, such as simulations under climate models. Climate models by simulation are determined by the changes in Greenhouse Gas (GHG) emissions assumed in the model. The assumptions of variables of socioeconomic and technological developments can assist the changes in Green House Gas (GHG) emissions (IPCC, 2007).

2.3.2 IPCC simulation scenarios

The IPCC Special Report on Emissions Scenarios (SRES) (Nakicenovic et al., 2000) described a series of scenarios for future greenhouse gas emission named “SRES scenarios” which are used as the basis of climate simulation scenarios in this study. The storylines in the scenario assume four directions for future developments. They summarize a change of future characteristics such as population growth, economic development and technological change.

The IPCC SRES Scenarios (Special Report on Emission Scenarios): The SRES scenario set consists of four storylines for the 21st century. Each storyline assumes a definitely different way for future developments, SRES emissions scenarios consist of four distinct groups (A1, A2, B1 and B2) as follows (START, 2010):

a. A scenarios were developed to focus on the economy and A1 scenarios focus on development of international cooperation and technology transfer. A2 scenarios assume more regional cooperation.

The A1 scenarios storyline and simulation scenario delineates a very rapid economic growth of a future world, low population growth, and the rapid adoption of new and efficient technologies (START, 2010).

The underlying patterns are merged among regions, capacity building, and increased cultural and social interactions, with a concrete reduction in per capita income. The A1 simulation scenario is divided into four groups that describe the energy system in the directions of technological change. The A1 scenarios are of a more integrated world. The A1 scenario is characterized by:

- Rapid economic growth.
- A global population that reaches 9 billion in 2050 and then gradually declines.
- The quick spread of new and efficient technologies.
- A merged world - income and way of life converge between regions, social and cultural interactions worldwide.

The A2 storyline and simulation scenario delineates a very heterogeneous world. The underlying theme is preserved in local identities. Fertility themes among regional convergences are slow and there is a high population growth. Economic development is primarily regional in emphasis and per capita economic growth and technological changes are slower than in other storylines (START, 2010).

The A2 simulation scenario is characterized by:

- A world of independently operating, self-reliant nations.
- Continuous population growth.
- Regional economic development.
- Slower technological changes and developments per capita income.

b. B Scenarios is the one that conserves the environment and social sustainability

The B1 storyline and simulation scenario delineates a convergent world with the same low population growth as in the A1 storyline, but with rapid changes in economic structures through a service and an economy, with reductions in material use, and the initiative of clean and resource-efficient technologies. The oriented global solution is on economical, social, and environmental sustainability, including improved equity, but without additional climate initiatives (START, 2010).

The B1 scenarios are of an integrated world, and more ecologically friendly. The B1 scenarios are characterized by:

- Rapid economic growth the same as in A1, but with rapid changes through a service and an economy.
- Population increasing to 9 billion in 2050, after that decreasing as in A1.
- Reductions in material and the initiative of clean and preserved resource-efficient technologies.
- An importance placed on global solutions to economical, social and environmental balance.

The B2 storyline and simulation scenario explains that a world is oriented on local solutions to economical, social, and environmental sustainability. It is a moderate population growth, intermediate levels of economic development, and low rapid and more diverse technological change than in the B1 and A1 storylines. While the emphasis is on environmental protection and social equity, it focuses on local and regional levels (START, 2010).

The B2 scenarios are more ecologically friendly. The B2 scenarios are characterized by:

- Continuously rising population, but at a lower rate than in A2.
- Emphasis on local region rather than global solutions to economical, social and environmental balance.
- Intermediate levels of economic development.
- Lower, rapid and more fragmented technological change than in A1 and B1.

2.3.3 Climate change scenarios in high resolution at the local scale: downscaling

The effect of climate emissions on the global climate are addressed using global climate models (GCMs). GCMs delineate the physical elements and processes in the atmosphere, oceans and land surface that create the climate condition system. One drawback is that the GCMs scale is very coarse, normally a few hundred kilometres in resolution. In the study of climate change impact, finer scales of future climate model are needed. Downscaling, as used for global climate models, refers to a procedure in which global information on climate change or atmospheric composition is translated to a finer spatial scale in the local and regional impacts. Two general approaches are needed in downscaling (Wilby et al., 2007) as follows:

a. Dynamic downscaling (also called regional modelling), where a high resolution regional climate model (RCM) with a better representation of local terrain simulates climate over the region of interest. Downscaling techniques are divided into four main types: a) dynamical climate modelling, b) synoptic weather typing, c) stochastic weather generation, or d) transfer-function approaches. The techniques are briefly described below:

- Dynamical climate modelling

Dynamical downscaling computation, is the embedding of a higher resolution Regional Climate Model (RCM) in a coarser resolution GCM. RCMs are computationally demanding and RCMs can compute smaller-scale atmospheric conditions, such as orographic precipitation or low-level jets better than the host GCM. Additionally, RCMs can be used to explore the correlation between different external forces, such as terrestrial-ecosystem or atmospheric chemistry changes.

- Synoptic weather typing

Weather typing approaches involve the relationship between nesting local, meteorological data and widespread patterns of atmospheric circulation. Weather downscaling therefore links climate on the large scale and the local scale. Potentially, the limitation of precipitation changes are computed by the frequency of weather pattern changes and are displayed in the host GCM.

- Stochastic weather generators

Climate change scenarios are generated stochastically using revised parameter sets scaled in line with the outputs from a host GCM. The main advantage of the technique is that it reproduces many observed climate statistics and so is widely used, particularly for agricultural impact assessment. Additionally, stochastic weather generators provide an efficient production of scenarios for risk analysis.

- Transfer functions

The transfer function downscaling approach can summarize relationships between local scale predictors and regional scale predictors. The processes of predictor variable or statistical fitting are provided by the mathematical transfer function. The weather typing methods, transfer approach assume the precision of the model parameters within future climate conditions, and the sensitivity of downscaling is presented by predictor variables and the statistical framework.

b. Statistical downscaling (also called SDS), where large scale climate features are statistically related to coarse regional scenarios of climate change.

General Circulation Models (GCMs) describe increasing concentrations of greenhouse gases on both global climate and regional climate scales. Downscaling techniques are used to assess local climate change impacts, so an SDSM (Statistical Downscaling Model) will support the development of multiple, low-cost and single-site scenarios of daily surface weather variables under present and future climate systems. The tasks consider data quality, control and transformation, predictor variable pre-screening, automatic model calibration, basic diagnostic testing, statistical analyses and graphing of climate data. The UKSDSM, for example, performs daily predictor variables provided for model calibration and downscaling at sites over the UK (Wilby et al., 2007). The variables delineate the atmospheric circulation, thickness, stability and moisture content at several levels in the atmosphere, under climate conditions observed during the period 1961 to 1990. Equivalent predictor variables are provided for four GCM experiments of climate change between 1961 and 2099. In addition, the SDSM techniques are applied to regions other than the UK and may provide predictor variable regions (Wilby et al., 2007).

The source of model calibration is the National Centre for Environmental Prediction (NCEP) that re-analyse data set. The data are re-gridded by the grid system of HadCM3 and the basis of a Global Circulation Model (GCM), the impact of climate change (double carbon dioxide concentration) is presented for the mean summer climate of HadCM3. The surface temperature is considered in the warming across the whole of the Indo-Pacific sector. The land regions warm up more than the sea due to the large heat capacity of the water. It leads to a warming occurrence in the northern part of the hemisphere (Timmermann et al, 2004). Thus, the El Niño event leads to the warming in the equatorial Pacific Ocean, the east being warmer than the west. The correlation between warming and mean climate can reduce the equatorial temperature gradient zone, possibly leading to change in some monsoons. The increase in carbon dioxide is only 1% per year so that the warming of the El Niño event tends to suppress the increasing rainfall in Southeast Asia and other areas.

In particular, the influence of greenhouse forcing on the Asian summer monsoon presents increasing daily precipitation during the summer season. In India, for example, the HadCM3 model (double carbon dioxide) is examined. As a result, increasing precipitation occurs along the Indian west coast and the north Bay of Bengal, while it is dry in the north peninsular (Ashrit et al. 2003).

The HadCM3 model presents the largest of the El Niño (warming) in future climate scenarios. Indeed, artificial tuning of the scientific parameters is created for the HadCM3 model that is suitable for the ENSO presentation in the future (Collins et al, 2001). Thus, the HadCM3 model is selected for downscaling.

For example, the appropriate SDSM 4.2 software consists of seven core procedures, along with the UKSDSM data achievement and recommendation (Wilby et al., 2007)(Fig. 2.21).

- Quality control and data transformation

The simple quality control checks in SDSM are provided through the identification of initial data and errors, specification of missing data codes and outliers prior to model calibration. In some cases it may be appropriate to transform predictors and the predictand prior to model calibration. The transform facility enables and applies selected data files and transformations (e.g., logarithm, power, inverse, lag, binomial, etc).

- Screening of downscaling predictor variables

Both gridded predictors (such as mean sea level pressure) and single site predictands (such as station precipitation) are linked empirically to each other as the chief statistical downscaling methods. The main purpose of the Screen Variables section is to assess suitable downscaling predictor variables. The decision process is complicated in that the individual predictor variables change both spatially and temporally. Screen variables support the examination of seasonal variations in predictor values.

- Model calibration

The calibration model computes the parameters of multiple regression equations via an optimization algorithm and provides a particular predictand and a set of predictor variables (either dual simplex of ordinary least squares). The model structure identifies monthly weather, seasonal or annual trends and sub-models as required, the process is either unconditional or conditional. The unconditional models are the relationships between the predictors and the predictand (e.g., local wind speeds may be a function of regional airflow indices). In conditional models, the intermediate process has both regional forcing and local weather (e.g., local precipitation amounts depend on the occurrence of wet-days, which in turn depend on regional-scale predictors such as humidity and atmospheric pressure).

- Weather generator

The weather generator operation produces synthetic daily weather series and observed atmospheric predictor variables. The examination of calibrated models generates the synthesis of time series for current climate conditions. Synthetic time series are to detect specific output files for later statistical analysis, graphing and modelling impacts.

- Data analysis

SDSM provides the determination of both downscaled scenarios and observed climate data with the summary statistics and frequency analyses. Basic outputs are the sub-period, output file name and selected statistics. In addition, SDSM has a suite of diagnostics including monthly, seasonal and annual measures of dispersion, correlation and extremes series.

- Graphical analysis

Three sections for graphical analysis consist of the frequency analysis, comparison of results, and time series analysis. The frequency analysis plots extreme value statistics of the selected data files. The comparison supports plots of monthly statistics produced by the summary statistics. Either bar or line charts may be chosen for display purposes. The graphs show the comparison of two data sets and the assessment of downscale, observed, or presented with the future climate scenarios. The time series analysis produces time series plots for up to five variables. The data can be analysed as monthly, seasonal, annual or water year periods for statistics such as Sum, Mean, Maximum, Winter/Summer ratios, partial duration series, percentiles and standardized precipitation index.

- Scenario generation

The scenario generator supports the daily weather series for atmospheric predictor variables produced by a climate model (both present and future climate experiments), rather than observed predictors. The input files are either the weather generator or scenario generator options, but are not the same length as those used to obtain the model weights during the calibration phase.

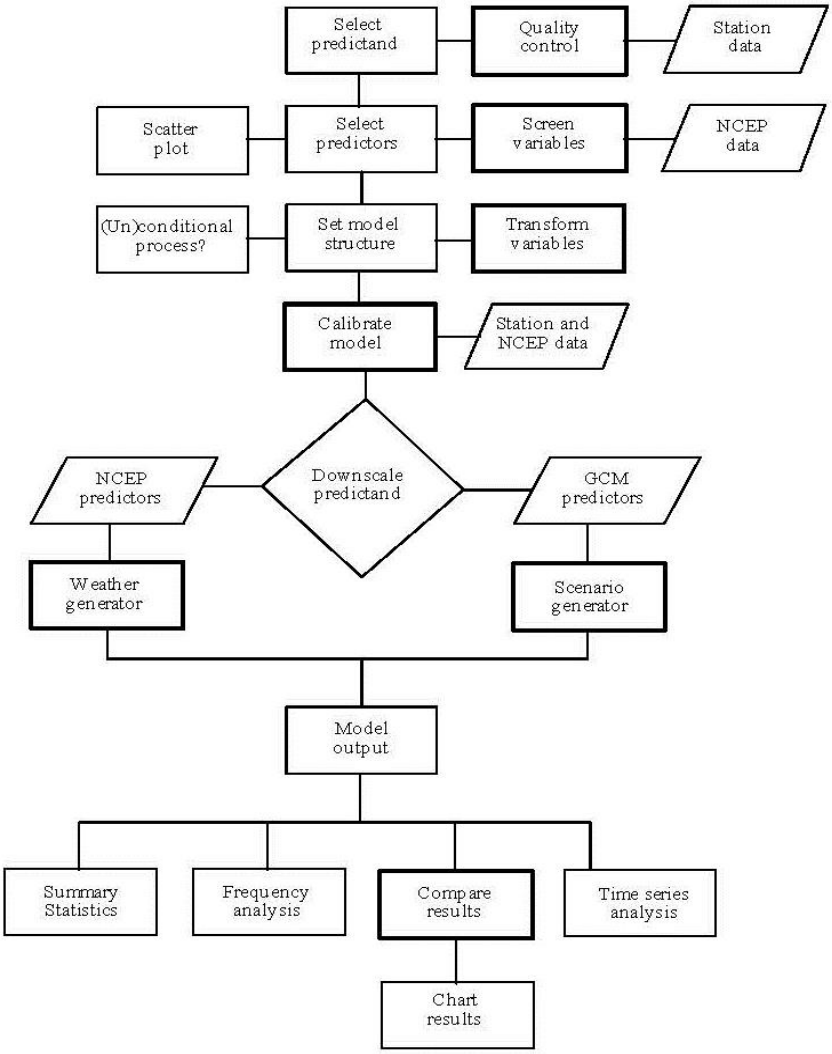

Figure 2.21 SDSM Version 4.2 climate scenario generation

These two approaches can be used in isolation or to complement each other. Therefore, the fundamental concept of statistical downscaling is that local climate condition is linked both by large-scale climate and by local physical features. Both large-scale patterns of climate elements (predictors) and local climate (the predictand) are linked by the statistical downscaling technique, and applied to the output from global or regional models. Climate change scenarios, which are based on mathematical model simulations, may differ among scenarios depending on how greenhouse gases affect the atmospheric condition.

The spatial distribution of future climate change under upper and lower simulation of greenhouse gas scenario, SRES A2 and B2 scenarios, is calculated using simulation PRECIS (Providing Regional Climates for Impacts Studies), a

regional climate model and uses the Global Circulation Model (GCM) ECHAM4 dataset as original data for calculation (Wilby et al., 2007).

2.3.4 The regional climate model in Thailand

The climate change data in Southeast Asia are assessed by the Southeast Asia START Regional Centre which is supported by the Hadley Centre, especially the precision of software, PRECIS and GCM datasets downscale in a regional climate model (START, 2012). The future climate system for mainland Southeast Asia is the future climate simulation at high resolution at a grid size of 20x20 km. and within a baseline during the years 1960 to 1999, which can be used for comparison, and the future period covers the years 2010 – 2099. (START provides precipitation forecasts for the years 2010 – 2099.)

Thus a climate scenario is developed based on simulation by PRECIS (providing regional climates for impacts studies) regional climate model, and using Global Circulation Model (GCM) ECHAM4 datasets as initial data for calculation. The simulations are summarized by the Intergovernmental Panel on Climate Change (IPCC) as emission scenarios A2 and B2. The result of the simulation operation presents the high resolution future climate projection in Thailand and neighbouring countries through to the end of the century. The PRECIS model uses the rescaling technique to process the final results with the observed weather data. Finally, the results of the future climate projections predict the trend of temperature, annual precipitation and wind speed in several regions in Thailand.

The assessment of climate change is only for a few decades, especially driven by precipitation data in order to consider the pattern of climate change on average. The accuracy of atmospheric greenhouse gas levels in the future, either modelled globally or regionally are calculated using uncertainty values under various climate simulation scenarios for planning. The annual rainfall volumes are presented for climate simulation scenarios A2 and B2, for example, in Uttaradit province during 2013 – 2099. The rainfall is a negligible fluctuation in both climate simulation scenario A2 and B2, while the rainfall of scenario A2 is higher than B2 as given in Fig. 2.22 and Fig. 2.23. In the first assessment report of the IPCC, the scenarios of atmospheric composition and climate change were prepared by atmospheric and climate scientists for scenario simulations. Hence, the environmental and social sustainability of climate scenario simulation B2 is

better than A2. These two climate scenario simulations are reported by IPCC (2007).

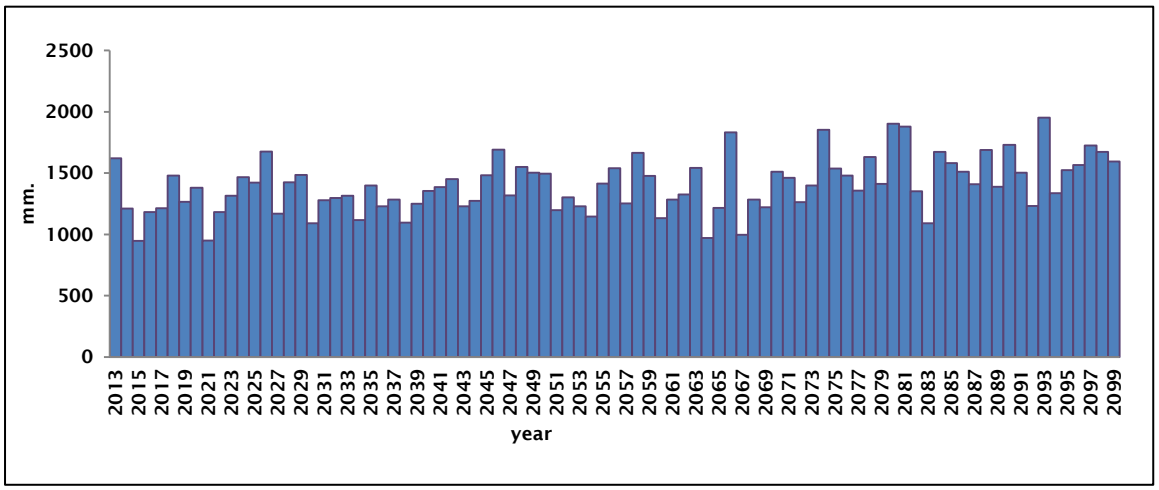

Figure 2.22 Predicted annual rainfall in Uttaradit province by scenario A2 during 2013 - 2099 (START, 2012)

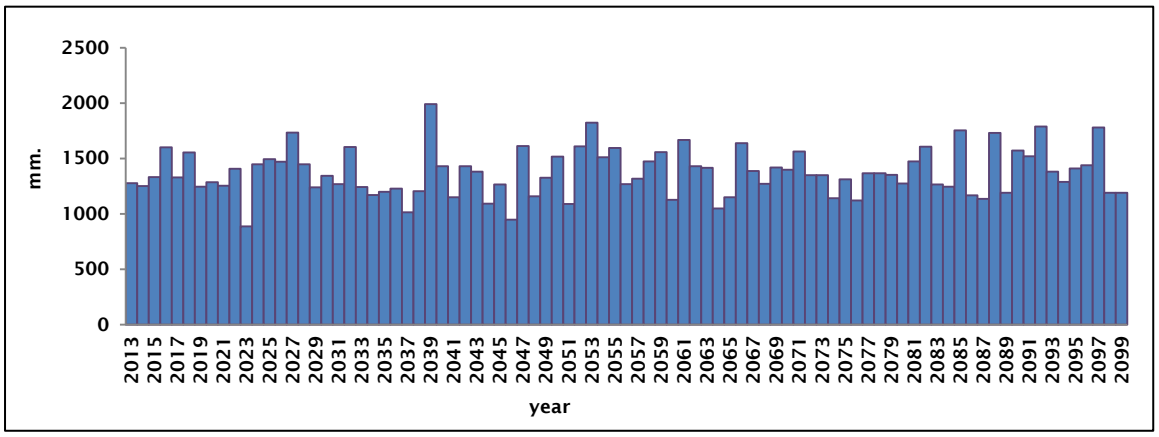

Figure 2.23 Predicted annual rainfall in Uttaradit province by scenario B2 during 2013 – 2099 (START, 2012)

Then, during the 1961-2099 period, the observed daily rainfall is provided by the rainfall processes of climate change, shown by the linkage between a Global Circulation Model (GCM) and the local rainfall by a Statistical Downscaling Model (SDSM) for three river basins: Mekong, Chi and Mun in Thailand. During 1961-2007, the observed daily rainfall covering eleven rain stations are computed. The rainfall data are presented for the 1961-1990 and 1991-2007 period, so the results of rainfall data for two periods are different in different locations in three river basins. For instance, an increase of annual maximum number of consecutive dry days (CCD) occurred in the Chi and the eastern part of the Mun basins. In this study, the basic statistical and physical features of observed rainfall procedure for calibration (1961-1975) and validation (1976-1990) are described by SDSM

technique. The statistical downscaling method forecasts the rainfall data from 1961-2099 under simulation scenario A2 and B2 by UK HadCM3 (HadCM3) model and the Canadian GCM3 (CGCM3) model. The results of these two models are different, while high uncertainty of simulation climate is obtained by the GCM3 (CGCM3) model. Thus, the HadCM3 model is chosen for local prediction (Artlert et al, 2013).

2.3.5 The relationship between climate and precipitation in Thailand

At the present time, climate change is having major influences around the world, especially producing abnormal precipitation. In several regions of the world, precipitation has increased rapidly, whereas others have become more arid, for instance, the temperature rise to 40C° in several European countries such as France, Italy, Netherlands, Portugal and Spain in 2003 (Houghton, 2009). Furthermore, the El Niño and La Niña phenomena have resulted (IPCC, 2007) in storm tracks and monsoon changes for the long term, leading to temperature and precipitation anomalies. The IPCC (2012) confirms the increase of extreme weather and rainfall intensity and runoff amount in high latitude and hilly terrain, which has an implication for landslide hazard. Maijandee (2014) presents the rainfall indices will be wetter in the rainy season and rainfall will be intense in dry the season in northern, western and north-eastern parts. Besides, the number of rainy days is higher and more scattered in central and north-eastern parts in the future climate.

In studying the relationship between warmer climate and precipitation, Archer (2010) indicates that the precipitation increases in widely spread regions because the increased air temperature leads to increased moisture in the atmosphere generally. Also, as evaporation has increased, greenhouse gases have affected precipitation over large areas. Therefore, the total amounts of heavy precipitation events have been observed to be widely spread.

Precipitation is also dependent on atmospheric circulation patterns which are caused by El Niño -Southern Oscillation, (ENSO) and other patterns of variability. The relationship between the atmospheric circulation change and climate change can still shift the storm track and the tropical sea-surface temperature patterns. El Niño-Southern Oscillation is an ocean-atmosphere phenomenon and involves warming of tropical surface water which is linked with ocean circulation. The Southern Oscillation leads to changes of the trade winds, which affect tropical

precipitation. Despite the fact that the global atmospheric circulation depends on the pattern of variability, this circulation is also associated with regional climate in each location in terms of storm track, poleward fluxes of heat, moisture and momentum. Furthermore, there are seasonal and longer time-scale effects associated with flooding, drought occurrence and other disasters (IPCC, 2007).

Jutakorn (2010) examines the beginning and end dates of the rainy season in Thailand during a normal weather year compared with the phenomena of El Niño and La Niña in each year by daily rainfall data across Thailand from the past to 2010. The beginning and end of the rainy season in years with normal climate are determined by correlation analysis. During the El Niño and La Niña period, the principles of time series are used to analyse the conditions of continuous rainfall for at least 5 days and at least 10 mm for cumulative rainfall. The beginning and end dates of the rainy season are different in each region of Thailand. During a La Niña year, the start date of the rainy season is earlier than in a normal year and the end date of the rainy season is later than in a normal year in several regions of Thailand. On the other hand, during an El Niño year, the starting date of the rainy season is later than in a normal year and the ending date of the rainy season is earlier than in a normal year. Therefore, during an El Niño and La Niña year, in the rainy season, the starting date of rainfall originate from the south-west, which slightly moves to the eastern part, the south-eastern, the north, the north-eastern and the central parts of Thailand respectively, while the beginning date of the rainy season in the central of north-eastern part is later than other parts.

2.3.6 The situation of ENSO in the present-day in Thailand

In February 2012, sea surface water temperature in the equatorial Pacific Ocean was lower than normal values by approximately 0.5-1.0 degrees Celsius, while in the west and the east of the Pacific Ocean temperature was higher than normal values by approximately 0.5-1.0 degrees Celsius. The surface temperature of the semi-deep sea water from 100 to 300 metres was higher than normal values. Overall, the temperature of sea water was determined to be normal. The trade winds at 850 hPa were stronger over the middle and the west of the Pacific in the equatorial Pacific Ocean. In the east side of the ocean, the westerly wind was rapidly stronger than normal values at 200 hPa level. The westerly stronger winds affected the central equatorial Pacific Ocean region, while, the

characteristic of air circulating counter clockwise in the Northern Hemisphere and the winds circulating clockwise in the Southern Hemisphere due to disorders of the atmosphere and the ocean, indicate the condition of La Niña reducing and becoming normal during March to May. As a result, heavy rainfall occurrences increased during the summer (March-April) however, the rainy season was otherwise normal that year (TMD, 2012d).

2.4 Landslides

2.4.1 Introduction

Landslides frequently occur on foothills and slopes and form and spread into the underlying bedrock as well as within various soil types. The causes of landslides are divided into three categories: 1) water, 2) seismic activity and 3) volcanic activity. Landslides can also be affected by soil type, soil moisture content, slope orientation, as well as slope angle. Saturated soils on slopes are therefore an important cause of landslides following intense rainfall, snowmelt, abnormal ground water level and changed surface water levels. Translational earth and rock slides are most common, with deep-seated rotation slides being uncommon. Debris flows and mud flows are common types of landslides and always occur in steep stream channels where additional water is incorporated into the sediment mass. The cause of landslides can basically be divided into two categories: natural and human induced (DMR, 2011a).

2.4.2 Type of landslides

The characteristics of landslide types can be identified on the basis of efficiency of movement. The movement of material depends on speed, volume of displacement and distance of run-out. Therefore, various material types are separated by rock types and soil types, while the type of movement depends on the landslide mass, such as fall, topple, slide, flow and spread (Table 2.1- Table 2.2 and Fig 2.24). Landslide movement types are classified as follows (USGS, 2004):

a. **Fall:** The mass movement of rock or earth, or both, falling abruptly down a steep slope along a surface until the terrain flattens. Falls are affected by gravity and movement is free with bouncing and rolling.

b. Topple: Toppling involves the forward rotation of rock down a slope as a unit or units around an axis below. The weight of material upslope is affected by gravity and the forces of fluids in cracks. The velocity may be extremely slow to rapid, depending on the distance of movement.

c. Flow: The movement of shear surfaces is continuous over a short space. The fundamental velocities of the displacing mass-flow is like a sticky liquid. The form changes from a slide to a flow depending on the composition and progress of water and mobility. Flows are divided into five basic types with fundamental differences.

- **Debris flow:** The pattern of movement of loose rock, soil and organic matter with water in large quantities flowing downwards. Debris flows are usually caused by intense surface-water flow, due to heavy or rapid rainfall, including the erosion of soil or rock on steep slopes. The velocity of rotational and translational slides, which consist of mass, causes loss of cohesion and water accumulation leads to debris flow. Sometimes, this causes loss of life due to rapid movements without warning. Debris flows occurs all over the world, especially in deforested areas and on slopes created by wildfires or clear-cutting. This form of flow occurs in both deep and long narrow channels and it is intense when occurring on a slope (USGS, 2004).

- **Debris avalanche:** The rapid to extremely rapid flow of debris.

- **Earth flow:** A characteristic of earth flow is its "hourglass" shape. It involves the mass movement of liquid down a slope, with a bowl shape at the head. Fine-grained materials, or clay-bearing rocks, usually expand and flow on moderate slopes and under saturated conditions. Sometimes, the flows of granular dry material will occur.

- **Mud flow:** A mud flow consists of at least 50 percentage sand material and clay-sized particles that are wet enough to flow rapidly. "Mud slides" is a variant name for mud flows and debris flows.

- **Creep:** Soil or rock flows slowly and steadily downwards because internal shear stress creates permanent deformity, which is, however, inadequate to create shear failure. Creep is divided into three types: (1) soil moisture content and soil temperature affect movement within the depth of the soil owing to seasonal

changes. (2) Shear stress continuously exceeds the strength of the material; and (3) slopes usually reach the point of failure as other types of mass movements. Creep is demonstrated by curved tree trunks, bent fences or retaining walls, tilted poles or fences, and small soil ripples or ridges.

d. Spread: The movement of soil or rock or both associated with the subsidence of the fractured mass expanding into liquid in the case of liquefaction spreads. Lateral spread always occurs on a slope or flat terrain in the stronger upper layer of rock and soil expands and moves above the soft layer. The expansion is separated into several layers. The fractures and expansion displace slowly, which leads to a stable layer covering a soft layer. In the spread, the stable layer covers a weak underlying unit through liquid flows. Sometimes, spreads occur in earthquake regions. The velocity may be slow to moderate, and with triggering mechanisms, the travel will be rapid (USGS, 2004).

<table>
<tr><td colspan="2" rowspan="3">Type of Movement</td><td colspan="3">Type of Material</td></tr>
<tr><td rowspan="2">Bedrock</td><td colspan="2">Soil</td></tr>
<tr><td>Predominantly coarse</td><td>Predominantly fine</td></tr>
<tr><td colspan="2">FALLS</td><td>Rock fall</td><td>Debris fall</td><td>Earth fall</td></tr>
<tr><td colspan="2">TOPPLES</td><td>Rock topple</td><td>Debris topple</td><td>Earth topple</td></tr>
<tr><td rowspan="2">SLIDES</td><td>ROTATIONAL</td><td rowspan="2">Rock slide</td><td rowspan="2">Debris slide</td><td rowspan="2">Earth slide</td></tr>
<tr><td>TRANSLATIONAL</td></tr>
<tr><td colspan="2">LATERAL SPREADS</td><td>Rock spread</td><td>Debris spread</td><td>Earth spread</td></tr>
<tr><td colspan="2" rowspan="2">FLOWS</td><td>Rock flow</td><td>Debris flow</td><td>Earth flow</td></tr>
<tr><td>(deep creep)</td><td colspan="2">(soil creep)</td></tr>
<tr><td colspan="2">COMPLEX</td><td colspan="3">Combination of two or more principal types of movement</td></tr>
</table>

Table 2.1 Types of movement and material (USGS, 2004)

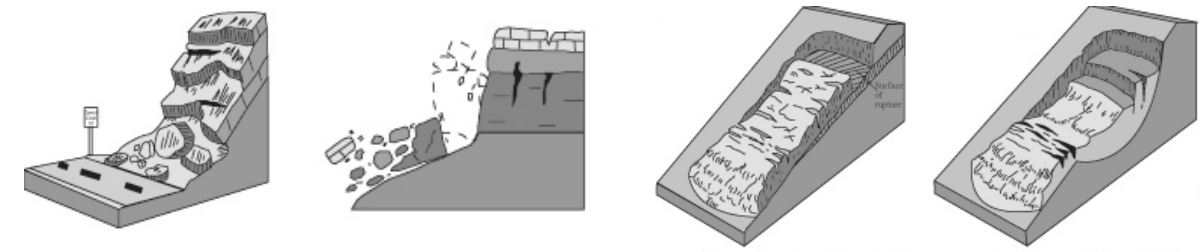

Rock fall Topple Rotational slide Translational slide

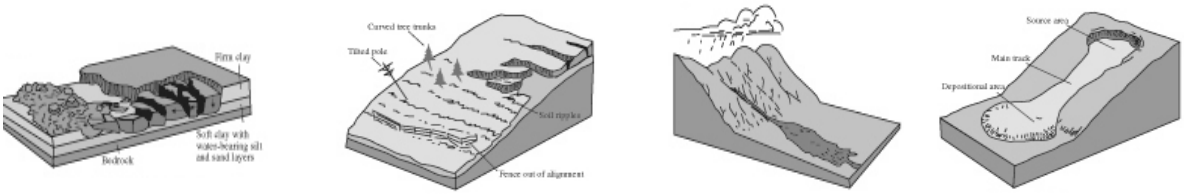

Lateral spread Creep Debris flow Earth flow

Figure 2.24 Movement and material types (USGS, 2004)

e. Slide: The movement of soils or rocks or both which with surface rupture or shear move downwards into large areas. The slope gradient ranges from about 20 to 40 degrees and the depth-to-length ratio from 0.3 to 0.1. The velocity is slow at first and then becomes more rapid, ranging from less than 0.31 metres every 5 years to 1.55 metres per month. Slides are caused by intense rainfall, which causes increased groundwater levels and saturation of the slope within the mass. In addition, slides are divided into two types: rotational slides and translational slides.

- Rotational slides

This involves the downward and upward rotation of rock or soil, or result in a curvilinear failure plane that does not parallel the slope contour. Rotational slides often occur in homogeneous material which slides down slopes of between 20 to 40 degrees with a depth-to-length ratio of 0.3 to 0.1. Intense rainfall leads to saturated slopes and raised groundwater levels in the mass, causing erosion of the slope (USGS, 2004) (Fig. 2.25).

Figure 2.25 Rotational landslide (USGS, 2004)

- Translational slide

The mass slides downwards and outwards along a roughly planar surface with little rotation or backward tilting. This is in contrast to rotational slides in that the material in translational slides fails along joints, bedding surface, or between the soil and rock. Transitional landslides frequently occur and are often shallow, occurring in the regolith with the bedrock surface acting as the failure plane. The failure surface may cover many kilometres and the velocity may be extremely moderate to rapid (1.8 m/hr) (USGS, 2004). In 2006, the past landslide occurrence was found in transitional slide form in Laplea district in Uttaradit province (Tepparnich et al, 2010). This landslide occurred between about 0.5 and 1 metre deep. The slope gradient is approximately 25°, 45° and 60°, which is representative of hilly and mountainous areas in Uttaradit province (Jotisankasa et al, 2008).

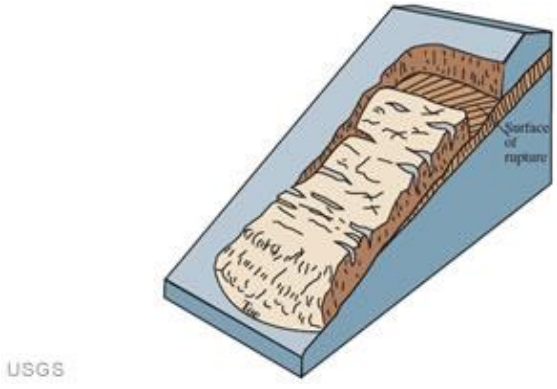

Figure 2.26 Translational landslide (USGS, 2004)

Landslide inventory are general classified on material type, movement type and movement rate in Table 2.2.

Landslide inventory	Description
Rock-fall	The mass movement of rock or earth, or both, falling abruptly down a steep slope along a surface until the terrain flattens. Falls are affected by gravity and movement is free with bouncing and rolling.
Topples	Toppling involves the forward rotation of rock down a slope as a unit or units around an axis below. The weight of material upslope is affected by gravity and the forces of fluids in cracks. The velocity may be extremely slow to rapid, depending on the distance of movement.
Debris flow	The pattern of movement of loose rock, soil and organic matter with water in large quantities flowing downwards. Debris flows are usually caused by intense surface-water flow, due to heavy or rapid rainfall, including the erosion of soil or rock on steep slopes.
Flow-slide	The movement of soils or rocks or both which with surface rupture or shear move downwards into large areas. The slope gradient ranges from about 20 to 40 degrees and the depth-to-length ratio from 0.3 to 0.1. Slides are caused by intense rainfall, that sand material and clay-sized particles that are wet enough to flow rapidly.
Soil-creep	Soil or rock flows slowly and steadily downwards because internal shear stress creates permanent deformity, which is, however, inadequate to create shear failure. Creep is divided into three types: (1) soil moisture content and soil temperature affect movement within the depth of the soil owing to seasonal changes. (2) Shear stress continuously exceeds the strength of the material; and (3) slopes usually reach the point of failure as other types of mass movements. Creep is demonstrated by curved tree trunks, bent fences or retaining walls, tilted poles or fences, and small soil ripples or ridges.
Rotational landslides	Rotational slides often occur in homogeneous material which slides down slopes of between 20 to 40 degrees with a depth-to-length ratio of 0.3 to 0.1. Intense rainfall leads to saturated slopes and raised groundwater levels in the mass, causing erosion of the slope
Translational landslide	Transitional landslides frequently occur and are often shallow, occurring in the regolith with the bedrock surface acting as the failure plane. The failure surface may cover many kilometres and the velocity may be extremely moderate to rapid (1.8 m/hr)

Table 2.2 Description of landslide inventory

2.4.3 The main factors affecting landslides in Thailand (DWR, 2010)

a. Slope: Slope affects the stability of soil. Moreover, the gradient of a slope has an effect on the probability of landslide occurrences. Slope gradient stabilities are divided into five levels: more than 70% (> 35°), 50-70% (26.7° -35°), 30-50% (16.7° -26.7°), 15-30% (8.5° -16.7°) and 0-15% (< 8.5°) (DWR, 2010). In addition, the slope angle and soil moisture are important factors for landslides during intense rainfall. The amount of rainfall together with the slope gradient is the main cause. The infiltration of rainwater and the soil slope area linked to the mechanisms of the landslide. The pore water pressure may affect the full soil thickness, which can be fully or nearly saturated. Then, this saturation of the soil slope reduces the shear strength of the soil and destabilizes the slope. The slope failure generally presents when the wetting front moves to the bottom of the soil slope, the change of the pore water pressure might act to destabilize the slope (Jotisankasa et al, 2008).

b. Soil types: Different soil types have different structural properties. The simulation of shear strength loss in residual soils affects soil stability which is affected by rainfall intensity owing to increasing moisture content. Moreover, soil type affects the potential for a landslide occurrence. Residual soil is classified into four types: granite, mudstone, shale and sandstone (mudstone), which are found in Uttaradit province (DWR, 2010).

c. Soil thickness: The potential for landslide occurrence is affected by soil thickness which can be divided into four levels: 0-0.5 metre, 0.6-2.0 metre, 2.1-4.0 metre and > 4 metre. The greater the soil thickness, the higher the potential for a landslide to occur (DWR, 2010).

d. Geology: The rock type indicates the geological conditions affecting the potential for a landslide to occur. The different rock types affect the decay properties of the weather layer which leads to reduced soil strength. The rock types in the study related to landslide hazard are divided into eight groups: Carboniferous-Permian granite, Jurassic-Cretaceous granite, Jurassic granite, Volcanic rock, Sedimentary rock (sandstone and mudstone), Metamorphic rock, Quaternary sediment and Limestone (Soralump et al, 2009).

The Geotechnical Engineering Research and Development Centre (GERD) proposed that the susceptible landslide areas are analysed by Unsaturated Soil

and Infinite Slope Stability theories in terms of the geotechnical engineering properties. The saturated soil condition can be identified by the behaviour of the shear strength due to increasing rainfall. The geological maps of Thailand are based on the scale of 1: 250,000 by the Department of Mineral Resources, and are then classified into eleven groups. Eight of the eleven geological groups are assigned into categories by the potential susceptibility to landslides. These groups are Granite Rock, Extrusive and Mafic Igneous Rocks, Predominantly Sandstone and Siltstone, Predominantly Shale and Mudstone, Interbedded Sedimentary Rocks, Metamorphic Rock, Carbonate Rock and Quaternary deposits. The percentages of recorded landslide events in each geological group are 11.45%, 4.23%, 10.25%, 3.05%, 22.69%, 8.28%, 7.71% and 32.34% respectively (Soralump et al, 2009).

e. Land use: This factor affects the occurrences of landslides in terms of soil surface cover. The probability of a landslide is high due to deforestation, which implies a root cohesion effect is lost, and in some agricultural areas after heavy rainfall. The soil quickly becomes saturated and on a slope can easily result in a landslide (DWR, 2010).

The vegetation type conditions were investigated by direct field observation in Thailand. The vegetation types are important for mass movement protection. In hill areas, there are primary natural forests, slash-and-burn agriculture, rubber plantations, orchards and bare lands. Therefore, the vegetation types are linked with the landslide distributions. The root size of common species differs according to slope conditions, including cliff surfaces and landslide scars (Nilaweera et al, 1994).

f. Rainfall: The volume of rainfall is one factor that directly affects with the occurrence of landslides, especially heavy rainfall. In many cases, landslides occur in areas where there are tropical cyclones and monsoons, so rainfall trends are a good indication of future landslide potential.

Finally, the rainfall amount is a significant factor, as well as the slope gradient, vegetation, and characteristic of the soil, due to the infiltration of rainwater and the soil slope related to the mechanisms of the landslide. Approximately 100 to 300 mm of past rainfall was recorded to initiate localized slope failure in Thailand (DMR, 2004). The antecedent rainfall and soil moisture conditions affect landslide occurrences (Crozier et al, 1980). After the accumulated rainfall increase, the soil

water content and pore water pressure increase. The saturation of soil slope will decrease the shear strength of soil. Then, approximately 90-95% of saturated slope can cause a progressive failure of the slope (Soralump et al, 2007).

2.4.4 Landslide model

Soil characteristics are a factor in landslide conditions affected by the environment and geology. In studying the relationship between ten landslide condition factors and the Adaptive Neuro-Fuzzy Inference System (ANFIS) models, Bui (2012) found that slope, aspect, curvature, lithology, land use, soil type, rainfall, distance to road, distance to river and distance to faults are associated with adaptive neuro-fuzzy inference system (ANFIS) models used to assess landslide susceptibility maps in the Hoa Binh province of Vietnam. The maps portrayed five susceptibility zones; very high, high, moderate, low and very low. The final results of this study, are shown in terms of susceptibility maps.

The observations of Guimarães (2003), on landslide areas of hill slopes are assessed using the SHALSTAB mapping model. The relationship between hydrological and the slope stability model is based on a digital elevation model (DEM). Furthermore, soil properties are the main parameters to be demonstrated for susceptible zones of shallow landslide using the SHALSTAB model. In the same manner, Bellugi (2011) concluded that the corresponding shallow landslide susceptibility can be assessed using SHALSTAB with accurate the precipitation predictions.

The above literature review reveals that the effect of various key landslide factors on models has been an issue in the use of models for predicting landslides for decades.

2.4.5 Case study of landslide occurrences in Thailand

In recent years, the occurrence of landslides has increased in Thailand, especially in the high and elevated hill areas. The northern mountain areas of Thailand are one region which is heavily affected by landslides. In most cases, heavy rainfall during rainstorms led to the landslides. In particular, several parts of Thailand were affected by the southwest monsoon and tropical cyclones. Most of the rain flows on the surface of the soil into the rivers and, as a result of increased moisture and saturated soils, landslides and flash floods occur, especially on high

angle slopes with thick layers of soil. The moisture and water in the soils on the slopes are moved by gravity as the soil reaches saturation point during heavy rain and groundwater levels on the hillside increase (DWR, 2010).

During heavy rainfall, the increase in the groundwater level leads to erosion or slippage on slopes, while the internal pressure of the soils is high, and the mass increases as water runs into the air space. Often the erosion, or slippage, of soil on the hillside occurs at the interface between the sedimentary rock layers. In the case of Thailand, soil creep occurs over slopes during heavy rainfall, leading to landslides. In Nakhon Si Thammarat province in the southern part of Thailand, for instance, landslides often occur in the mountains, which consist of sandy soil on the surface and granite below. Therefore, during heavy rainfall, the soil becomes saturated with water, with the loss of strength of the soil and subsequent erosion, (including increased groundwater levels) (Fig. 2.27).

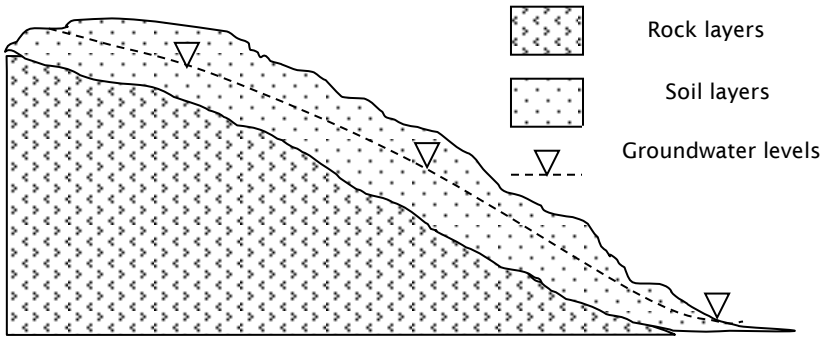

Figure 2.27 Rock and soil layers (DWR, 2010)

Jotisankasa (2008) discovered that the rainfall induced landslide is linked to the change of soil moisture and slope failure in hilly and mountainous areas, consequently landslides occurred during intense rainfall. Soil characteristics are investigated in terms of low plasticity, such as ML (silt with a low liquid limit), SM (Sand and Silt) and CL (clay with a low liquid limit) in debris flow areas in Thailand. The slope stability and slope failure are calculated by the infiltration model and the soil water characteristic curve. The movement of the soil water characteristic curve can identify the water content suction, the saturation level, shear strength variation and the permeability function. In this study, the top surface of soil is considered representative for suction measurement. The wetted soil properties depend on incident rainfall, therefore the soil water characteristic curves are used to estimate the rainfall induced and slope saturation. As a result,

the suction measurement and monitored pore water pressures can indicate the real time changes in the safety factor providing an early warning system.

2.5 The threshold value of rainfall for the initiation of cause landslides in Thailand

2.5.1 Introduction

The climate change problems have been affecting global communities, causing heavier rainfall, severe landslides, floods or longer consecutive dry days causing severe drought. Thailand also suffers from the effects of climate change, landslides cause severe damage including loss of life and properties and economic damage. Landslides occur in several regions in the southern and northern parts of Thailand, during the rainy season (DMR, 2011a).

In Fig. 2.28, are shown the number of landslide occurrences yearly in Thailand during 1988 to 2011, whilst Fig. 2.29 represents regions of Thailand and Fig. 2.30 shows landslide occurrences monthly in the same period of time. Overall it can be seen that the trend of landslide occurrences is related to threshold rainfall, but it does not depend on spatial location.

In Fig. 2.28, the number of landslide occurrences was around eleven in 2011 and around six in 2004 respectively while it was just under four in other years. Local anecdotal statements link the rainfall volumes as the main cause of landslide occurrences. In Fig. 2.29, landslide occurrences were high in the northern and the south eastern parts of Thailand; around fifteen and fourteen during 1988 to 2011, while the southwest experienced over six because of high rainfall values in this region. In Fig. 2.30, the total landslide occurrences were high in March: around eight in 2011. It was the same as November in all three years; there was around one event in 2003, two events in 2004 and approximately five events in 2010. There were around seven events in May and in August during the monsoon. Landslide occurrences have never been recorded in the four months of January, February, April and June.

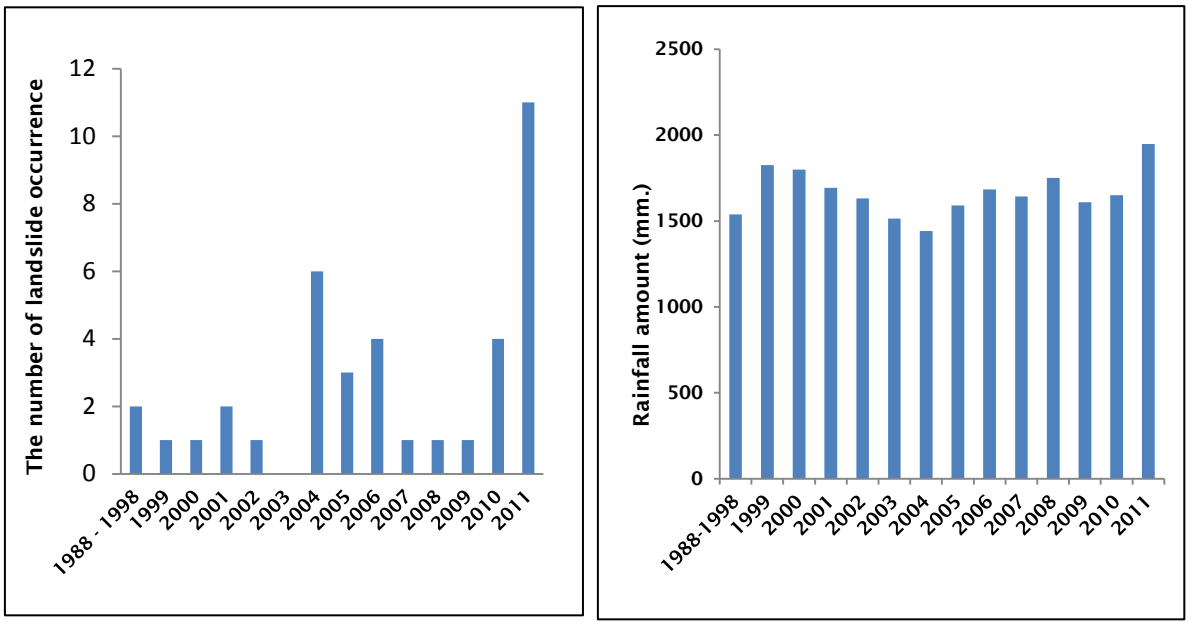

Figure 2.28 The chart of landslide occurrences (DMR, 2012) and rainfall amount (TMD, 2012b) during 1988-2011

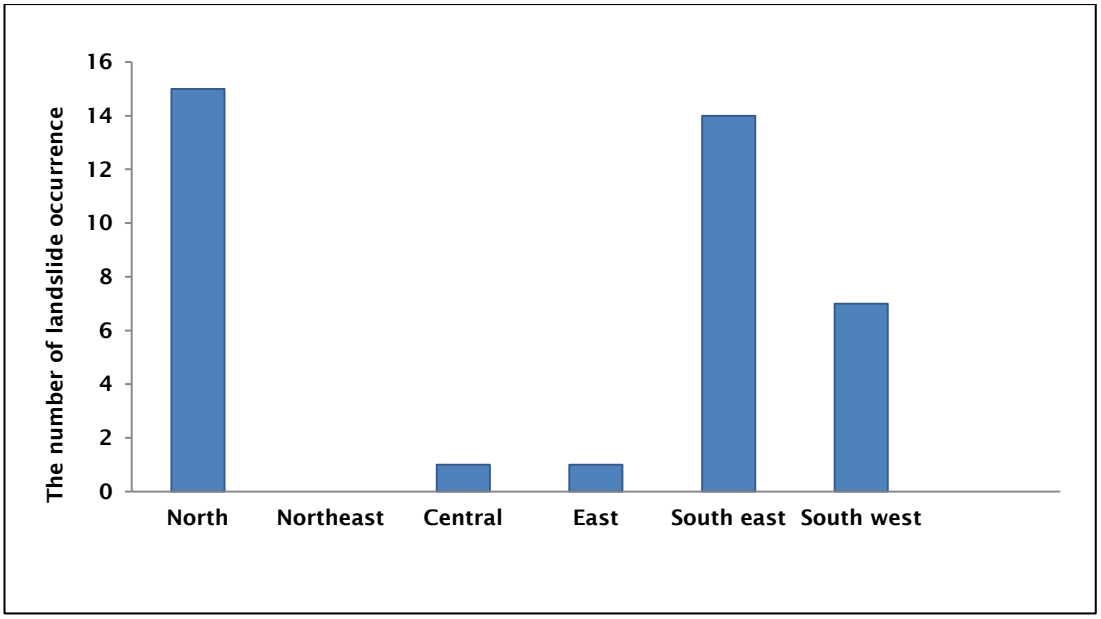

Figure 2.29 The chart of landslide occurrences in six regions (DMR, 2012)

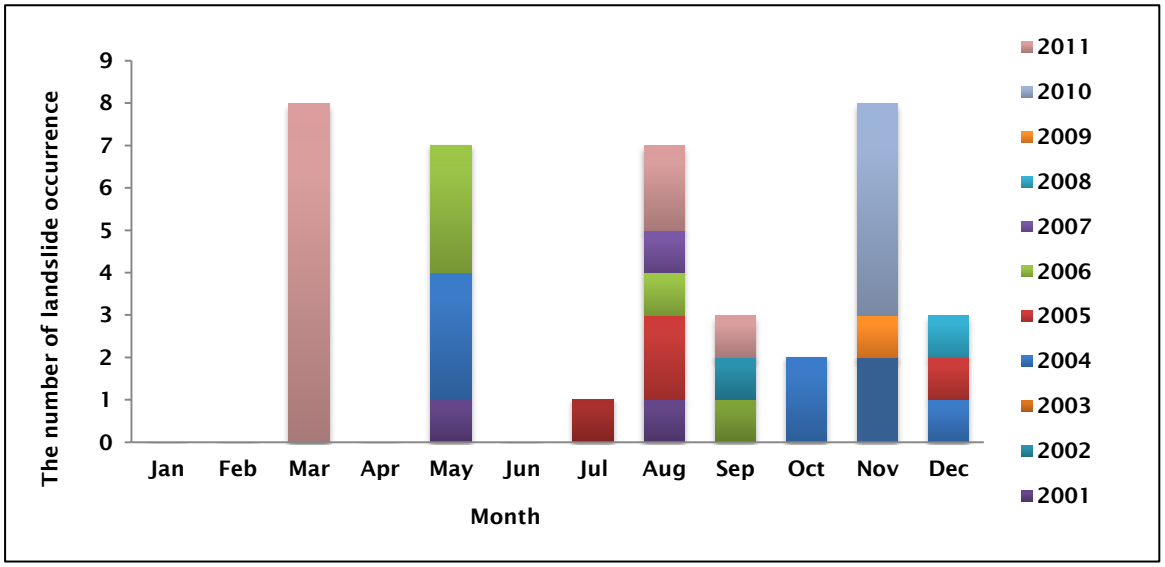

Figure 2.30 The bar chart of monthly landslide occurrences during 1988-2011(DMR, 2012)

2.5.2 The previous study of landslides induced by rainfall

Rainfall volume is therefore a vital factor in increasing damage caused by landslides. This factor is evident from case studies using past events. Some previous studies of landslides from rainfall in Thailand are reviewed in this section. Landslide occurrences are analysed by various techniques which are linked with rainfall amount using the past landslide occurrences in several regions and shown in four case studies of Thailand and in two case studies in China as follows:

Firstly, landslides occurred in Wang Chin district, Phrae province in 2001, because of heavy rainfall continuing for three consecutive days. The landslide type is debris flow, caused by intense rainfall and approximately 300 mm of rainfall in one day. Sixty houses and one bridge, as well as approximately 80% of agricultural areas were damaged. Hong village, Pasak village, Kham Muak village, Song Kwae village and Muag Kham village were violently destroyed by large volumes of water flowing from the hills. This area, therefore, is considered a risk area requiring prediction in the future in order to set up early warning (Teerarungsigul et al., 2007). Landslide hazard and prediction models of mountains and hills of the Mae Nam Yom basin in the scale 1:50,000 to 1:10,000 in Wang Chin District in Phrae Province, in the North of Thailand have been studied by both GIS and Remote Sensing. The Remote Sensing assessed landslide occurrences in terms of special mapping, whereas the technique of GIS is used to calculate landslide hazard assessment.

Secondly, Soralump, (2007) revealed that landslide hazard zoning can address the landslide problem and reduce the number of losses. In the south of Thailand, six provinces were selected in this case study: Phuket, Ranong, Trang, Phan-Gna, Satun and Krabi provinces. The landslide occurrences are more frequent because of disarrangement of land use in hazard areas. Geotechnical soil conditions have been used to analyse and weight factors for large zoning areas. The type of residual soil is considered in relation to potential landslides by geotechnical laboratory tests. The accumulated rainfall during three days (approximately 270 mm) is calculated by the Antecedent Precipitation Index (API) and the various soil/rock groups are influential to landslide occurrence. The relationship between the accumulated rainfall over three days in different periods of time and the technique of GIS are used in landslide hazard maps. Finally, rainfall intensity, i.e. was the intensity identified, is a main factor for analysis in landslide hazard modelling.

Landslides often occur in Chiang Rai province in the northern part of Thailand because this area has the highest rainfall average when compared with other provinces in the northern part. Therefore, an early warning system is important to reduce losses from landslides. Seven risk factors are considered in order to identify the type of areas, which are divided into three levels: high risk, normal risk and non-risk areas with landslide occurrences. Whereas, 101 mm of rainfall value is a main risk factor and other factors are identified: rock type, slope, forest cover, faults, wind direction and altitude. The risk factors thus depend on characteristics of the local area. Thus, the causal factors of landslides depend on seven risk factors which are classified into two groups: intrinsic factors and triggering factors. The risk areas are also determined and classified by the weighted Geographic Information System (GIS) program in order to create a hazard map (DMR, 2011b).

The landslide susceptibility model is created by the Department of Mineral Resources. According to the weather changes, a mathematic model is created adjusting the shear strength and the seepage of the soil properties under the conditions of soil moisture change, in order to analyse the susceptible landslide areas. In terms of geotechnical engineering, soil properties are determined in the geotechnical laboratory such as shear strength, angle of friction, soil types and permeability. The 30x30 metres of resolution in both the elevation and slope angle are obtained by a Digital Elevation Model, (DEM). The hourly rainfall data of

at least 24 hours (100-300 mm) is used to calculate for the dynamics of susceptible landslide because 24 hour duration relates to the susceptible landslide areas (three levels: high, medium and low) for early warning in the northern and southern parts of Thailand (DMR, 2011a).

Landslide occurrences have been studied by researchers in China, and have been classified into two cases studies. Kunlong, et al. (2007) found the prediction and time warning of landslide occurrence in terms of hazard risk assessment and management from rainfall and geology. The accuracy of warning is present for one hour. In this case, Yongjia City, Zhejiang Province in China is the study area. The geological and regional landslide hazard zonation is analysed by mathematical models, while, the triggering factors, such as rainfall-controlled warning models: 175 mm and 250 mm of daily rainfall can be estimated by short-time dynamic warning models, after that the information will show on maps by WebGIS.

This study is divided into two parts: prediction and time warning. The hazard prediction depends on two factors, firstly, the intrinsic factor is topography, slope, lithology, geology and human activities and rainfall is an extrinsic triggering factor. A quantitative model produces statistical predictors. A geo-hazard zoning map, in the scale 1:6,000,000 consist of intrinsic and triggering factors to be used to determine the boundary of landslide zones.

Another case study, Zhang (2011) studied a real time warning system of landslide occurrence by WEBGIS, divided into two regions: typhoon region and non-typhoon region. They showed the relationship between the landslide hazard region and rainfall via a statistic approach. There are many factors to analyse in respect of landslide occurrence, such as topography, geological structure, lithology, as well as slope instability, critical daily rainfall (175-250 mm), earthquake, excavation, loading and water fluctuation. The researchers selected Zhejiang Province in China because it is one of the provinces of highest economic growth, and has been experiencing serious geological disasters in the past, especially landslides, debris-flows and rock falls.

Typhoons and rainstorms have frequently been occurring from August to September every year. The spatial prediction results are integrated with time forecast in order to upload a spatial prediction zonation map, monitored data of geo-hazard and real time rainfall for warning via the Internet. The geological and

meteorological information are integrated for landslide warning in the region. In terms of intensity of landslide occurrence, the semi-quantitative analysis of regional landslide hazard is used to prove spatial landslide prediction. The information is considered from the history of landslide occurrence to show the relation between five environmental factors, such as slope gradient, lithological formation, faults distribution, water system, land-use type, and two triggering factors, such as the annual number of rainstorm days and human activities. These are seven factors to compose on a map in the scale 1: 100,000 to create either a quantitative information map or a GIS analysis function. Furthermore, seven information maps are generated in order to present the different hazard levels of the zonation map. Historical rainfall has influenced with landslide occurrence for two decades in Zhejiang Province. The rainfall statistics are examined for landslides that had occurred many times in June-September each year. Especially, effective rainfall (≥300 mm) has influenced large and moderate landslides in high hazard areas. Then, it is divided into three levels of hazard: low, moderate and high taking into consideration rainfall intensity and effective rainfall. In this case, the effective rainfall is compared in low, medium and high hazard in large and moderate landslides: 0-200 mm, 200-300 and ≥300 mm respectively. While, the effective rainfall is divided hazard levels of rainfall in small landslides: low, medium and high as 0-150, 150 -250 mm and ≥250 mm respectively. Using WebGIS, a real-time system of landslide hazard zonation mapping was developed for early warning on the internet (Zhang et al., 2011).

Summarizing these few, but often detailed studies, seven examples of threshold daily total rainfall values are given that were related to slope failures, together with one example of the API that caused slope failure. The lowest value of daily rainfall was 101mm and the greatest of daily rainfall was 300mm. so the hourly rainfall data of at least 24 hours (100-300 mm) is used to calculate for the dynamics of susceptible landslide in Thailand. Moreover, the Antecedent Precipitation Index (API), which is influential to landslide, is calculated for three days (approximately 270 mm) in the various soil/rock groups.

In China, approximately 175 mm and 250 mm of daily rainfall can be measured for short-time dynamic warning models on maps by WebGIS, while the low, medium and high hazard categories defined by Zhang (2011) for large and moderate landslides: 0-200 mm, 200-300 and ≥300 mm respectively, seems appropriate.

2.6 Models of slope failure for landslide analysis

2.6.1 Introduction

The slope stability analysis forms a key part of the mapping of potential landslide hazard which is determined by geology, site condition and soil properties within a Geographical Information Systems (GIS) framework to define the spatial distribution. The combination of hydrological data such as rainfall, runoff and surface water, accumulation areas, as well as infiltration, is also important for slope stability calculation (Kayastha et al., 2006). The infinite slope stability model and steady state runoff are also used to estimate potential shallow landslides. The mapping of potential landslides is divided into two processes: mapping created by observed shallow landslides linked with aerial photographs and field investigation and applying the categories of local geology and topography to the analysed landslide hazard map, at the watershed scale. The digital terrain model (DTM) data are presented to assess the landslide hazard potential in terms of the SHALSTAB model. The accuracy of the model is associated with landslide hazards in a landscape (Dietrich et al., 1998). Another slope stability model, the SINMAP (Montgomery et al., 1994) (Stability Index Mapping) model is a model for assessing slope stability and landslide hazard. This model is applied to assess the shallow translational landslide by shallow groundwater flow convergence in terms of susceptible areas, slope instability and slope failure in a slope stability model at sites based on several factors: slope, lithology, landform, geological structure and hydrology. Shallow surface flow convergence, increased soil saturation and shear strength reduction are indicators for assessing the debris flow and landslide occurrences including within a digital elevation model (DEM). The scale of DEM data can be resolved in terms of GIS and mapping to pinpoint the location of hazard areas.

2.6.2 Slope failure models

a. GIS for Slope Stability Analysis

The Geographic Information System (GIS) can manage and analyse information in the form of spatial data linked to a database and displayed as a smart map. GIS is a good way of analysing and developing geotechnical models for slope stability analysis, especially for landslide hazard mapping. Both homogenous and non-homogenous slopes can be identified by this method and the slope stability index

is another safety factor which depends on the geotechnical, physical and mechanical parameters. The slope stability analysis of the GIS application can refer to the area of landslide hazard zonation, including the estimated potential landslide hazard or mass movement, on a map and showing the spatial distribution of the hazard classes. In terms of safety factors, geometric data, shear strength data, unit soil weight and pore water pressure are required to calculate a reliable model (Kayastha et al., 2006).

b. Infinite slope stability model

The infinite slope model is used to analyse and estimate hazard zonation in terms of regional scale as these failures are common in Thailand in contrast to infrequent rotational failures. Slope stability is estimated and applied by a combination of various physical processes. Furthermore, several types of digital data are still used in the analysis such as land use, spatial distribution of soil types, vegetation and digital elevation model (DEM) data. The infinite slope method can be used to calculate the slope stability factor, while the proportion of stable and unstable force (Fig. 2.31) is estimated by Acharya (2006) and De Vleeschauwer and De Smedt (2002) from Montgomery and Dietrich (1994) and Westen and Terlien (1996), as follows:

$$Fs = \frac{C_s + C_r}{D\gamma_e \ sin\,\theta} + \left[1 - m\frac{\gamma_w}{\gamma_e}\right]\frac{tan\,\emptyset}{tan\,\theta} \qquad \text{(eg 1)}$$

Fs is the safety factor

Cs and *Cr* are the soil and root cohesion (kNm^2) by soil and vegetation types

D is the thickness of soil layer on the top of bedrock (m)

$\emptyset$ is the angle of internal friction (degree)

θ is the slope angle

γ_w is the unit weight of water (kNm^3), and

γ_e is the effective unit weight of soil (kNm^3) given as

$$\gamma_e = \frac{q\cos\theta}{D} + \mathrm{m}\gamma_\mathrm{s} + (1 - \mathrm{m})\gamma_\mathrm{d} \qquad \text{(eg 2)}$$

Then,

γ_d is the dry unit weight of the soil (kNm^3)

γ_s is the saturated unit weight of the soil (kNm^3), and

q is any surcharge on the soil surface(kNm^2).

Parameter 'm' in both equations is the soil saturation index, related with wetness of the soil.

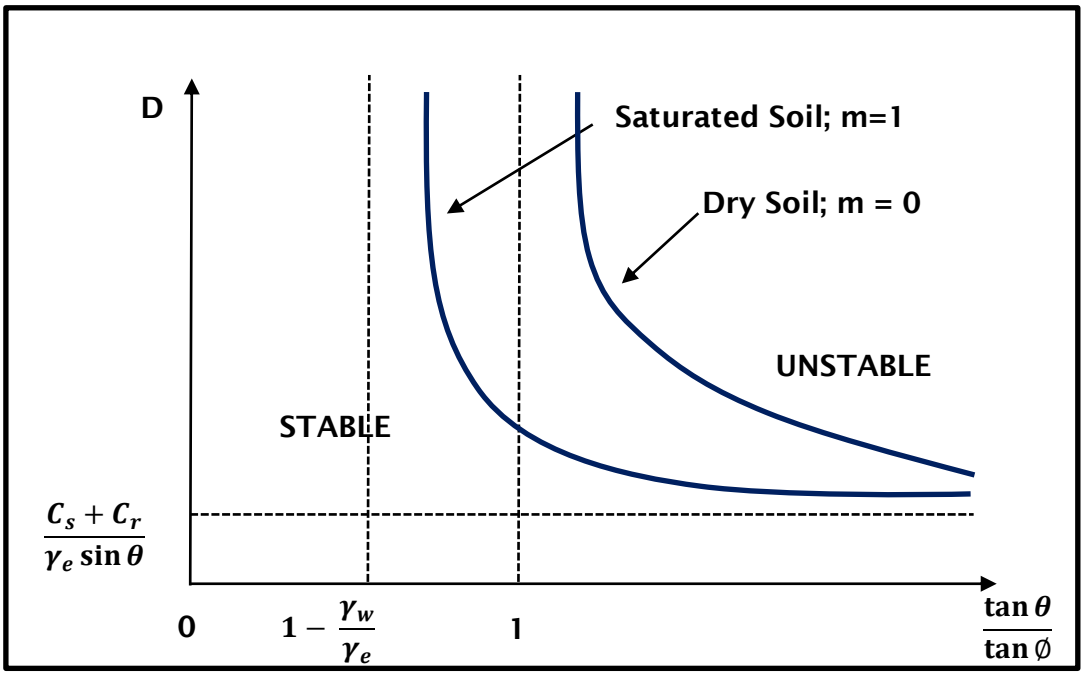

Figure 2.31 The proportion of stable and unstable forces

Four slope stability classes are used to calculate the model concept in terms of environmental phenomena, soil saturation, water saturation and soil depth affecting slope failure. The failure conditions can be estimated in terms of saturated soil depth and the slope depending on the ground-water level. The slope is also linked with the critical soil saturation index, if the soil saturation index is less than 1, the slope is unsafe (Table 2.3).

Safety factor	Slope stability	Remarks
FS>1.5	Stable	Only major destabilizing factors lead to instability
1.25 < FS < 1.5	Moderately Stable	Moderate destabilizing factors lead to instability
1 < FS < 1.25	Quasi Stable	Minor destabilizing factors lead to instability
0.5< FS < 1.0	Lower threshold	Stabilizing factors may be responsible for stability
FS < 1.0	Upper threshold	Stabilizing factors are needed for stability

Table 2.3 Classification of stability classes (Province of British Columbia, 1995)

c. SHALSTAB

SHALSTAB is a physical model which uses both steady state runoff and infinite slope stability to determine shallow landslide occurrences. The parameters of precipitation and soil transmissivity (q/T) are used by the SHALSTAB model for assigning the landslide hazard. The ratio of subsurface flow to drainage areas, including local slope are calculated by the Digital Terrain Model (DTM) to compare slope stability and various landscapes over large areas. Both steady state runoff and infinite slope stability are associated with the SHALSTAB model. The basic assumption of this model is the balance of subsurface and saturation overland flow (Dietrich et al., 1998).

The SHALSTAB model is a basic model which is assigned in the form of a digital terrain model for potential shallow landslide mapping and landslide hazard prediction. There are important factors to be considered in this model, such as soil bulk density, water volume, soil stiffness strength, as well as leakage from underlying bedrock. The saturated overland flow is more significant in the lower gradient soils than very steep soils. The trend of soil thickness effects is correctly predicted by the model in the channel among valleys and on ridges, thus slope convergence depends on the characteristic of soil and thickness. Shallow subsurface flow convergence is the focus of topography. Runoff flow in the underlying bedrock and the decline in depth of runoff on the surface can be identified by the elevation potential at the hill slope gradient. Shallow landslides and soil mantle ridges often occur on soil bedrock, while the mobilization of landslides down slopes for short distances and other landslides travel into a debris flow on steep channel slopes for long distances as well as accumulate sediment downstream. Landslide maps are also shown in terms of shallow landslide occurrences in steep lands. Colluvium is released during landslide occurrences. As a result, root strength and soil thickness are reduced, increasing susceptibility to failure during great storms.

- **SHALSTAB model parameters**

There are several parameters for evaluating shallow landslides. There are four parameters in terms of the characteristics of soil and the effect of precipitation: soil bulk density (ps), the angle of internal friction (ø), the soil transmissivity (T) and the effective precipitation (q). The calculated drainage areas of landslide scar and width scar are important elements of the SHALSTAB model. The local ground

slope is also considered at the failure site. The SHALSTAB model is certainly suitable for field mapping of potential landslide locations alone or in conjunction with field observation (Dietrich et al., 1995).

- **How to use SHALSTAB model**

There are four well-defined prior uses for the SHALSTAB model: displaying a hazard map, reducing potential shallow landslide occurrences for planned forests, road network planning in order to reduce failure and watershed management. The SHALSTAB model can evaluate levels of risk: high, medium and low potential slope instability. The process in this approach involves the following: 1. using the best topographic data; 2. creating an accurate landslide scar map based on field observation and aerial photographs; 3. estimating a log (q/T) value (the effective precipitation, q/the soil transmissivity, T) for each scar location from the SHALSTAB results; and 4. showing the relationship between the landslide mass and different (q/T) values to make a decision on the threshold values required. In terms of hazard mapping, the high-risk areas are identified by the SHALSTAB model as part of a public safety program. The structures are often identified by debris flow and travel for long distances along a valley. The steeper channel areas are estimated to be more than the threshold channel gradient, whereas the watershed management is classified by the stability in SHALSTAB. This principle compares the percentage of areas of shallow landslide and the landscape scale in order to predict the match for observed landslide frequencies.

- **The expectation of SHALSTAB model in the future**

At the present time, the SHALSTAB model is a physical model based on a digital terrain model which is associated with shallow slope stability potential across a landscape. This model is successful in predicting future potential sites of instability from landslides. The parameters are used for ranking on the map by stability, leading to the identification of high, medium and low hazard classes. Local parameters are essential to define large hazard areas in a practical context. Shallow landslides respond with steep, high drainage areas. Generally, the assumptions are identified by the comparison between landslide scar maps and model outputs. Furthermore, the relationship between slope stability and hazard includes land use assigned to natural forest cover. The effect of root strength is not identified by this model. However, a new advanced SHALSTAB model (Dietrich et al., 1995), classified as SHALSTAB.C, SHALSTAB.V and SHALSTAB.D

considers rooting depth. The detail of testing SHALSTAB.C shows that a spatially constant soil depth is subject to root cohesion as well as the effect of root strength data in the forest cover, influencing hill slope instability. Moreover, in advanced models, this process depends on the characteristic of soil, and soil depth, which leads to outputs in the model of instability, including root strength and vertically diverse saturated hydraulic conductivity, considered within SHALSTAB.V. Finally, the SHALSTAB.D model will consider more parameters; a debris flow algorithm and a grid-based model for high solution topographic data.

- **The efficiency of SHALSTAB model**

According to Fontes et al. (2003), the SHALSTAB model can be used to predict susceptible landslide areas and potentially unstable slopes, especially hill slopes during heavy or intense rainfall in tropical areas. The slope stability and hydrological model are linked, based on the infinite slope equation. A digital elevation model (DEM) is generated for assessing the risk areas in the terrain, thus this method can be used with Arc View software. In this case study, the shallow landslides are tested by the SHALSTAB model to predict susceptible landslide areas. Therefore, 1: 50,000 scale mapping is used to identify initial landslide hazard areas, including 1: 10,000 scale mapping necessary to increase model performance in risk areas. Incidentally, Cervi et al., (2010) applied three different models (Weight of Evidence, Fuzzy Logic and SHALSTAB) to assess landslide susceptibility mapping. In this case study areas of about 450 km in the northern Apennines in Italy were tested according to rainfall data in April 2004. Shallow landslides occurred over areas of several kilometres squared. All models were run according to the same geo-environmental causal factors of soil type, soil thickness, land cover, possibility of deep drainage into the bedrock, slope angle and upslope contributing areas. The assessment of model performances are shown by the threshold independent approach, thus the statistical weight of Evidence and Fuzzy Logic model have an accuracy as high as 0.77. The SHALSTAB model, meanwhile had an accuracy equal to 0.56, which gives less reliable results because the assumptions of slope hydrology adopted by SHALSTAB do not include the case of fine-grained soils. Model performance also depends on the quality of input data that is necessary to present the spatial variability of parameters over large areas. In each case study, the different models depend on the perspective of problems and planning use.

d. Slope stability in SINMAP model

The SINMAP model has been developed for use with Arc GIS by computing in terms of slope stability index mapping and the hydrological model. Based on the SINMAP approach, a combination of shallow ground water flow is used for application to analysed transitional shallow landslides. Environmental management in terms of forest planning and forest engineering and other geo-hazards are studied with the SINMAP model. The SINMAP model is based on the infinite slope stability model linked to saturated soil depth and pore water pressure, which are balanced with the proportion of discharge in catchment areas. There are many parameters to be calculated and input with the SINMAP model, such as topography, specific catchment areas, quantitative soil properties and climate, especially soil properties identified by soil cohesion and root cohesion. The digital elevation model can be determined in terms of topographic, values including uncertainty values. The stability index equation is defined by SINMAP as follows (Hammond et al, 1992):

$$FS = \frac{C + \cos\theta\left[1 - min\left(\frac{R\ \ a}{T sin\,\theta'}, 1\right) r\right] tan\,\emptyset}{sin\,\theta} \qquad \text{(eg 3)}$$

where

C is the combination of root (*Cr*) and soil cohesion (*Cs*) (kNm^2)

R is the recharge rate (m/day)

T is the transmissivity (m^2/day)

Ø is the internal friction angle of the soil (degree)

Furthermore, the combination of hydrological and geotechnical parameterization are determined by the mapping (SINMAP) model in terms of lower and upper values (Fowze et al., 2012) to predictions.

The requirement of the SINMAP model consists of four terms as follow,

- **Digital elevation model (DEM) for the case study**

Based on Arc GIS software, the grid DEM is shown using a raster dataset where the elevation or slope angles may be represented in digital maps of the study areas. In this study, the grid DEM in 30 metres resolution was downloaded from *www.gdem.ersdac.jspacesytems.or.jp/* and each pixel was calculated by 30 metres on the ground.

- **Geotechnical data : *C* and *Ø* values as follows:**

Combined Cohesion = $C_r + C_s$ (N/m^2)

Soil weight = $h\,\rho_s\,g$ (N/m^2)

C (Dimensionless Cohesion) = $(Cr+Cs)/(h\,\rho_s\,g)$

C_s = soil cohesion (N/m^2)

C_r = root strength (N/m^2)

C = $Cs\,/(h\,\rho_s\,g)$

ρ_s = wet soil density (kg/m^3)

h = soil depth (m)

g = gravitational acceleration (9.81 m/s^2)

- **Hydrological model : the ratio *R/T***

T = soil transmitivity ($T = ks \times h$)

ks = the saturated permeability of the material (standard values depend on soil type)

R = rain (mm./hr)

- **The past landslide point themes**

Parameters: *C*, *Ø* and the ratio *R/T* are shown in terms of lower and upper values in default values as follows:

Dimensionless Cohesion (lower value). Default value: 0.0. This is the lower value that takes into account both root and soil cohesion.

Dimensionless Cohesion (upper value). Default value: 0.25. This is the upper value that takes into account both root and soil cohesion.

Phi [degrees] (lower value). Default value 30°. This is the lower value of the soil friction angle.

Phi [degrees] (upper value). Default value 45°. This is the upper value of the soil friction angle.

T/R (lower value). Default value: 2000 m. This is the lower value for the ratio of transmissivity to the effective recharge rate.

T/R (upper value). Default value: 3000 m. This is the upper value for the ratio of transmissivity to the effective recharge rate.

Soil Density (ρ_s) Default value: 2000 kg/m^3.

The infinite slope stability model factor of safety is calculated by the SINMAP model;

$$SI = FS = \frac{Cr + Cs + cos2\,\theta\,[\,\rho s\, g(D - Dw) + (\rho s\, g - \rho w\, g)Dw]\tan\Phi}{D\rho s\, g\sin\theta\,\cos\theta} \qquad \text{(eg 4)}$$

The output of SINMAP models is divided into five classes: Stable Slope Zone, Moderately Stable Zone, Quasi-stable Zone, Lower threshold and Upper threshold (Table 2.4).

Various stability classes approached in the SINMAP Model		
Condition	**Class**	**Predicted State**
SI > 1.5	1	Stable Slope Zone
1.5>SI> 1.25	2	Moderately Stable Zone
1.25>SI> Minor destabilizing 1.0	3	Quasi-stable Zone
1.0>SI> 0.50	4	Lower threshold
0.50>SI> 0.0	5	Upper threshold

Table 2.4 Various stability classes approached in the SINMAP Model (Province of British Columbia,1995)

2.6.3 The comparison of slope stability both the SHALSTAB and SINMAP models for landslide risk assessment

The Shallow Landslide Stability Model (SHALSTAB) and Stability Index mapping (SINMAP) models (Table 2.5) have been determined for landslide hazard and management. The theoretical basis of SHALSTAB and SINMAP are related by mathematical derivations and applied into GIS. The combination of a hydrological model and an infinite of slope stability model based on catchment areas and hill slopes are calculated by both models. The shallow surface flow convergence leads to increased pore pressure (wetness) and soil saturation and shear strength reduction (Montgomery et al., 1994). The SHALSTAB and SINMAP models are also more efficient in assessing the DEM at scales of 10-metres and 30-metres, whereas the DEM can manage watershed in digitized contour patterns on topographic sheets on a scale of 1: 24,000 with a 10-metre or 30-metre mesh grid overlaid on the top. The elevation is calculated by inverse distance weighting interpolation in each grid cell. The limitation of both models is that neither applies to deep-seated instability, deep earthflows and rotational slumps.

SINMAP	SHALSTAB
1. The accuracy of DEM leads to the accuracy of output (landslide initiation zones). 2. Seven parameters need to apply: the root and soil cohesion, angle of internal friction, the soil transmissivity (hydraulic conductivity x soil thickness), recharge (rain) and soil bulk density. 3. T/R lower bound (values) and T/R upper bound (values) are calculated for ratio of transmissivity to the effective recharge rate. 4. Three parameters: dimensionless cohesion, T/R and Phi degree (soil friction angle) are calculated for upper and lower bounds (values) of SINMAP.	1. High resolution DEM in an ASCII grid file format. 2. Six parameters need to apply: the effective cohesion, the angle of internal friction, the soil transmissivity (hydraulic conductivity x soil thickness) and the effective precipitation (q) and soil bulk density. 3. The lowest of q/T values are calculated by areas (least precipitation amount required for instability). 4. Four parameters: the bulk soil density, the angle of internal friction, the soil transmissivity and the effective precipitation are calculated for SHALSTAB.

Table 2.5 The comparison between SINMAP and SHALSTAB

There are two reasons why the SINMAP model is more suitable than SHALSTAB in Uttaradit province as follows:

1. In terms of SINMAP, the single lower and upper value calibration parameter values are represented for areas in three parameters: dimensionless cohesion, T/R and Phi degree (soil friction angle). It means the lower and upper values of parameters cover the whole area (study site) because parameter values are not homogenous and small soil samples are taken over a large area, while the parameter values of SHALTAB are not used the range (the lower and upper values). Therefore, the parameter values of SINMAP are more accurate than SHALTAB.

2. In Uttaradit province, the clearance of agricultural land and deforestation are problems and lead to landslide occurrences, so the root strength values are important to calculate for cohesive values. The root strength is important in contributing to cohesion values in this area, since root strengths of some vegetation can make strong cohesion. For example, abundant vegetation in the

mountain areas (strong root cohesion reduces the occurrence of landslides) is found in Faktha district.

SHALSTAB is not clear as to how to derive root strength values, while root strength values are input as cohesion values in SINMAP. Thus, the parameters of the SINMAP model are more complete to evaluate landslides than the SHALSTAB model for the landslide analysis. The SINMAP model is more suitable in Uttaradit province (study site) than the SHALSTAB model. In addition, the SINMAP model can be integrated and linked with ARC GIS version 10.1 which is more up-to-date.

There are five studies in five locations to present the procedure of SINMAP. First of all, according to the observations of Lan et al.(2004), lithology, structure, slope angle, slope aspect, elevation and off fault distance influence Stability Index Mapping. The spatial database of the landslides in the Xiaojiang watershed in China is evaluated by techniques of GIS in terms of the susceptibility maps. The landslide factors are classified and calculated by the Certainty Factor model (CF) values for the hazard class of landslide zonation. In addition, the comparisons of the threshold precipitation values are still identified by the instability classes of the landslide hazard map.

Secondly, the Stability Index Mapping (SINMAP) model, which was developed by the state of British Columbia coordinating with the Canadian government, uses the Geographic Information System (Arc view) for landslide prone areas analysis. The potential of shallow landsliding is presented by National Forest and Transportation Management. The slope stability index is based on the 30 metres resolution of the Digital Elevation Model (DEM). In this study, six classes of stability index are presented by areas (km^2) and percentages of a region, then, classified into three levels: moderate to high, low to moderate and none to low. The 30 metres of each pixel of DEM are calculated as a horizontal plan view of the ground, but 30 metres of pixel size might have a slight error on the ground slope of fills, cuts, and especially where the natural hill slopes are steep within a watershed. Therefore, the areas on the ground by SINMAP are less than 30 metres in each pixel, as the edge calculation is neglected. For example, in tests carried out by SINMAP, the 30 metre pixel size of DEM can calculate areas on the ground less than 30 metres in each pixel (Michael and Dixon, 1998). The landslide-prone areas are based on five main factors: the history of landslides, the characteristic

of the soil, ground slope, contributing drainage areas and vegetation (root strength) (Michael and Dixon, 1998).

Thirdly, Acharya et al. (2006) presented the slope stability analysis covering 409 km^2 of the Himalayas in the northern part of Rasuwa district in Nepal. Landslides often occur in the rainy season. In this study, SINMAP software was used on GIS Arc View 8.1. In terms of digital data, the spatial soil types, DEM, land-use and vegetation are used to compute the slope stability factor. The combination of hydrological data and slope angle are calculated, the wetness of soil depended on during the extreme rainfall period and the slope angle of a DEM. The Digital Elevation Model presented the slope ranges between 0^o and 64^o on the Himalayan mountains. The increase of saturated groundwater flows correlated with slope failure regions. The scenario of dry soil, half and fully-saturated soil are used to increase the wetness of soil from dry to a saturated condition, the safety factor decreases but it depends on the slope angle. Then, the scenarios of the extreme daily rainfall events in both a 1 year and 10 year return period are compared to the percentage of slope stability classes. There is a small difference in saturated conditions. As a result, the impact of storm events are overestimated by saturated and non-saturated (dry sand) conditions. It easily becomes an unstable class in saturated conditions under a steep slope of more than 30^o. The agricultural areas or areas of deforestation are also dominant in association with slope failure during the monsoon season.

Fourthly, the relationship between Stability Index Mapping (SINMAP) and the Frequency Ratio model (FR) as a simple method (logistic regression& neural network) are two main factors in the causes of slide: ground water pressures and toe erosion. Yilmaz (2009) found that indicated the relationship between landslide factors and landslide occurrence location to create the susceptibility classes in the landslide susceptibility maps. There are several factors to consider in this case, such as the distance from drainage systems, faults and roads, slope angle and aspect, topographic elevation, topographical wetness index and vegetation cover, including rainfall which is a main factor in identifying landslide susceptibility. The quality of this model is tested for validation under the statistical frequency ratio (FR) model.

In another case, Pack (1998) concluded that the infinite slope stability model and the steady state hydrology model are linked with the three factors of topography,

rainfall and soil to evaluate the spatial distribution of shallow debris slides in the Kilpala watershed, which is sub-drainage of the Nimpkish Watershed in northern Vancouver Island, British Columbia in Canada. The stability classification map is identified in this case.

To summarize, the distribution of rainfall and the extremes of monsoons and typhoons across Thailand are described for the climate condition. As raining in Thailand is caused by monsoons and storms, so scattering of rainfall for all year round is different in each region. The extreme of monsoons and typhoons is also linked with rainfall conditions, which lead to landslide occurrences. The initiation of a landslide is linked with the threshold rainfall value. Furthermore, the regional climate change impacts in future climate scenarios are downscaled by both SDSM and START. The change in the rainfall pattern due to climate change in the future will be predicted. The pattern of landslides is linked with the model of slope failure to use for landslide analysis, especially SINMAP. Thus, the main factor of literature review describes the linkage between the change in rainfall pattern due to climate change and the landslide model, showing the risk areas in the future.

CHAPTER 3 PARAMETERISING SINMAP

To address the research objectives, the methods are described in this chapter: set-up and calibration of the SINMAP model, sensitivity of the SINMAP model, geotechnical laboratory, landslide assessment at present calibration and landslide assessment under future climate simulation scenario A2 and B2. First of all, in the SINMAP calibration, the model is set up and calibrated against the landslide hazard mapping from the past landslide inventory triggered by rainfall values in Thapla and Laplea districts in Uttaradit province in 2006. As a result, the relationship between the output of the SINMAP model and the occurrence of past landslides are compared in terms of the landslide hazard mapping. Secondly, the SINMAP parameters are considered by sensitivity for accuracy, such as trends of slope angle of hilly terrain, rainfall values, soil depth, soil density, permeability values, shear strength values and friction angle. Additionally, the SINMAP parameters will be extended to use primary data obtained from the geotechnical laboratory at Kasetsart University in Thailand, as well as field data collected in Uttaradit province as part of this research.

At the present calibration, the average rainfall data during 1954 – 2012 is used to assess the rain triggered landslide hazard analysis in slope stability mapping in terms of hydrological data, as well as land cover/land use and a digital elevation model (DEM), rock type and geotechnical data including permeability, soil density, soil classification, shear strength and the angle of friction values. As a result, the stability hazard class definition is described for landslide hazard mapping.
In addition, the average arrival rainfall during 2013 – 2099 under climate simulation scenarios A2 and B2 will be analysed by the Statistical DownScaling Model (SDSM) version 4.2 for the landslide hazard mapping in the future.

Finally, the landslide hazard mapping will be compared and shown by areas (km^2) both in the present day and in the future under climate simulation scenarios A2 and B2 in Uttaradit province. [An overview of the work plan is shown in Fig 3.1.]

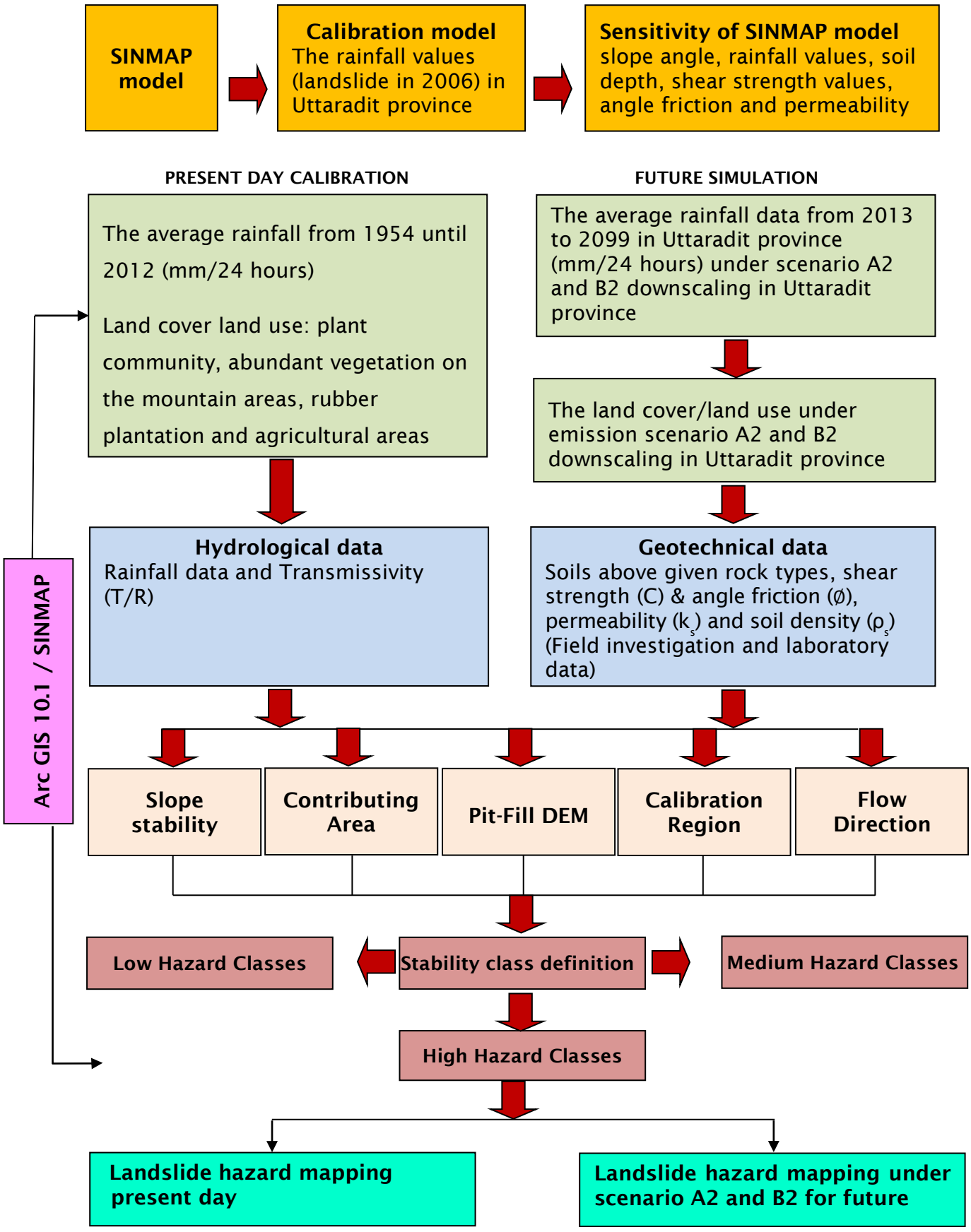

Figure 3.1 Conceptual frame work for the project

3.1 The rainfall conditions in Uttaradit province

Climate conditions were dominated by the southwest and the northeast monsoons, the tropical cyclones which usually come during May to October affected rainfall values in several parts of Thailand. The tropical cyclone, depression level, moved to cover the Bay of Bengal and the Andaman Sea. In 2006, thirty-four tropical cyclones moved into the western Pacific Ocean, the South China Sea and the Bay of Bengal, but only sixteen tropical cyclones affected Thailand, and only two tropical cyclones directly came into Thailand. The first tropical cyclone was typhoon level, called XangSane, and moved into the upper part, especially in the north-eastern part of Thailand in October. The second, named Durian, was depression level, moving into the southern part in December. Therefore, heavy rainfall occurred in several regions, especially in northern and southern parts (TMD, 2007a).

Rainfall conditions are associated with the southwest monsoon season during April to September. Especially in April, the low pressure area was located in the middle of the country and spread throughout several regions, such as the northern, the north eastern and the southern parts. It occurred during the warm weather in this month as the season changes from summer to rainy. During the May to September period, the low pressure area covered the northern and the north-eastern parts of Thailand throughout the eastern part and the Gulf of Tonkin. As a result, the wind moved from the Indian Ocean through the Bay of Bengal, the China Sea and the Gulf of Thailand, into the central part of Thailand. This wind moved from the south-western part into the north-eastern part. It is called the southwest wind, which originates from the southwest monsoon. Wet days usually dominate by the power of the southwest monsoon and the low pressure area.

In Uttaradit province, on May 23, 2006 landslides and flash floods occurred in Muang, Laplea and Thapla districts. This situation led to 83 people killed, 33 people lost, 673 houses damaged, including 481,830 hectares (481.803 km^2) of agricultural area damaged, to a total value of $9.15 million (DMR, 2012). According to the Department of Methodological reports, the Intertropical Convergence Zone moved over the upper of the northern and north eastern parts on 22 May 2006, so it led to heavy rainfall conditions, approximately 263.7 mm in Muang district and 330 mm in Laplea district in Uttaradit province, especially at tambon Khungtapao in Muang district on 22 May 2006 over 200 mm of rainfall

was measured around 3 pm until 11 pm as shown in Fig 3.2. Note that these threshold values are consistent with those recorded in the literature review at the end of section 2.5. The comparison between the average standard rainfall values (the average annual rainfall from 1981 to 2010) and the annual rainfall values in 2006 were calculated for the intensity of rainfall in 2006. The rainfall values in 2006 were greater than the average normal rainfall values in Uttaradit province (Fig 3.3). Three districts were affected by landslides on 23 May 2006; Muang, Laplea and Thapla districts, while the mud and timber flowed down into Bantuek, Sisatchanalai district in Sukhothai province around 3 am.

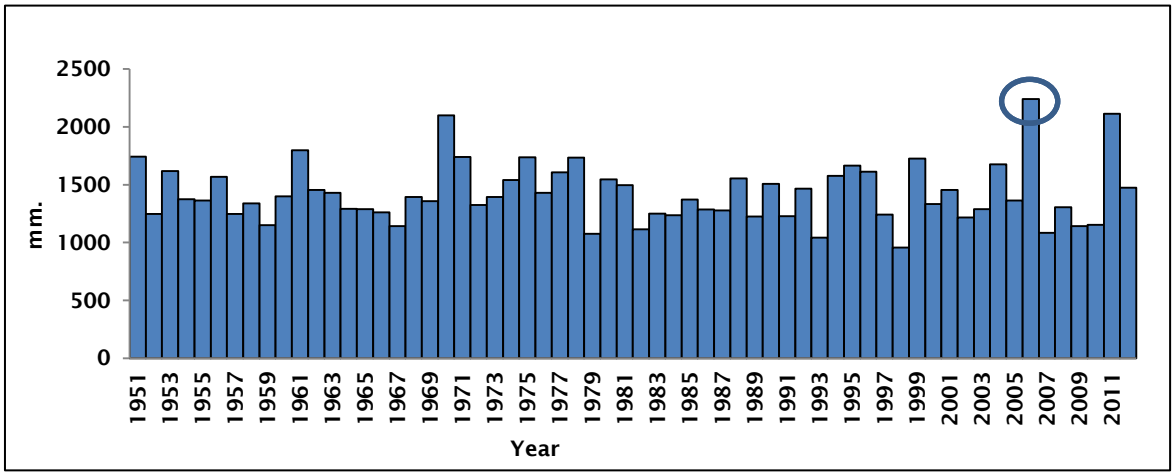

Figure 3.2 The critical point of annual rainfall values in central rain station in Uttaradit province in 2006 (TMD, 2012b)

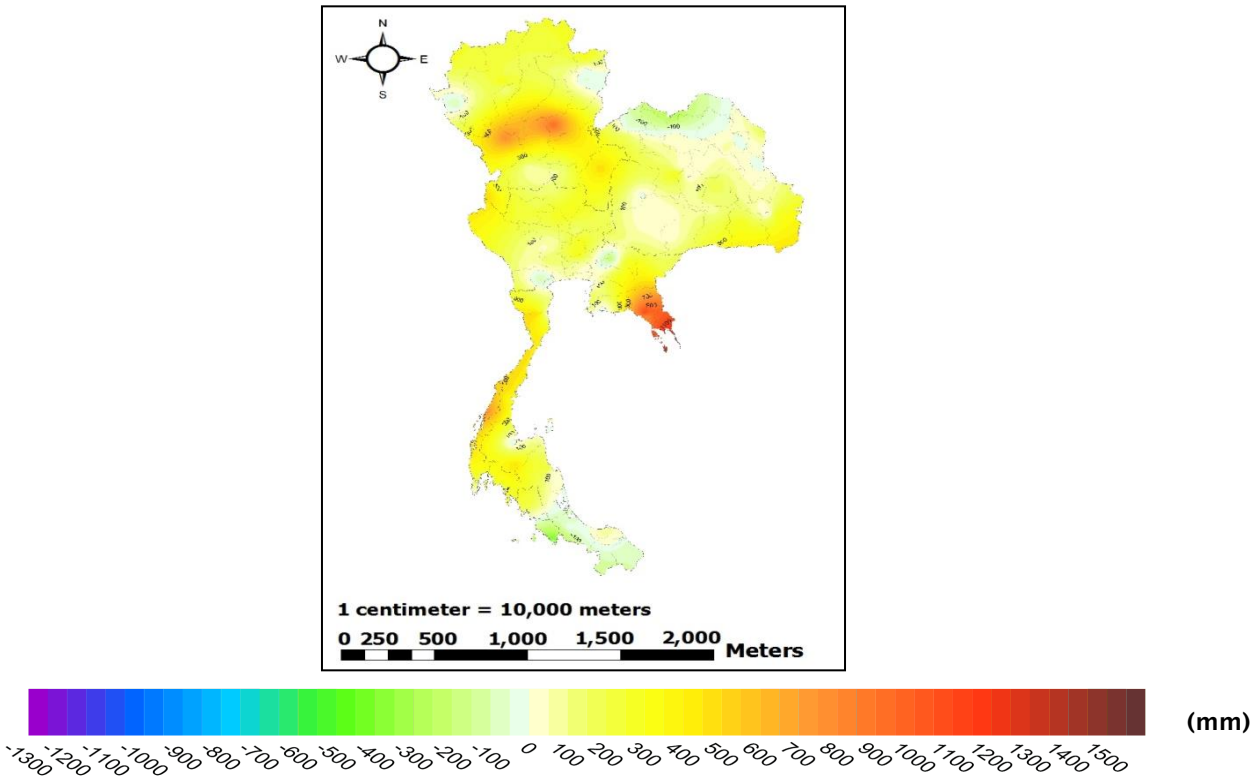

Figure 3.3 The variability of rainfall in Uttaradit province in 2006 (TMD, 2012b)

Then, landslides occurred again on 9th September, 2011 in Nampat district in Uttaradit province because of heavy rainfall. It was about 242.8 mm (DMR, 2011). At the end of July, 2011, Thailand was influenced by the tropical storms, which became the depression moving into Nan province. Afterwards it changed into a low pressure area which overspread into several provinces in the northern part.

Then, on 9th September, the extreme daily rainfall (242.8 mm) occurred because the low pressure area and the southwest monsoon led to the landslide occurrence in Nampat district in Uttaradit province. This landslide occurred in five villages in Nampat district: Bantonkanoon, Banhuaidua, Banhuaikom, Banklongnean and Bankhokmi. The Department of Mineral Resources reported that five people died, two people were lost and houses and infrastructure were damaged by these landslide occurrences. Another cause of landslide occurrences, in the general topography of this area, is the surrounding high mountains and steep cliffs which lead to landslides and mud slides (DMR, 2011a).

Finally, approximately 600-700 mm of the annual rainfall was higher than the average annual rainfall (1981-2010) and was presented in Uttaradit province, especially Laplea and Muang districts as presented by the interpolation map in 2006. These situations are linked with the history of landslide areas in this year. In 2011, the annual rainfall was higher than normal years since the rain storm started from March until October in this year. Therefore, landslides occurred in several regions of Thailand, especially in Uttaradit province in the northern part.

3.2 Pit data collection and geotechnical soil testing

Soil testing was carried out to define the basic and index properties, including the residual soils collected from Uttaradit Province. In the field, undisturbed block of 200 mm size was extracted for each sampling.

3.2.1 Field investigation and sampling

A field investigation and sampling programme was undertaken during December 2013. The selected locations in Uttaradit province were seven test pit locations in elevated and mountainous terrains, as shown in Fig 3.4. The first five test pit locations were in the same area of past landslides: the first test pit location was in Muang district (TP1), the second test pit location in Laplea district (TP2), the third and the fourth test pit locations in Thapla district (TP3 and TP4) and the fifth test pit location in Nampat district (TP5) respectively. Another two test pit

locations were not in the area of past landslides: the sixth and seventh test pit locations were in Bankhok district (TP6) and Faktha district (TP7). Five block samples of 200 mm sides were extracted from each test pit location and were hand dug to a depth of 0.5 m below the ground surface, while approximately 3 m depth for soil occurs above given rock types in the hilly terrain (GERD, 2012). After extraction, the box samples were sealed by paraffin wax to preserve loss of moisture and were analysed in the geotechnical laboratory at Kasetsart University; the procedure of sampling.

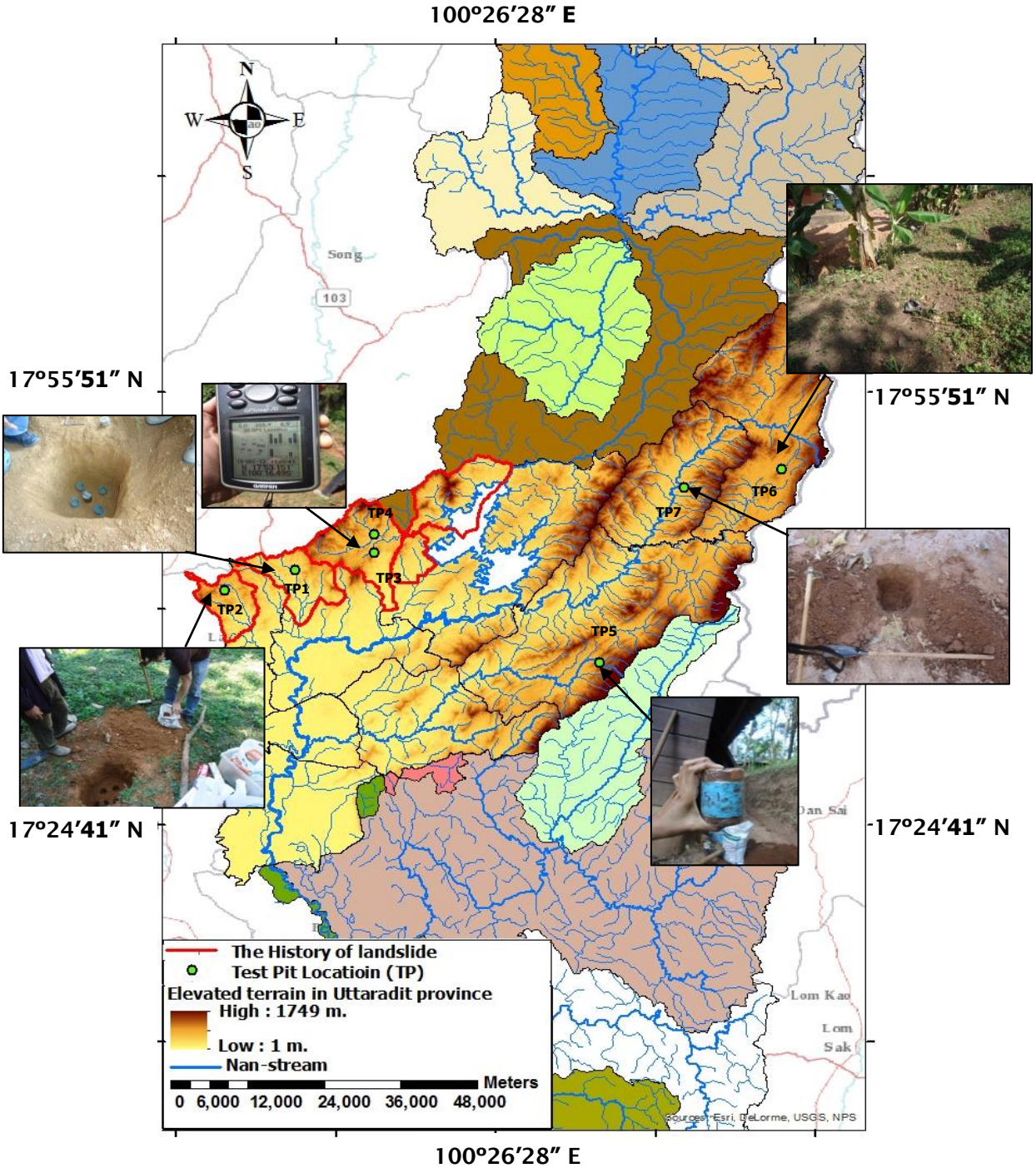

Figure 3.4 The test pit location in Uttaradit province

Nonetheless, the exploration of the seven test pit locations showed an absence of large trees due to deforestation, but shallow root systems were found to a depth of 0.5 metres at some locations. The vegetation type conditions were investigated by direct field observation in Uttaradit province. There were primary natural forests for survey such as slash-and-burn agriculture, rubber plantations, annual crops, galangal oil, orchards and bare lands. Therefore, the vegetation types were linked with the landslide occurrences, especially on hill slopes. Because the root size of common species was different on slope conditions, including cliff surfaces and landslide scars (Nilaweera et al, 1994), Nilaweera (1994) determined that the type of vegetation related to the landslide occurrences in four vegetation types: plant community, abundant vegetation on the mountain areas, rubber tree plantations and agricultural areas. The effect of tree roots on slope stability was considered by the species of vegetation types. Therefore, seven tree species in four vegetation types were selected for shearing tests in the laboratory and reported by Nilaweera (1994) in Table 3.1.

Tree species	**Vegetation types**	**Root strength values (k/Nm^2)**	**The total of root strength values (k/Nm^2)**	**District**
Hibiscus macrophyllus	Plant community	2.2526	2.2526	Nampat, Thongsaenkhun
Dipterocarpus alatus	Abundant vegetation on the mountain areas	4.0634	2.9417	Faktha
Hopea odorata		3.1723		
Ficus benjamina		1.5896		
Alangium kurzii	Rubber plantation	3.0254	2.7140	Bankhok
Alstonia macrophylla		2.4026		
Hevea brasiliensis	Agricultural area	1.1014	1.1014	Laplae, Thapla Muang, Phichai, Tron

Table 3.1 The root strength results of roots in each vegetation type (Nilaweera, 1994)

3.2.2 Soil classification

a. Grain size analysis (Sieve test)

Grain size analysis tests were undertaken in engagement with ASTM D 422 and referred to the particle size distribution test. The particle size analysis was separated into shapes and a range of sizes. The sieving technique was applied for gravel and sand size (coarser) materials with sedimentation. The range of particle sizes could be tested with a simple sieving test on clean sand and gravel to determine the components of clay-silt-sand-gravel mixture. The appropriate size of six standard diameter numbers, namely 3/8”(9.5mm), 4”(4.75mm), 10”(2mm), 40”(0.425mm), 100”(0.150mm) and 200”(0.075mm) was selected to be sieved.

b. Atterberg limits

A clay soil condition can be changed by the range of the moisture content. The softening of clay by additional water could be identified by a well-known example. The liquid limit (LL) tests of a clay soil were performed to determine the range of moisture content using ASTM D 4318. The plastic limit (PL) was determined by the same method as the liquid limit. The plasticity index (PI) (Fig 3.5) could be calculated from the liquid and the plastic limit measurements.

The selected soil samples from the test pit locations in Uttaradit province, were classified by the sieve and the Atterberg tests as soil types of silt in test pit locations 1-4 and clay in test pit locations 6-7, the exception was test pit location 5, which was sand. The Atterberg test was used to calculate plasticity:

- Low plasticity (L.L. less than 35%)

- Medium plasticity (L.L. 35% - 50%)

- High plasticity (L.L. more than 50%)

And, plasticity index (P.I.= L.L.-P.L.)

The Atterberg test of the seven residual soils from the test pit locations were divided into five soil groups and linked with the chart of plasticity index in Fig 3.5:

a. Test pit location 1 and 2: ML/OH as silt (low liquid limit) and organic (high liquid limit)

b. Test pit location 3: MH/OH as silt (high liquid limit) and organic (high liquid limit)

c. Test pit location 4 ML/OH as silt (low liquid limit) and organic (high liquid limit)

d. Test pit location 5: SM (sand and silt)

e. Test pit location 6 and 7: CL as clay (low liquid limit)

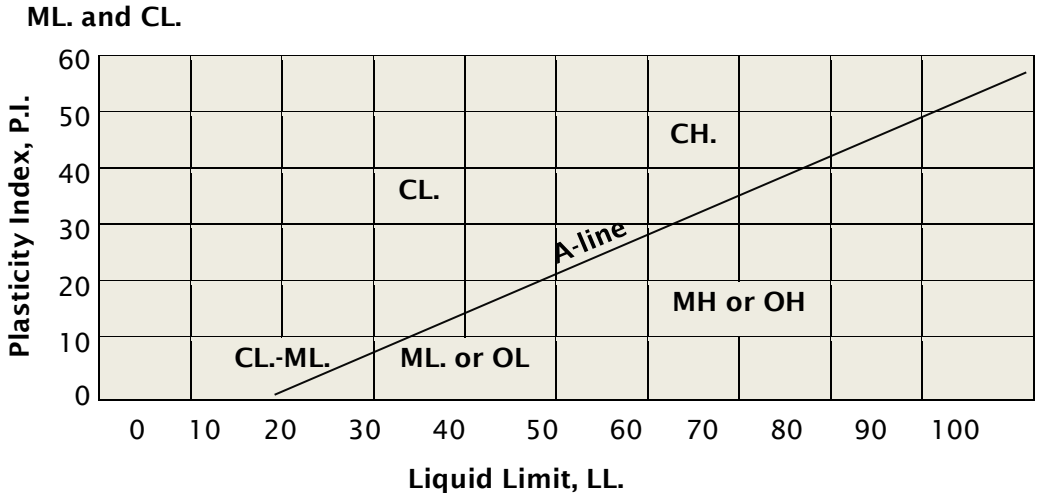

Figure 3.5 The chart of plasticity index (Kangsasitiam et al., 2004)

Both Sieve test and Atterberg (Kangsasitiam et al., 2004) are used to classify and are presented by a chart (Table 3.2).

TP	Atterberg			Sieve test (% passing)						Soil type	
	Liquid Limit (LL)	Plastic Limit (PL)	Plastic Index (PI)	#3/8 (9.5 mm)	#4 (4.75 mm)	#10 (2mm)	#40 (0.425 mm)	#100 (0.15 mm)	#200 (0.075 mm)		
1	47.05	27.85	19.20	97.04	94.24	91.53	89.67	84.27	81.53	ML/OH	Silt
2	49.59	31.70	17.82	98.61	96.67	93.30	90.97	83.91	77.79	ML/OH	
3	62.08	37.15	24.93	100.00	99.29	98.94	97.68	95.88	94.36	MH/OH	
4	47.33	31.2	16.13	100.00	99.92	99.72	99.07	94.44	90.19	ML/OH	
5	NP			100.00	100.00	99.90	99.28	72.18	38.36	SM	Sand
6	29.15	18.2	10.95	100.00	100.00	99.92	96.55	91.42	80.88	CL	Clay
7	27.75	17.88	9.87	100.00	98.53	88.32	84.20	80.52	73.35	CL	

Table 3.2 The classification of soil by Atterberg limits and Sieve test

The result of the soil classification can be related to the cohesiveness and permeability values of soil in the seven test pit locations. Cohesiveness is a key factor, for example a cohesionless situation is possible in sand and silt, but not in clay (Peck et al., 1967).

3.2.3 Index of soil properties

a. Direct shear tests

The test of shear strength of soils in the laboratory were run on the ASTM D 3080. The movement of two halves of the shear box test along a horizontal surface of sliding were selected for the samples. The values of measurement of the shear strength of soils depend on the soil conditions. The drained shear strength of the cohesive soils was carried out with the rate of shearing slow enough to permit drainage to displace during shear. The rate of displacement was dependent on the drained soil characteristics and the permeability of the soil. The permeability of soils were corresponding with the coefficient of consolidation. The consolidation stages can calculate the appropriate time failure, hence the rate of displacement (0.5 mm/minute) can be determined in the samples.

b. Permeability tests

A test to determine coefficient of permeability was undertaken in accordance with ASTM D 422. The permeability coefficients generalized by Darcy's law describe that the rate of flow of fluid through a porous granular medium under stable

conditions is proportional to the excess pressure leading to the flow and inversely proportional to the glutinousness of the fluid. The constant of permeability identifies the characteristics of soils with a high permeability constant, such as sand, and those with low and intermediate permeability constants, such as silts and clays. The results of drained shear strength of cohesive soil and permeability of soil in the seven test pit locations in geotechnical laboratory are shown in Table 3.3.

Test pit	**Soil type**	**Cohesion soil (Kpa)**	**Angle friction**	**Soil density kg/m^3**	**Permeability cm./sec.**
1	ML or OH	6.96	26.23	1568	4.006E-06
2	ML or OH	10.30	32.23	1762	2.918E-05
3	MH or OH	12.85	33.13	1822	6.081E-06
4	ML or OH	16.18	28.86	1916	1.172E-06
5	SM	7.85	30.09	1716	3.415E-04
6	CL	14.02	24.62	1477	1.175E-06
7	CL	6.96	26.23	1984	8.187E-05

Table 3.3 The result of soil properties in geotechnical laboratory

3.3 Implementation of stability index mapping (SINMAP)

The procedure of SINMAP software is provided for the terrain stability mapping tool and based on infinite slope stability. In this study, the mathematical theory of SINMAP is applied by shallow translational landsliding and run by Arc GIS 10.1.

3.3.1 The Stability Index (SI)

The landslide hazard mapping analysis is performed using the Stability Index Mapping (SINMAP) model, incorporating both hydrological and geotechnical parameterizations in terms of an infinite slope (Pack et al., 1998). As outlined in the first step of the GIS technique, the geotechnical and hydrological parameters are calibrated for calibration regions through the uniform of probability distribution and presented for lower and upper bounds (values) on uncertain parameters in SINMAP model analysis: Transmitivity (T)/Recharge (R) (lower-upper bounds), Cohesion (lower-upper bounds), Angle friction (degrees) (lower-upper

bounds) and Soil density (kg/m^3). Furthermore, default values may be included in the SINMAP software, including the gravity constant (9.81 m/s^2) and water density (1,000 kg/m^3).

Accordingly, the stability index, SI, which is equivalent to the factor of safety, FS, can be divided into three classes. By default, the stability index has been defined with six SI values, 0 (defended), 0-0.5 (upper threshold), 0.5-1.0 (lower threshold), 1.0-1.25 (quasi stable), 1.25-1.5 (moderately stable), and >1.5 (stable). In this study, the result of SI values is reclassified into three classes as follow (Fowze et al., 2012):

a. High hazard classes (0.0-1.0), are defined with three SI values, 0 (defended), 0-0.5 (upper threshold) and 0.5-1.0 (lower threshold) SI values of less than 1 would refer to failure regions.

b. Medium hazard classes (1.0-1.5), are defined with two SI values, 1.0-1.25 (quasi stable) and 1.25-1.5 (moderately stable).

c. Low hazard classes (>1.5) are defined as stable.

The SINMAP model has been developed for use with Arc GIS version 9.0 or higher by computing in terms of slope stability index. Based on the SINMAP approach, a combination of shallow ground water flow is applied to analyse transitional shallow landslides, while the rotational slump and deep earth flow are not applied. The infinite slope stability model is linked with saturated soil depths and pore water pressures which are balanced with the proportion of discharge in catchment areas. All kinds of parameters can be calculated using the SINMAP model, such as specific catchment areas and quantitative soil properties, especially soil properties identified by soil cohesion and root cohesion values. The digital elevation model (DEM) can be determined in terms of topographic values including uncertainty values. The stability index equation was defined by SINMAP (Kayastha et al., 2006).

3.3.2 Model variables and model parameters

The description of the SINMAP model requires four variable parameters as follows: *C*, (cohesion), $\varnothing$ (Internal friction angle), the ratio *R/T* and the soil density.

The variable parameter values are linked with the digital elevation model (DEM) to calculate the values for each pixel. An inventory of landslides is used for validating the model output.

3.3.3 Flow direction of slope angles

The flow direction can be calculated by various methods to assign the flow direction in each grid cell in the steepest downward slope: the eight flow directions method, the multiple flow direction method (Quinn et al., 1991), the random direction method (Fairfield and Leymarie, 1991) and the grid flow tube method (Costa-Cabral and Burges, 1994).

The eight flow directions method determines the flow from each cell to one of its eight neighbours and is widely respected due to the proven disadvantages having been solved. Otherwise, SINMAP uses the multiple flow direction approach introduced by Tarboton (1997). In this approach, the flow direction angle measured counter clockwise from the east in quantity between 0 and 2π and this angle is assigned the direction of the steepest downward slope on the eight triangular facets formed in a 3 x 3 grid cell window centred on the grid cell.

A block-centred delegate is applied with each elevation value taken to indicate the elevation of the centre of the relationship between grid cells. Eight planar triangular facets are formed between each grid cell and its eight neighbours. Each of these has a downslope vector, while it draws outwards from the centre, an angle lies within or outside the 45° ($\pi/4$ radian) angle range of the facet at the centre point. While the slope vector angle is within the angle facet, it displays the steepest flow direction on that facet. If the slope vector angle is outside, the steepest flow direction is associated with the facet that is taken along the steepest border. The slope and the flow direction linked with the grid cell is taken as the magnitude and direction of the steepest downslope vector from all eight facets. This procedure was presented by Tarboton (1997).

The boundary of the study area is delineated by the topography of the districts and provinces. The Laplea and Thapla districts are delineated using digital

topographical maps for calibration of the SINMAP model and the Uttaradit province is delineated using a digital topographical map between latitude 17° 7′ and 18° 24′north and between longitude 99° 5′and 101° 17′east. The topographical maps are divided by slope angle from an altitude angle in nine districts in Uttaradit province.

3.3.4 Landslide inventory points theme

The landslide inventory points theme is a vector dataset used in order to calibrate the model. GPS technique is used to provide the geospatial position of the past landslide inventory points theme in four districts: Maung, Laplea, Thapla and Nampat.

3.3.5 Geotechnical data: Cohesion and internal friction angle

The characterization of local residual soils and land use using digital mapping in six districts such as Muang, Laplea, Thapla, Nampat, Bankhok and Faktha, were collected in the field in Uttaradit during December 2013. The local residual soils data consisted of soil thickness, cohesive soil, permeability and wet soil density values. Otherwise, the land cover/land use was surveyed and represented by vegetation type corresponding with the landslide occurrences, the root cohesion values were calculated for the species of vegetation types. In other words, shear strength, angle friction, permeability and wet soil density values of residual soils could be referred to realistic values of geotechnical parameters in the study area, analysed in the geotechnical laboratory.

The dimensionless cohesion form of the infinite slope stability model combines both soil and root properties. The relationship between the ratio of cohesive strength and the weight of soil contribute to slope stability. In addition, the internal friction angle of soils (∅) also contributes to slope stability. The soil angle friction is one parameter in geotechnical data, which was directly input in the SINMAP software (Hammond et al., 1992).

Then, the combination of soil density (ρ_s) and soil thickness (h) also corresponded with the Dimensionless Cohesion(C) which leads to the infinite slope stability model.

3.3.6 Hydrological data: R/T as required by the software

The transmissivity (T) of the hydrological data input is assigned as the vertical significant hydraulic conductivity of soil and is defined by:

T = soil transmissivity ($T = ks \times h$) (eg 1)

Where the k_s value is the saturated permeability of the material of interest. The k_s value is tested by the American Standard Test Method (ASTM) in the geotechnical laboratory including soil thickness for calculation of transmissivity (T) values.

The R parameter in the SINMAP model is equivalent to the effective recharge for a critical period of wet weather linked with the trigger landslides and is given by:

R = Rainfall – Evapotranspiration – Deep Percolation (eg 2)

The evapotranspiration and deep percolation are negligible values to calculate during rainstorms causing landslides. Due to a steady rainfall, the evapotranspiration and deep percolation would be minimal values. Given this condition, the deep percolation and the evapotranspiration could be ignored (Fowze et al., 2012).

In Uttaradit province, for example, on May 23, 2006, landslides and flash floods occurred in Muang, Laplea and Thapla districts. According to the Department of Methodological Reports, the Intertropical Convergence Zone moved over the upper of the northern and north eastern parts on 22 May 2006, so it led to heavy rainfall conditions, approximately 263.7 mm in Muang district and 330 mm in Laplea district in Uttaradit province. Three districts were affected by landslides on 23 May 2006; Muang, Laplea and Thapla districts. The threshold of rainfall values in the past for landslide occurrences is 206.4 mm in Thapla district and 330 mm in Laplea district in 2006 (DMR, 2011a).

3.4 Digital Elevation Model (DEM) grid theme and pit filled DEM

Execution of the SINMAP model involved first processing of the DEM (fig 3.6) to determine the flow direction, the slope stability, and the specific catchment area. A brief description of the terms and procedures involved in the determinations are discussed in the following section.

Pits in digital elevation model data (DEMs) (Fig 3.6) can be set or indicated by grid elements around higher altitude values in the form of DEM without draining outward. The natural and general topography cannot be exactly shown in the DEM. These features are eliminated by using a "flooding approach" which adjusts at the elevation of each pit grid cell within the DEM to the elevation of the lowest pour point on the pit border (Jenson and Domingue, 1988), for example, the pit-filled DEM of the Thapla district (Fig 3.7).

Based on Arc GIS software, the grid DEM is shown using a raster dataset where the elevation or slope angles may be represented in digital maps of the study areas. In this study, the grid DEM in 30 metres resolution was downloaded from *www.gdem.ersdac.jspacesytems.or.jp/* and each pixel was calculated by 30 metres on the ground. The output of SINMAP is mapped and defined for the areas of potential terrain instability. The combination of SINMAP Arc map toolbar and an Arc map document of GIS create and display the topographic grid data. Then, the topographic basis of a SINMAP was defined by a DEM grid. The grid of soil and hydrological terrain parameters were classified for calibration regions.

In this study, the slope stability index was based on the 30 metres resolution of Digital Elevation Model (DEM). Three classes of stability index are presented by areas (km^2) and percentages of region: moderate to high, low to moderate and none to low. The 30 metres of each pixel of DEM are calculated on the ground (Micheal and Dixon, 1998) and presented in kilometre squares. A perspective view of the digital elevation model (DEM) of the study area is shown in Uttaradit province (Fig 3.4).

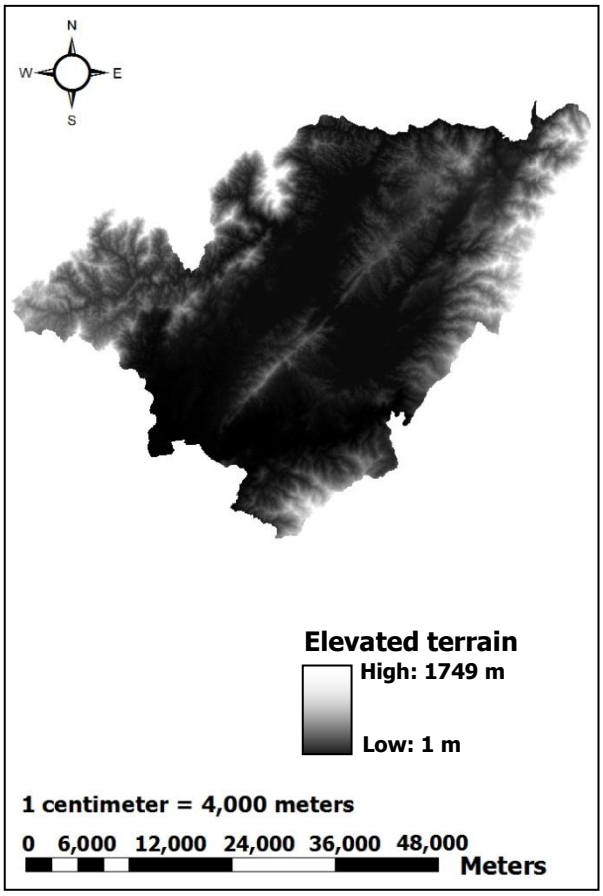

Figure 3.6 The original DEM of Thapla district

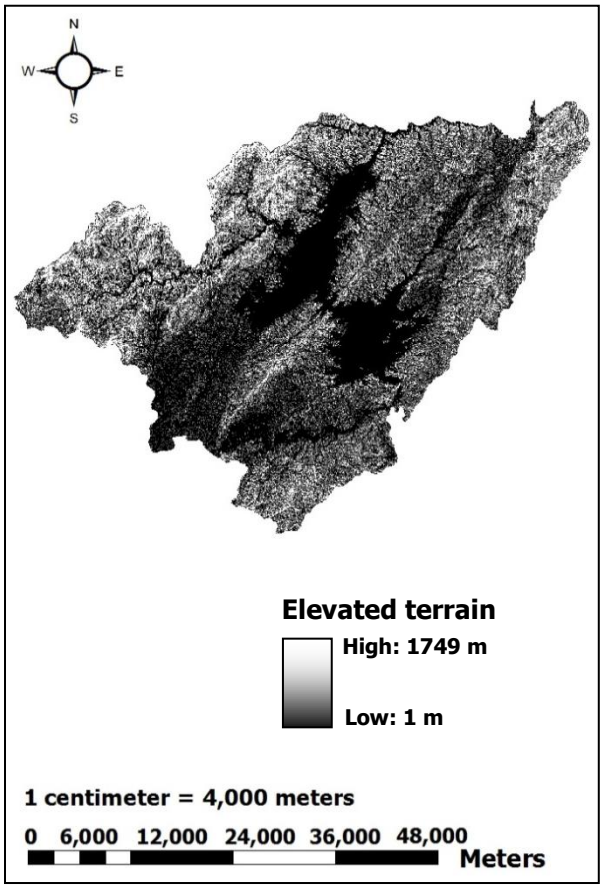

Figure 3.7 The pit fill DEM of Thapla district

3.5 SINMAP Model calibration

In the study area, several parameters are used to regionalize the geology and the land use in digital mapping data. The geotechnical parameters characterize the slope stability due to the contribution of root and soil cohesion values. The reclassification of land use is grouped by various land use types in Uttaradit province, such as slash-and-burn agriculture, rubber plantations, annual crops, galangal oil, orchards and bare lands which were surveyed by the author during December 2013. Whereas, the reclassification of vegetation was grouped by the species of vegetation types, and the root cohesion values referred to by Nilaweera (1994).

Former studies of several investigators using different techniques, including direct shear test, root strength information linked with vertical root model equations reported typical values of root cohesion, ranging from 1 kPa to 17.5 kPa (Coppin et al, 1990).

The land use surveys showed primary natural forests, slash-and-burn agriculture, annual crops, orchards and bare lands in Laplea and Thapla districts. Therefore, 0-1.1014 kPa of the range of root strength values were the best selection in this study area (Laplea and Thapla districts).

Geological data are based on previous studies; group 1: Granite rock, group 2: Extrusive and Mafic Igneous rocks, group 3: Predominantly Sandstone and Siltstone, group 4: Predominantly Shale and Mudstone, group 5: Interbedded Sedimentary rocks, group 6: Predominantly Metamorphic rock, group 7: Predominantly Carbonate rock and group 8: Quaternary deposits. The percentages of landslide events in each geological group are 11.45%, 4.23%, 10.25%, 3.05%, 22.69%, 8.28%, 7.71% and 32.34% respectively (GERD, 2013).

In this study, the geological data were grouped into eight groups, while there were two groups in Uttaradit province; group 2: Extrusive and Mafic Igneous rocks and group 6: Predominantly Metamorphic rock. Only group 2 and group 6 are classified to indicate the shear strength and the angle of friction values in each geological group in Uttaradit province. Only 4.23% of Extrusive and Mafic Igneous rock and 7.71% of Predominantly Metamorphic rock are obtained for the probability of landslide occurrences.

As for the SINMAP, variable geotechnical parameters were initially used such as the saturated permeability, strength tests, internal friction angle and soil classification. The corresponding susceptibility classes between the landslide scars and the result of the SINMAP model were compared for model calibration.

To provide samples for the geotechnical laboratory analyses, three test pit sample locations in Laplea and Thapla districts were observed and selected according to past landslide occurrences and mountainous areas. One test pit sample was selected in tambon Maephun in Laplea district: TP2 (Ban Na Kham), and two test pit samples were selected in tambon Nam Man in Thapla district: TP3 (Ban Nam Ta) and TP4 (Ban Nam Lee) because of the past landslide occurrence in 2006. A multi region polygon theme was, accordingly, divided by geological group in Table 3.4 and directly tested the soil above the rock types in the permeability and the soil density including using the techniques of consolidate drain (CD) soaked sample in the shear strength and the angle of friction in Table 3.5. In terms of the direct shear test, a consolidation stage was provided for estimating a suitable time of failure, so the rate of displacement related to the coefficient of consolidation. A consolidate drain (CD) technique requires that the consolidation is completed and the pore water pressure changes during shear are prevented by allowing draining. It requires that at least 95% dissipation of excess pore pressure should occur. The consolidation time may be long because of the soil thickness which must be drained.

The basis of SINMAP consists of the infinite slope stability and topographic wetness index and is defined by the stability index (SI). SI means the factor of safety that is a measure of the destabilizing factor (increased wetness). Thus, the consolidate drain (CD) technique is consistent with the assumption of SINMAP which defined the increased saturated trend and wetness index model (Montgomery and Dietrich, 1994).

No.	Soil types	N	E	Depth (m.)	Geology group
TP1	ML or OH	17° 48.620	100° 06.918	0.5	Group 6
TP2	ML or OH	17° 46.057	99° 58.558	0.5	Group 6
TP3	MH or OH	17° 53.151	100° 16.495	0.5	Group 6
TP4	ML or OH	17° 50.872	100° 16.459	0.5	Group 2
TP5	SM	17° 36.756	100° 43.636	0.5	Group 6
TP6	CL	18° 01.513	101° 05.410	0.5	Group 6
TP7	CL	17° 59.226	100° 53.728	0.5	-

Table 3.4 Geological data and soil types in seven test pit locations

Test Pit	Soil types	Rock group	Testing condition			
			CD Soaked Sample		Permeability(k_s) (cm/sec)	Soil density(ρ_s) (kg/m^3)
			C´ (kpa)	ø (degree)		
TP2	ML or OH	Group 6	10.30	32.23	2.918E-05	1762
TP3	MH or OH	Group 6	12.85	33.13	6.081E-06	1822
TP4	ML or OH	Group 2	16.18	28.86	1.172E-06	1916

Table 3.5 The geotechnical parameters in soil above rock types in Laplae and Thapla districts

The SINMAP model was executed initially using the results of the shear strength values (C_s) and the angle of friction values (ø) in terms of the upper and the lower values.

The complete set of parameters for the predictions are considered as equivalent to the apparent soil depth (m), the soil density (kg/m^3), the root cohesion (KPa), the soil cohesion (KPa), the angle of friction, the combined cohesion (KPa), the hydraulic conductivity (cm/sec), the transmitivity (m^2/day), the recharge (mm/day) and T/R (m). The root strength values were calculated for the upper values and no root strength values were calculated for the lower values in Laplea district in Table 3.6, while the calculation of SINMAP parameters in Thapla district were the same as in Table 3.7.

The apparent soil density value was 1762 kg/m^3 in Laplea district and the soil density value was 1822 and 1916 kg/m^3 in Thapla district. The root cohesion value of 1.1014 kPa was defined as the effect of vegetation in agricultural areas and the root cohesion value of 0 kPa was defined for bare land. The angle of friction values were 32.23° in Laplea district and 28.86°, 33.13° in Thapla district.

The hydraulic conductivity values collected by the geotechnical laboratory in Laplea and Thapla districts were 2.918E-05 and 1.172E-06, 6.081E-06 in units of cm/sec. In this calculation, the effective recharge values are equivalent to the rainfall values referred to by the landslide occurrences in 2006, in both Laplea district and Thapla district, as 330 mm and 206.4 mm respectively (DMR, 2011a).

The transmissivity unit was changed into m^2/day, and then T/R was calculated in terms of metre units. The SINMAP calculation in Laplea district (Table 3.6) gave these geotechnical parameters: the cohesion values and the angle of friction values were 11.31° and 32.23°. In terms of hydrological parameters (T/R) are 381 and soil density was 1,762 kg/m^3.

Test pit location	Geological group	Soil depth (h) (m)	Soil density (Kg/m^3)	Root Cohesion (KPa)	None-root Cohesion (KPa)	Soil Cohesion (KPa)	Combined Cohesion (KPa)	Dimensionless Cohesion	Friction Angle	Hydraulic Conductivity (ks) cm./sec	Transmitivity (m^2/day)	Recharge (mm./day)	T/R (m.)
TP2	Group 6	0.5	1,762	1.014	0	10.30	11.31	1.3192	32.23	2.9180E-05	126	330	381

Table 3.6 The calculation of SINMAP parameters in Laplea district

Test pit location	Geological type	Soil depth (h) (m)	Soil density (Kg/m^3)	Root Cohesion (KPa)	None-root Cohesion (KPa)	Soil Cohesion (KPa)	Combined Cohesion (KPa)	Dimensionless cohesion	Friction Angle	Hydraulic Conductivity (ks) cm./sec	Transmitivity (m^2/day)	Recharge (mm./day)	T/R (m.)
TP3	Group 6	0.5	1,822	1.014	0	12.85	13.86	1.437	33.13	6.081E-06	26.27	206.4	127.5
TP4	Group 2	0.5	1,916	1.014	0	17.19	16.18	1.561	28.86	1.172E-06	5.06	206.4	24.56

Table 3.7 The calculation of SINMAP parameters in Thapla district

Upper and lower thresholds were characterized by regions. The uncertainty of parameter value ranges were quantified by the probability distribution of the upper and lower values. In cohesive values, for example, the soil cohesion and root strength were set at zero for cohesionless situations (Wu and Sidle, 1995), thus the lower value of dimensionless cohesion was set at zero.

The calculation of SINMAP parameters in Thapla district, hence, are described in Table 3.7. The cohesion values were 1.561 in the upper value and the angle of friction values were 33.13º in the upper value and 28.86º in the lower value. The hydrological parameters (T/R) were 127.5 and 24.57; soil density parameters were 1822 and 1916 kg/m^3 respectively.

3.6 Landslide hazard mapping

A rainfall analysis was first used to define the probability of daily rainfall events and reporting the probability of landslide occurrences in terms of their triggering factors. Fifty-nine years of annual rainfall data (1954-2012) were recorded by the Thailand Meteorological Department (TMD) and high values occurred in 2006 and 2011. In 2006, the monthly rainfall value was high in May (600 mm) (Fig 3.8). High daily rainfall values corresponded with landslide occurrences on May 23, 2006 during the rainy season. The extreme daily rainfall was approximately 320 mm on 22rd May, 2006 (Fig.3.9), while the past landslides occurred on 23rd May, 2006 in Laplea and rainfall values was equivalent to 330 mm/24 hours (DMR, 2011a).

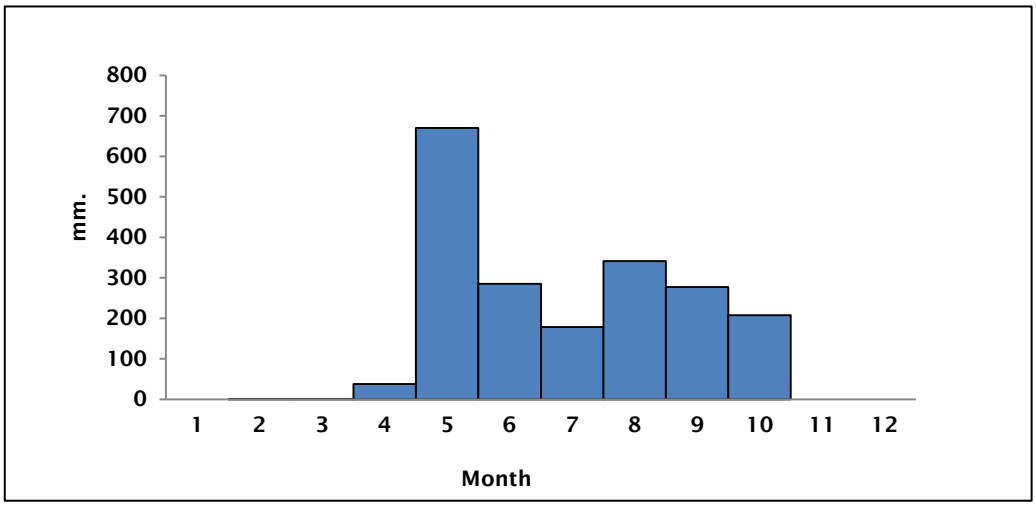

Figure 3.8 The trend of monthly rainfall in Laplea district in 2006

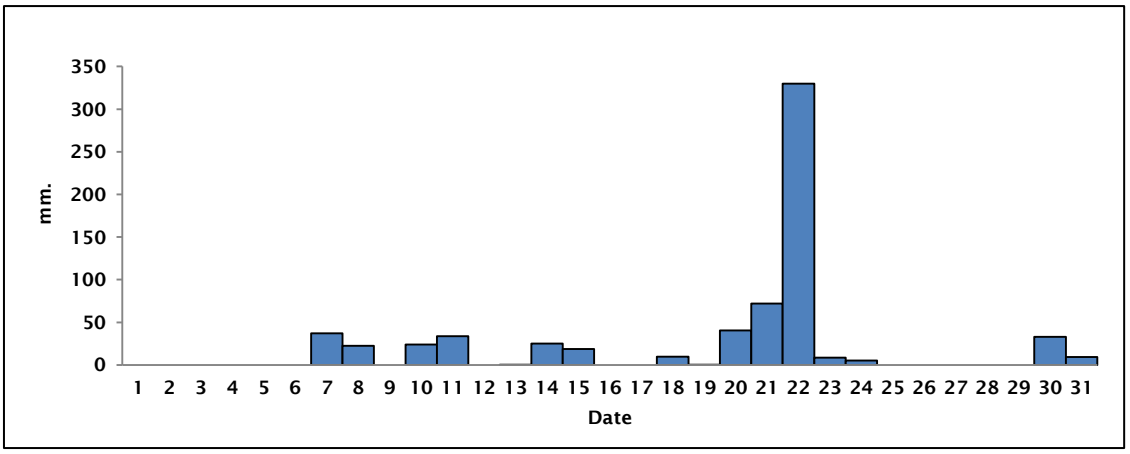

Figure 3.9 The trend of daily rainfall in Laplea district in 2006, May

The description of Thapla district was calculated into low, medium, and high risk classes in the boundary of tambons calibrated with the observed landslides falling in the high and medium classes in tambon Namman, Nang Phaya, Thafaek, Thapla and Chrim. According to the Department of Mineral Resources (DMR), the landslides which occurred in tambon Namman, Nang Phaya and Chrim destroyed approximately 110 houses in 5 villages because of approximately 206.4 mm of rainfall values on May 23, 2006 (DMR, 2011a).

3.7 Sensitivity Analysis in SINMAP model

The sensitivity of the SINMAP model is an important part in the probability of landslide assessment. The uncertainty and sensitivity of parameters are computed for each pixel and shown by areas (km^2) Furthermore, the assessment of the

sensitivity analysis directly affects the outcome of the model. The ranges of sensitivity of SINMAP parameters are calculated for the determination of the probability of stability assessment.

The rain-triggered landslide hazard analysis was actualized by the relationship between the hydrological and the geotechnical parameterizations. Thus, the sensitivity analysis of the slope stability index model was undertaken by utilizing combined geotechnical and hydrological data. Six parameters were described, analysed and manipulated by sensitivity analysis. In terms of geotechnical data, (3) the variability of soil depth, (4) permeability, and (5) the effective recharge (rainfall values) in hydrological data were presented. The sensitivity of (6) slope angle was derived from the digital elevation model (DEM) and linked with the sensitivity index of the Slope Stability Index (SINMAP) model. Available sections and descriptions in the SINMAP model are listed below.

3.7.1 Sensitivity of geotechnical data

The variable of shear strength and angle of friction values affect the slope stability index (SINMAP) model, then the shear strength values and root strength were tested for the sensitivity assessment. The variable of the dimensionless cohesion values were modelled, while the other parameter values were default. The sensitivity of the tested dimensionless cohesion (the ratio of cohesion and soil weight) parameters varied in the range of 0–1.5. The dimensionless cohesion interval was between 0.25 and 0.5, the ranges of dimensionless cohesion values considered were 0-0.25, 0–0.5, 0–1.0, 0.5–1.0 and 1.0–1.5 (Table 3.8).

Condition	Dimensionless Cohesion	Friction of Angle	Transmissivity m^2/day (h=1 m.)	T/R (R=100 mm.)
Very Soft	0 – 0.25	30 – 45	86.4	864
	0 – 0.5			
Soft	0 – 1.0			
Medium	0.5 – 1.0			
Soft Strong	1.0 – 1.5			

Table 3.8 The calculation of dimensionless cohesion in each condition in SINMAP model

Then, the angle of friction parameter values were varied in these ranges: 5º – 10º, 10º – 15º, 15º – 20º, 20º – 25º, 25º – 30º, 30º – 35º and 35º - 45º as given in Table 3.9, which included eight ranges. The angle of friction values parameters directly affects the trend of the hazard classes, while the range of 30º - 45º is default values by SINMAP software (Pack et al., 1998).

Dimensionless Cohesion	Friction Angle	Transmissivity m^2/day (k=0.00001) (cm./sec.)	H (m.)	T/R (m.)	Recharge (mm./day)
0 – 0.25	5 - 10	86.4	1.0	864	100
	10 - 15				
	15 - 20				
	20 - 25				
	25 - 30				
	30 - 35				
	35 - 45				

Table 3.9 The variability of friction angle in SINMAP model

3.7.2 Sensitivity of hydrological data

The evaluations of variable soil depths and permeability were linked with the sensitivity of the SINMAP model, including the default values of dimensionless cohesion and angle of friction values used; and the coefficient of permeability (k) was used in loam type (1E-05 cm/sec) for variable soil depths, This soil type was used to calculate in the ratio of T/R (i.e. $T = ks \times h$ and ks = the saturated permeability of the material (cm/sec), h = soil depth (m) and R = rain (mm/ 24hours)) as shown in Table 3.10.

The standard of recharge values was used in average daily rainfall values (100 mm) by the Land Development Department (LDD), 2012, for variable soil depths and permeability. The change of transmissivity values (*T)* depends on variable soil depth, computed at intervals of 0.25 – 0.5 metres as 0.25, 0.5, 1.0, 1.5, 2.0 and 2.5 metres respectively and T/R was varied by 216, 432, 864, 1,296, 1,728, and 2,160 metres, while 1.25 Kpa was selected for the lower value of cohesion because MH or OH (silt) was presented in test pit location 3 (Thapla district). Although the lowest value of MH or OH (silt) was used for dry sand (cohesionless soil) (Kangsasitiam et al., 2004), 0 Kpa was used for the lower value of cohesion. In this case, 0 Kpa cannot use the lower value of cohesion because the value of 0 Kpa was not varied for sensitivity. So, the lowest cohesion value of clay (2.5 Kpa) (Srinil et al., 2001) was divided by 2, the 1.25 Kpa of cohesion value represented

the lower value of dimensionless cohesion of silt (i.e. *C*: (Dimensionless Cohesion) = (*Cr*+*Cs*)/($h \rho_s g$): [1.25/(0.25x2.0x9.89)]) (Table 3.11), since, silt consists of organic and sedimentary clay (Kangsasitiam et al., 2004). On the other hand, the cohesive value of test pit location 3 (Thapla distric) was selected for the upper value of dimensionless cohesion(*C*) and soil density (ρ_s): 12.8 Kpa and 1,822 respectively (Table 3.7) (i.e. dimensionless cohesion (*C*) = $Cs / h \rho_s g$) as given in Table 3.11.

Furthermore, the sensitivity of permeability was varied by soil types (1E-04 – 1E-07 cm/sec) and T/R was presented by 8,640, 864, 86.4 and 8.64 metres as given in Table 3.12.

The sensitivity of the tested effective recharge parameters (ie. rainfall) values varied in 50, 100, 150, 200, 250 and 300 mm respectively. The variable recharge values have affected the changed T/R values as 1,728, 864, 576, 432, 345.6 and 288 metres respectively (Table 3.13), while the other parameters are default.

Soil type	**K**
	(cm/sec)
Gravel	**1.0-100**
Coarse sand	**1.0-0.01**
Fine sand	**0.01-0.001**
Loam	**0.001-0.00001**
Clay	**< 0.000001**

Table 3.10 The constant of the coefficient of permeability (k) values of soil type

Dimensionless Cohesion	**Friction Angle**	**Transmissivity m^2/day (k=0.00001) (cm/sec)**	**H (m)**	**T/R (m)**	**Recharge (mm/day)**
0.25 – 2.56	**30° - 45°**	**21.6**	**0.25**	**216**	**100**
0.125 – 1.28		**43.2**	**0.5**	**432**	
0.0625 – 0.64		**86.4**	**1.0**	**864**	
0.0416 – 0.42		**129.6**	**1.5**	**1,296**	
0.0312 – 0.32		**172.8**	**2.0**	**1,728**	
0.025 – 0.256		**216.0**	**2.5**	**2,160**	

Table 3.11 The variability of soil depth in SINMAP model

Dimensionless Cohesion	Friction Angle	Transmissivity m^2/day	H (m)	T/R (m)	Recharge (mm/day)
0 – 0.25	30 - 45	864 (k=1E-04 cm./sec)	1.0	8640	100
		86.4 (k=1E-05 cm./sec)		864	
		8.64 (k=1E-06 cm./sec)		86.4	
		0.864 (k=1E-07 cm./sec)		8.64	

Table 3.12 The variability of permeability in SINMAP model

Dimensionless Cohesion	Friction Angle	Transmissivity m^2/day (k=0.00001) (cm/sec)	H (m)	T/R (m)	Recharge (mm/day)
0 – 0.25	30 - 45	86.4	1.0	1,728	50
				864	100
				576	150
				432	200
				345.6	250
				288	300

Table 3.13 The variability of recharge (rainfall values) in SINMAP model

3.7.3 Sensitivity to initial: The digital elevation model

Given the slope angle values of hilly terrain, the digital elevation model (DEM) with a resolution of 30 metres was used. Based on Arc GIS software, the grid DEM which was downloaded from *www.gdem.ersdac.jspacesytems.or.jp/* was shown using a raster dataset where the elevation or slope angle may be represented by the hilly elevation from 1metre to 1,749 metres in digital maps of the study areas. In Arc GIS 10.1, the slope angles are classified into six angle ranges: 0° – 5°, 5° – 10°, 10° – 15°, 15° – 25°, 25° – 35° and 35° – 65° in Uttaradit province. Accordingly, the stability index, SI, which is equivalent to the factor of safety, FS, can be divided into three classes. Fowze (2012) estimated three hazard classes based on six classes of stability definition. In this study, the slope angle falls into three: high, medium and low hazard classes, 25° - 65°, 10° - 25° and 0° -10° respectively. These slope angle ranges of the hilly terrains in Uttaradit province are presented for sensitivity assessment. With some other parameters, the slope angles are variable, but the shear strength, angle friction, permeability, soil depth and rainfall values are default as given in Table 3.14.

Dimensionless Cohesion	Friction Angle	Transmissivity m^2/day (k=0.00001) (cm/sec)	h (m)	T/R (m)	Recharge (mm/day)	Slope angle
0 – 0.25	30 - 45	86.4	1.0	864	100	0° -10°
						10° - 25°
						25° - 65°

Table 3.14 The variability of slope angle in SINMAP model

3.8 Calibration of present day conditions

Average annual daily rainfall data are used herein during the 1954-2012 period as recorded by the Thailand Meteorological Department (TMD) in Uttaradit province. One hundred and twenty-one rain gauges cover seventy-six provinces of Thailand. Rainfall distribution is described by calculation using nine rain stations covering eleven provinces of Uttaradit: Tak, Pisanulok, Khon kean, Udontani, Lampang, Petchaboon, Phrae, Loei, but there are no complete rainfall values in two rain stations in Sukhothai and Nong Bao Lum Phu. There are nine rain stations which related to the downscaling of the daily precipitation scenario in the future simulation from latitude 16° 26′and 18° 37′ north and between longitude 98° 52′ and 103° 05′ east in SDSM software (Fig 3.10). In general, the rainfall values are usually high in the rainy season (mid-May to October), but this approach calculates the wet days all through the year, due to the probability of landslide occurrences corresponding to heavy rainfall not only in the rainy season but also in other seasons

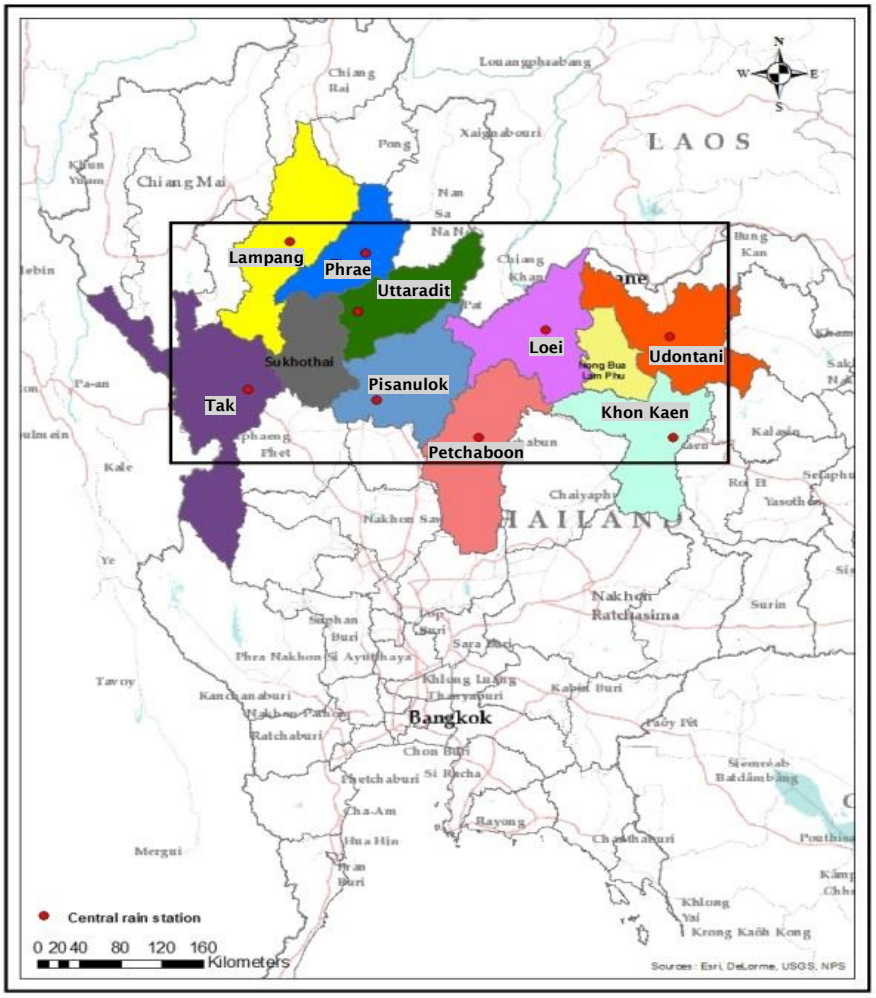

Figure 3.10 Downscaling by SDSM in the northern and northeastern parts of Thailand

3.8.1 Data preparation

The Uttaradit province is defined by using digital topographical maps, which show the specific form of slope angle associated with hilly terrains in the nine districts of Thapla, Laplea, Muang, Nampat, Phichai, Bankhok, Faktha, Thongsaengkhun and Tron in Uttaradit province. The landslide inventory points themes were linked with past landslide occurrences. In this study, the Global Positioning System (GPS) technique was used to provide the geospatial position of the past landslide inventory points theme, on 23 May 2006 in Thapla, Laplae and Muang districts and on 9 September 2011 in Nampat district, the same location of soil sampling.

The evapotranspiration and deep percolation are negligible values to calculate during rainstorms causing landslides. The threshold of rainfall values are analysed, with hydrological data described by the rainfall value rates. The rainfall values should be calculated for the wet time period for the landslide analysis (defined as mm of rainfall per twenty-four hours), in the SINMAP software

(Montgomery and Dietrich, 1994). The rainfall calculation was a consideration of both daily rainfall and three-hourly rainfall (Fig 3.11). Both daily rainfall and three-hourly rainfall during 1981-2010 are used to calculate the standard hours of daily rainfall. Three hourly data observed rainfall values obtained at the times: 1am, 4 am, 7am, 10am, 1pm, 4pm, 7pm and 10pm (Thai Meteorological Department) and are used to calculate three-hourly rainfall rates for the nine rain stations: 351201 (Uttaradit province), rain station 376201 (Tak province), rain station 378201 (Pisanulok province), rain station 381201(Khon Kaen province), rain station 354201 (Udontani province), rain station 328201 (Lampang province), rain station 379201 (Petchaboon province), rain station 330201(Phrae province) and rain station 353201 (Loei province). In terms of extreme rainfall indices, a wet day is defined as a day that has a rainfall amount greater than or equal to 1 mm (Maijandee et al., 2014). Figure 3.11 shows the processing steps in the rain analysis.

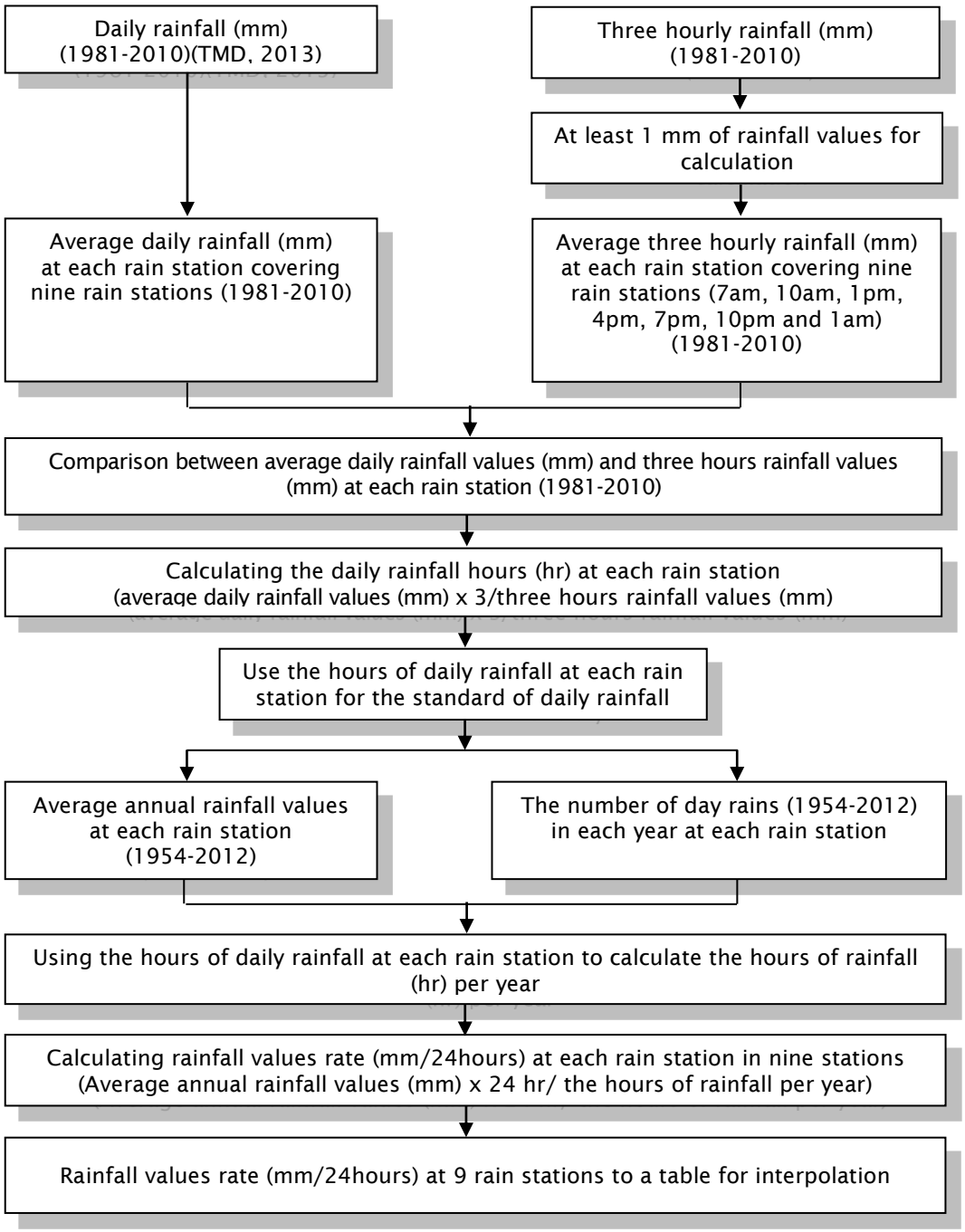

Figure 3.11 Methodology of rainfall values analysis

Over the baseline period 1954 to 2012, for nine central rain stations covering nine provinces, the mean annual rainfall was approximately 1,404.9 mm for Uttaradit, 1,036.9 mm for Tak, 1,352.6 mm for Pisanulok, 1209.1 mm for Khon Kaen., 1,414.1 mm for Udontani, 1059.9 mm for Lampang, 1142.2 mm of Petchaboon, 1099.4 mm for Phrae and 1,241.1 mm for Loei respectively. During the period 1981 to 2010, average three-hourly rainfall values are described for each rain station over the nine provinces as shown in Table 3.15.

Province	1 am	4 am	7 am	10 am	1 pm	4 am	7 am	10 pm	Average
Uttaradit	8.67	8.89	7.11	6.00	5.36	7.20	8.40	8.36	**7.86**
Tak	6.26	6.11	6.05	5.26	5.02	7.36	7.67	6.46	**6.57**
Pisanulok	8.25	7.87	7.17	6.69	6.46	7.10	8.86	8.79	**7.65**
Khon Kaen	9.33	8.28	7.62	6.26	7.16	9.08	9.03	10.26	**8.80**
Udontani	9.13	8.83	9.04	6.47	7.83	7.64	8.71	9.20	**8.77**
Lampang	7.48	6.85	6.08	6.11	5.44	6.46	8.40	7.31	**7.65**
Petchaboon	7.41	7.16	5.96	6.35	5.52	6.76	6.38	7.49	**6.93**
Phrae	7.84	7.53	6.67	5.65	5.33	6.42	7.79	6.71	**6.75**
Loei	8.30	6.82	7.67	6.98	6.51	8.83	9.06	8.57	**7.84**

Table 3.15 Average three hourly rain (mm) per day from 1981 to 2010

The relationship between average three-hourly rainfall and daily rainfall values (mm) are used to calculate the hours of daily rainfall over nine rain stations in Table 3.16, then the hours of annual rainfall will be calculated with annual rainfall values and describe a rainfall rate (mm/24 hours). Then, nine rain stations covering nine provinces will be averaged by the interpolation approach and represented by the rainfall value rates in mm/24 hours in Uttaradit province.

The interpolation is used for this case because there is only one central rain station in Uttaradit province. The achievement of interpolation which is a part of Arc GIS, is used to estimate the rainfall values, so the average rainfall thresholds are from nine provinces: Tak, Pisanulok, Khon Kaen, Udontani, Lampang, Petchaboon, Phrae, Loei including Uttaradit.

Province (rain station)	Average three hourly rain from 1981-2010 (mm)	Average daily rainfall from1981-2010 (mm)	Average hours rainfall per a day (hours)	The number of day rain per a year (day)	The number of standard days rain per a year (day rain: accumulated rain within 24 mm)
Uttaradit(351201)	7.86	11.56	4	117	19days
Tak(376201)	6.57	10.66	4.5	100	18days
Pisanulok(378201)	7.65	10.95	4	119	19days
Khon Kaen(381201)	8.8	11	3.5	108	15days
Udontani(354201)	8.77	10.86	3.5	123	18days
Lampang(328201)	7.65	9.5	3.5	114	16days
Petchaboon(379201)	6.93	9.0	4	120	20days
Phrae(330201)	6.75	9.27	4	113	18days
Loei(353201)	7.84	9.69	3.5	129	18days

Table 3.16 The calculation of rainfall rate covering nine provinces

3.8.2 Landslide hazard mapping

The 1954-2012 period is used for the baseline of rainfall data at the present calibration, and the period 2013-2099 is used for future simulation. Two time series will be input in the SINMAP program in terms of hydrological data and a comparison made between the present calibration and the future simulation for landslide hazard mapping of Uttaradit province.

For the period 1954-2012, the mean annual rainfall (mm) covering the nine central rain stations noted above was calculated in rainfall mm/24 hours in Uttaradit, Tak, Pisanulok, Khon Kaen, Udontani, Lampang, Petchaboon, Phrae and Loei as 73.94 mm, 57.61 mm, 71.18 mm, 80.6 mm, 78.56 mm, 66.25 mm, 57.11 mm, 61.07 mm, and 73.94 mm respectively.

Then, the distribution of rainfall occurrences was used for analysis in the nine districts in Uttaradit province by interpolated mapping. The rainfall rate (mm/24 hours) above, described by interpolated mapping, was obtained for each district in Uttaradit province and inputted into the hydrological part of SINMAP software

covering the nine districts of Phichai, Bankhok, Faktha, Laplea, Muang, Nampat, Thapla, Thongsaengkhun and Tron. Then, SINMAP output will be mapped by a DEM grid of both soil and hydrologic data so that the areas of potential terrain instability or high hazard classes (km^2) can be defined.

3.9 The future simulation

The General Circulation Model (GCM) describes the relationship between the rising greenhouse gasses and climate conditions at a global and regional scale. But the GCM cannot extend to describe climate change conditions at the local scale, as it displays at too coarse a spatial resolution. Therefore, the simulation of the Regional Climate Model (RCM) is useful to assess the impact of climate change at the local scale.

For climate change in Thailand, the future climate scenarios are simulated at both spatial and temporal scales. The precipitation input is needed to predict for future climate, and the Statistical Downscaling Model (SDSM), was used to assess the simulation scenario of future change for latitude 16^{o} 26 $'$ and 18^{o} 37 $'$ north and between longitude 98^{o} 52 $'$ and 103^{o} 05 $'$ east in the SDSM software as given in (section 3.8) Fig 3.10. The baseline period of observed daily rainfall data (mm) 1961-1990 was generated for SDSM calibration for each of the nine central rain stations.

3.9.1 Statistical Downscaling Model (SDSM)

The modelled rainfall data is obtained by the SDSM program, HadCM3 and CGCM2 will be analysed by the grid cell at the National Centre for Environment Prediction (NCEP). Over the period 1961-2099, the daily predictor values are generated by HadCM3 and CGCM2 under simulation scenario A2 and B2. The highest rise of carbon dioxide is presented for simulation scenario A2, while B2 scenario is more ecologically friendly as noted above. The appropriate software for these is SDSM 4.2 consisting of seven core procedures, along with the UKSDSM data achievement and recommendation. The conditional mode is identified for the daily precipitation amount in the downscaled SDSM process, while the unconditional mode is set for temperature. The annual mode is used for the model type (Wilby and Dawson, 2007).

a. The quality control and the data transformation

Nine meteorological stations in nine Provinces have 100% complete and accurate daily rainfall data sets, used from 01/01/1961 to 31/12/1990.

b. Screening of downscaling predictor variables

This procedure describes that the predictor variables are chosen in the predictor description window and the default dates of the screen variables are set at the start and end dates (1961-1990). Otherwise, the conditional mode is selected for determining the daily precipitation amount in the downscaled SDSM process.

c. SDSM calibration

The SDSM calibration process involves setting the time period of rainfall, the start and end dates might be changed in the screen setting, the period 1961-1990 are the default dates. In this study, observed daily rainfall values should be used to generate the predicted rainfall data covering the nine central rain stations over nine provinces. The conditional mode is selected for determining the daily precipitation amount in the downscaled SDSM process. The 1961-1990 period is selected for the SDSM calibration set, as well as the conditional mode for residual analysis, the annual mode is selected for the model type. It is found that the annual modelled rainfall values are best correlated with annual observed rainfall values and the annual modelled rainfall values are used for the prediction from 2013 to 2099.

d. Weather generator

The weather generator operation defines the ensembles for a synthetic daily weather series. The ensemble members are needed to consider the equally possible local climate scenarios that are identified by a regional scale predictor. The default of the ensemble size is 20 and the maximum ensemble size is 100. In this case, the 100 member ensembles of synthetic rainfall time series are suitable for analysis.

e. Data analysis

SDSM provides the determination of both downscaled scenarios and observed climate data with the summary statistics and frequency analyses. The SDSM is performed in the summary statistics and diagnoses both observed and synthetic

data, including the variable mean, maximum, minimum, variance, percent wet-days and wet/dry days, spell lengths computed on a monthly, seasonal, annual basis. In terms of percentage, wet days and maximum wet spell periods are selected for this case.

f. Frequency analysis

The frequency analysis is plotted by the distribution of diagnostics for both modelled and observed data. The quantile-quantile plot is presented for comparison between modelled data and observed data files. In this case, the quantile-quantile plot of daily rainfall (downscaled from HadCM3) is present for the period of 1961-1990.

g. Scenario generation

The scenario generation operation creates the ensemble of synthetic daily weather. The daily rainfall predictors are supplied by a GCM, in this study, HadCM2 and HadCM3 have a year's length of 360 days and predict from 1961to 2099 for both scenarios A2 and B2.

3.9.2 The result of downscaled future climate precipitation by SDSM

Over the period 1961 – 2012, the comparison between observed annual rainfall and modelled annual rainfall is presented by graphs (Chapter 5) (Section 5.2.1) in nine rain stations in nine provinces. Over the 1961-2012 period, the gap between observed and modelled annual rainfall was approximately 3-10% yearly for each of the nine rain stations. The 100 member ensembles of synthetic rainfall time series and threshold 0.2 are indicated for the best condition in SDSM software (Kalanay et al., 1996).

Only 360 daily rainfall values per year were forecasted by the SDSM program. Over the period 2013-2099, the number of predicted wet periods covering nine central rain stations in nine provinces is the same as the present calibration. The wetness of daily rainfall occurrences is described for the SINMAP program. Although the rain gauge is located in a central district in each of the nine provinces, it represents the best available record characterising each province.

The average annual rainfall is used to calculate the rainfall rate (mm/24 hours). The number of wet days (here defined as the number of standard rainy hours from 1981 to 2010) is used to calculate wet days per year in the annual rainfall

values in each rain station for future climate simulation (2013-2099). The unit should be set to define (mm) rainfall within twenty-four hours in the SINMAP program. The average rainfall of mm/24 hours during 2013-2099 will be described in nine central rain stations covering nine provinces, and rainfall values will be averaged by the Interpolation approach as shown by the rainfall data on the map (Chapter 5)(Section 5.5.2). The mm/24 hours rainfall values are presented on the map in Uttaradit province.

3.9.3 Southeast Asia START Regional Centre

The future climate projection was forecasted by the Southeast Asia START Regional Centre (Southeast Asia region on climate change impact) for simulation scenarios A2 and B2. The dataset describes long periods of climate conditions represented by the changing of greenhouse gases, such as carbon dioxide. The database must describe a multi-annual time period. It cannot specify an annual cycle alone.

The model uses a grid size of 20x20 km. In this study, both latitude and longitude were indicated in each province covering nine provinces of Uttaradit, Tak, Pisanulok, Khon Kaen, Udontani, Lampang, Petchaboon, Phrae and Loei as given in Fig 3.12.

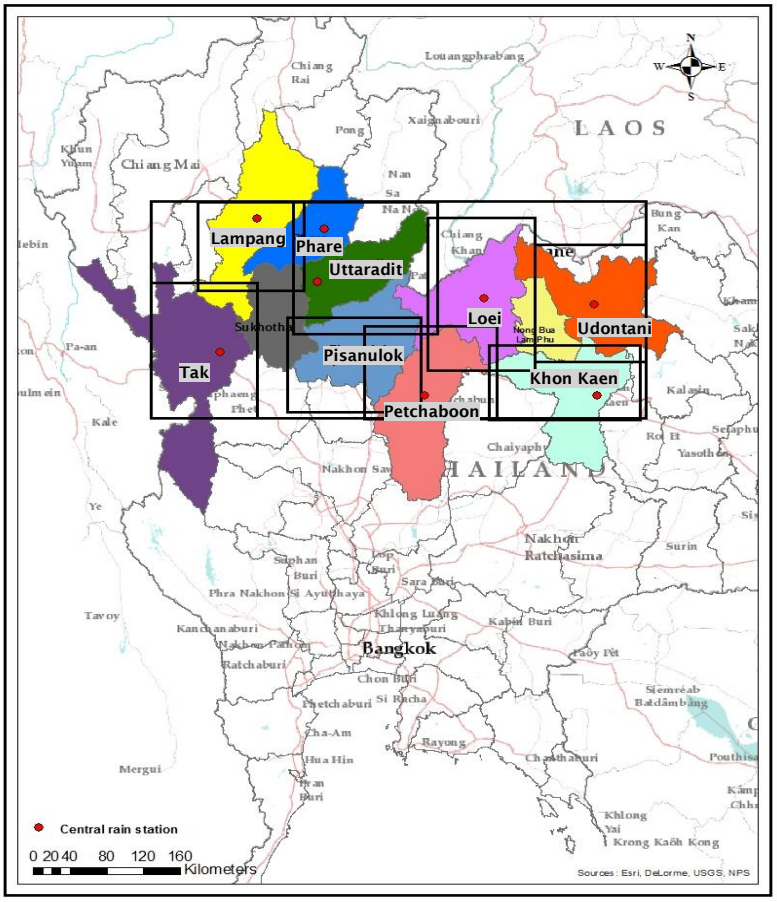

Figure 3.12 Latitude and longitude in each province covering nine provinces by START

Daily rainfall data, only 360 days per year, was verified by START from 1961 to 2099 under simulation scenario A2 and B2. Daily data, forecasted by START, consist of precipitation (mm), wind speed (m/s), wind direction (degree from north and solar radiation (w/m^2), Tmax (c^o) and Tmin (c^o). In this study, the precipitation data (START) was used to correlate with SDSM graphically in terms of annual rainfall during the 1961-2099 period, whereas observed annual rainfall was described by graphs, during 1961-2012 (section 3.9.5). In addition to the number of hours of daily rainfall (defined using the three hours data) from 1981 to 2010, the number of these wet time periods is used to calculate the rainfall rate (mm/24 hours) in the period 2013-2099 for each rain station.

3.9.4 The result of downscaled future climate of precipitation

For the period 1961-2012, observed rainfall was a baseline for calibration in SDSM and START software covering nine rain stations in the nine provinces of Uttaradit, Pisanulok, Loei, Tak, Khon Kaen, Phrae, Udontani, Lampang and Petchaboon in the northern and northeastern parts of Thailand between latitude 16^o 26 $'$ and 18^o 37 $'$ north and between longitude 98^o 52 $'$ and 103^o 05 $'$ east. This

ensemble was used to compare observed and modelled annual rainfall during the 1961-2099 period for both climate scenarios A2 and B2. The SDSM output, derived from the HadCM3 model, was chosen for precipitation prediction during the period 1961-2099 under simulation scenarios A2 and B2, whilst, the climate change data in Southeast Asia are assessed by the Southeast Asia START Regional Centre (supported by the Hadley Centre), especially the precision of software, PRECIS and GCM datasets are downscaled in a regional climate model (START, 2012). The precipitation data predicted by START and SDSM are described by graphs (Chapter 5) (Section 5.2.1) covering the nine rain stations.

During the period of 2013-2099, the annual precipitation of climate scenario A2 and B2 were represented by graphs for both SDSM and START. Then, the observed annual rainfall during 1961-2012, and the annual rainfall volumes of both START and SDSM during 1961-2099 will be represented by nine graphs in each rain station in nine provinces as rain station 351201 (Uttaradit province), rain station 376201 (Tak province), rain station 378201 (Pisanulok province), rain station 381201(Khon Kaen province), rain station 354201 (Udontani province), rain station 328201 (Lampang province), rain station 379201 (Petchaboon province), rain station 330201(Phrae province) and rain station 353201 (Loei province).

3.9.5 Landslide hazard mapping

The distribution of rainfall events will be used to analyse in the nine districts in Uttaradit province by interpolation, the average and intense rainfall values which are presented on the interpolated map. The rainfall values (mm/24hours) will focus on the Uttaradit province and will be presented in each district: Muang, Laplea, Thapla, Nampat, Bankhok, Faktha, Thongsaengkhun, Phichai, and Tron.

Finally, this chapter consists of calibration and sensitivity of SINMAP, geotechnical laboratory, change in rainfall condition under present-day conditions and in the future simulation. Both calibration and sensitivity are confirmed for accuracy of SINMAP parameters. The technique of geotechnical laboratory is applied for the SINMAP model. Both SDSM and START techniques are used to downscale in the north and north-eastern part of Thailand. The change in rainfall condition in each district in Uttaradit province is used to analyse the landslide risk both under present-day conditions and in the future simulation. Thus, the risk areas under present-day

conditions and in the future simulation are presented by the landslide hazard mapping.

CHAPTER 4 CALIBRATION AND SENSITIVITY OF SINMAP MODEL

This chapter is divided into two sections. The first section presents the setup and calibration of the SINMAP model through comparison between landslide areas of the SINMAP output and past landslides in 2006 in Laplea and Thapla districts in Uttaradit province. The second section describes analysis of the sensitivity of the SINMAP model parameters: dimensionless cohesion, angle of friction, soil thickness, permeability, rainfall and slope angles are varied and output is shown by the zonation of hazard classes (km^2).

4.1 Calibration of SINMAP model

Calibration is used to show the relationship between the past landslides (landslide scars which show the areas) and the three hazard class areas: high, medium and low (calculated by SINMAP software) in terms of square kilometre units. The past landslide, on May 23, 2006, occurred in tambon Maephun in Laplea district and tambon Namman, Nang Phaya and Chrim in Thapla district. Approximately 330 mm of rainfall over 24 hours occurred in Laplea district and about 206.4 mm of rainfall in Thapla district (DMR, 2011) a, both observed rainfall values were used for standardizing the calibration model. The landslide scars were also used for calibration only in tambon Maephun in Laplea district and in tambon Namman in Thapla district because data was only available for these two tambons.

The Department of Mineral Resources (DMR) presented the boundary of landslide scars in a polygon shape in both tambons Meaphun and Namman. The landslide scars were obtained from satellite images, after landslides occurred and the boundaries of the landslide scars were calculated in terms of square kilometres (DMR, 2006).

As for SINMAP, the geotechnical data: soil depth (m), the soil density (kg/m^3), the combined cohesion (KPa)_(the root & the soil cohesion), the angle of friction, the hydraulic conductivity (permeability: cm/sec) and hydrological data (the transmitivity: m^2/day), the rainfall (mm/day)) were modelled for the resulting zonation risk (Table 3.6 and Table 3.7). The exploration of soil and land cover/land use in the past landslide areas (tambon Maephun and Namman) were considered in this analysis. Most of the agricultural areas noted in the field during December 2013 were on mountainous and hilly terrains in tambon Maephun in Laplea district and in tambon Namman in Thapla district, showing annual crops and orchards.

The SINMAP output was divided into three Stability Index (SI) ranges of hazard classes: 0-1 (high hazard classes: failure region), 1-1.5 (medium hazard classes: instability) and >1.5 (low hazard classes: safe areas) High hazard classes would refer to failure regions.

The digital elevation model (DEM) with a resolution of 30 metres was used in SINMAP, to show the slope angle values of hilly terrain in Laplea and Thapla districts (1 pixel is equal to 900 m^2 on the ground), six ranges of slope gradients were classified by Arc GIS: 0^o – 5^o, 5^o – 10^o, 10^o – 15^o, 15^o – 25^o, 25^o – 35^o, 35^o – 65^o. Then, the six ranges were condensed to three ranges: flats (0^o – 10^o), low slopes (10^o – 25^o) and steep slopes (25^o – 65^o). Tepparnich (2010) surveyed the range of slope gradients in Uttaradit province and classified them as low slopes (slope angle of < 25^o) and steep slopes (slope angles of 45^o and 60^o) of hilly and mountainous areas, showing 0.5 – 1 metre deep past shallow landslides. Therefore, in this study, slope gradients of both 10^o – 25^o and 25^o – 65^o were selected for low slopes and steep slopes respectively, while slope gradients of 0^o – 10^o were considered to flats.

As for calibration, the comparison of landslide scars overlapped with slope gradients of steep slopes (25^o – 65^o), low slopes (10^o – 25^o) and flats (0^o – 10^o) and the output of SINMAP (high, medium and low hazard classes) was considered in terms of areas (km^2).

Both slope gradient and SINMAP output areas were calculated at a resolution of 30 metres within the DEM with each pixel equal to 900 square metres. The edge calculation is neglected for the output of SINMAP areas, the hazard class areas on the ground are less than 30 metres in each pixel, which was also reported by Michael and Dixon, (1998). Michael and Dixon, (1998) tested the SINMAP model. The upper Weiser River area in the central west of Idaho State, USA was used for the study site. In this case, the 30 metres resolution of the DEM was used for the SINMAP model, so each pixel represented a 30 metre square on the ground. But the 30 metres pixel size cannot exactly represent ground slopes on fill, cuts, and slopes directly adjacent to a stream. Therefore, the areas under SINMAP software were less than 30 metres on the ground.

In this study, the real areas of GIS on slope gradients were compared with the SINMAP output. The landslide scar areas were calculated both by GIS software and SINMAP output in tambon Maephun in Laplea district. Therefore, the landslide

scar areas according to GIS software and by SINMAP output were 31.8 km^2 and 26.79 km^2 respectively. The landslide scar areas according to the GIS software were higher than the SINMAP output: approximately 15.7% as shown in Fig 4.1 – Fig 4.2.

A) GIS

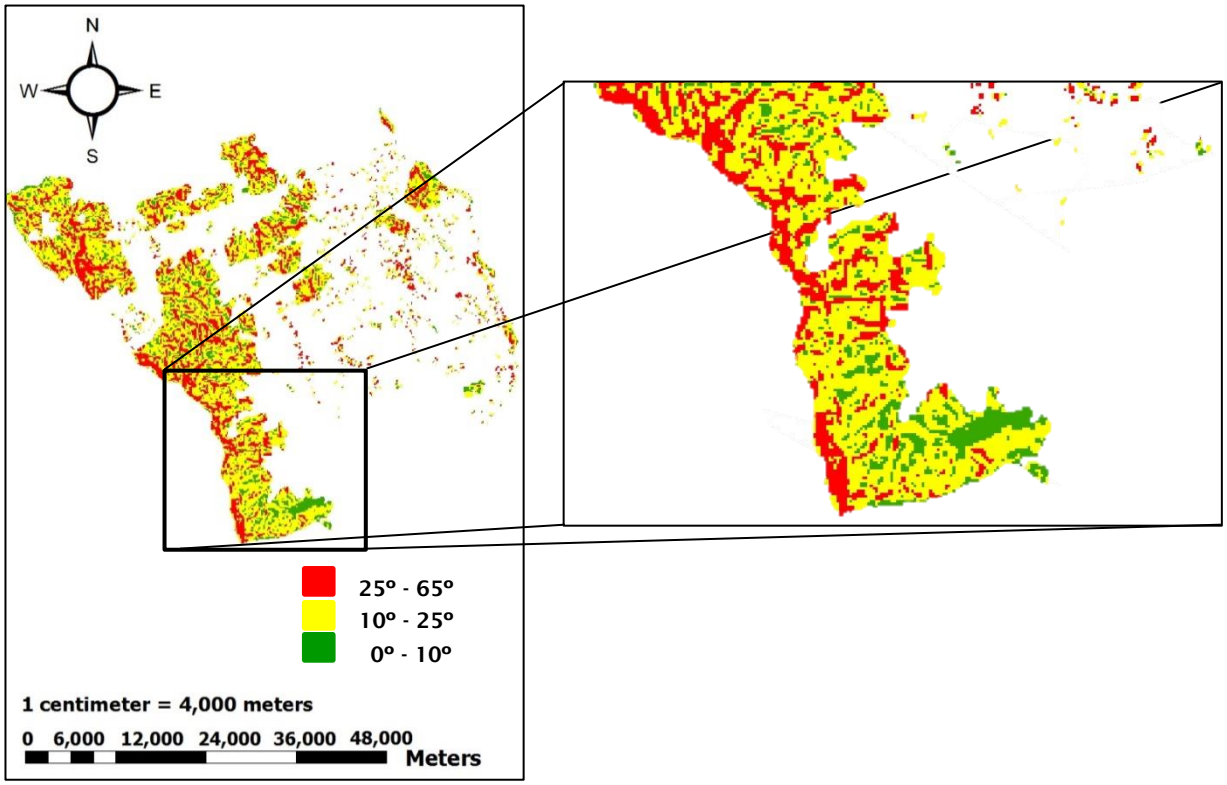

Figure 4.1 The comparison of landslide scar between the neglected edge calculation for the output of SINMAP areas, showing the neglected ground slopes on fill, cuts, and slopes directly adjacent to a stream in the cycle (left) and the edge calculation for the slope gradients area according to GIS software, showing the ground slopes on fill, cuts, and slopes directly adjacent to a stream in the square (right)

B) SINMAP

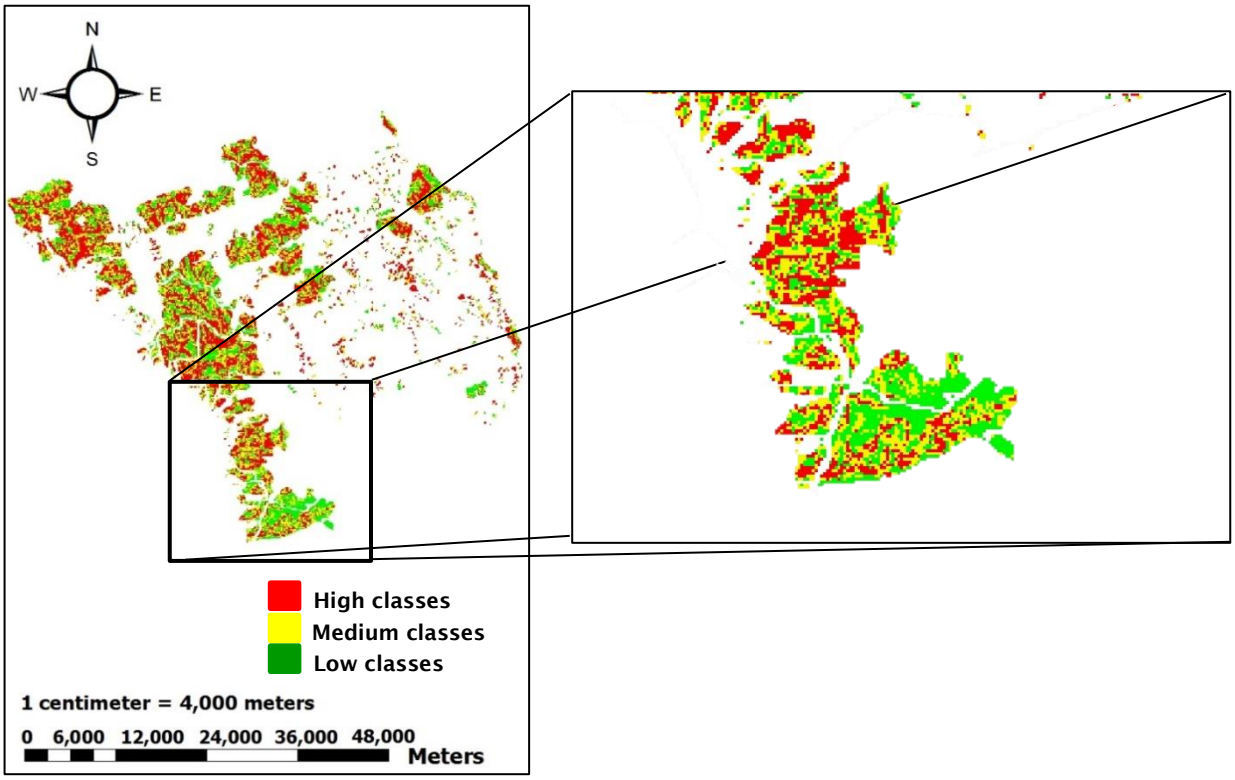

Figure 4.2 The comparison of landslide scar between the neglected edge calculation for the output of SINMAP areas, showing the neglected ground slopes on fill, cuts, and slopes directly adjacent to a stream in the cycle (left) and the edge calculation for the slope gradients area according to SINMAP software, showing the ground slopes on fill, cuts, and slopes directly adjacent to a stream in the square (right)

Areas by SINMAP output (hazard classes)		Areas by GIS software (slope gradients)	
pixel	Km^2	pixel	Km^2
29767	26.79	35332	31.8

Table 4.1 The comparison of landslide scar areas between the calculation of the SINMAP output and the calculation of GIS software

For the calibration, the landslide scar areas, both SINMAP output (hazard classes) and GIS software (slope gradients), were compared with all tambon Maephun areas as follows:

4.1.1 The result of calibration in Laplea district

a) The results of SINMAP output areas between landslide scar areas and all the area of Laplea district were calibrated.

The output of SINMAP is presented for high, medium and low hazard classes: high class areas occurred in three tambons: Maephun, Nanokkok and Failuang. The past landslides occurred only in tambon Maephun in 2006 because the southwest monsoon approached on the western side of the study area. The southwest monsoon led to heavy rainfall in the western part of Laplea district, so the landslides occurred only in tambon Maephun. Therefore, this tambon was used for calibration. The output of SINMAP areas presented for high, medium and low hazard classes and the GIS software areas presented the range of slope gradients: steep slopes, low slopes and flats which both corresponded to the landslide scar areas in tambon Maephun in Laplea district (DMR, 2011).

According to DMR (2006), the total of landslide scar areas was 34.3 km^2, while the landslide scar areas of SINMAP output in tambon Maephun is approximately 26.8 km^2, because some part of the mapped landslide scar areas were in Sukhothai province: about 7.5 km^2 (an area outside this study) (Fig 4.3). Approximately 11.24 km^2 (41.9%), 8.77 km^2 (32.8%) and 6.78 km^2 (25.3%) of landslide scar areas are found in the high, medium and low hazard classes respectively as given in Table 4.2. In addition, 41.04 km^2 (35.3%) of high, 40.69 km^2 (35.0%) of medium and 34.53 km^2 (29.7%) of low classes were presented in all areas of tambon Maephun as shown in Table 4.2. Some parts of high, medium and low hazard class areas did not overlap with the landslide scars (Fig 4.3). The comparison of hazard level areas: high, medium and low classes in the landslide scar areas and hazard level areas: high, medium and low classes in all areas of tambon Maephun are shown in Table 4.2.

Three hazard class areas in boundary of landslide scar					**Three hazard class areas in boundary of tambon Maephun**				
Stability Index (SI)	**Hazard classes**	**Pixel**	**Sq.Km.**	**Percentage**	**Stability Index (SI)**	**Slope gradient**	**Pixel**	**Sq.Km.**	**Percentage**
0-1	**High**	**12486**	**11.24**	**41.9**	**0-1**	**High**	**45600**	**41. 04**	**35.3**
1-1.5	**Medium**	**9747**	**8.77**	**32.8**	**1-1.5**	**Medium**	**45211**	**40.69**	**35.0**
More than 1.5	**Low**	**7534**	**6.78**	**25.3**	**More than 1.5**	**Low**	**38366**	**34.53**	**29.7**
Total		**29767**	**26.79**	**100**	**Total**		**129177**	**116.3**	**100**

Table 4.2 The comparison of three hazard classes of SINMAP output areas in the landslide scars and in tambon Maephun in Laplea district

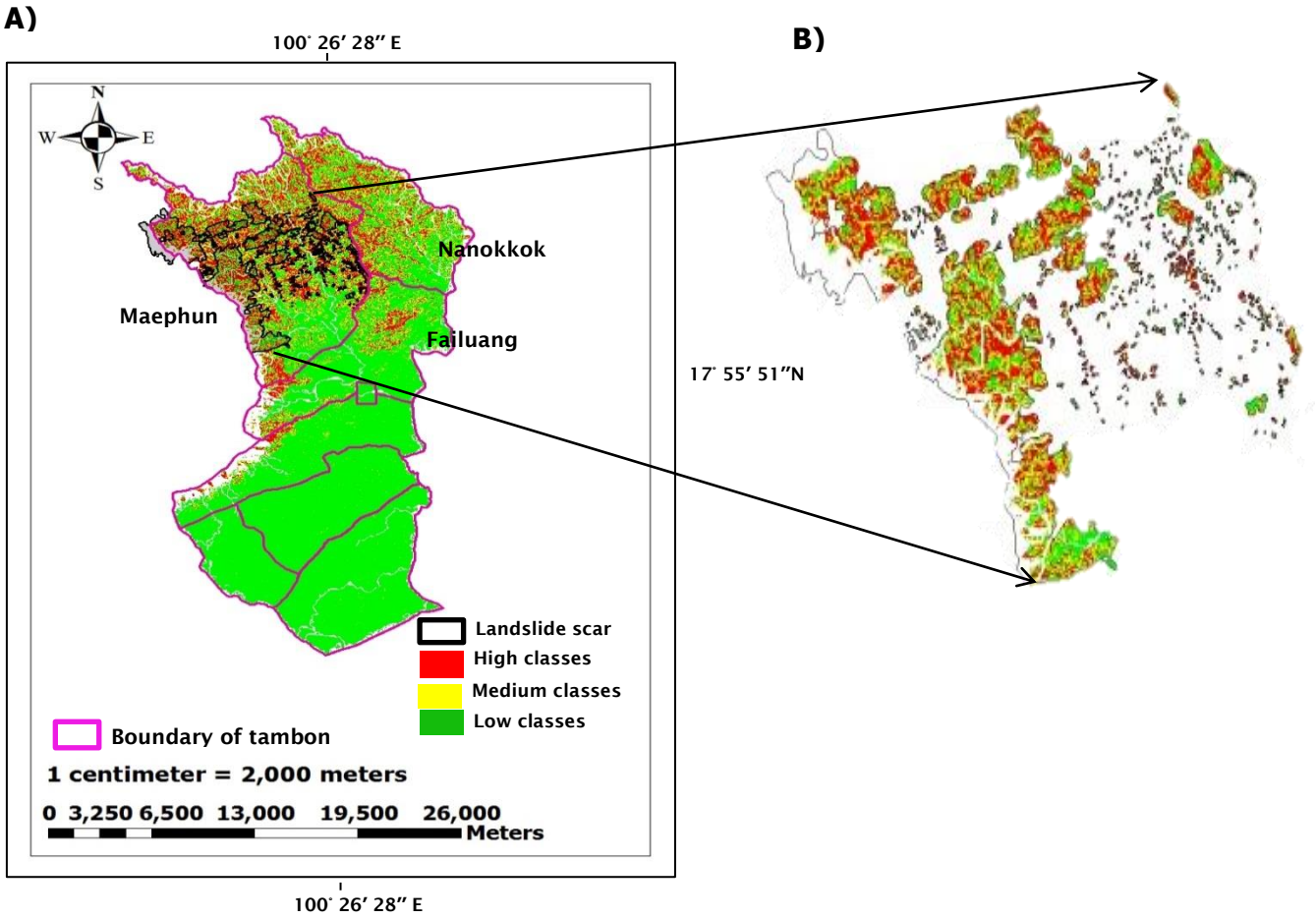

Figure 4.3 Landslide scars covering three hazard classes: high, medium and low and in tambon Maephun, showing the landslide scar areas (on the right) and three hazard classes: high, medium and low in all areas of Laplea district (on the left)

b) The results of the slope gradient areas between landslide scar areas and all areas of Laplea district were calibrated. The landslide scar areas were presented by GIS software: about 31.8 km^2 in tambon Maephun. Table 4.3 showed that the areas of slope gradient of steep slopes (25° – 65°), low slopes (10° – 25°) and flats (0° – 10°) present in tambon Maephun.

According to DMR (2006), the total of landslide scar areas was 34.3 km^2, while the landslide scar areas according to GIS software in tambon Maephun is approximately 31.8 km^2, because some part of the landslide scar areas were in Sukhothai province: about 2.5 km^2 (an areas outside this study) (Fig 4.4). Approximately 8.93km^2 (28.1%), 18.84 km^2 (59.3%) and 4.03 km^2 (12.6%) of landslide scar areas are found in the steep slopes, low slopes and flats respectively as given in Table 4.3. Furthermore, 29.9 km^2 (22.8%) of steep slope, 74.6 km^2 (56.8%) of low slope and 26.8 km^2 (20.4%) of flat areas are presented in

all areas of tambon Maephun as shown in Table 4.3. As a result, some areas of slope gradients: steep slopes, low slopes and flats were not overlapped by the landslide scars. The comparison of slope gradient areas: steep slopes, low slopes in the landslide scars and in all areas of tambon Maephun are shown in Table 4.3.

Three hazard class areas in boundary of landslide scar					Three hazard class areas in boundary of tambon Maephun				
Slope type	Slope gradient	Pixel	Sq.Km.	Percentage	Slope type	Slope gradient	Pixel	Sq.Km.	Percentage
Steep slope	25°- 65°	9919	8.93	28.1	Steep slope	25°- 65°	33222	29.9	22.8
Slope	10°- 25°	20935	18.84	59.3	Slope	10°- 25°	82888	74.6	56.8
Flat	0°- 10°	4478	4.03	12.6	Flat	0°- 10°	29777	26.8	20.4
Total	0°- 65°	35332	31.8	100	Total	0°- 65°	145887	131.3	100

Table 4.3 The comparison of slope gradient areas in the landslide scars and in tambon Maephun in Laplea district

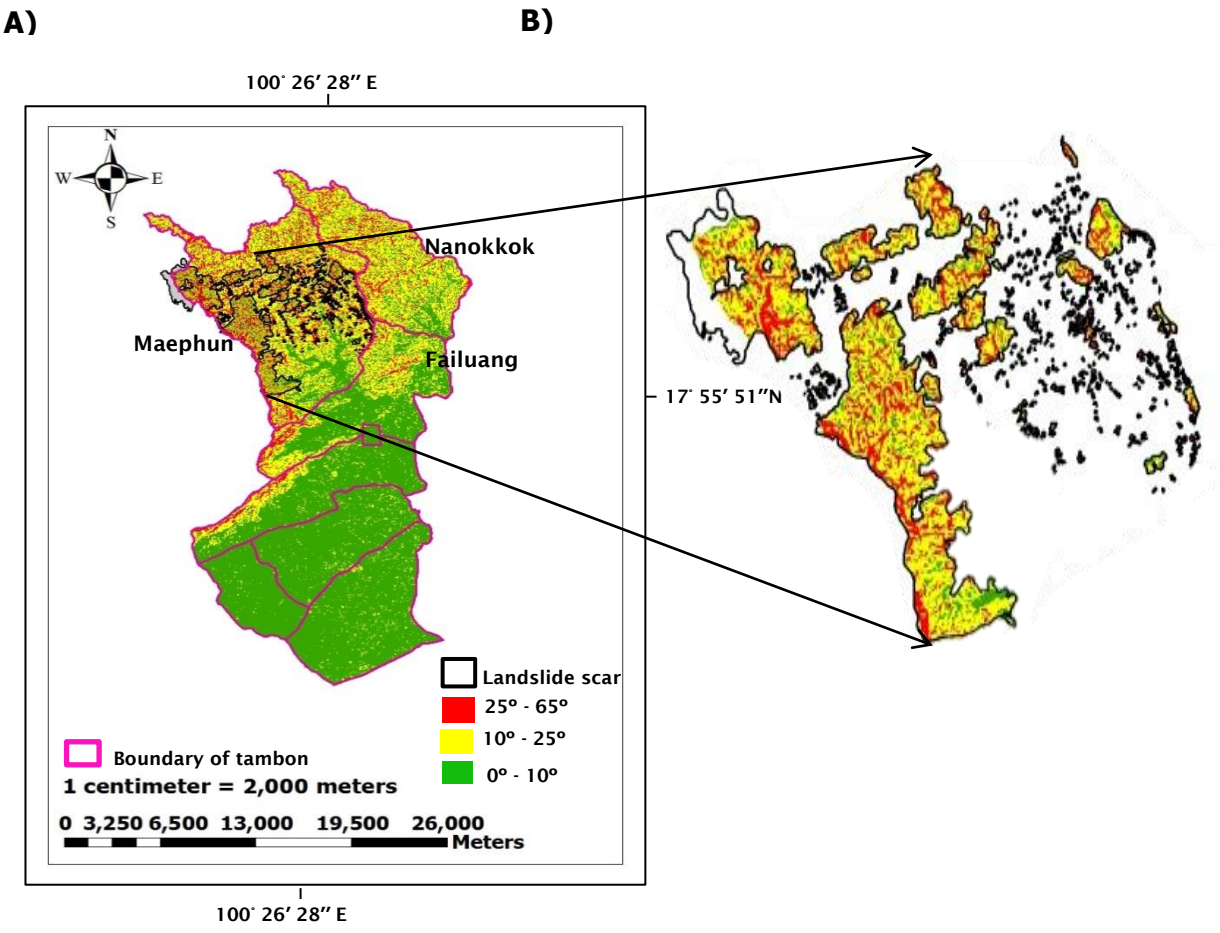

Figure 4.4 The comparison between three slope gradients: steep slopes (25° – 65°), low slopes (10° – 25°) and flats (0° – 10°), showing the landslide scar areas in tambon Maephun (on the right) and all areas of Laplea district (on the left)

As a result, the three hazard class areas: high, medium and low and the slope gradient areas: steep slopes, low slopes and flats were different, both for landslide scars and all tambon Maephun, but the ratio of area percentages was nearly the same between the landslide scar and all areas of tambon Maephun. Finally, the landslide scars presented approximately 74.7% of both high and medium class areas and presented about 87.4% of gradient areas, both steep slopes and low slopes in tambon Maephun (Table 4.2 and Table 4.3).

The past landslide scar cover three hazard classes and the slope gradients of three ranges, while three hazard class areas related to slope gradient areas of three ranges as above. Since hilly and mountainous terrains consist of steep slopes, low slopes and flats, so the landslide scar covered all three ranges of slope gradients. Another reason the landslide scar covered flat areas are because the mass of soil from steep gradient areas slide onto low slope areas around the foot of the mountains.

As a result, the landslide scar areas covered some parts of all the three hazard classes and three ranges of slope gradients in tambon Maephun because heavy rainfall occurred in all parts of the mountains. Orographic rain is associated with the elevation of mountains, when the moist air rises over the mountain and it rains on the windward side. In addition, the cyclonic effects and the upward motion influence the rainfall occurrence on the windward side. On the other hand, the rainfall amounts are less on the leeward side; called “the rain shadow”. In Thailand, orographic rain occurs during May to October because of the southwest monsoon and comes in the western part of country. There are many mountains and orographic rainfall is a main factor of landslide occurrence.

4.1.2 The result of calibration in Thapla district

a) The results of SINMAP output areas between landslide scar areas and all area of Namman district were calibrated.

In this case, the high classes of SINMAP output presented in six tambons: Namman, Nang Phaya, Chrim, Thapla, Thafaek and Phalueat (Fig 4.4). The past landslides, on May 23, 2006, occurred in tambon Namman, Nang Phaya and Chrim, in the west of Thapla district because of the southwest monsoon. This monsoon blew into the western part of Thapla district which led to heavy rainfall (206 mm), while tambon Namman was only available for the landslide scar data (DMR, 2006). So the SINMAP output areas: high, medium and low classes were

calibrated with landslide scar areas in tambon Namman. The total of landslide scar areas was presented by the SINMAP output: 13.1 km^2 in tambon Namman, while 10.1 km^2 (77.1%) of high, 1.12 km^2 (8.5%) of medium and 1.89 (14.4%) of low class areas as given in Table 4.4. The SINMAP output also presented in high, medium and low in all area of tambon Namman: 139.8 km^2 (60.2%), 27.4 km^2 (11.8%) and 65.1 km^2 (28.0%) respectively (Table 4.4). Some parts of high, medium and low hazard class areas did not overlap with the landslide scars (Fig 4.5). The comparison of hazard level areas: high, medium and low classes in the landslide scar areas and hazard level areas: high, medium and low classes in all areas of tambon Maephun are shown in Table 4.4.

Three hazard class areas in boundary of landslide scar					**Three hazard class areas in boundary of tambon Namman**				
Stability Index (SI)	**Hazard classes**	**Pixel**	**Sq.Km.**	**Percentage**	**Stability Index (SI)**	**Slope gradient**	**Pixel**	**Sq.Km.**	**Percentage**
0-1	**High**	**11198**	**10.1**	**77.1**	**0-1**	**High**	**155370**	**139.8**	**60.2**
1-1.5	**Medium**	**1244**	**1.12**	**8.5**	**1-1.5**	**Medium**	**30459**	**27.4**	**11.8**
More than 1.5	**Low**	**2099**	**1.89**	**14.4**	**More than 1.5**	**Low**	**72295**	**65.1**	**28.0**
Total		**14541**	**13.1**	**100**	**Total**		**258124**	**232.3**	**100**

Table 4.4 The comparison of landslide scar areas and output of SINMAP areas in tambon Namman in Thapla district

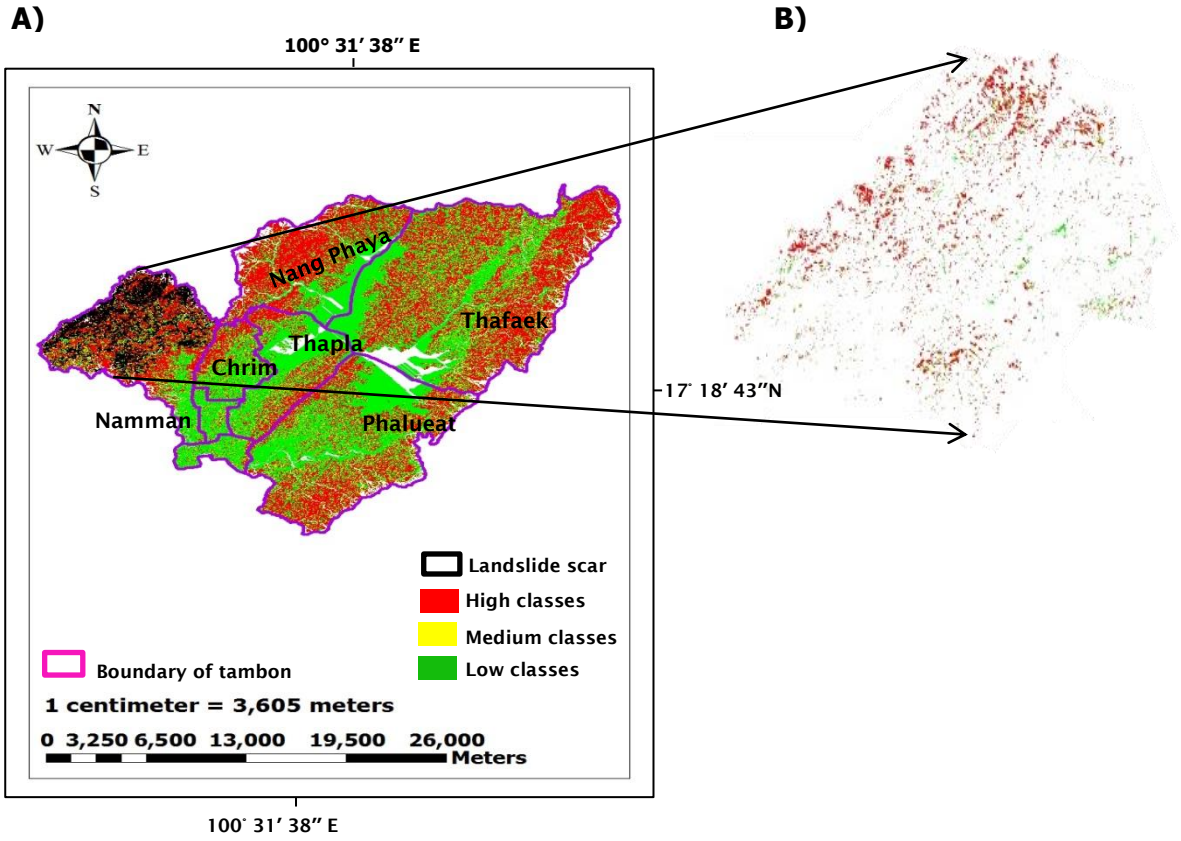

Figure 4.5 Landslide scar covering three hazard classes: high, medium and low in tambon Namman (right hand side) and three hazard classes: high, medium and low in all area of Thapla district (left hand side)

The past landslide scars covered three hazard classes: high, medium and low, but 10.1 km^2 (77.1%) is presented in high class areas. Only 1.89 km^2 (14.4%) is present in low class areas (Table 4.4) because the boundary of landslide scars extended into flat areas around the mountains. The mass of soil slide moved around the foot of the mountains when the landslide occurred.

b) The results of slope gradient areas between landslide scar areas and all area of Thapla district were calibrated. The landslide scar areas were presented by GIS software: about 15.4 km^2 in tambon Namman. Table 4.5 and Fig 4.6 show that the areas of slope gradient of steep slopes (25° – 65°), low slopes (10° – 25°) and flats (0° – 10°) presented in tambon Namman and in Thapla district. The total of landslide scar area was presented by the GIS software: 15.4 km^2 in tambon Namman, while 5.63 km^2 (36.4%) of steep slopes, 7.56 km^2 (49.2%) of low slopes and 2.22 (14.4%) of flats as given in Table 4.5. All areas of Thapla district also presented in steep slopes, low slopes and flats: 56.7 km^2 (21.4%), 140.4 km^2 (53.1%) and 67.3 km^2 (25.5%) respectively (Table 4.5).

Three ranges of slope gradient areas in boundary of landslide scar					Three ranges of slope gradient areas in boundary of tambon Namman				
Slope type	Slope gradient	Pixel	Sq.Km.	Percentage	Slope type	Slope gradient	Pixel	Sq.Km.	Percentage
Steep slope	25°- 65°	6230	5.63	36.4	Steep slope	25°- 65°	62996	56.7	21.4
Low slope	10°- 25°	8397	7.56	49.2	Low slope	10°- 25°	156001	140.4	53.1
Flat	0°- 10°	2465	2.22	14.4	Flat	0°- 10°	74731	67.3	25.5
Total	0°- 65°	17092	15.4	100	Total	0°- 65°	293728	264.4	100

Table 4.5 The comparison of landslide scars and slope gradients in tambon Namman in Thapla district

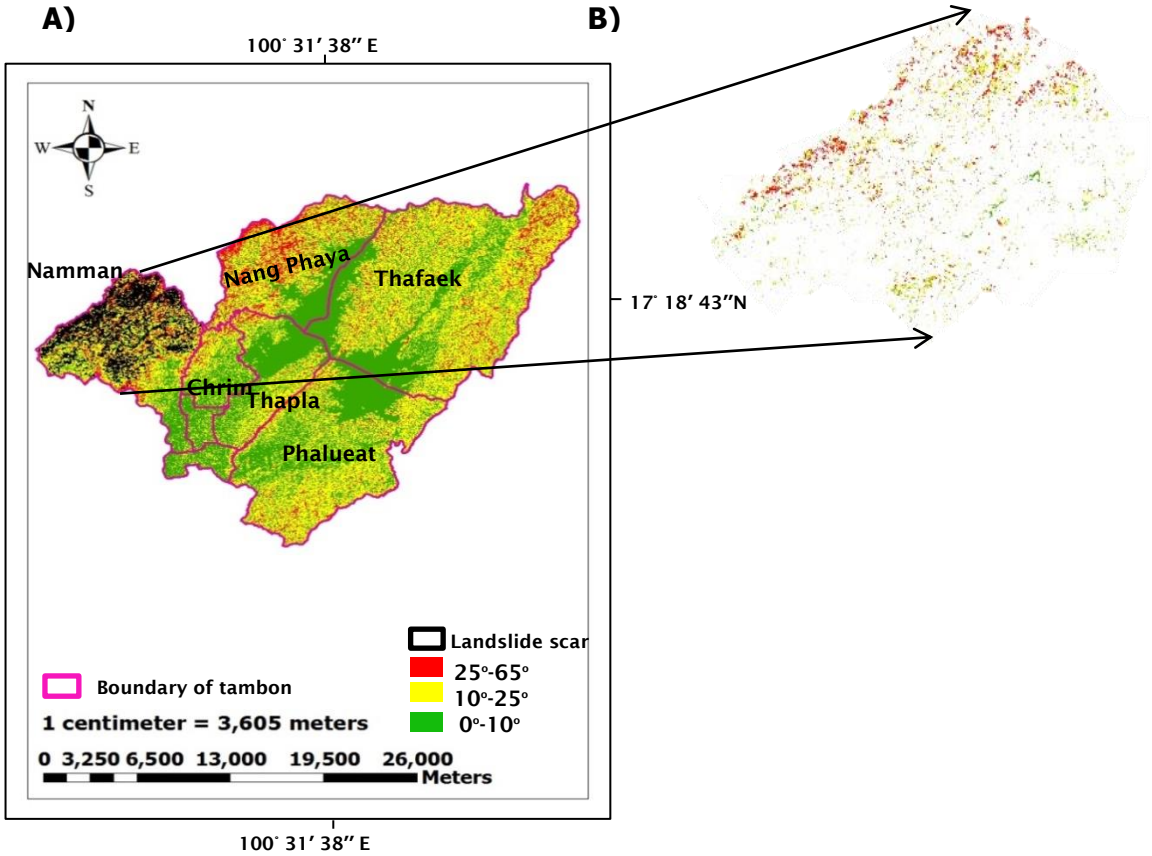

Figure 4.6 The comparison between landslide scar covering three slope gradients: steep slopes (25° – 65°), low slopes (10° – 25°) and flats (0° – 10°) in tambon Namman (right hand side) and three slope gradients: steep slopes, low slopes and flats in all areas of Thapla district (left hand side)

The slope gradients of three ranges are presented in the scar areas, while about 85.6% is showed both 25° – 65° (steep slope) and 10° – 25° (slope) since hilly and mountainous terrains consist of slope gradients of three ranges as above (Table 4.5). The reason is the same as the landslide scar in tambon Maephun.

As for calibration, most of landslide scar areas covered both steep slopes and low slopes, approximately 13.19 km^2 (85.6%) of all areas of landslide scars, while steep slope and low slope areas presented approximately 197.1 km^2 (74.5%) in all areas of Thapla district. Both steep slope and low slope areas of the landslide scar and all areas of Thapla district were different. The landslide scar areas covered some parts of the mountains because orographic rain occurred in some parts of the mountains. When the moist air rises over the mountain, and it rains on the windward side, the cyclonic effects and the upward motion influence the rainfall occurrence on the windward side. On the other hand, the rainfall amounts are less on the leeward side; called “the rain shadow”. In Thailand, orographic rain often occurs during May to October because of the southwest monsoon. Therefore, the landslide occurred on the windward side of the mountains.

4.1.3 Analysis results of calibration in Laplea and Thapla districts

The landslide scar areas both tambon Meaphun in Laplea district and tambon Namman in Thapla districts were presented for the SINMAP calibration under observed rainfall conditions in 2006, the landslide scar overlapped with three hazard classes: high, medium and low and also overlapped slope gradients of steep slopes, low slopes and flats. The high percentages of landslide scar areas overlapped with high and medium hazard classes and both steep slopes and low slopes. On the other hand, the low percentages overlapped with the low classes and flats. When the past landslide occurred, soil mass moved downward along a roughly planar surface. The failure covered several kilometres, so the low hazard class (safety areas) and slope gradients of 0^o – 10^o (flat) were found in the landslide scar areas.

As for the calibration in two tambons, approximately 80.15% of SINMAP output (averaged by adding the percentage of both high and medium classes in two tambons) and 86.5% slope gradients (averaged by adding the percentage of both steep slopes and low slopes in two tambons) were presented as above. It means that both high and medium classes and steep slopes and low slopes are linked to each other. These two percentages can confirm the efficiency of the SINMAP model, that it is suitable for landslide analysis. Therefore, in this study, the zonation of landslide risk should cover all areas of high and medium classes, and cover about, 19.85% of low class areas (percentage remaining i.e. (100-80.15)).

4.2 Output of sensitivity of SINMAP model analysis

Sensitivity analysis was used to determine the impact of variable input parameters under model analysis. The output of sensitivity analysis was simulated by the relationship between the geotechnical and the hydrological parameters, including the slope angles, by the digital elevation model (DEM). The variable of each parameter was obtained by sensitivity analysis and shown by three hazard class areas (km^2): high, medium, and low. The total areas of SINMAP output (km^2) corresponded with all areas on the ground (km^2). As for the sensitivity of SINMAP parameters, the slope gradients were shown in Uttaradit and five SINMAP parameters: dimensionless cohesion, angle of friction, soil depth, permeability and rainfall were presented in Thapla district as follows:

4.2.1 Output of sensitivity SINMAP model in slope angle ranges

Three ranges of slope gradients: steep slopes (25^o – 65^o), low slopes (10^o – 25^o) and flats (0^o – 10^o) as shown in Fig 4.7 below, are presented for nine districts in Uttaradit province. The slope gradients of 25^o – 65^o, 10^o – 25^o and 0^o – 10^o were related to the digital elevation model (DEM). Based on Arc GIS software, showing the slope gradient areas of hilly terrain, the digital elevation model (DEM) with a resolution of 30 metres was used and calculated for 900 m^2 in each pixel, and changed into km^2 units. Therefore, three slope gradient areas were calculated in nine districts: Muang, Laplea, Thapla, Nampat, Faktha, Bankhok, Thongsaenkhun, Phichai and Tron as shown in Fig 4.8. Both Phichai and Tron districts were found to be only 1% hilly terrains, so the slope gradients of steep slopes (25^o – 65^o) and low slopes (10^o – 25^o) are small areas and 99% is flat terrain (0^o – 10^o) as shown in Fig 4.7 and Fig 4.8.

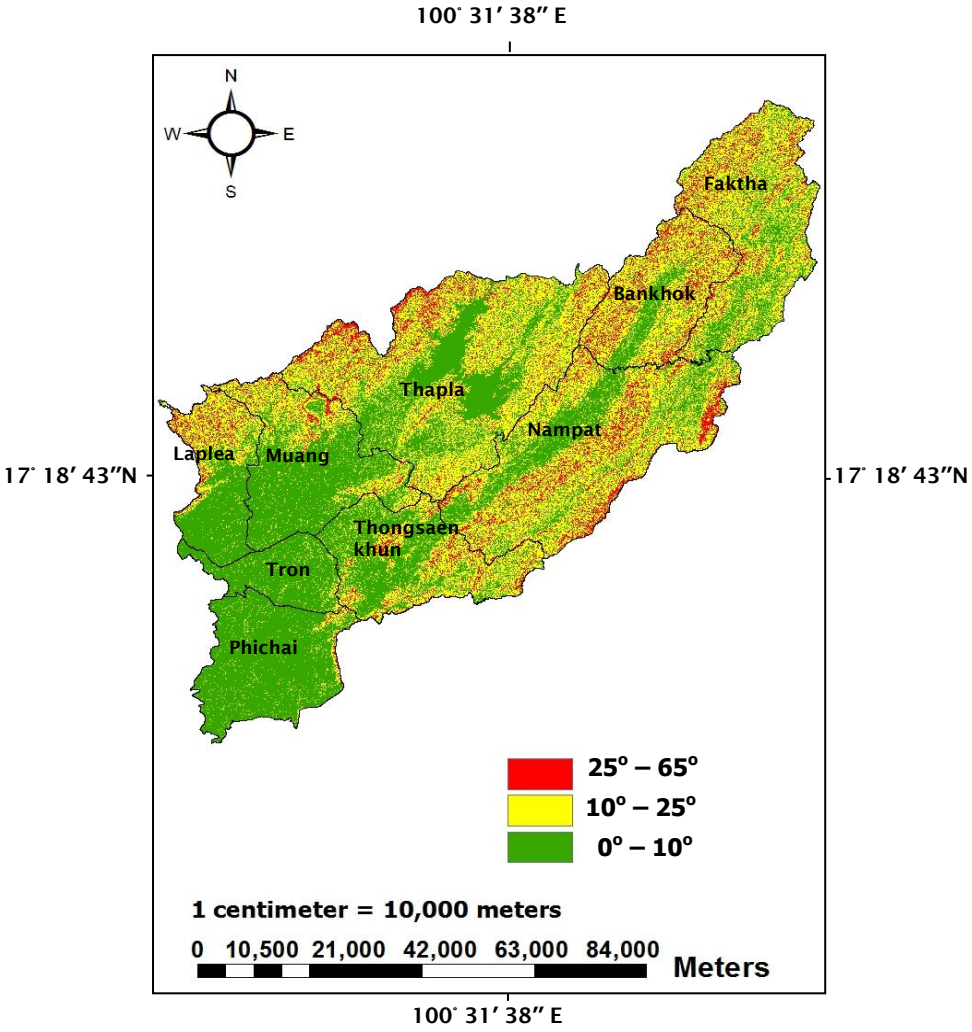

Figure 4.7 The classification of slope gradient areas: steep slopes (25° – 65°), slopes (10° – 25°) and flats (0° – 10°) in nine districts in Uttaradit province

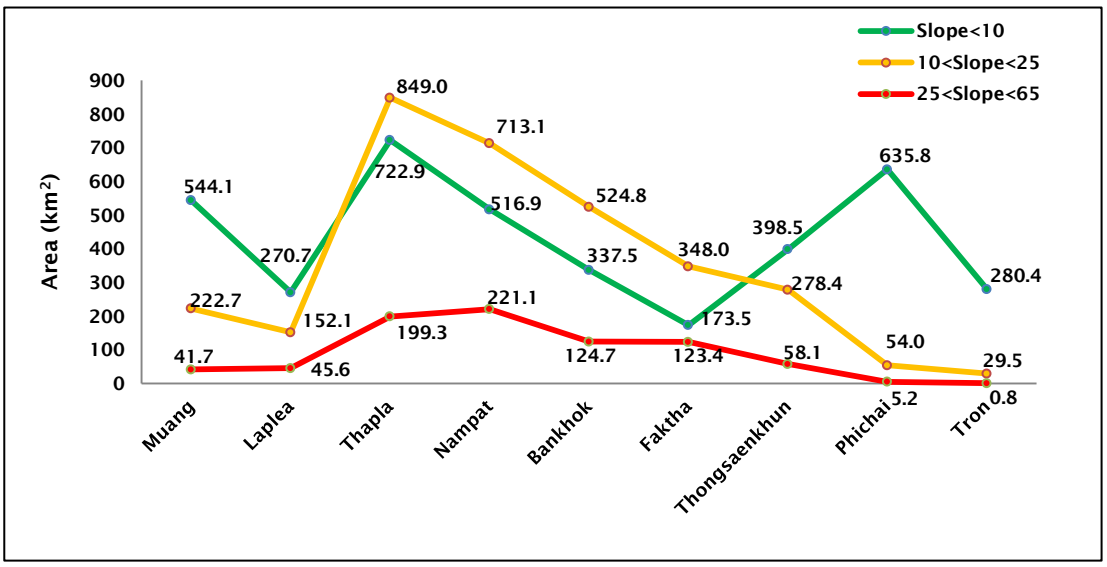

Figure 4.8 Three ranges of slope gradient areas in each district in Uttaradit province

In the literature review, slope gradients affect the probability of landslide occurrences: in these results. The probability of landslide is more than 70%, when slope gradients are more than 35°, while the probability of landslide is between 50% and 70%, with slope gradients of 26.7° - 35°. The probability of landslide is between 30% and 50% on slope gradients of 16.7° - 26.7°. The probability of landslide is between 15% and 30% on slope gradients of 8.5° - 16.7°, while the probability of landslide impacts is between 0% and 15% on slope gradients of 0° - 8.5° (DWR, 2010).

Therefore the Digital Elevation Model (DEM) by GIS software, classified in three ranges of slope gradients in Uttaradit province as above, was tested by the SINMAP model. As for SINMAP parameters, the hazard classes were presented for high, medium and low hazard classes, using the default values of each geotechnical parameter in the SINMAP model, while 100 mm/24 hours of rainfall value (probability of landslide occurrences as defined by DMR, 2011) was used for sensitivity of hydrological parameters. This rainfall value is the smallest observed for landslide risk areas and a more conservative estimate, when compared with observed rainfalls in this study, so the DMR value was applied for sensitivity analysis. Three hazard classes: high, medium and low were presented in a map (Fig 4.9), while the areas of the three hazard classes calculated for the 900 m^2 in each 30 metres pixel of DEM, and converted into km^2 units (Fig 4.10).

As a result, the relationship between the location of slope gradients: steep slopes (25° – 65°), low slopes (10° – 25°) and flats (0° – 10°) and the location of high, medium and low hazard classes are presented by maps as shown in Fig 4.7 and Fig 4.9. The area of high classes (red), medium (yellow) and low (green) and the area of steep slopes (red), low slopes (yellow) and flats (green) in two graphs. Both Fig 4.8 and Fig 4.10 were compared for the area of three slope gradients and three hazard classes. The total area of three classes: high (940.8 km^2), medium (1,274.3 km^2), low (5,013.1 km^2) and the total area of three ranges of slope gradients: steep slopes (819.9 km^2), low slopes (3,171.6 km^2) and flats (3,880.3 km^2) presented in all nine districts. The high class and steep slope areas were nearly the same in each district, while the medium class were less than low slope areas and the low class were higher than flat areas. Finally, the high classes related to steep slopes, while the medium and the low classes related to both low slopes and flats, so all three ranges of slope gradients directly affect three hazard classes in the SINMAP model.

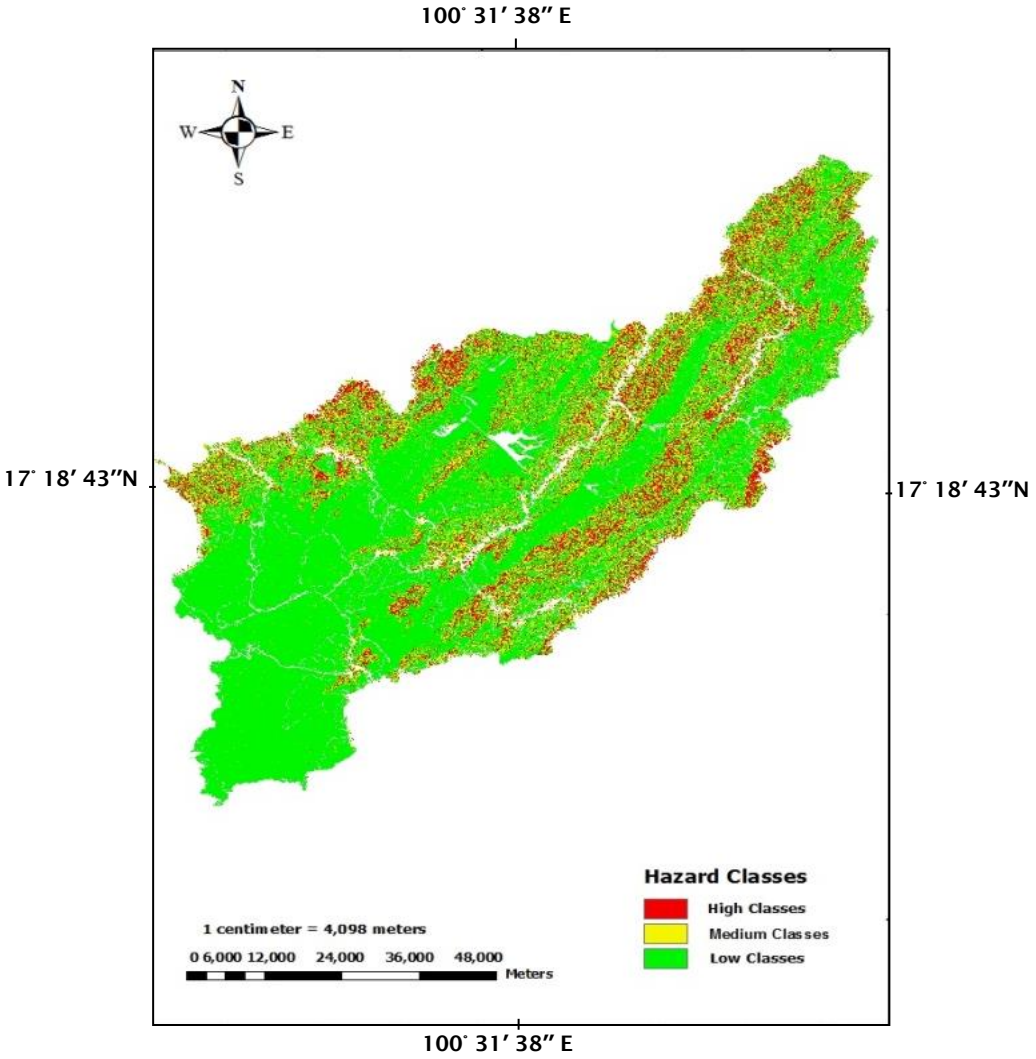

Figure 4.9 The landslide hazard mapping in Uttaradit province

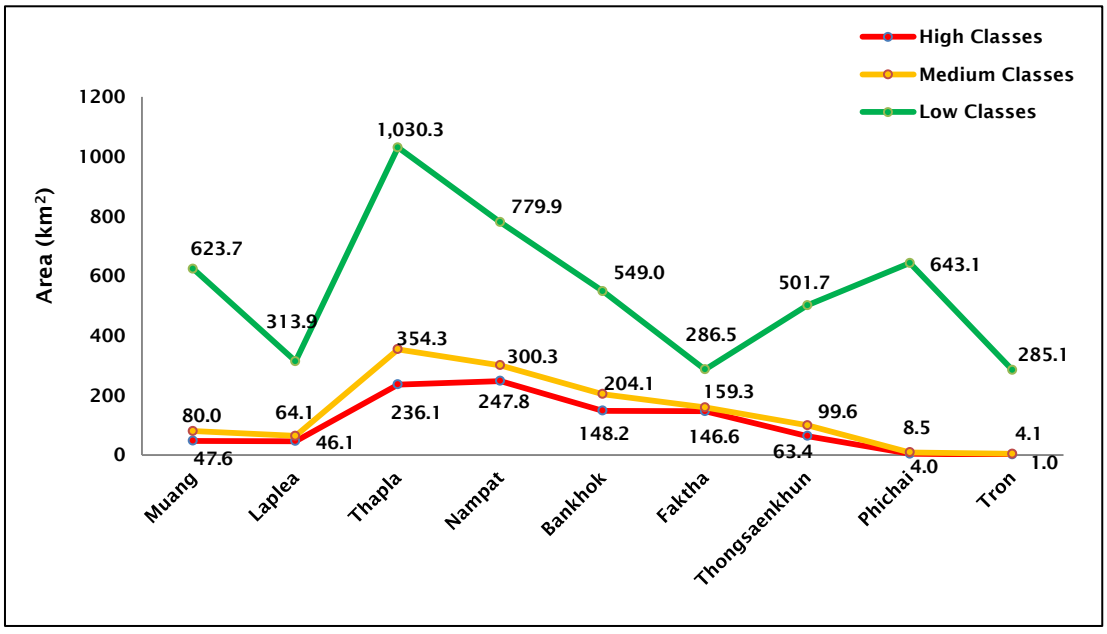

Figure 4.10 The hazard class areas: high, medium and low in each district in Uttaradit province

The high class areas were related to the same location of slope gradients of 25° – 65° (steep slope) in seven districts: Muang, Laplea, Thapla, Nampat, Bankhok, Faktha, Thongsaenkhun, while the high class areas were not found in Phichai and Tron districts, since less than 1% of steep slope areas were found in both districts.

Furthermore, the areas of slope gradients in Thapla district (Fig 4.11) were presented in 199.3 km^2 of steep slopes, 849.0 km^2 of low slopes and 722.9 km^2 of flats, while the location of three ranges of slope gradients were used to link with the sensitivity map of other parameters: dimensionless cohesion, angle friction, soil depth, permeability and rainfall. First the high risk areas will occur in steep slope areas, then it will occur in low slope and flat areas.

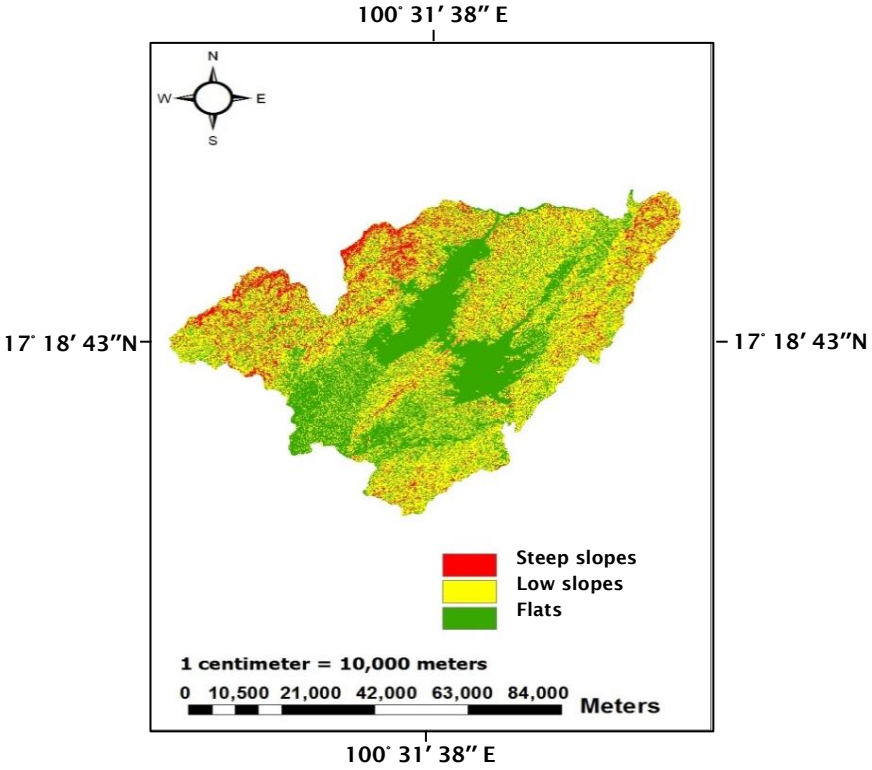

Figure 4.11 The slope gradient areas: steep slopes, low slopes and flats in Thapla district

4.2.2 Output of sensitivity of SINMAP model in the geotechnical data

A. The geotechnical data section: the variable shear and root strength values were linked within the dimensionless cohesion values as 0 – 0.125(Fig 4.12(1)), 0.125 – 0.25(Fig 4.13), 0.25 – 0.5(Fig 4.14), 0.5 – 1.0(Fig 4.15) and 1.0 – 1.5 (Fig 4.16) respectively.

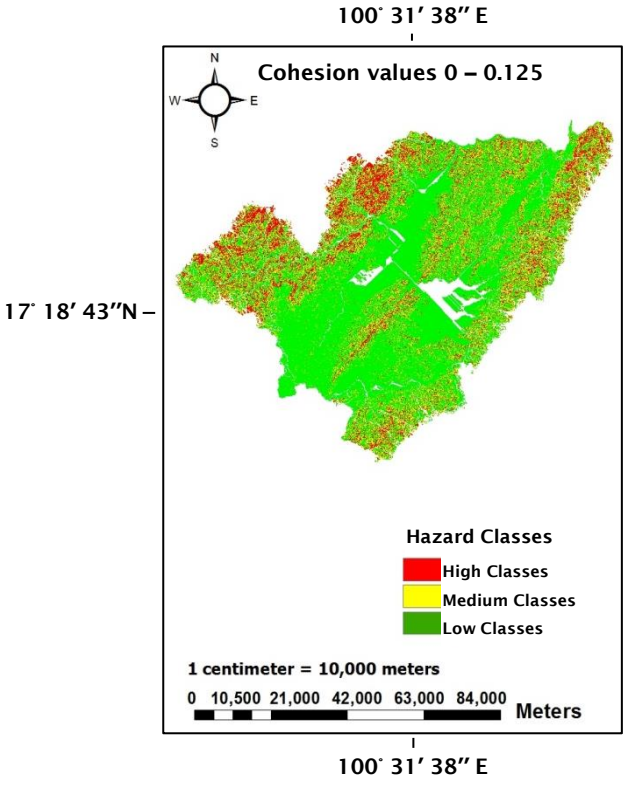

Figure 4.12 The sensitivity of landslide hazard mapping (cohesion values 0 – 0.125)

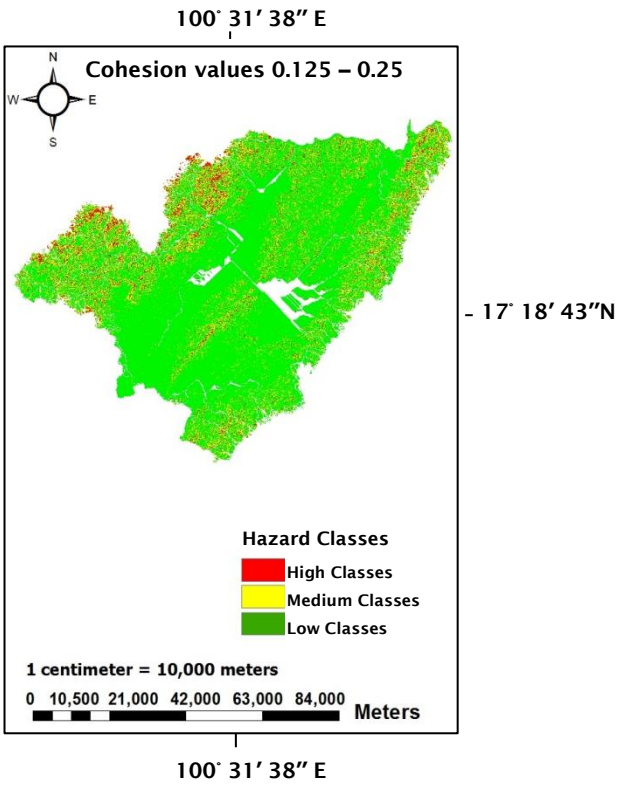

Figure 4.13 The sensitivity of landslide hazard mapping (cohesion values 0.125 – 0.25)

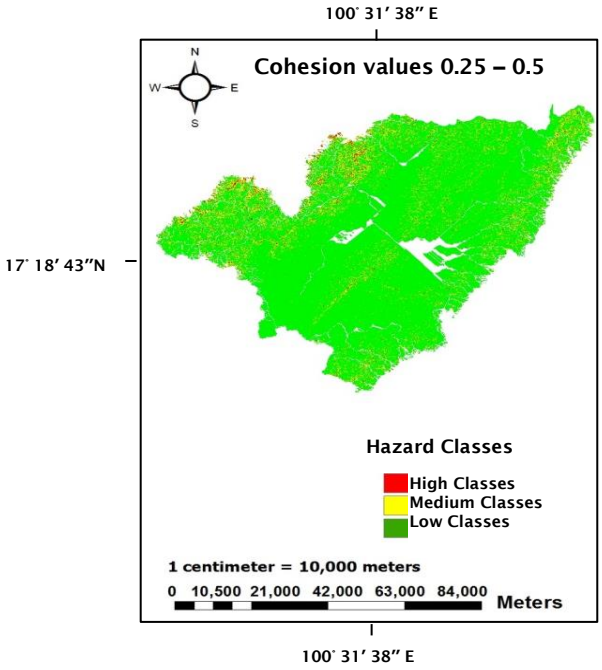

Figure 4.14 The sensitivity of landslide hazard mapping (cohesion values 0.25 – 0.5)

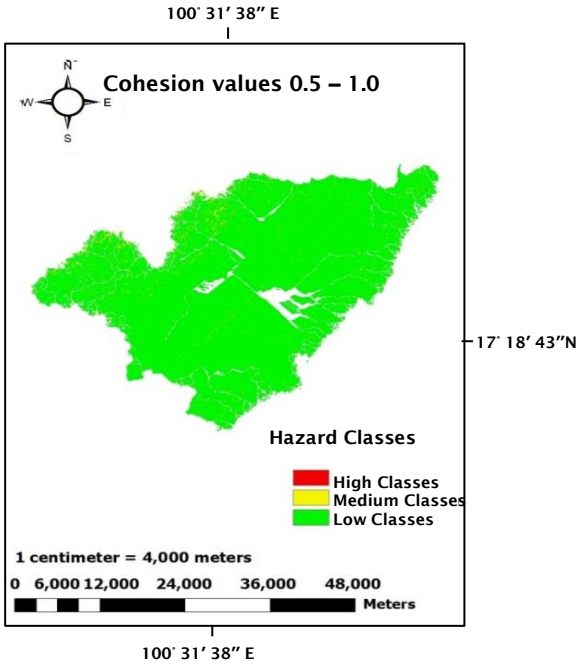

Figure 4.15 The sensitivity of landslide hazard mapping (cohesion values 0.5 – 1.0)

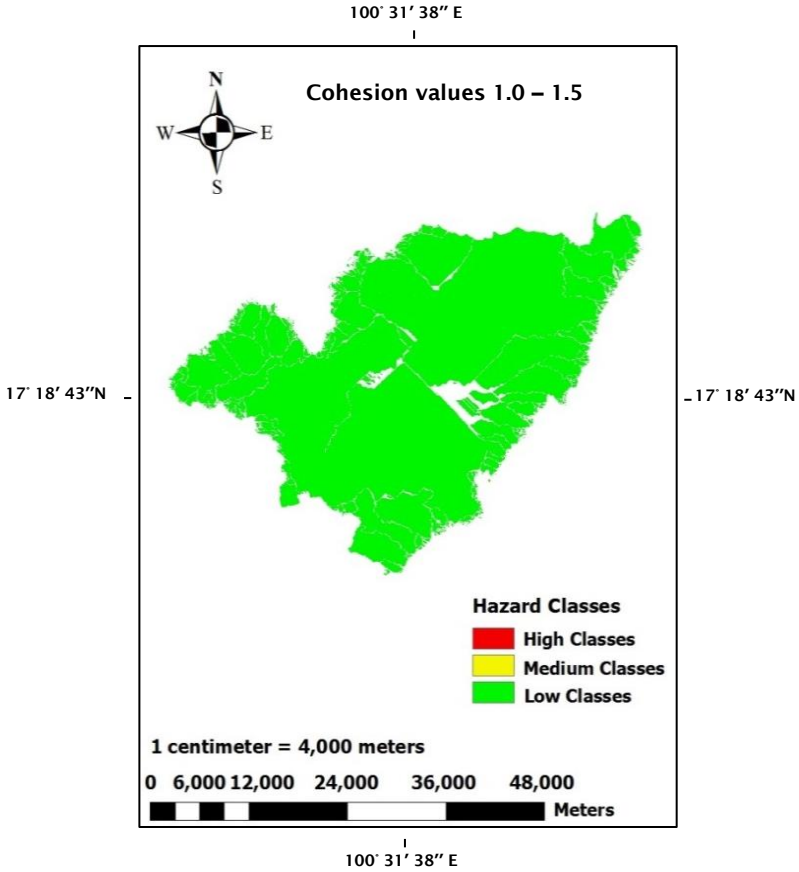

Figure 4.16 The sensitivity of landslide hazard mapping (cohesion values 1.0 – 1.5)

The sensitivity of the tested dimensionless cohesion parameters varied in five ranges: 0 – 0.125, 0.125 – 0.25, 0.25 – 0.5, 0.5 – 1.0 and 1.0–1.5. Both high and medium hazard classes steadily decreased, but low classes increased when dimensionless cohesion ranges increased.

The high class areas overlapped in steep slope areas and medium class areas overlapped in low slope areas, but the low class areas overlapped in some parts of low slope and flat areas in three ranges of dimensionless cohesion: 0 – 0.125, 0.125 – 0.25, 0.25 – 0.5 (Fig 4.12 - Fig 4.14), while the high and medium class areas are so small in ranges of 0.5 – 1.0 and cannot be detected in the range of 1.0 – 1.5, despite being hilly terrain. The hazard class areas (km^2): high, medium and low in nine districts showed in a graph as in Fig 4.17. Three hazard classes (Fig 4.12 – Fig 4.16) related to three slope gradient areas: steep slope, low slope and flat in Thapla district (Fig 4.11). The total km^2 unit of high, medium, low hazard class areas (by adding high, medium, low hazard class areas) was 1,620.8

km². The total area of three hazard class areas was the same in the Thapla area (1,620.8 km²) by the SINMAP outputs (Fig 4.17).

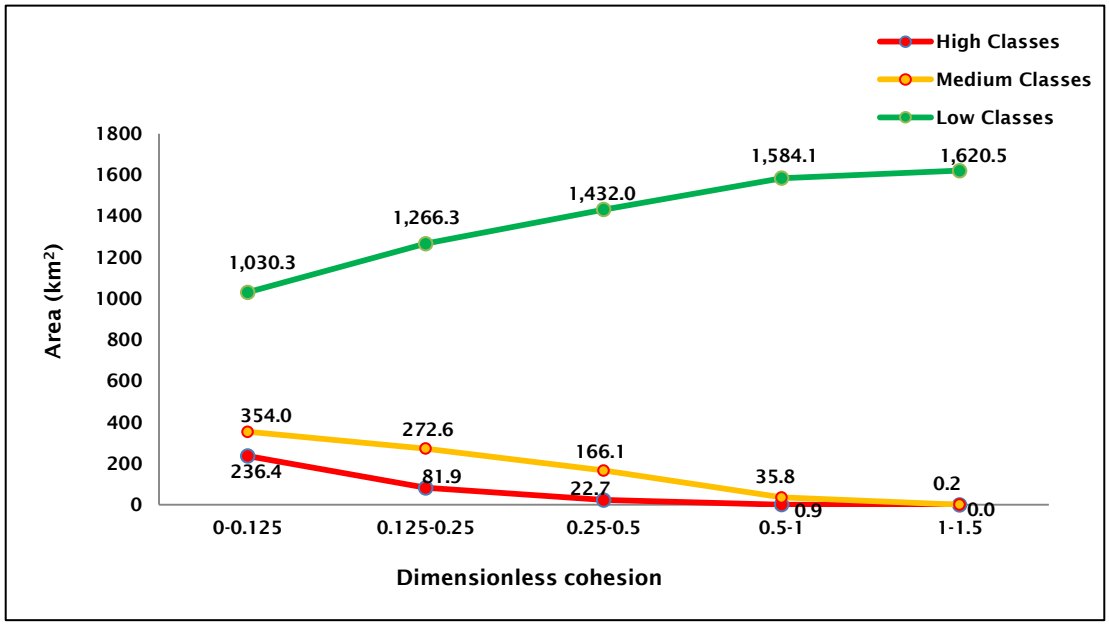

Figure 4.17 The behaviour of dimensionless cohesion in three hazard class areas: high, medium and low

The high hazard class areas were approximately 236.4 km², 81.9 km², 22.7 km², 0.9 km² and 0 km², and medium hazard class areas were 354.0 km², 272.6 km², 166.1 km², 35.8 km² and 0.2 km², while low hazard class areas were approximately 1,030.3 km², 1,266.3 km², 1,432.0 km², 1,584.1 km² and 1,620.5 km² in the dimensionless cohesion ranges of 0 – 0.125, 0.125 – 0.25, 0.25 – 0.5, 0.5 – 1.0 and 1.0 – 1.5 respectively. The high and medium class areas decreased, but low class areas increased when dimensionless cohesion ranges increased. As a result, increased dimensionless cohesion ranges could reduce high (failure region) and medium (instability) class areas in hilly and mountainous areas, becoming low hazard class areas (safe).

The influence of cohesive values is quite high sensitivity within the SINMAP software. The high cohesive values can reduce failure regions in hilly terrains and it become safety areas. On the other hand, the literature describes that the shear strength loss in residual soils affects soil stability under rainfall intensity owing to increasing moisture content (DWR, 2010). Hence, the dimensionless cohesion parameters affect all three hazard class areas in the SINMAP model.

B. The variability of the angle of friction values were shown: 5° – 10° (Fig 4.18), 10° – 15° (Fig 4.19), 15° –20° (Fig 4.20), 20° – 25° (Fig 4.21), 25° – 30° (Fig 4.22), 30° – 35° (Fig 4.23) and 35° – 45° (Fig 4.24), the angle of friction values steadily dropped in high hazard classes, on the other hand low hazard classes slightly increased, as given in Fig 4.25.

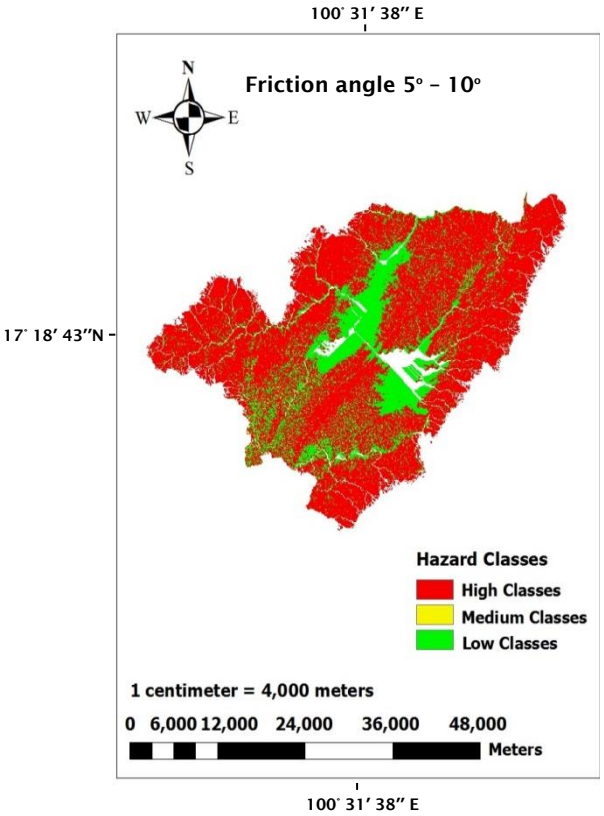

Figure 4.18 The sensitivity of landslide hazard mapping (friction angle 5° – 10°)

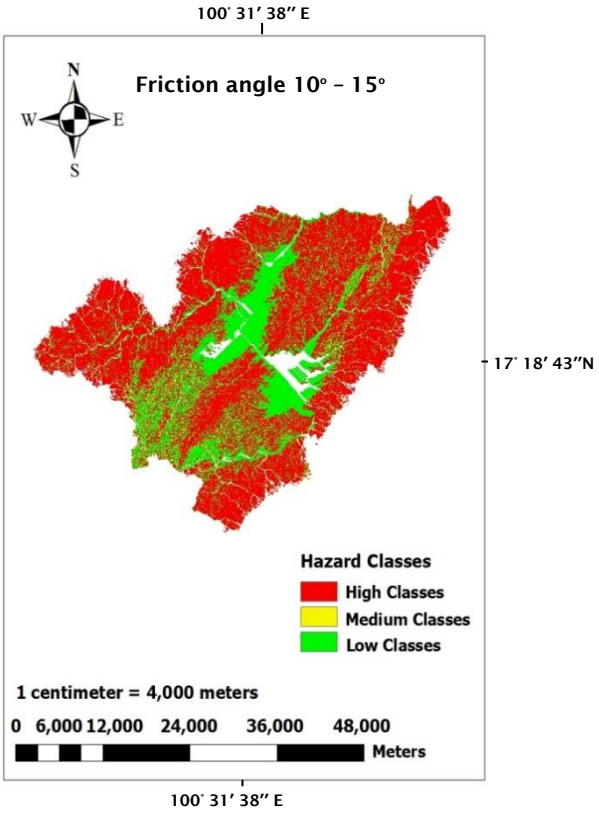

Figure 4.19 The sensitivity of landslide hazard mapping (friction angle 10° – 15°)

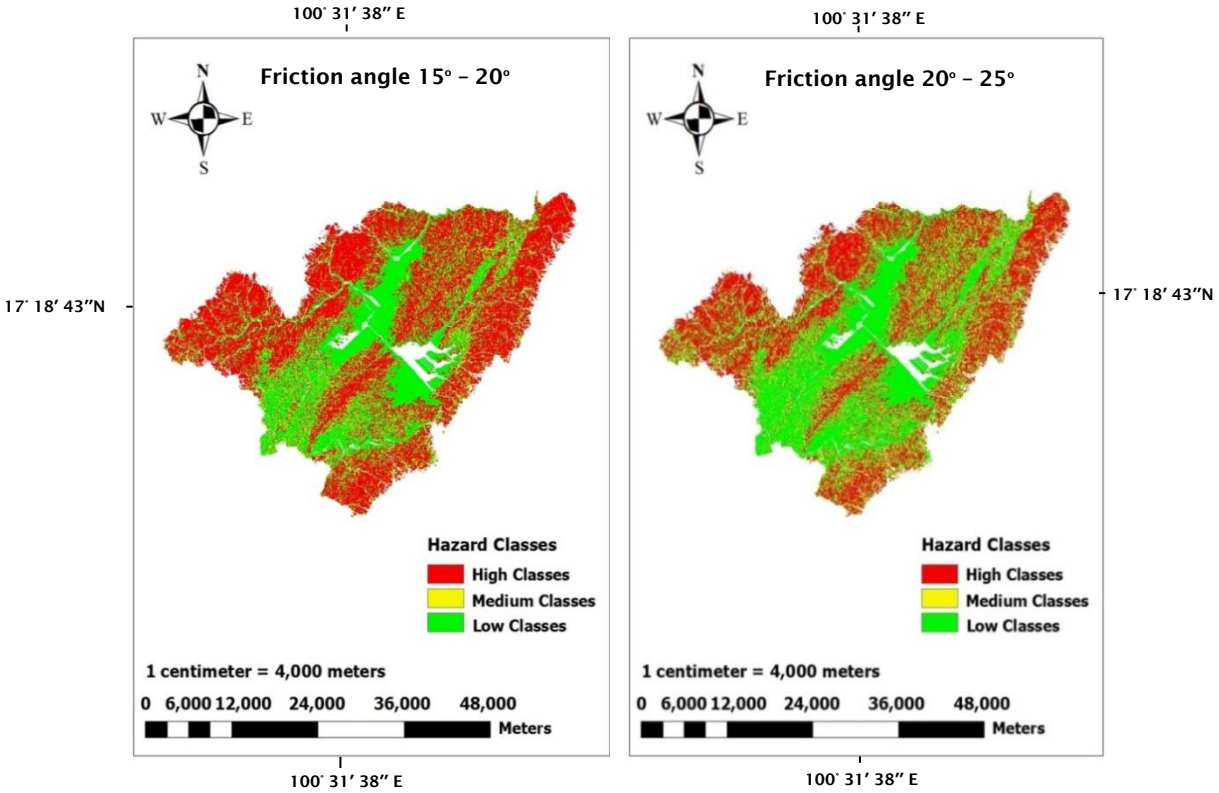

Figure 4.20 The sensitivity of landslide hazard mapping (friction angle 15° – 20°)

Figure 4.21 The sensitivity of landslide hazard mapping (friction angle 20° – 25°)

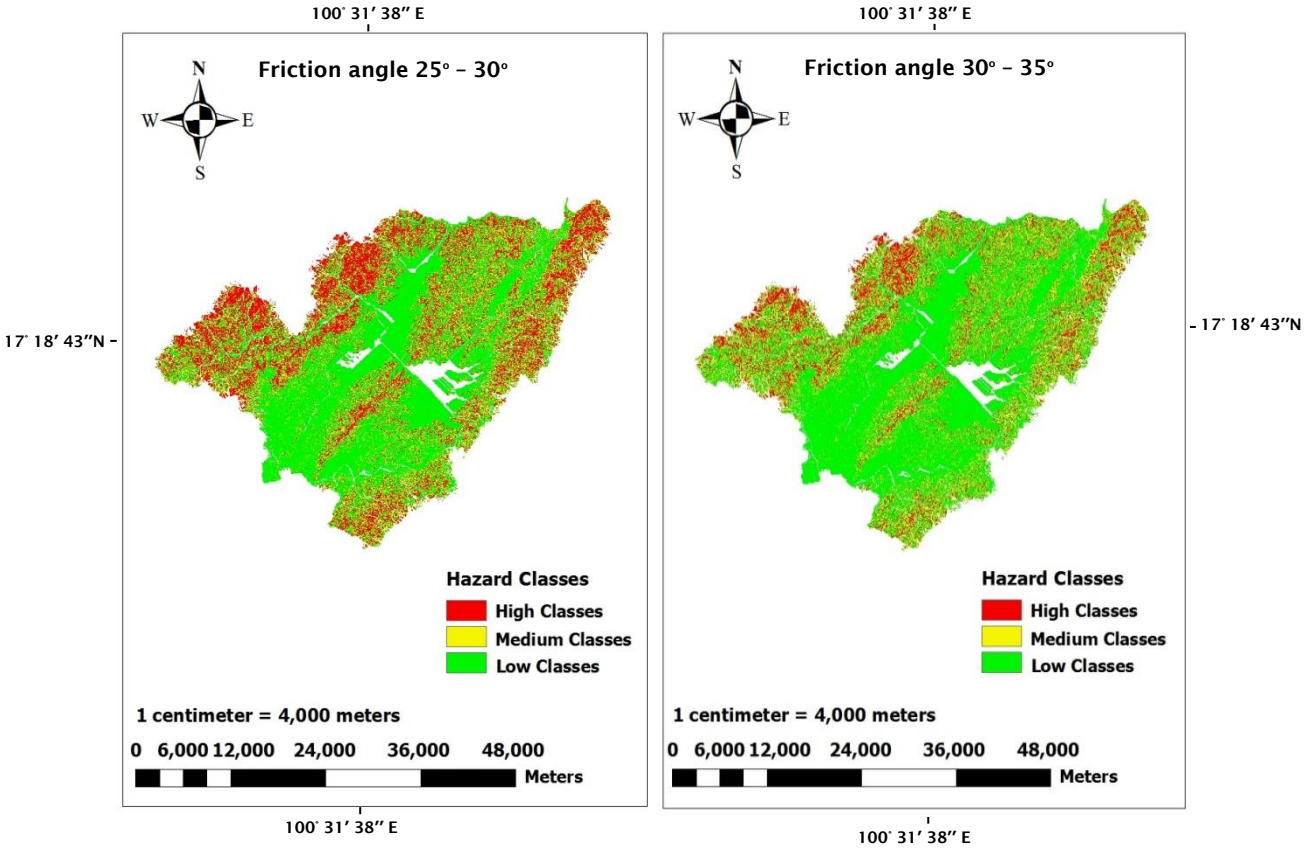

Figure 4.22 The sensitivity of landslide hazard mapping (friction angle 25° – 30°)

Figure 4.23 The sensitivity of landslide hazard mapping (friction angle 30° – 35°)

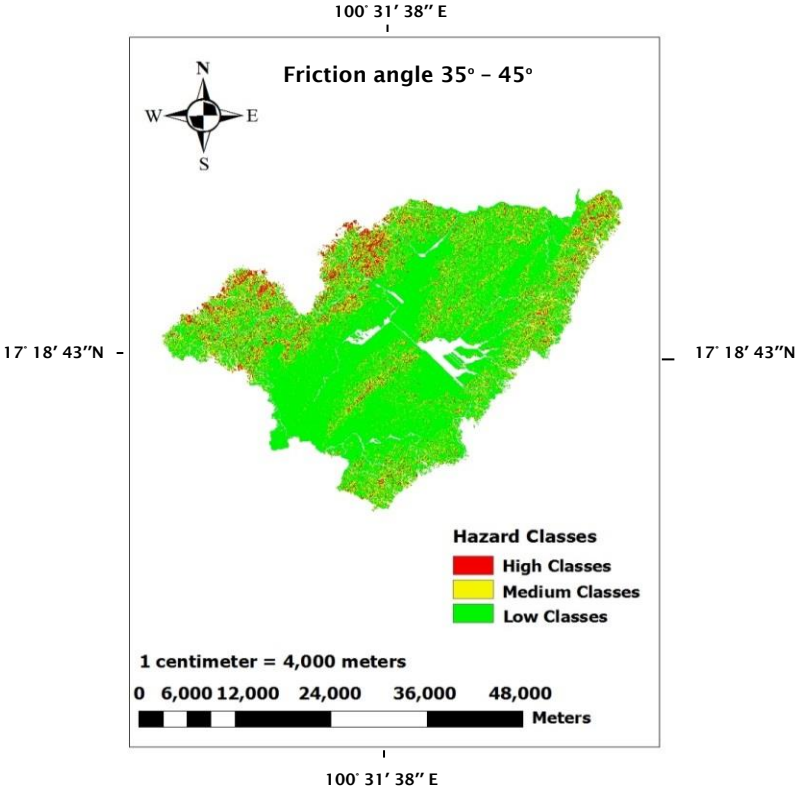

Figure 4.24 The sensitivity of landslide hazard mapping (friction angle 35° – 45°)

The interval of angle of friction values of 5° – 45° were tested for sensitivity, but the range of 25° – 45° was found in soil testing in this study (Section3, Chapter 3). In four ranges of 5° – 10°, 10° – 15°, 15° – 20° and 20° – 25°, the high class areas slightly decreased, while the low and medium class areas increased. First the high classes covered three ranges of slope gradients: steep slopes, low slopes and flats. Then high classes covered only steep slope and low slope areas, while the medium and low class areas covered more areas of low slope and flat areas.

In the angle of friction ranges of 25° – 30°, 30° – 35° and 35° – 45°, the high hazard class areas slightly decreased, as 418.9 km^2, 236.3 km^2 and 120.0 km^2 respectively, while medium hazard class areas slowly increased: 348.0 km^2 and 354.2 km^2, and then it decreased: 291 km^2. Both high and low hazard class areas were inversed in these three ranges as shown in Fig 4.25. The total area (km^2) of high, medium and low hazard class areas (by adding high, medium, low hazard class areas) was the same in the area of Thapla district (1,620.8 km^2) by the SINMAP outputs (Fig 4.25).

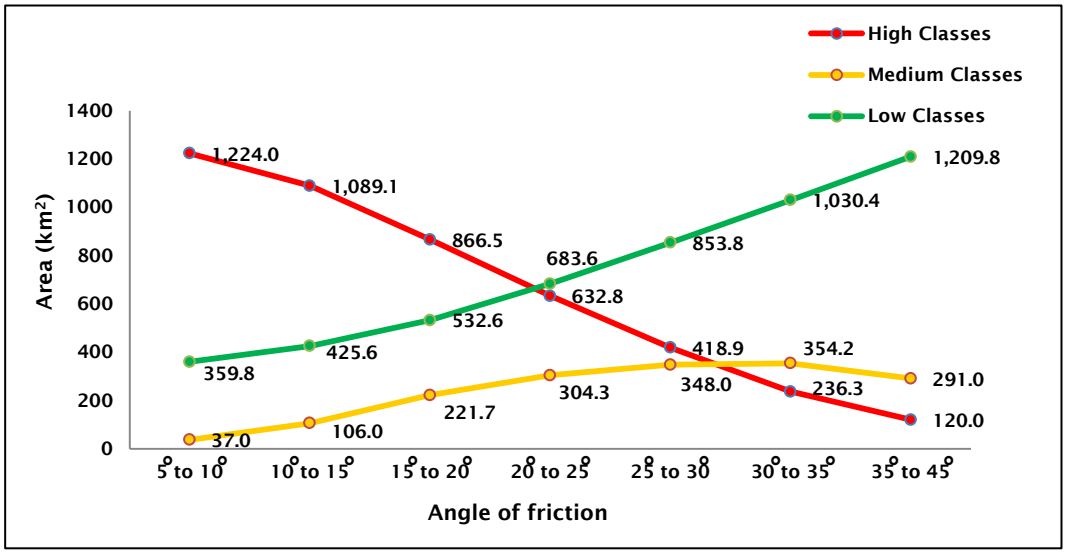

Figure 4.25 The behaviour of angle of friction in three hazard class areas: high, medium and low

The interval of angle of friction values of 5° – 45° lead to a decrease of high hazard class areas, while the low hazard class areas increased. The medium class areas increased from 5° – 10° to 20° – 25°, but it decreased from 25° – 30° to 35° – 45°.

As a result, the small ranges of angle of friction (5° – 10°) lead to big areas of high classes (failure region) and medium classes (instability) which covered steep slope, low slope and some part of flat areas, while medium and low class areas covered only small areas of flat (Fig 4.11 and Fig 4.18). On the other hand, the big range of angle of friction from 25° – 30° to 35° – 45° lead to the small areas of high and medium classes, covering only steep slope and some parts of low slope areas, while low class areas covered in higher areas of low slope areas and in flat areas. The increasing of angle of friction from 25° – 30° to 35° – 45° can reduce the high and medium hazard class areas (failure regions and instability), showing the same behaviour as in dimensionless cohesion values. The high range of dimensionless cohesion can reduce the high and medium hazard class areas because the angle friction parameter is a part of dimensionless cohesion parameter.

4.2.3 Output of sensitivity of SINMAP model in hydrological data

A. The evaluation of variable soil depths corresponded with the sensitivity of the SINMAP model, including the default values of shear strength and angle of friction values which were obtained. The coefficient of permeability (k) used is that for the loam type because the calculation of this type was nearly the default values of T/R in SINMAP software (T/R = 2000-3000) and the 100 mm/24 hours of rainfall values was used for calculation (the smallest rainfall value for probability of landslide (DMR, 2011)). The output of the SINMAP model for variable soil depths (Table 3.10) are presented for 0.25m (Fig 4.26), 0.5 m (Fig 4.27), 1 m (Fig 4.28), 1.5 m (Fig 4.29), 2 m (Fig 4.30) and 2.5 m (Fig 4.31) and is shown by the areas of high, medium and low hazard classes in km^2. The high hazard and medium classes in five maps were the same location in steep slopes and low slopes (Fig 4.11).

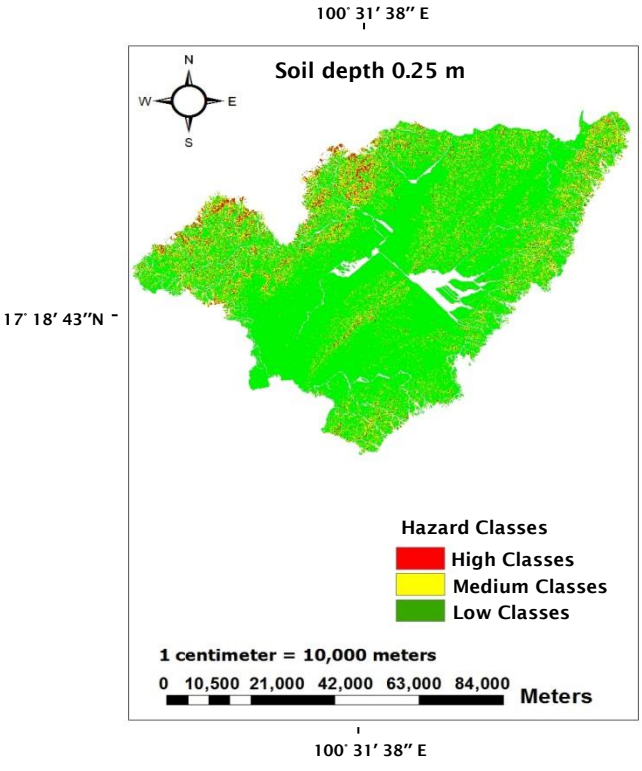

Figure 4.26 The sensitivity of landslide hazard mapping (soil depth 0.25 m)

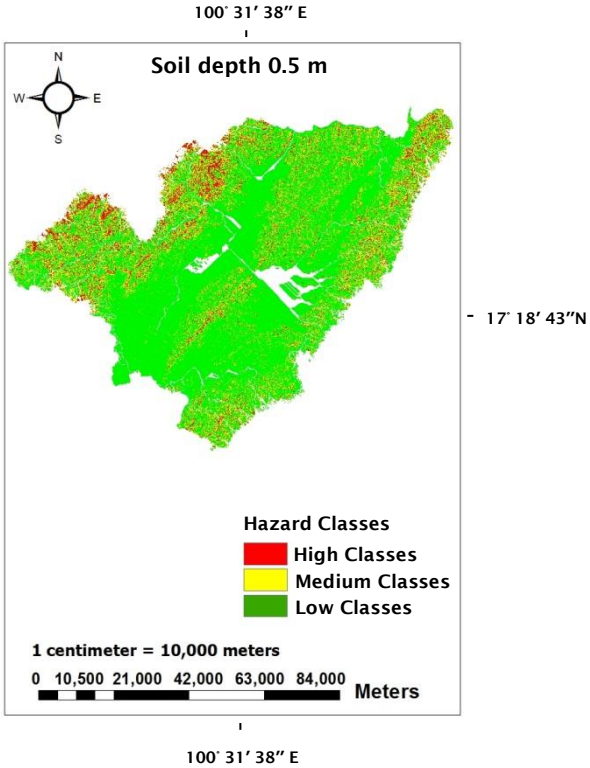

Figure 4.27 The sensitivity of landslide hazard mapping (soil depth 0.5 m)

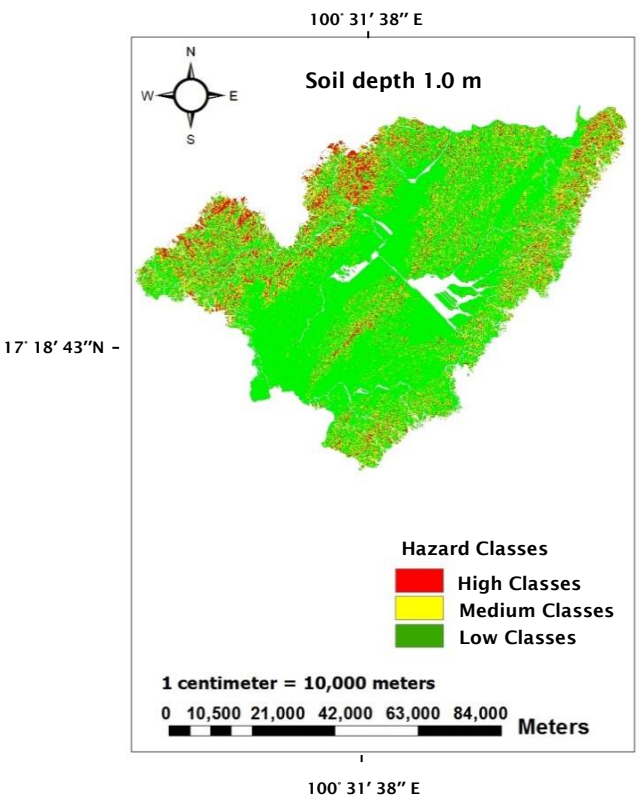

Figure 4.28 The sensitivity of landslide hazard mapping (soil depth 1.0 m)

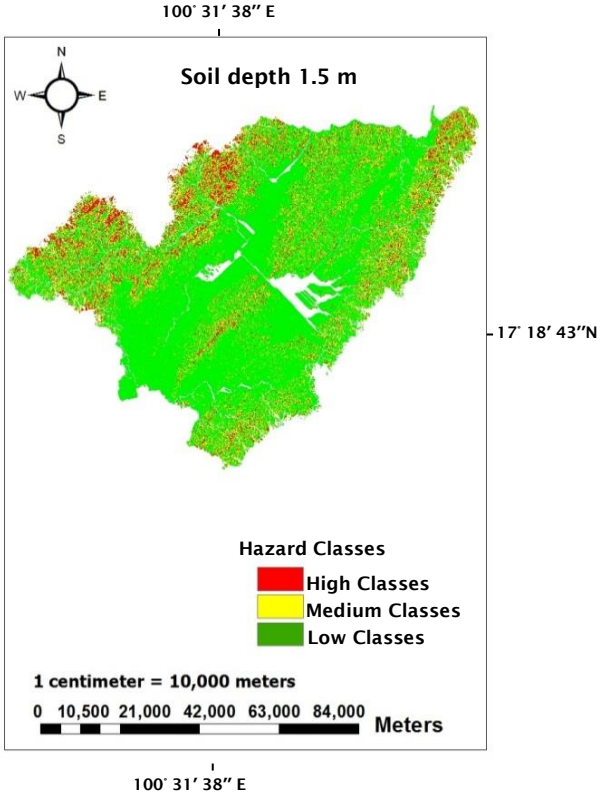

Figure 4.29 The sensitivity of landslide hazard mapping (soil depth 1.5 m)

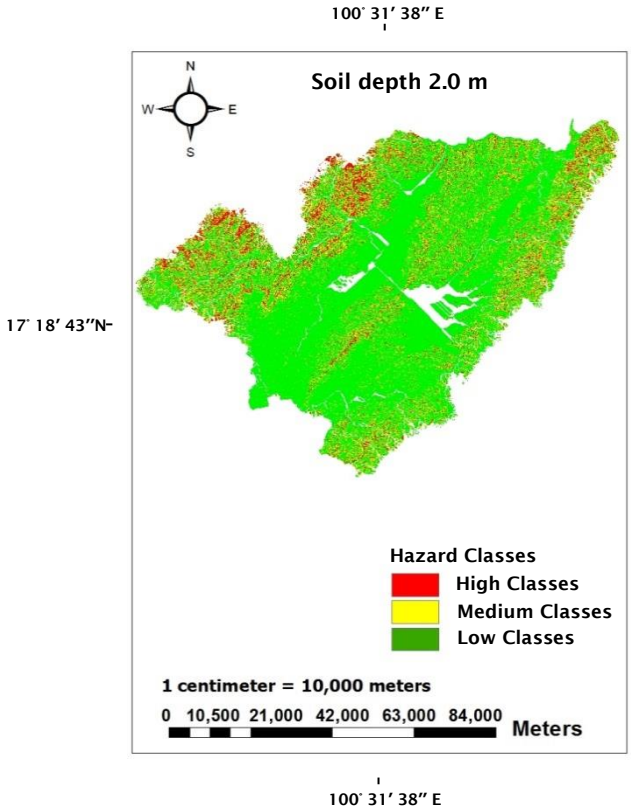

Figure 4.30 The sensitivity of landslide hazard mapping (soil depth 2.0 m)

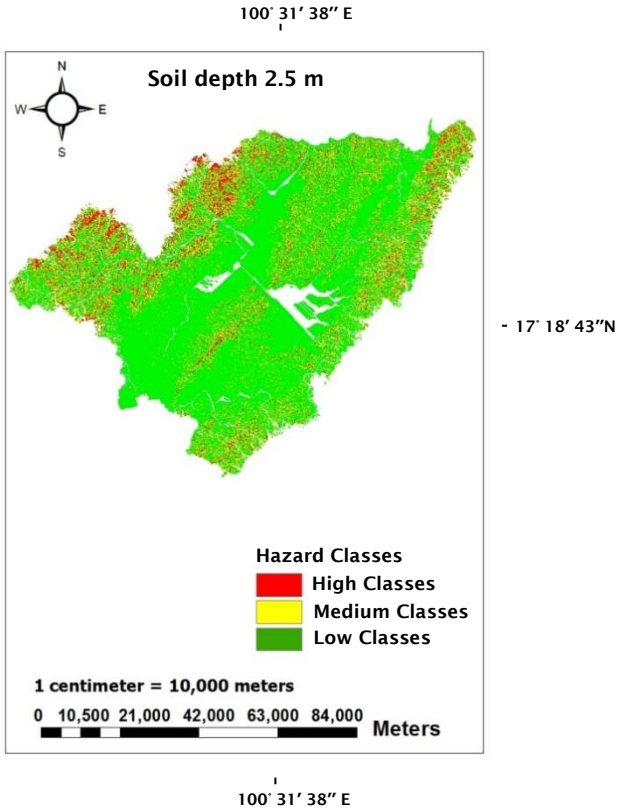

Figure 4.31 The sensitivity of landslide hazard mapping (soil depth 2.5 m)

The sensitivity of the soil depths were varied in the range of 0.25 – 2.5 metres, and the SINMAP output of the high, medium and low hazard classes were nearly the same in soil depths from 0.25 metres to 2.5 metres as show in five maps (Fig 4.26 -Fig 4.31). The high hazard classes increased from 0.25 metres to 1 metre of soil depth, and slowly decreased from 1metre to 2.5 metres of soil depth. On the other hand, the low hazard classes slightly decreased from 1metre to 1 metre of soil depth and slowly increased from 1metre to 2.5 metre of soil depth. The total area (km^2) of the high, medium and low hazard class areas was the same in the area of Thapla district (1,620.8 km^2) by the SINMAP outputs (Fig 4.32).

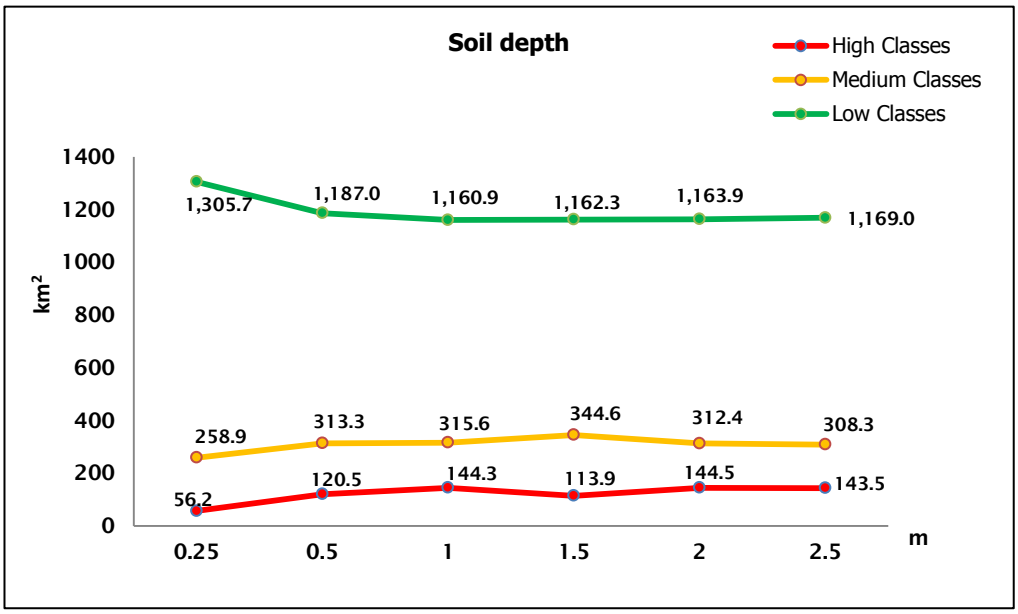

Figure 4.32 The behaviour of soil depth in three hazard class areas: high, medium and low

The high, medium and low classes of soil depth (0.25 – 2.5 metres) are quite stable, while the high class areas occur in hilly terrains (steep slope areas: 199.3 km^2) and low class areas occur in flat terrains (flat areas: 722.9 km^2) and occur in some parts of low slope (low slope areas: 849.0 km^2). The increasing of high class areas (failure regions) are 56.2 km^2, 120.5 km^2 and 144.3 km^2 in deep soil: 0.25 metre, 0.5 metre and 1.0 metre respectively (Fig 4.32), after 1.0 metre of soil depth the high class areas slowly decrease. Approximately 1 metre of soil depth was a critical depth in SINMAP model. As stated in the Literature Review, soil thickness is divided into four levels: 0-0.5 metres, 0.6-2.0 metres, 2.1-4.0 metres and > 4

metres, which affect landslide occurrence (DWR, 2010). The literature review shows the deeper soil on steep and low slopes presents increased risky areas.

As for SINMAP, it is applied for shallow translational landslides, corresponding to shallow ground water flow convergence, while it did not apply for deep-seated instability, including deep earthflows. The past landslides are shallow landslides, about 0.25 and 1 metre deep was reported by Jotisankasa (2008). Therefore, a critical deep link with the past shallow landslide, only shallow soil on steep and low slopes (1 metre of soil depth) is considered. The soil depths (1.5 – 3.0 metres) are over the detection limit that is why the high hazard class areas slowly decrease.

As a result, the variable soil depths have an impact of only 1 metre of soil depth in the SINMAP software and only 1.0 metre of soil depth is indicated by shallow landslides, so variable soil depths (1.5 – 3.0 metres) are not considered.

B. The variable permeability values were part of the sensitivity of the SINMAP model, whereas the shear strength and friction of angle values were default (Section3, Chapter3). The standard of rainfall values was 100 mm (DWR, 2011) and the soil depth used was 1 metre. The coefficient of permeability (k) was variable in four soil types: E-04: cm/sec (Fig 4.33), E-05 cm/sec (Fig 4.34), E-06 cm/sec (Fig 4.35) and E-07 cm/sec (Fig 4.36) (soft, medium, strong, hard) (Terzaghi et al., 1948) (Table 3.12), covering the soil types in the study site as shown for the areas of high, medium and low hazard classes in km^2 unit as given in Fig. 4.33–Fig. 4.37.

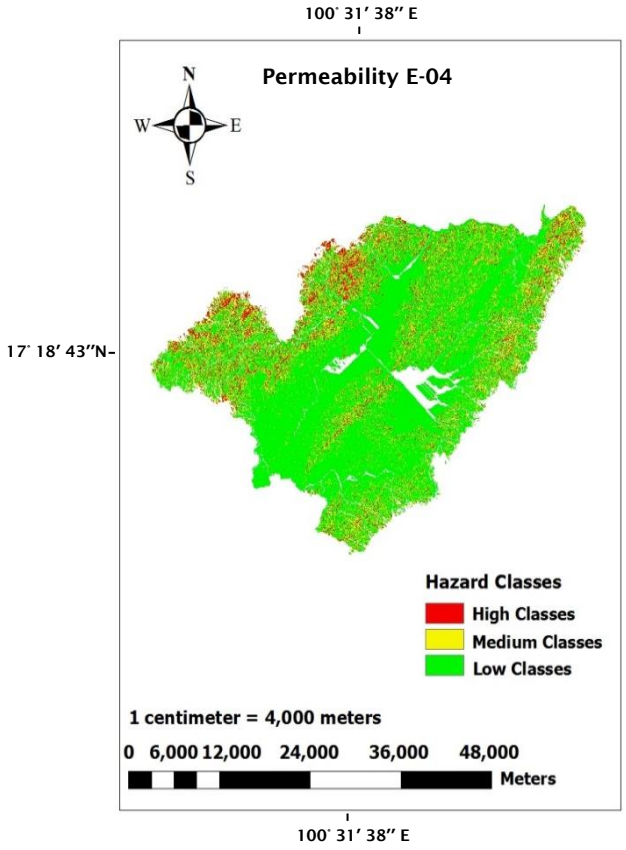

Figure 4.33 The sensitivity of landslide hazard mapping (permeability E-04 cm/sec)

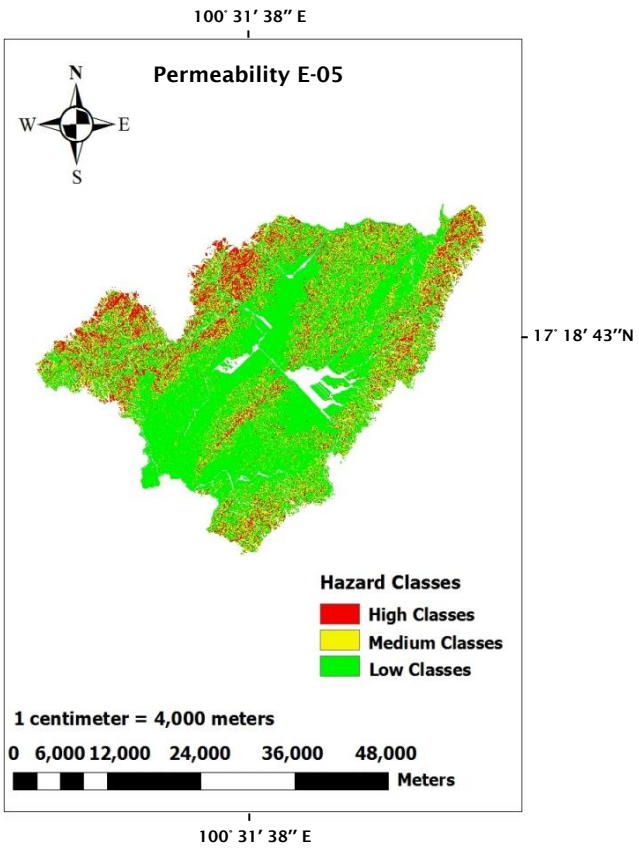

Figure 4.34 The sensitivity of landslide hazard mapping (permeability E-05 cm/sec)

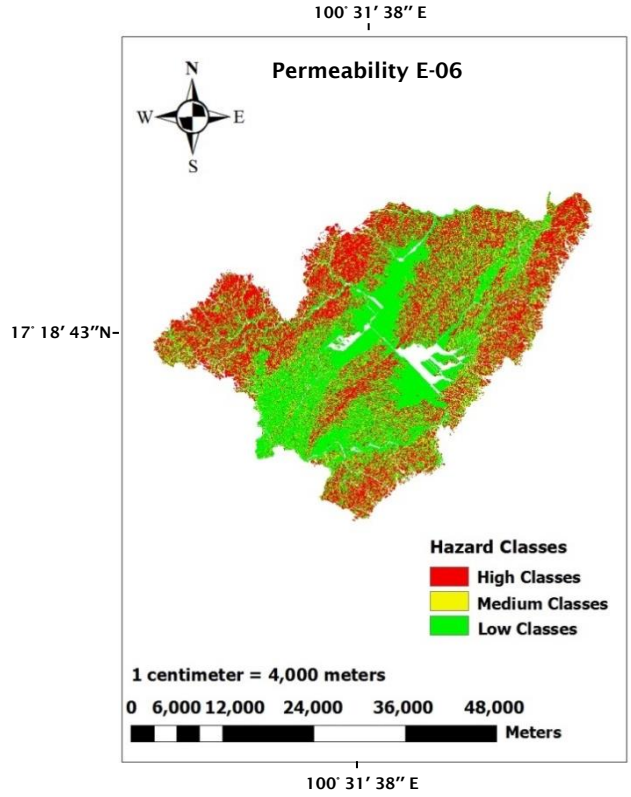

Figure 4.35 The sensitivity of landslide hazard mapping (permeability E-06 cm/sec)

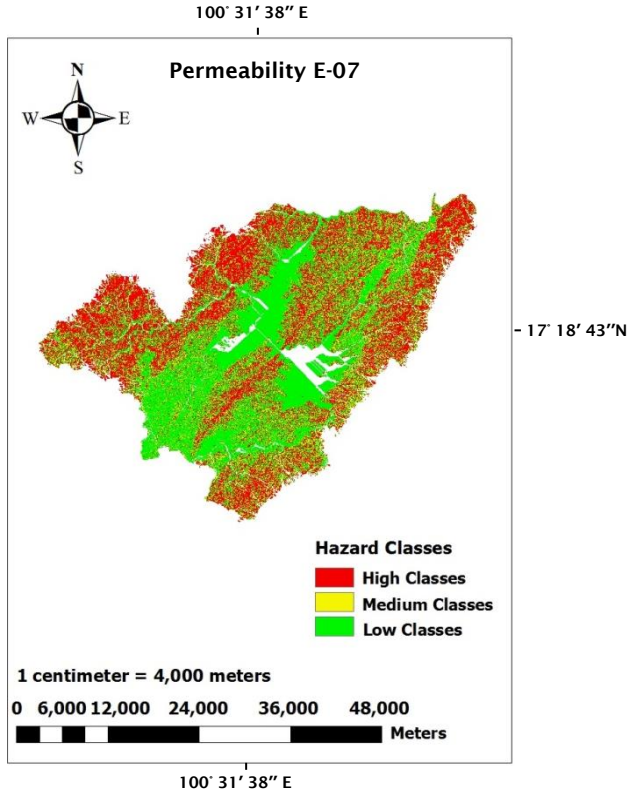

Figure 4.36 The sensitivity of landslide hazard mapping (permeability E-07 cm/sec)

The sensitivity of the tested permeability parameters varied in five values: E-04, E-05, E-06 and E-07, which related to soil types: soft, medium, strong, hard respectively. When high class areas increased, low class areas decreased, while medium class areas were nearly the same in five values (Fig 4.37).

First the high classes occurred in steep slope areas, and then in low slope areas and some parts of flat areas respectively (Fig 4.32 – Fig 4.36). Both high and medium class areas increased from E-04 to E-05 cm/sec, while low class areas decreased because both high and medium classes covered steep slope and low slope areas, so only some parts of low slopes remained showing in low classes.

In the range of E-05 to E-06 cm/sec, the high hazard class areas increased, while medium and low class areas decreased because the high class areas covered three ranges of slope gradients: steep slopes, low slopes and flats. So low slope and flat areas lost, the medium and low class areas decreased. Both Fig 4.11 and Fig 4.32 presented that the medium and low classes occurred in low slope and flat areas. The total km^2 unit of high, medium, low hazard class areas in each district was 1,620.8 km^2 (adding by high, medium, low hazard class areas). The total area of high, medium, low hazard class areas in each district was the same as the area of Thapla district (1,620.8 km^2) according to the SINMAP outputs (Fig 4.16). The high hazard class trend of the SINMAP output gradually increased and became constant, whereas the low hazard classes slightly decreased and became constant as shown in Fig 4.37. The areas of high hazard classes were contrasted with the permeability values in terms of km^2 units.

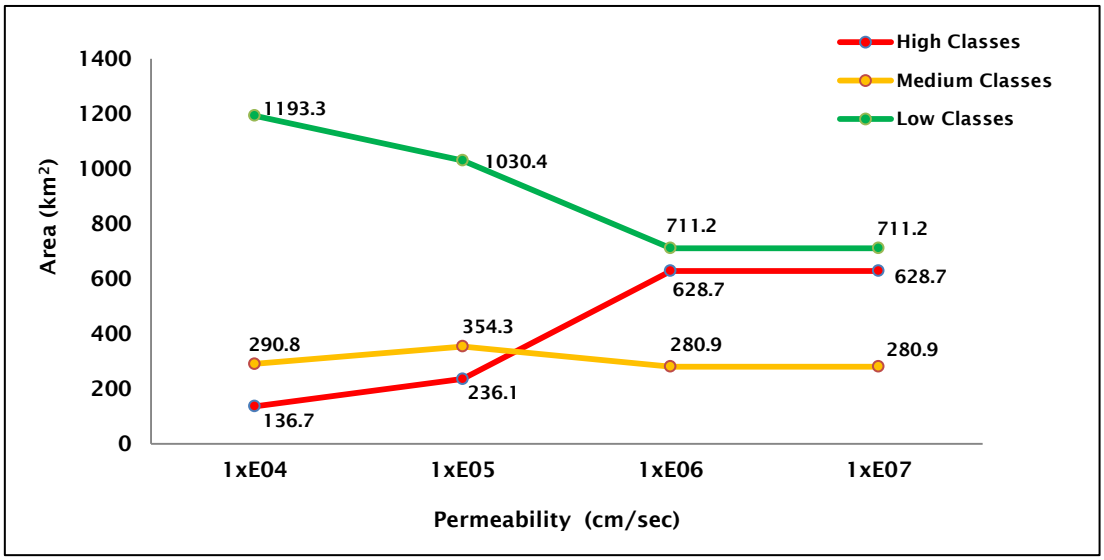

Figure 4.37 The permeability values of landslide hazard mapping in high, medium and low class areas

The permeability values are varied by soil types: E-04(sand), E-05(silt), E-06(silt) and E-07(clay) (Peck et al., 1948). Based on the SINMAP approach, a combination of shallow ground water flow is applied to analyse transitional shallow landslides, while the infinite slope stability model is linked with saturated soil depths and pore water pressure which are balanced with the proportion of discharge in catchment areas. The permeability values of both E-06 and E-07 are saturated soil so high class areas (failure region) are higher than other soils, covering three ranges of slope gradients: steep slope, low slope and some parts of flat areas. On the other hand, in E-04 of permeability value, most of high hazard class areas occur in steep slope areas (Fig 4.11 and Fig 4.32). As a result, the permeability value is an important parameter for the SINMAP model.

C. The sensitivity of the threshold rainfall values varied in the range of 50 – 300 mm/day, while 100 - 300 mm/day of rainfall values were recorded as associated with the past landslides (DMR, 2011). The 50 mm/day of rainfall values was presented for the smallest values because this value was often recorded by TMD (2011) in the rainy season. So this value is necessary to test for sensitivity. The high hazard class areas of the SINMAP output gradually increased from 50 (Fig 4.38), 100 (Fig 4.39), 150 (Fig 4.40), 200 (Fig 4.41), 250 (Fig 4.42) to 300 (Fig 4.43) mm/day respectively.

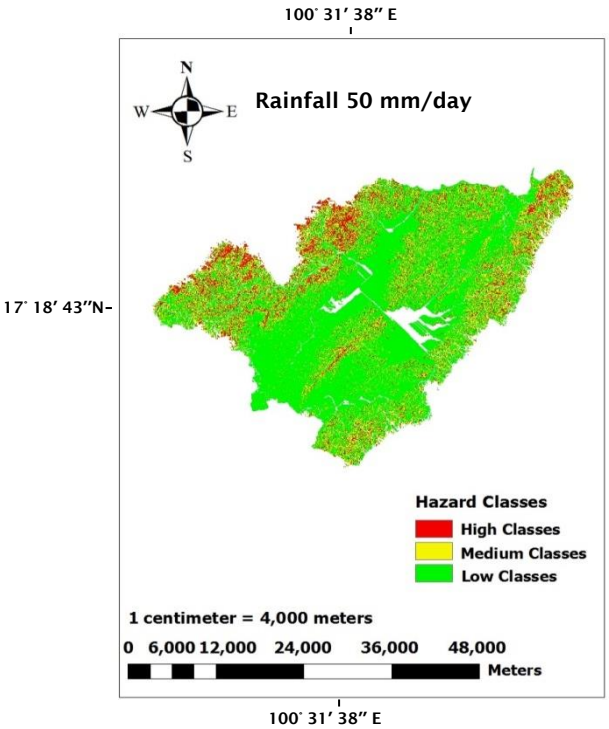

Figure 4.38 The sensitivity of landslide hazard mapping (rainfall 50 mm/day)

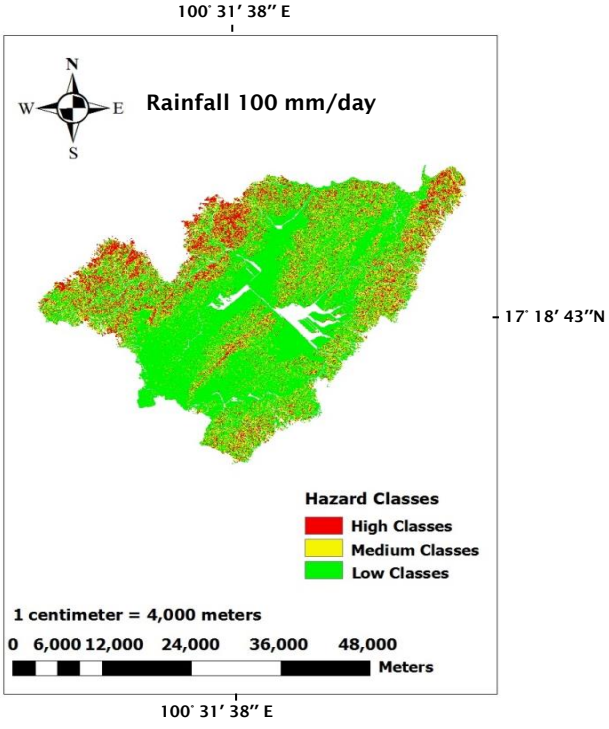

Figure 4.39 The sensitivity of landslide hazard mapping (rainfall 100 mm/day)

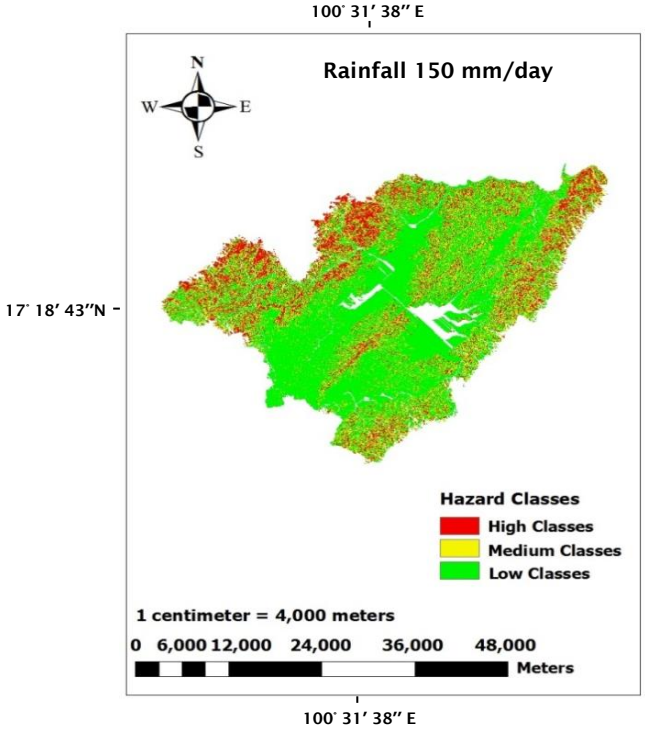

Figure 4.40 The sensitivity of landslide hazard mapping (rainfall 150 mm/day)

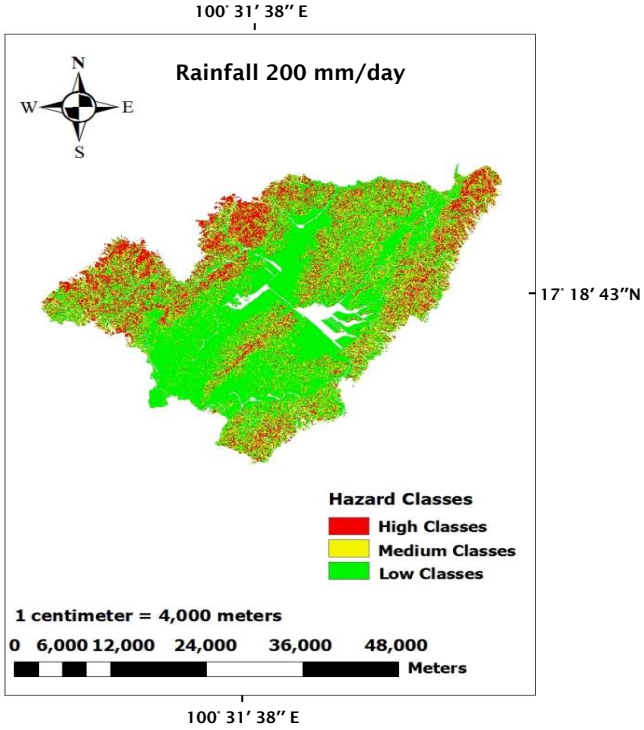

Figure 4.41 The sensitivity of landslide hazard mapping (rainfall 200 mm/day)

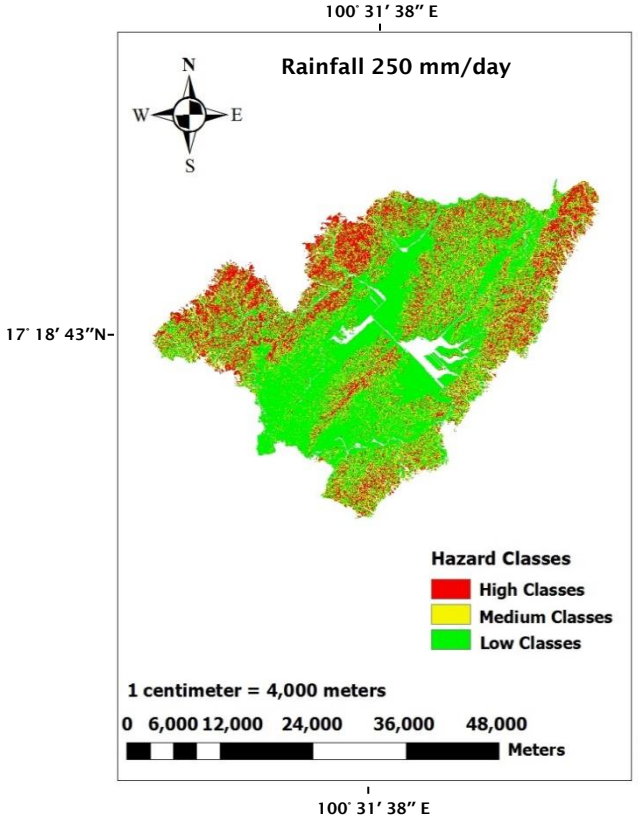

Figure 4.42 The sensitivity of landslide hazard mapping (rainfall 250 mm/day)

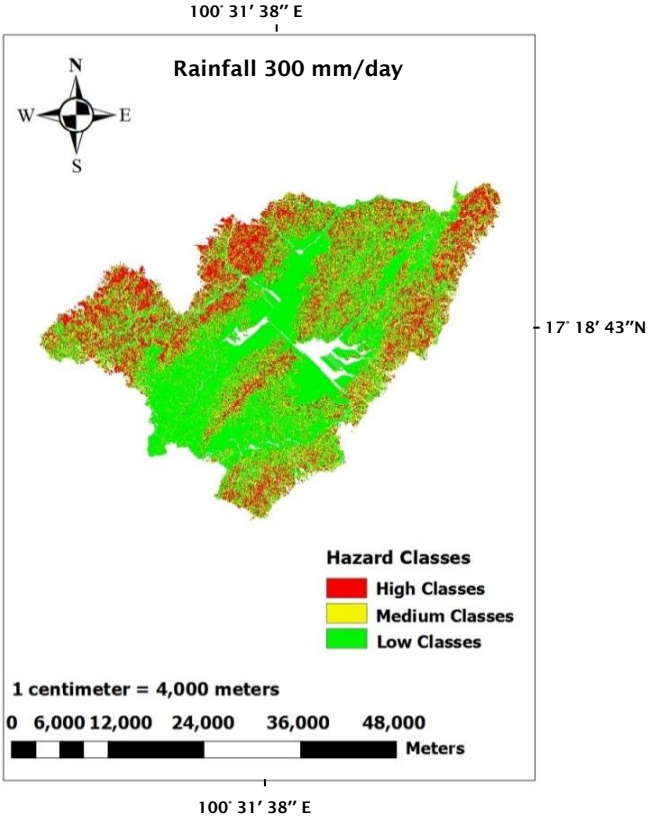

Figure 4.43 The sensitivity of landslide hazard mapping (rainfall 300 mm/day)

The high hazard class areas gradually increased, and the medium hazard class areas remained constant, whereas the low hazard class areas slightly decreased (Fig 4.38 to Fig 4.43). First the high hazard class areas occurred in steep slope areas, and then in low slope and flat areas respectively, when high class areas increased from 50 mm/day to 300 mm/day. The medium class areas occurred in the steep slope, low slope and flat areas that remained from the high classes. When the high class areas increased, the high class areas covered some parts of medium class areas. The medium class areas covered some parts of low class areas, and then low class areas decreased as shown in Fig 4.11 and in Fig 4.38 – Fig 4.43.

The total km^2 unit of high, medium and low hazard class areas was 1,620.8 km^2 (by adding high, medium, low hazard class areas). The total area of high, medium, low hazard class areas in each district was the same as the area of Thapla district (1,620.8 km^2) by the SINMAP outputs (Fig 4.44).

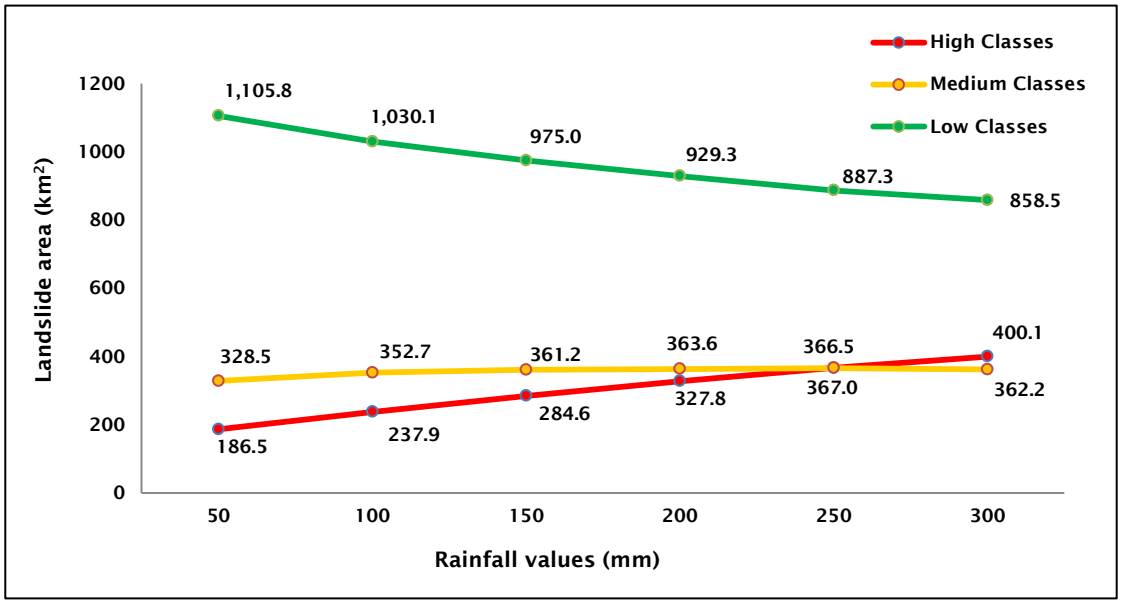

Figure 4.44 The rainfall values of landslide hazard mapping in high, medium and low class areas

In addition, the slope gradients and soil moisture are important factors for landslides during intense rainfall. The amount of rainfall, together with the slope gradients are the main cause. The infiltration of rainwater and the soil slope area are linked to the mechanisms of the landslide (DWR, 2010). As a result, the increased rainfall values lead to the increase of high class areas (failure region), covering steep slopes, low slopes and flat areas, while the medium class areas are

quite stable, covering low slope and flat areas, so some areas of steep slopes and flats remained in low classes.

4.2.4 Dominant parameters of SINMAP model

There are five main parameters: slope gradients, dimensionless cohesion, angle of friction, permeability and rainfall. First, the most important is slope gradients and rainfall, since the high hazard class relates to steep slope areas, while medium and low classes occur in low slope and flat areas when it rains. The rainfall is also most important because rainfall is the main cause for landslide (hydrological data (T/R) it is impossible for R to show zero). Next, three parameters: dimensionless cohesion, angle of friction and permeability of are equal importance. The soil depth of 1.5 – 3.0 metres is not sensitive, since it is over the detection limit of the SINMAP model. All parameters are considered only in 1 metre of soil depth, because of shallow landslides (applied by SINMAP model). As a result, the high hazard class areas (failure regions) are considered for sensitivity analysis. The high values of rainfall lead to saturated soil, while dimensionless cohesion and permeability values decrease on a steeper slope. The processes of slope failure occur. Thus, the low values of both dimensionless cohesion range and angle of friction present for high areas of high hazard class (failure regions), while the low values of permeability (saturated soil) also increase the high hazard class areas. All high class areas are related through hilly and mountainous terrains (both steep slopes and low slopes).

As for sensitivity, the high hazard class areas increase from 186.5 to 362.2 km^2 when rainfall values increase values from 50 to 300 mm/day (Fig 4.44), on the other hand the high hazard class areas decrease from 236.4 to 0 km^2, while the range of dimensionless cohesion increases from 0 – 0.25 to 1 – 1.5 (Fig 4.17). In terms of angle of friction, the high hazard class areas decrease from 1,224 to 120 km^2, while the range of angle of friction increases from 5^o – 10^o to 35^o – 45^o (Fig 4.25). The high hazard class areas increase from 136.7 to 628.7 km^2 when permeability values decrease values from E-04 to E-05 cm/sec (Fig 4.37). The corresponding of four parameters relate to landslide and SINMAP theory, including slope gradients. The reason, as analysed above, is that the regression of four parameters are shown in high hazard class areas.

Regression analysis is used to show the correlation in terms of linear regression. As described in the graph, the regression of relationship of high class areas and

main four parameters: dimensionless cohesion, angle of friction, permeability and rainfall are presented as shown in Fig 4.45 - Fig 4.48. The regression between rainfall values and high class areas has a regression r^2= 0.99 for SINMAP model, on the other hand the regression between high class areas and all three parameters: dimensionless cohesion, angle of friction, permeability have negative slopes. The value of the correlation coefficient both rainfall and angle of friction are so good (r^2=0.99), and higher than other parameters. The correlation coefficient of dimensionless cohesion and permeability are presented: (r^2=0.75) and (r^2=0.57). The reason, as analysed above, is that five parameters are sensitive for landslide analysis in SINMAP model, while the most important is slope gradients and rainfall.

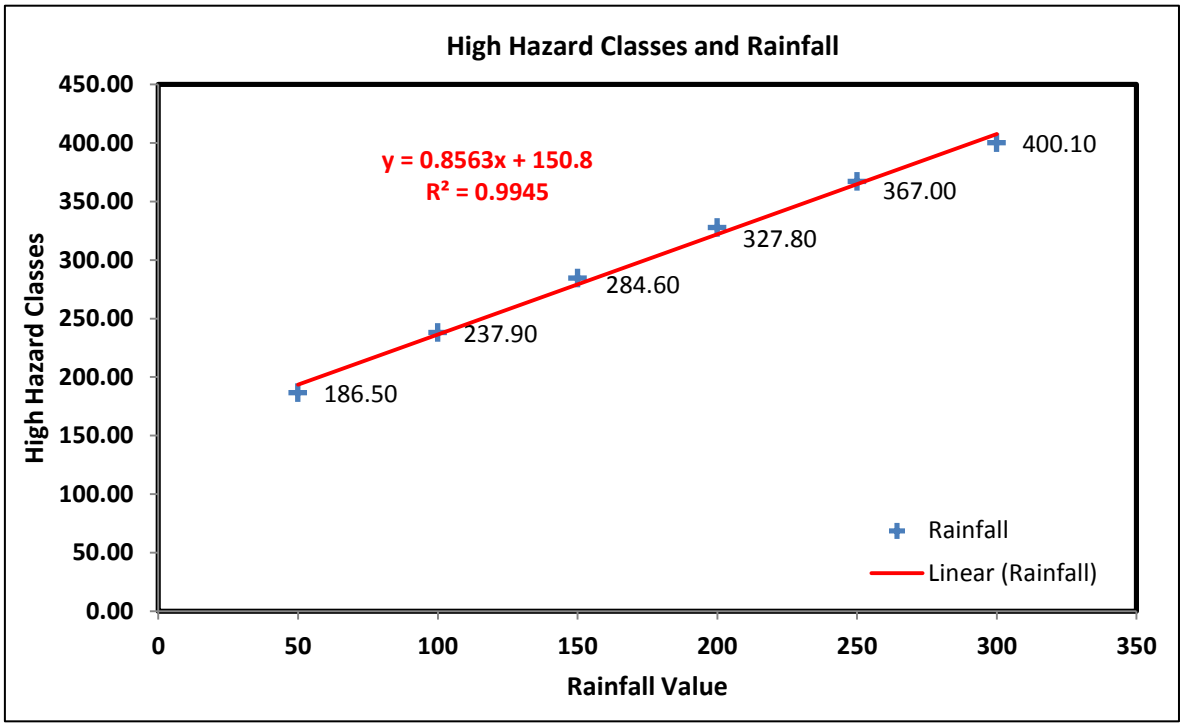

Figure 4.45 The correlation coefficient of rainfall related to the high hazard class areas (km^2) (failure regions)

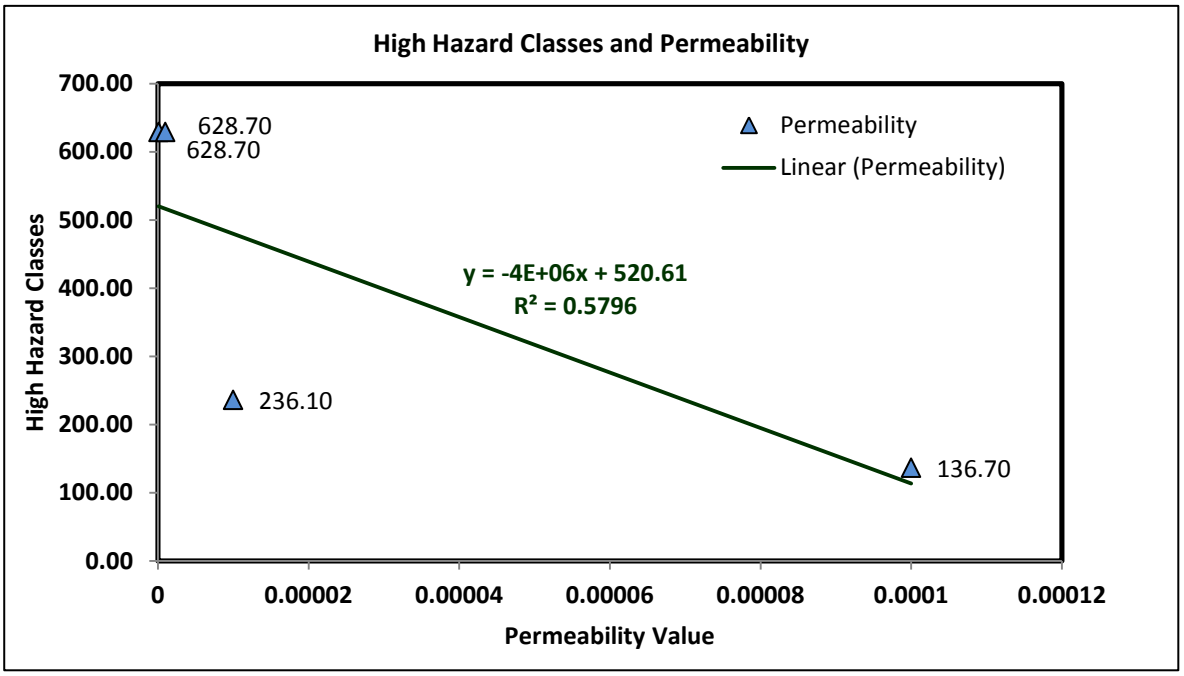

Figure 4.46 The correlation coefficient of permeability related to the high hazard class areas (km²) (failure regions)

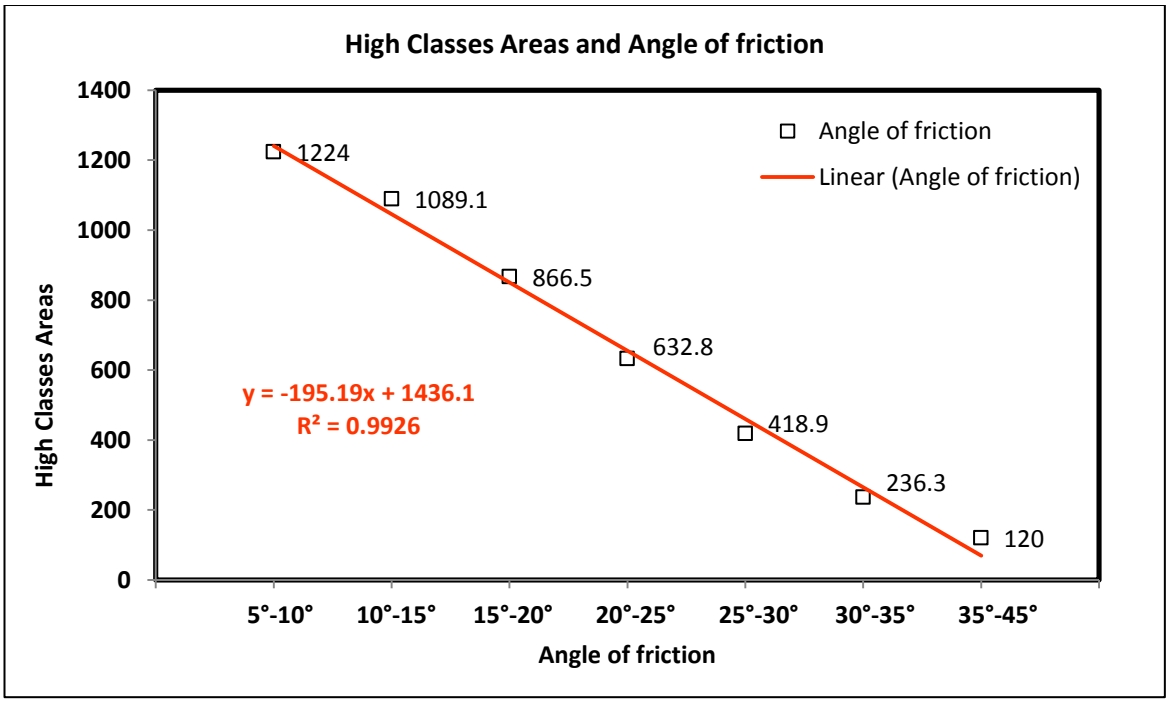

Figure 4.47 The correlation coefficient of angle of friction related to the high hazard class areas (km²) (failure regions)

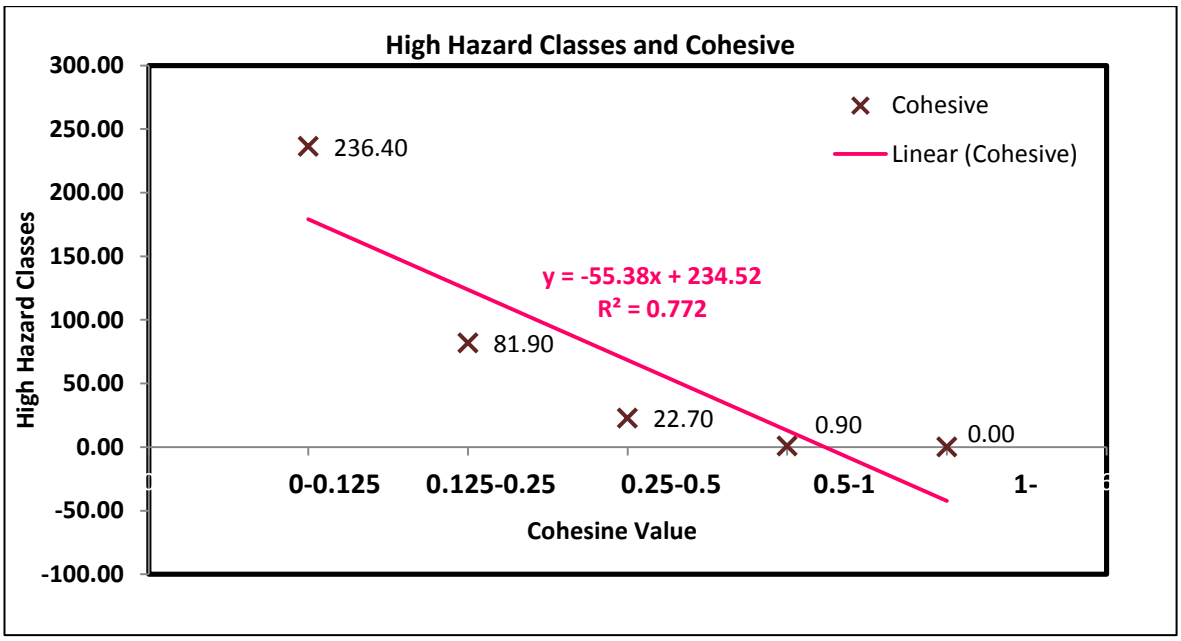

Figure 4.48 The correlation coefficient of dimensionless cohesion related to the high hazard class areas (km^2) (failure regions)

It can be seen in the sensitivity of the SINMAP model, first, the most important is slope gradients and rainfall. Next, three parameters: dimensionless cohesion, angle of friction and permeability are of equal importance. The SINMAP model is based on the infinite slope stability model linked to saturated soil depth and pore water pressure, which are balanced with the proportion of discharge in catchment areas. These three parameters affected landslide occurrences and associated with landslide theory. Jotisankasa (2008) presented that the pore water pressure may affect the full soil thickness, which can be fully or nearly saturated. Then, this saturation of the soil slope reduces the shear strength of the soil and destabilizes the slope. The slope failure generally presents when the wetting front moves to the bottom of the soil slope, the change of the pore water pressure might act to destabilize the slope. All of parameters are linked each other.

Eventually, both the calibration and the sensitivity are related to the SINMAP analysis. Although the zonation of landslide risk covered more areas than just the landslide scars, the percentage of risk areas (both high and medium hazard class areas) and slope gradients (both steep and low slope areas) are linked to each other. First the percentage of risk areas covers almost all areas of steep and low slopes, then it covers some parts of flat areas. So, the output of SINMAP is linked with slope gradients. Sensitivity, slope gradients and rainfall are dominant parameters for SINMAP. The high class areas increase on steep slopes, low slopes and flats respectively when rainfall increases. The characteristics of soil (cohesive

soil, permeability and angle of friction) also affect the risk areas. The high value of cohesive soil can reduce the failure region in steep and low slope areas.

CHAPTER 5 THE RESULTS OF LANDSLIDE HAZARD MAPPING COMPARING PRESENT-DAY CONDITIONS AND FUTURE SIMULATION

This chapter is divided into three sections. The first section describes the landslide hazard mapping for the present-day conditions in Uttaradit province, calculating rainfall values from 1954 to 2012. Then in the second section, the landslide hazard mapping in the future simulation during 2013-2099 will be forecast by SDSM program version 4.2 and START. Finally, the comparison of zonation of landslide risk (km^2) in the landslide hazard mapping, between both the calibration of present-day conditions and the future simulation, are presented by SINMAP software on Arc GIS version 10.1.

5.1 Landslide hazard mapping calibrated for present-day conditions

5.1.1 Hydrological data

In present-day conditions, the average observed rainfall values between 1954 and 2012 were calculated, covering nine provinces: Uttaradit, Tak, Pisanulok, Khon Kaen, Udontani, Lampang, Petchaboon, Phrae and Loei. This spatial scale was selected as the downscaling of the SDSM version 4.2 covered all nine provinces, including the study site (Section 3.8.1, Chapter 3). The average annual rainfall values were calculated in mm/24 hours for the landslide analysis because this unit will show accumulated rainfall within 24 hours, i.e. the wet time period, according to SINMAP software (Table 5.1). Thus, average three-hourly rainfall totals from 1981 to 2010 were used to calculate the standard of days rain per year for each rain station covering nine provinces (Section 3.8.1, Chapter 3). The days-rain per year and annual rainfall were used to calculate rainfall in mm/24 hours as in Table 5.1

Rainfall values (1954-2012)	Uttaradit	Tak	Pisanulok	Khon Kaen	Udontani	Lampang	Petcha boon	Phrae	Loei
Average annual rainfall	1,412.4	1,039	1,303.8	1,200	1,420.1	1,061.1	1,123.2	1,110.9	1,248.8
Days rain per a year	19	18	19	15	18	16	20	18	18
Average daily rainfall (mm/24 hours)	74.3	57.7	68.6	80	78.9	66.3	56.2	61.7	69.4

Table 5.1 The average annual rainfall and the rainfall value rates from 1954 to 2012

The interpolation function in Arc GIS software was used to average rainfall values for each rain station covering the nine provinces for spatial analysis as shown in Fig. 5.1. Then, the interpolation map is presented with rainfall values (mm/24 hours) covering the nine provinces.

The rainfall values analysis focuses on Uttaradit province, the strongly intense rainfall present in three districts: Maung, Laplea and Tron districts: 78.2 mm/24 hours, while Nampat, Phichai and Thongsaenkhun districts are 69.6 mm/24 hours, and between 65.5- 69.6 mm/24 hours in Thapla district. The rainfall values, calculated by T/R will be calculated for all districts. Only one rainfall value is presented for each district.

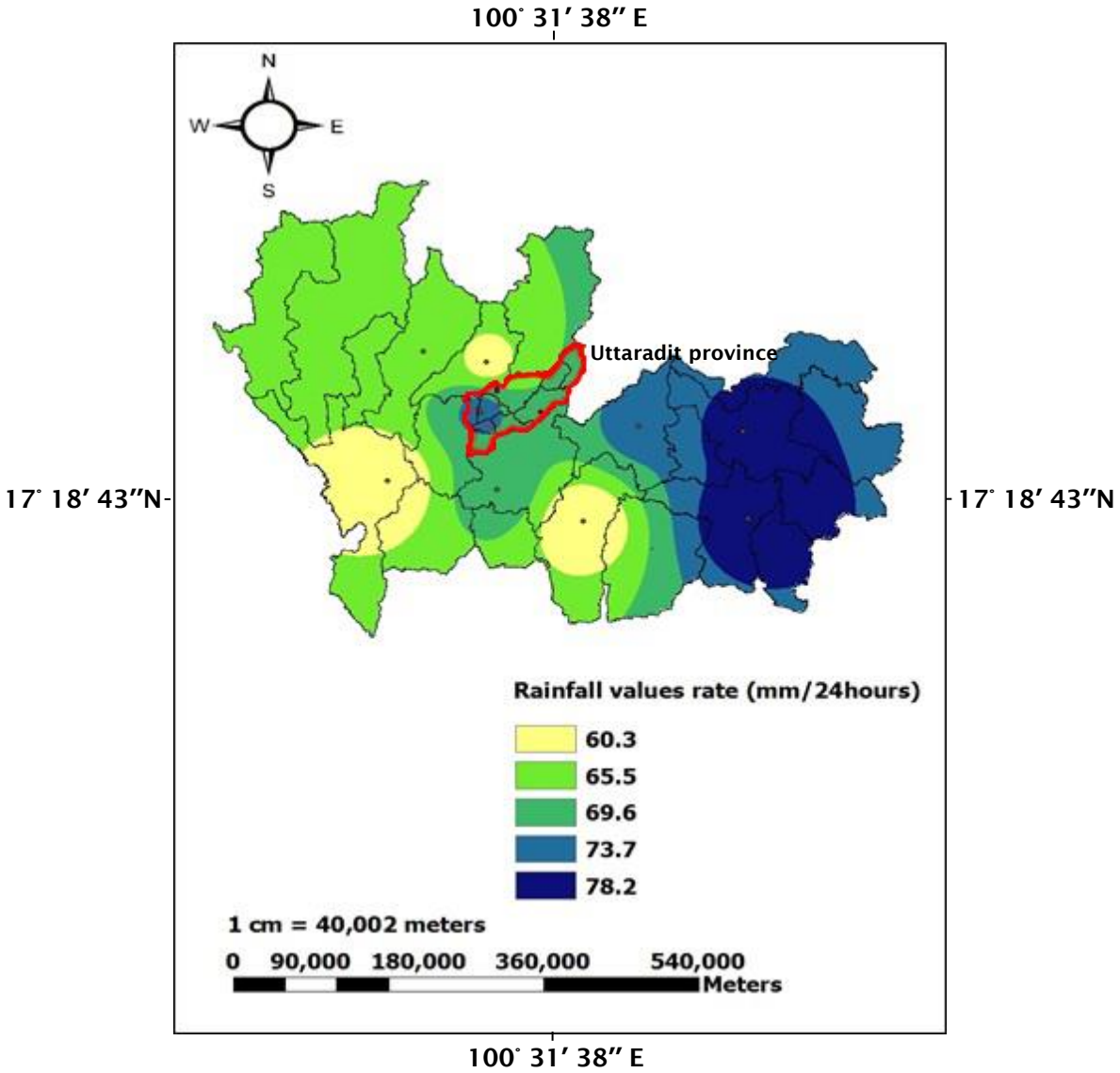

Figure 5.1 The interpolated map covering nine rain stations from 1954 to 2012 and the rainfall values focusing on Uttaradit province

5.1.2 Geotechnical data

The required SINMAP parameters were assembled from the geotechnical soil data. Soil and root cohesion, friction angle, permeability (hydraulic conductivity), soil depths and soil density were obtained from the geotechnical laboratory results for each district (Section 3.5, Chapter 3) and hydrological data (interpolated rainfall values from 1954 to 2012) (Fig 5.1), as shown in Table 5.2. The upper value of dimensionless cohesion was used from the geotechnical laboratory results from each district, while the lower value of sand and silt (ML or OH, MH or OH and SM) was used for dry sand (cohesionless soil) (Kangsasitiam et al., 2004) and the lower value of clay was used for the lowest cohesive soil parameter.

As for silt and sand, silt (ML/OH and MH/OH) and sand (SM) consist of sand and organic material. The test pit locations 1, 2 and 4 presented: ML/OH as silt (low liquid limit) and organic (high liquid limit) and the test pit location 3 presented: MH/OH as silt (high liquid limit) and organic (high liquid limit), while the test pit location 5 presented: SM (sand and silt). The liquid limit (LL) was measured to determine the range of moisture content, while the liquid limit (LL) was less than 35%, showing a low value of plasticity.

Therefore, dry sand (cohesionless soil) can be found in test pit location 1- 5. On the other hand, clay exhibits cohesive soil, so the cohesionnless soil could not present the lower values of dimensionless cohesion of clay (Head et al., 1994). Clays were found in TP6 and TP7 and linked with dimensionless cohesion values: 2.34 in Bankhok district, and 1.017 in Faktha district, while dry sands (cohesionless) did not present in both districts. The lowest cohesion value of clay was approximately 2.5 Kpa (Srinil et al., 2001). The test pit location 7 (Faktha district) as shown in Table 5.2 represented the lower value (i.e. *C*: (Dimensionless Cohesion) = $(Cr+Cs)/(h\rho_s g)$: [2.5/(0.5x1.984x9.89)]). Therefore, the lower dimensionless cohesion value was 0.256 in clay.

As for root strength, the vegetation type was investigated by direct field observation in Uttaradit province in December 2013. There were four vegetation types: orchards, semi-natural and plantation forest (mountain areas), rubber tree plantations and horticultural areas in six districts, which types are explained below.

The effect of tree roots on slope stability was considered by the species of vegetation. Seven tree species in four vegetation types were selected for shearing tests in the laboratory and reported by Nilaweera (1994) (Section 3.2.1, Chapter 3). Four vegetation types are classified by seven tree species as follows:

a. Orchards: Hibiscus macrophyllus

b. Semi-natural and plantation forest (teak): Dipterocarpus alatus, Hopea odorata and Ficus benjamina

c. Rubber tree plantations: Alangium kurzii and Alstonia macrophylla

d. Agricultural area (slash-and-burn agriculture annual crops and galangal oil): Hevea brasiliensis

Given the geotechnical data described, the seven test pit locations of the six districts (Muang (TP1), Laplea (TP2), Thapla (TP3, TP4), Nampat (TP5), Bankhok (TP6), Faktha (TP7)) were used as data sources. The other three districts were not used for soil samples: Phichai, Tron and Thongsaenkhun, so soil samples were used from another test pit location which was near. Both Tron and Phichai, were used from the second test pit location (TP2) and Thongsaenkhun (TP5) was used from the fifth test pit location (TP5) for the SINMAP calculation because both Phichai and Tron districts were found in small areas of hilly terrain or mountains. Hilly and mountainous areas in Thongsaenkhun and Nampat districts are adjacent to each other.

Test Pit	District	Soil type	Soil depth (h) (m)	Soil density (ρ_s) (Kg/m^3)	Root Cohesion (KPa)	No root Cohesion (KPa)	Cohesionless (KPa)	Soil Cohesion (KPa)	Combined Cohesion (KPa)	Lower dimensionless cohesion	Dimensionless cohesion	Friction Angle	Hydraulic Conductivity (ks) (Permeability) cm/sec	Transmitivity (m^2/day)	Recharge (rainfall value) (mm/day)	T/R (m)
TP1	Muang	ML or OH	0.5	1568	1.1014	0	0	6.96	8.06	0	1.048	26.23	4.006E-06	17.305	73.7	234.8
TP2	Laplea	ML or OH	0.5	1762	1.1014	0	0	10.30	11.40	0	1.32	32.23	2.918E-05	126	73.7	1709
TP3	Thapla	MH or OH	0.5	1822	1.1014	0	0	12.85	13.86	0	1.56	33.13	6.081E-06	26.27	69.6	377.4
TP4		ML or OH	0.5	1961	1.1014	0	0	16.18	17.281	0	1.75	28.86	1.72 E-06	22.69	65.5	401.1
TP5	Nampat	SM	0.5	1716	2.2526	0	0	7.85	10.10	0	1.20	30.09	3.415E-04	1475.3	69.6	21196.8
TP6	Bankhok	CL	0.5	1477	2.7140	0	2.5	7.85	14.02	0.256	2.34	24.62	1.175E-06	5.076	69.6	72.9
TP7	Faktha	CL	0.5	1984	2.9417	0	2.5	7.85	6.96	0.256	1.017	26.23	8.187E-05	353.7	69.6	5081.9

Table 5.2 The calculation of SINMAP parameters in six districts

5.1.3 Landslide hazard mapping in Uttaradit province

In this study, both geotechnical and hydrological data were input into the SINMAP program for each district because the characteristic of soil and rainfall values were not the same for each district. Then, the landslide hazard mapping was presented for nine districts of Uttaradit province.

For each of the nine districts: three levels of hazard classes: high, medium and low, are shown in Fig 5.2 and Fig 5.3. The hazard class areas: (high (red), medium (yellow) and low (green)) were presented for each district and also the total area for each of the districts (purple) in Fig 5.3. Four districts were areas of past landslides: Muang, Laplea, Thapla, Nampat, five districts were not areas of past landslides: Bankhok, Faktha, Phichai, Tron and Thongsaenkhun. Two of five districts: Phichai and Tron were found in particularly steep and low slope areas. Both steep and low slope areas were only 0.75% - 7.77% of all areas in Phichai district and 0.26 – 9.49 % of all areas in Tron district. The 5.2 km^2 of steep slope, 54 km^2 of low slope and 635.8 km^2 of flat areas showed in Phichai district, include the total area of the district (695 km^2), while 0.8 km^2 of steep slope, 29.5 km^2 of low slope and 280.4 of flat areas showed in Tron district, include the total area of the district (310.7 km^2). The slope gradient areas (km^2) in each district are shown in a map (Fig 5.4). The real areas (i.e. areas according to GIS software) also presented for three slope gradient areas in each district: steep slopes (25^o – 65^o), low slopes (10^o – 25^o) and flats (0^o – 10^o) and are shown by the three colours: red, yellow and green respectively, and include the total area of all the districts (purple) as shown in Fig 5.5. The SINMAP output areas (i.e. areas according to SINMAP software) were less than the real areas of GIS software (on the ground) (Section 4.1.1, Chapter4). The SINMAP output areas (all three hazard class areas: high, medium and low) of the nine districts were compared with the real areas by GIS software (all three slope gradient areas: steep slopes, low slopes and flats) as shown in Table 5.3.

Area	Muang	Laplea	Thapla	Nampat	Bankhok	Faktha	Thong saenkhun	Phichai	Tron
Total slope gradient areas (km^2)	808.5	468.5	1771.2	1451.2	987.0	644.9	735.1	695.0	310.9
SINMAP out areas(km^2)	751.4	424.0	1620.7	1328.0	901.2	592.4	669.8	655.6	290.2
Missing areas(km^2)	57.1	44.5	150.5	123.2	85.8	52.5	65.3	39.4	20.7
Missing areas%	7.0	9.5	8.5	8.5	8.7	8.1	8.9	5.7	6.7

Table 5.3 The comparison between the real areas of GIS software and SINMAP output areas of nine districts in Uttaradit province

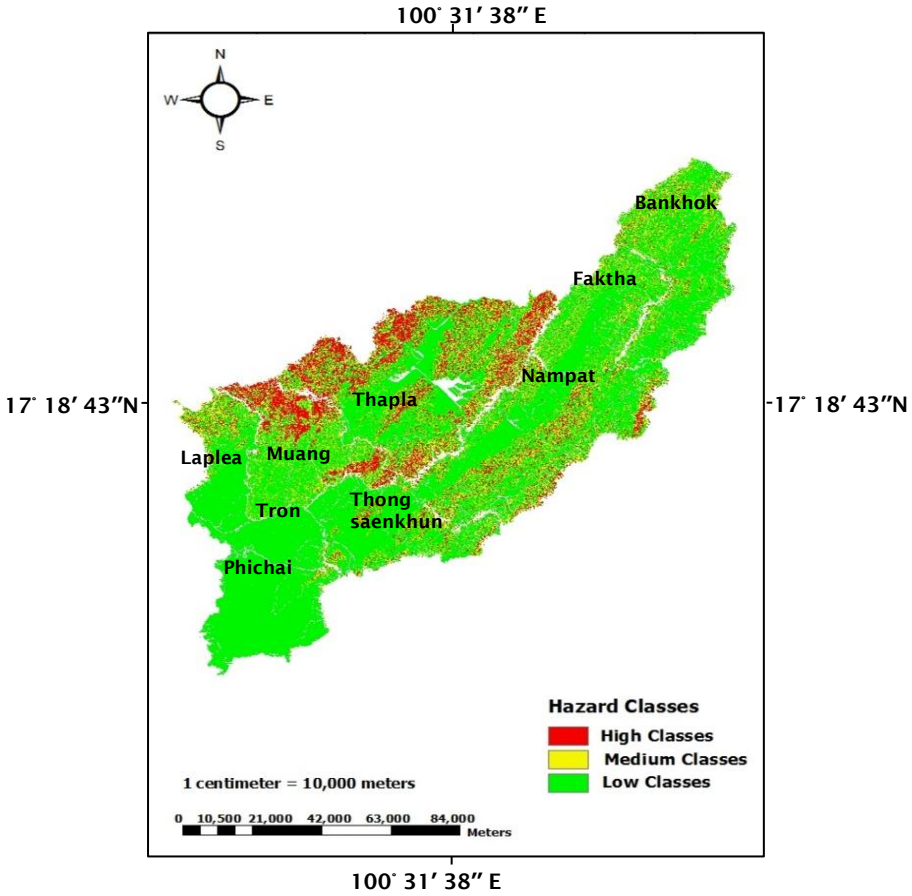

Figure 5.2 The hazard class areas: high (red), medium (yellow) and low (green) showing in each district for landslide hazard mapping in Uttaradit province for the present-day conditions

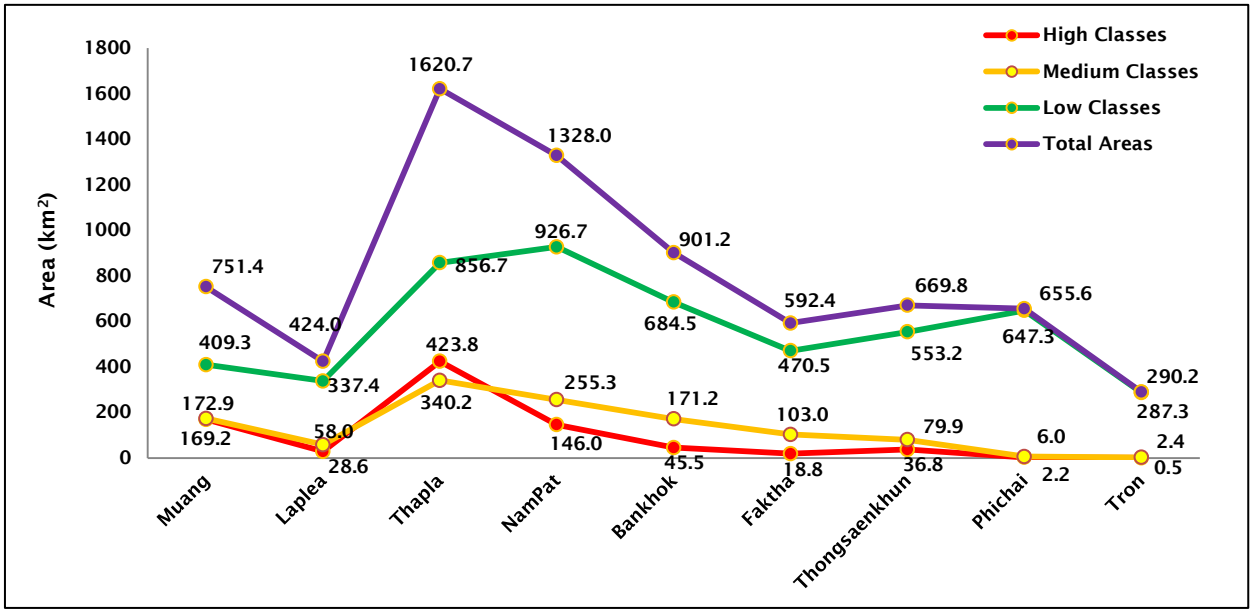

Figure 5.3 The hazard class areas (km²): high (red), medium (yellow) and low (green) showing in each district and also the total area of all districts (purple) in Uttaradit province

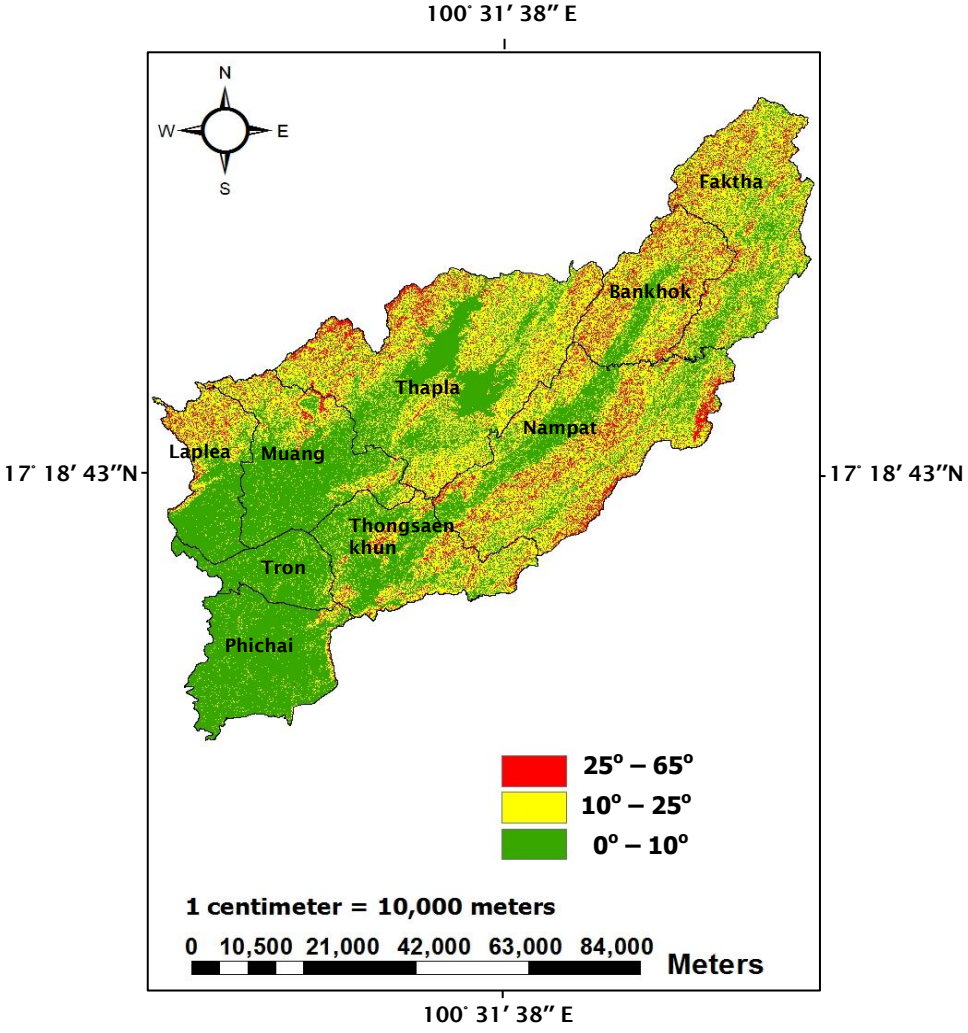

Figure 5.4 The classification of slope gradient areas: steep slopes (25° – 65°), low slopes (10° – 25°) and flats (0° – 10°) in the nine districts in Uttaradit province

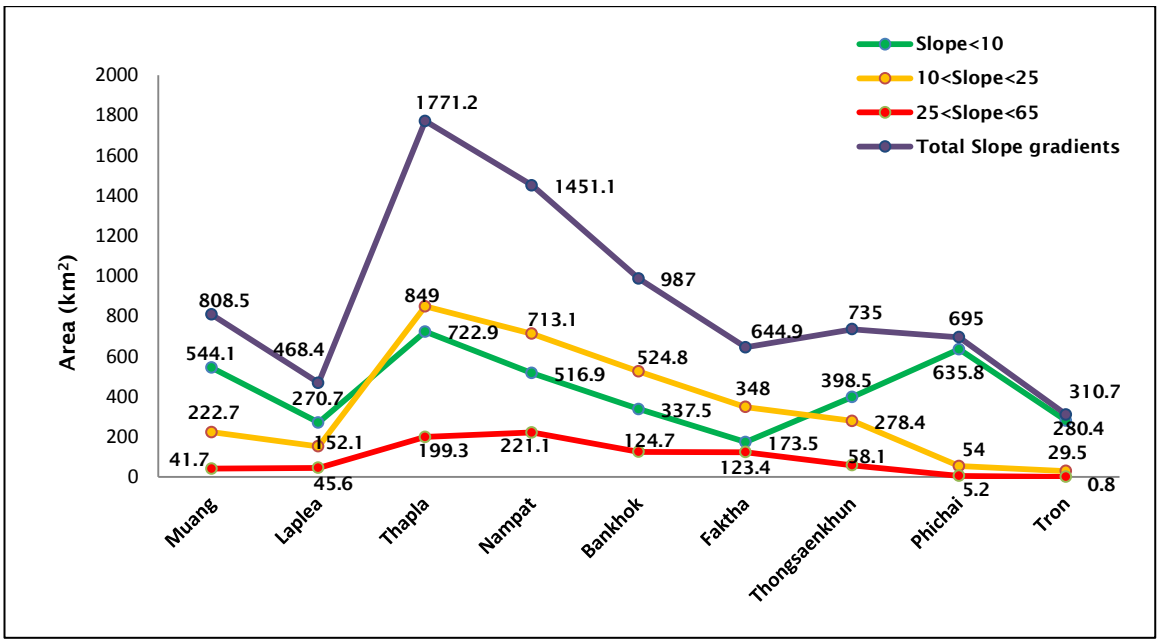

Figure 5.5 The real areas of GIS showing slope gradient areas: steep slopes (25° – 65°), low slopes (10° – 25°) and flats (0° – 10°) in each district and also all areas of districts (purple) in Uttaradit province

In this study, the landslide hazard mappings are divided into three levels of hazard classes: high (failure regions), medium (instability) and low (safety areas) As for the calibration, in tambon Maephun in Laplea district, approximately 74.7% of SINMAP output (averaged by adding the percentage of both high (41.9%) and medium (32.8%) classes in this tambon) and 87.4% slope gradients (averaged by adding the percentage of both steep slopes (28.1%) and low slopes (59.3%) in this tambon). In tambon Namman in Thapla district, approximately 85.6% of SINMAP output (averaged by adding the percentage of both high (77.1%) and medium (8.5%) classes in this tambon) and 85.6% slope gradients (averaged by adding the percentage of both steep slopes (36.4%) and low slopes (49.2%) in this tambon). Both high and medium classes and steep slopes and low slopes are linked to each other and the percentages of high and medium classes and steep slopes and low slopes are quite high. Lastly, most failure regions and instabilities occurred in hilly and mountainous areas. All areas of both high and medium classes are selected for the zonation of landslide risk.

Then, 25.3% of low classes in tambon Maephun and approximately 14.4% of low classes in tambon Namman are present in landslide scar areas. Approximately 19.85% of low class areas are selected for the zonation of landslide risk because of the average percentage of low classes in these two tambons (i.e. calculated:

(25.3% + 14.4%)/2). The 19.85% of landslide scar areas were presented in low classes because of the slide of soil mass from steep gradient areas onto low slope areas around the foot of the mountains. In addition, 13.5% of landslide scar also presented in flats in two tambons (i.e. averaged: 12.6% of tambon Maephun + 14.4% of tambon Namman/2) because flat areas were found in the high mountains. Therefore, all areas of high and medium hazard classes and 19.85% of low class areas are selected for the zonation of landslide risk.

The relationship between the three hazard classes and three slope gradients were presented for each district. The zonation of landslide risk presented in all areas of high and medium classes and 19.85% of low class areas and also classified as steep slope, low slope and flat areas in nine districts: Muang, Thapla, Laplea, Nampat, Thongsaenkhun, Faktha, Bankhok, Tron and Phichai as follows:

a) Muang district

The zonation of landslide risk covered all steep slope, low slope areas and also covered some parts of flat areas. The high class (failure regions) areas are clearly shown in the map (Fig 5.6), as this class covered: 35.8 km^2 (21.2%) of steep slopes, 124 km^2 (73.3%) of low slopes and 9.4 (5.6%) of flats respectively. The steep slope areas are less than low slope areas because the steep slope areas are only 41.7 km^2 (5.16%) of all the areas of Muang district (Fig 5.5).

In Muang district, approximately 9.4 km^2 (5.6%) of flat areas were found in the high hazard class. The flat areas were found in high hazard classes because some flat areas were found around the top of mountains. The high class (failure region) frequency occurs only in hilly and mountainous terrains. First the high risk zone covered almost all areas of steep slope and then it covered low slope and flat areas because steep slopes, as low slopes and flats were mixed together in the mountains. The flow directions is to assign flow from each grid cell, either adjacent or diagonally, in the direction of the steepest downward slope. Thus, the increase of infiltrated rainfall related to the slope gradient, can increase the high hazard class areas as the infinite slope model is related to slope length (Montgomery and Dietrich, 1994).

The medium classes covered both 45 km^2 (26%) of low slope areas and 127.6 km^2 (73.8%) of flat areas, while most of the flat areas was found in low class: 374.2 km^2

(91.4%). Most of the flat areas was found around mountains, so about 127.6 km^2 (73.8%) of flat areas occurred in the medium classes (Table 5.4).

There were four parameters: dimensionless cohesion, angle of friction, permeability and rainfall, which were considered. In this case, the dimensionless cohesion value of [1.048] (shear strength & root strength values) and permeability value of [4.006E-06 cm/sec] were low, when compared with other districts. The angle of friction value was also low: 26.23^o. On the other hand, 78.2 mm/24 hours of rainfall in terms of T/R was higher than other districts (Table 5.2). The permeability, dimensionless cohesion and friction angle were small, while rainfall value was high that is why these four parameters led to the highest of zonation risk in this district.

These four parameters lead to big areas of zonation of landslide risk. Finally, in Muang district, the zonation of landslide risk is presented in a map (Fig 5.6). Steep slope, low slope and flat areas were calculated by adding 100% of high & medium classes and 19.85% of low class areas (zonation of landslide risk), covered approximately 36.5 km^2 of steep slopes (by adding of high (35.8 km^2), medium (0.3 km^2) and low (0.4 km^2) classes), 203.6 km^2 of low slopes (by adding of high (124 km^2), medium (45 km^2) and low (34.6 km^2) classes) and 183.2 km^2 of flats (by adding of high (9.4 km^2), medium (127.6 km^2) and low (46.2 km^2) classes (i.e. the zonation of landslide risk: 36.5+203.6+183.2 = 423.3 km^2) as shown in Table 5.4. Three- dimensional representation of slope gradients is shown in Fig 5.7 and Fig 5.8. Steep slopes, low slopes and flats presented in three hazard classes: high, medium and low as shown in Fig 5.9.

Muang district	Hazard classes											
	High				Medium				Low			
	Slope gradient areas (km^2)				Slope gradient areas (km^2)				Slope gradient areas (km^2)			
	steep slopes	low slopes	flats	total	steep slopes	low slopes	flats	total	steep slopes	low slopes	flats	total
	35.8	124	9.4	169.2	0.3	45	127.6	172.9	0.4	34.6	374.2	409.2
	21.2%	73.3%	5.6%	100%	0.2%	26.0%	73.8%	100%	0.1%	8.5%	91.4%	100%

Table 5.4 The relationship between the three hazard classes and three slope gradients, including the zonation of landslide risk (high, medium and low classes) showing steep slope, low slope and flat areas in Muang district under present-day conditions

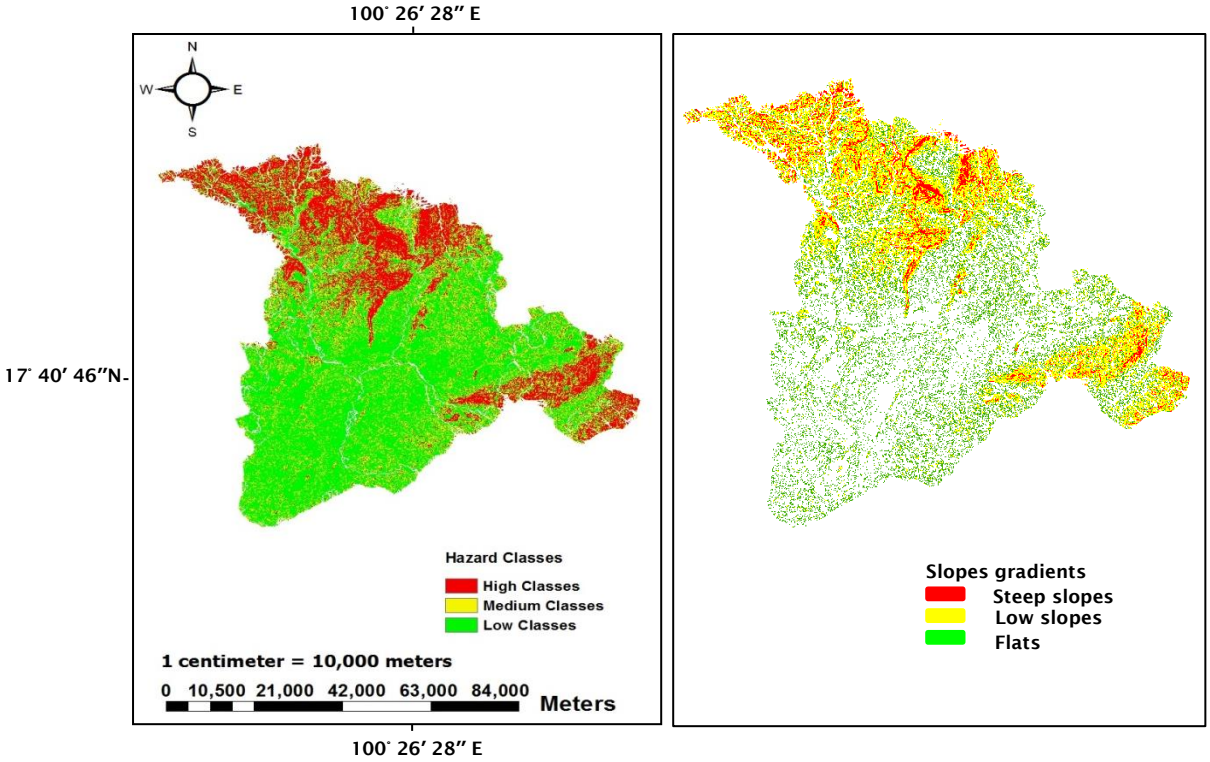

Figure 5.6 The comparison between steep slope, low slope and flat areas showing the zonation of landslide risk (right hand side) and landslide hazard mapping (left hand side) in Muang district under present-day conditions (i.e. 3D area is between latitude 17° 45' 57" north and longitude 100° 13' 35" showing slope gradients in the mountainous areas)

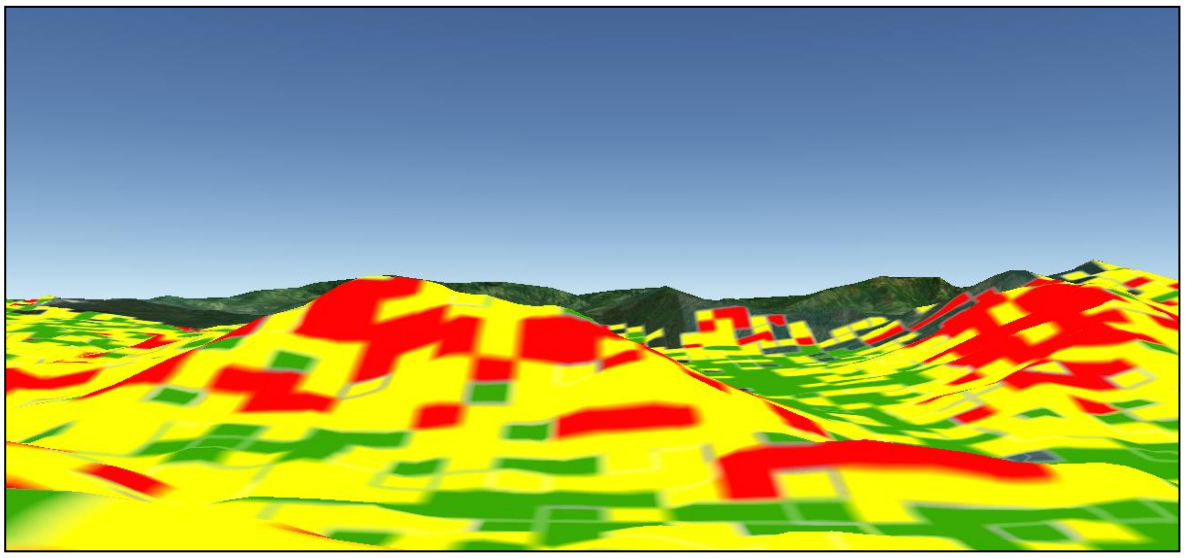

Figure 5.7 Three-dimensional representation of steep slope, low slope and flat areas showing between latitude 17° 45' 57" north and longitude 100° 13' 35" east in Muang district

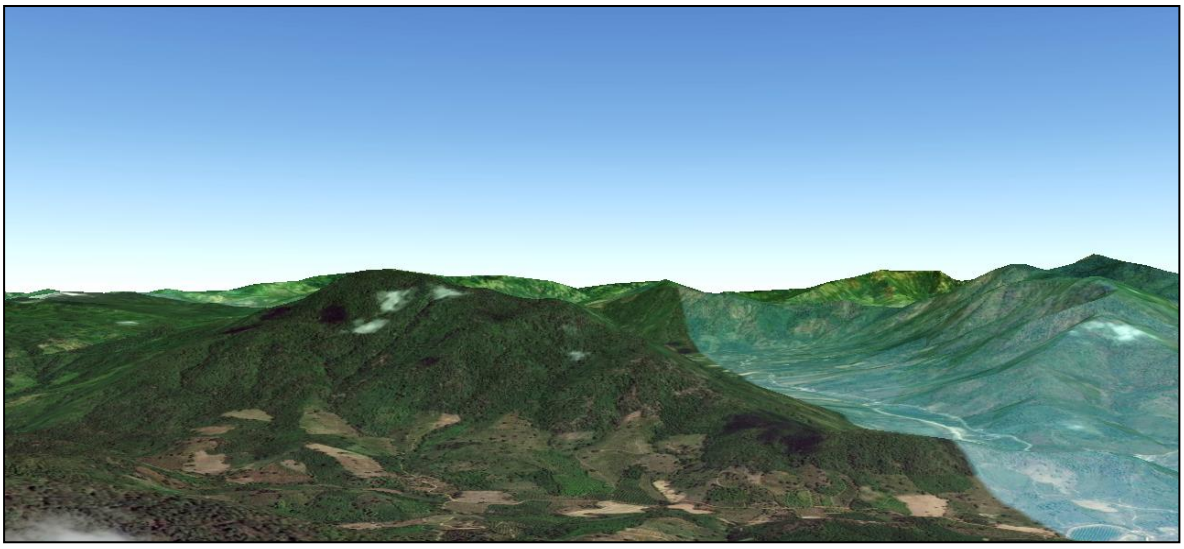

Figure 5.8 Three-dimensional representation of real hilly and mountains by google earth showing the mixture of steep slopes, low slopes and flats between latitude 17° 45' 57" north and longitude 100° 13' 35" east in Muang district

Steep slopes, low slopes and flats in the zonation of landslide risk (Fig 5.7) and steep slopes, low slopes and flats in the real hilly and mountain terrains (Fig 5.8) were presented in the same areas. Figure 5.9 confirm that the mixture of steep slopes, low slopes and flats in real hilly and mountains by Google earth.

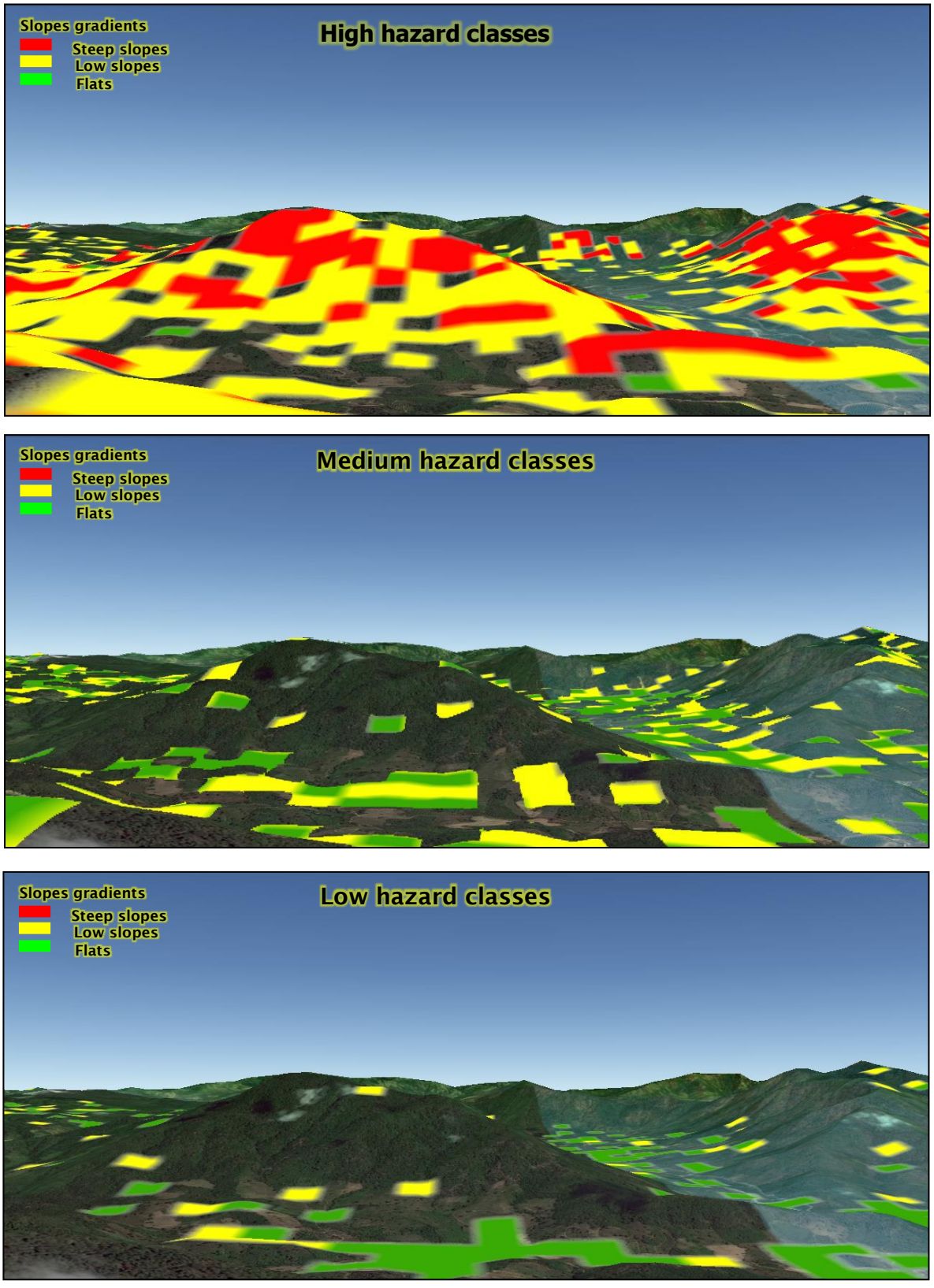

Figure 5.9 The comparison between steep slope, low slope and flat areas showing in the high, medium and low hazard classes in a three-dimensional representation of hilly and mountainous areas in Muang district

b) Thapla district

The zonation of landslide risk in Thapla district covered the steep slope, low slope and flat areas in this district. The high classes covered 163.8 km^2 (38.7%) of steep slope, 256.6 km^2 (60.5%) of low slope and 3.4 km^2 (0.8%) of flat areas. The high risk covered almost all areas of steep slope: 199.3 km^2 in Thapla district (Fig 5.5). Then high class covered some parts of low slope areas. Approximately 296.3 km^2 (87.1%) of low slope areas were found in medium classes because the low slope areas, were quite high and some low slope areas remain from the high classes. In low classes, 243.7 km^2 (28.4%) of low slopes and 607.6 km^2 (70.9%) of flats were presented. In this case, the high percentage of steep slope areas showed in high classes and the high percentage of low slope areas presented in medium classes and the high percentage of flat areas showed in low classes (Table 5.5). As a result in Table 5.2, the permeability value of 6.081E-06 cm/sec was small, but the dimensionless cohesion of 1.56 and the friction angle of 33.13^o were quite high. Approximately 65.5 – 69.6 mm/24 hours of rainfall presented in this area (Fig 5.1). The impact of the small permeability value led to the zonation of landslide risk, but the high values of dimensionless cohesion and friction angle also affect the zonation of landslide risk. So, the zonation of landslide risk in Thapla district is less extensive than in Muang district (Section 4.2.1, Chapter4). Steep slope, slope and flat areas were calculated by adding all areas of high, medium and 19.85% of low classes (zonation of landslide risk) (Fig 5.10), so the zonation of landslide risk covered: 178.4 km^2 of steep slopes (by adding of high (163.8 km^2), medium (9.2 km^2) and low (5.4 km^2) classes), 717.5 km^2 of low slopes (by adding of high (256.6 km^2), medium (296.3 km^2) and low (164.6 km^2) classes) and 38.2 km^2 of flat areas (by adding both high (3.4 km^2), medium (34.8 km^2) (i.e. the zonation of landslide risk: 178.4+717.5+38.2 = 934.1 km^2) as shown in Table 5.6. The three-dimensional representation of slope gradients and mountainous areas are shown in Fig 5.11 and Fig 5.12. Steep slopes, low slopes and flats presented in three hazard classes: high, medium and low as shown in Fig 5.13.

Thapla district	Hazard classes											
	High				Medium				Low			
	Slope gradient areas (km^2)				Slope gradient areas (km^2)				Slope gradient areas (km^2)			
	steep slopes	low slopes	flats	total	steep slopes	low slopes	flats	total	steep slopes	low slopes	flats	total
	163.8	256.6	3.4	423.8	9.2	296.3	34.8	340.3	5.4	243.7	607.6	856.7
	38.7%	60.5%	0.8%	100%	2.7%	87.1%	10.2%	100%	0.6%	28.4%	70.9%	100%

Table 5.5 The relationship between the three hazard classes and three slope gradients, including the zonation of landslide risk (high, medium and low classes) showing by steep slope, low slope and flat areas in Thapla district under present-day conditions

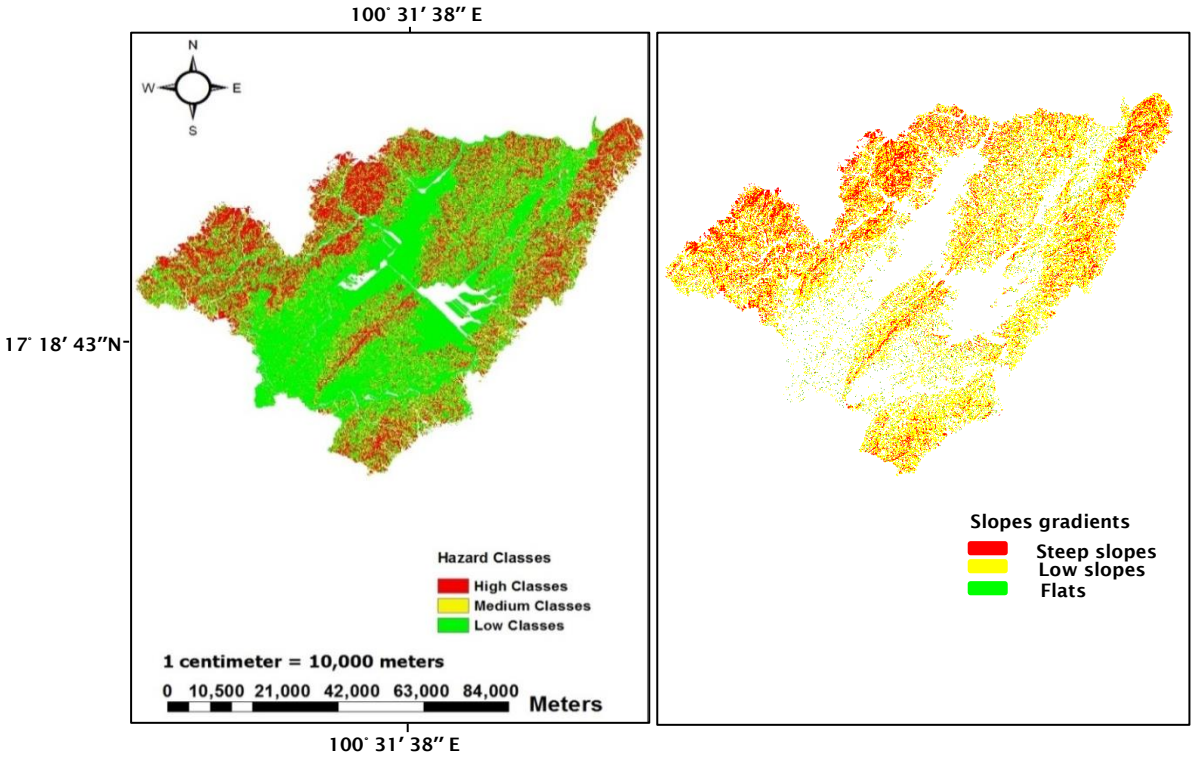

Figure 5.10 The comparison between steep slope, low slope and flat areas showing the zonation of landslide risk (right hand side) and landslide hazard mapping (left hand side) in Thapla district under present-day conditions (i.e. 3D area is between latitude 17° 55' 00" north and longitude 100° 15' 34" showing slope gradients in the mountainous areas)

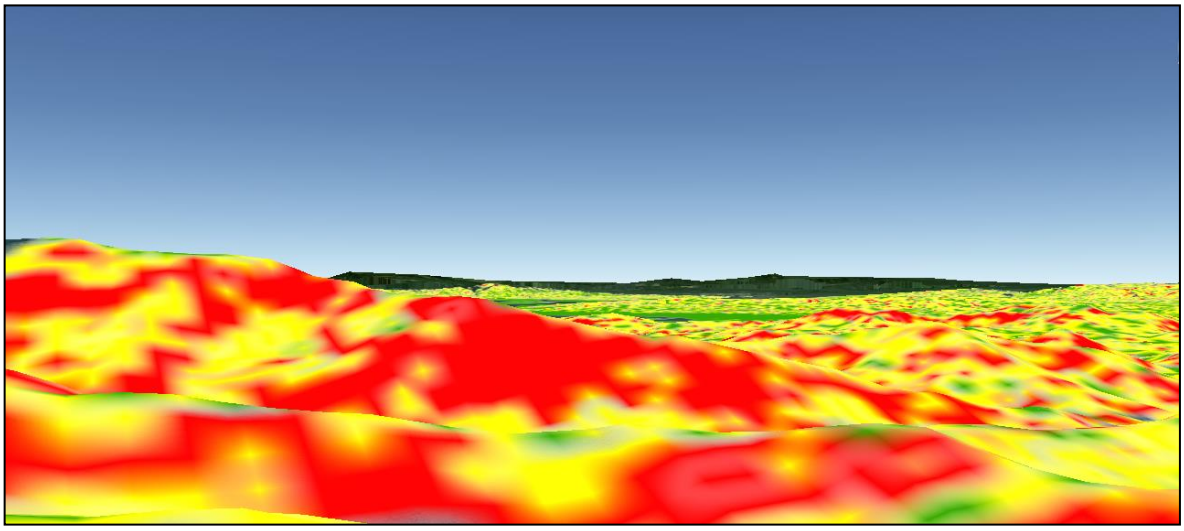

Figure 5.11 Three-dimensional representation of steep slope, low slope and flat areas showing between latitude 17° 55' 00" north and longitude 100° 15' 34" east in Thapla district

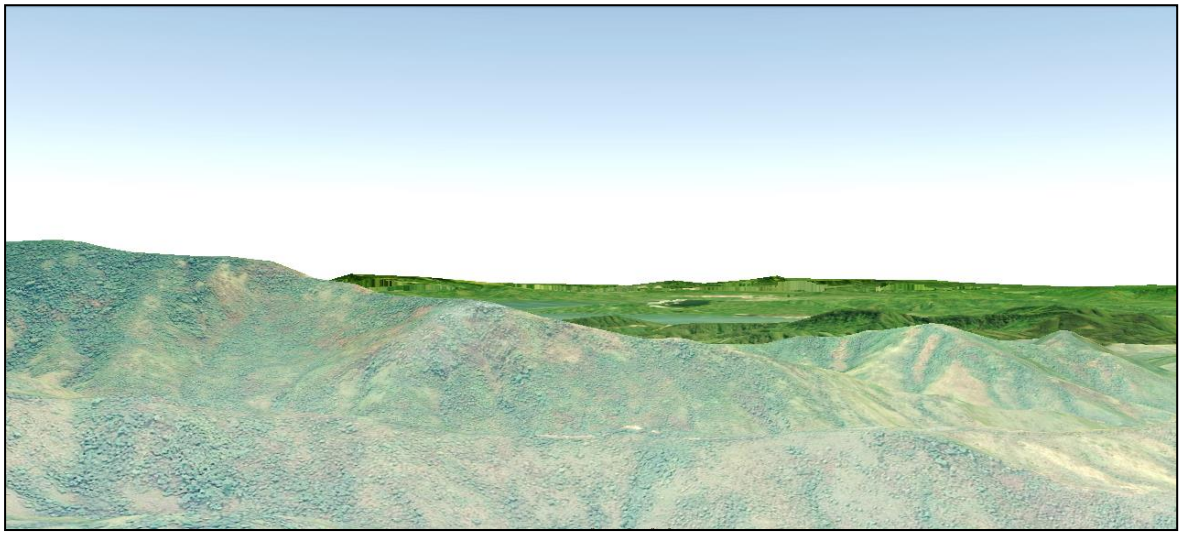

Figure 5.12 Three-dimensional representation of hilly and mountains by google earth showing the mixture of steep slopes, low slopes and flat between latitude 17° 55' 00" north and longitude 100° 15' 34" east in Thapla district

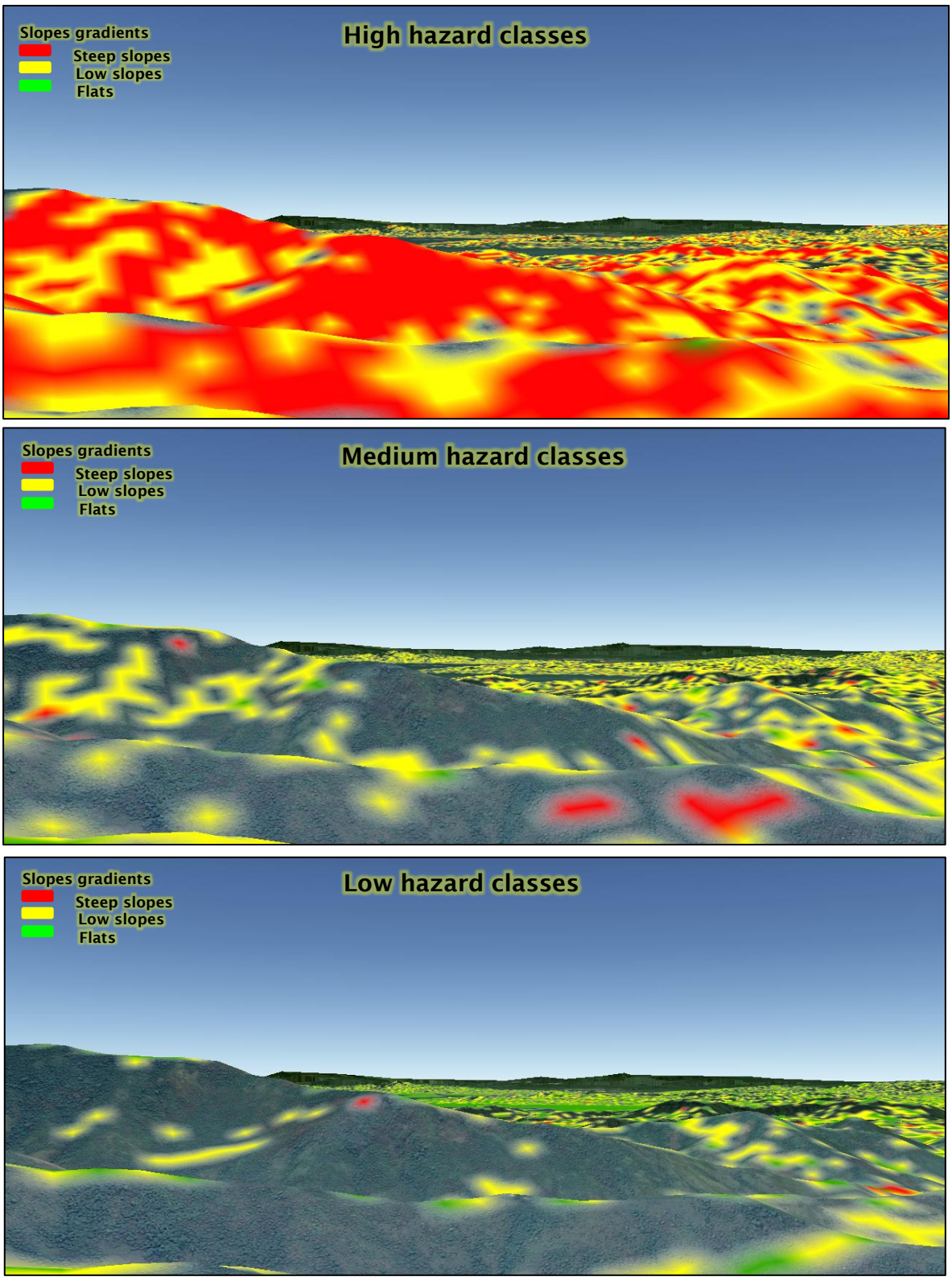

Figure 5.13 The comparison between steep slope, low slope and flat areas showing in the high, medium and low hazard classes in three-dimensional representation of hilly and mountainous areas in Thapla district

c) Laplea district

The zonation of landslide risk was found in steep slope, low slope and flat areas. The 19.2 km^2 (67.1%) of steep slope and 9.3 km^2 (32.5%) of low slope areas were found in high classes, while 15.9 (27.4%) of steep slope areas and 40.6 km^2 (69.9%) were also found in medium classes. In this area, the high classes were quite low so some parts of steep slopes and low slopes remained showing in medium classes, while approximately 69.9% of low slope areas were also found in medium classes. All flat areas showed in low classes: 248.9 km^2 (73.8%) (Table 5.6). In terms of characteristic of soil (Table 5.2), the dimensionless cohesion of 0-1.32 and the friction angle of 32.23^o were quite high, while the permeability of 2.918E-05 cm/sec and 73.7 mm/24 hours (Fig 5.1) of rainfall values were also high, so the zonation risk was quite small and the steep slope areas were found in both high and medium classes. Steep slope, low slope and flat areas were calculated by adding 100% of both high and medium and 19.85% of low classes (zonation of landslide risk), so the zonation of landslide risk indicated 38.8 km^2 of steep slopes (by adding of high (19.2 km^2), medium (15.9 km^2) and low (3.7 km^2)), 113.2 km^2 of low slopes (by adding of high (9.3 km^2), medium (40.6 km^2) and low (63.3 km^2)) and 1.7 km^2 of flats (by adding of high (0.1 km^2), medium (1.6 km^2) (i.e. the zonation of landslide risk: 38.8+111.2+1.7 = 151.7 km^2) (Table 5.6) and presented in a map (Fig 5.14). The three-dimensional representation of slope gradients and mountainous areas were shown in Fig 5.15 and Fig 5.16. Steep slopes, low slopes and flats presented in three hazard classes: high, medium and low as shown in Fig 5.17.

Laplea district	Hazard classes											
	High				Medium				Low			
	Slope gradient areas (km^2)				Slope gradient areas (km^2)				Slope gradient areas (km^2)			
	steep slopes	low slopes	flats	total	steep slopes	low slopes	flats	total	Steep slopes	low slopes	flats	total
	19.2	9.3	0.1	28.6	15.9	40.6	1.6	58.1	3.7	84.8	248.9	337.4
	67.1%	32.5%	0.3%	100%	27.4%	69.9%	2.8%	100%	1.1%	25.1%	73.8%	100%

Table 5.6 The relationship between the three hazard classes and three slope gradients, including the zonation of landslide risk (high, medium and low classes) showing by steep slope, low slope and flat areas in Laplea district under present-day conditions

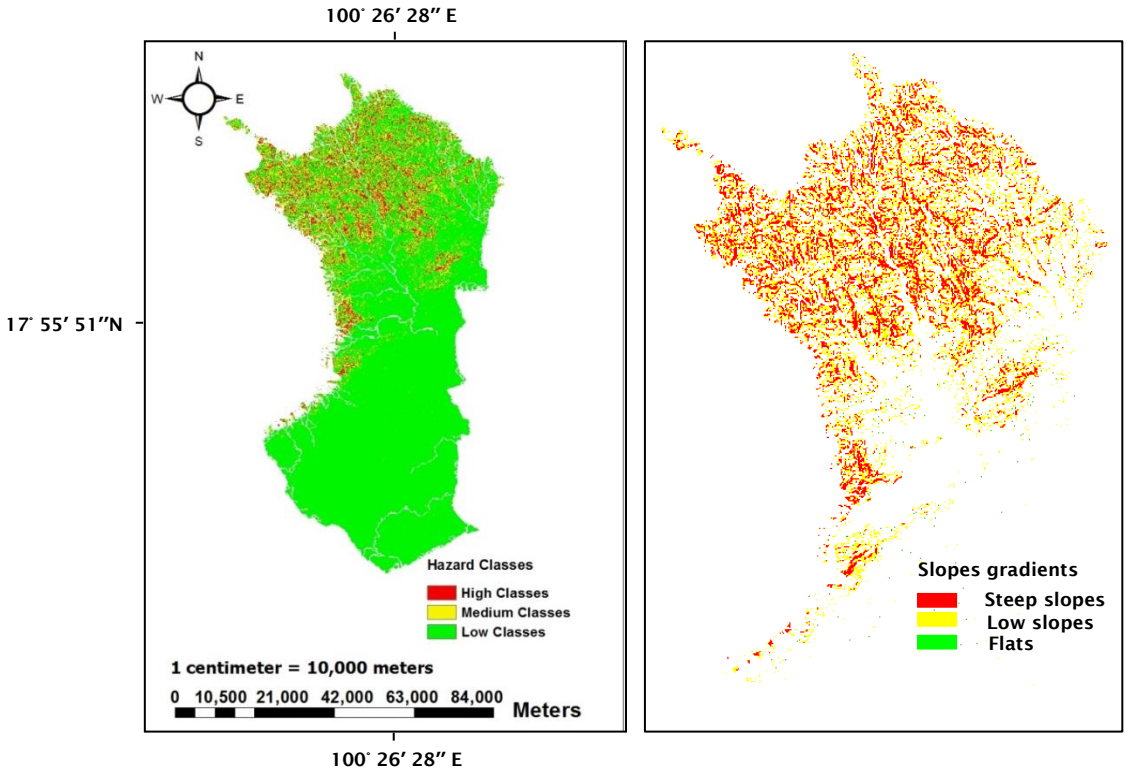

Figure 5.14 The comparison between steep slope, low slope and flat areas showing the zonation of landslide risk (right hand side) and landslide hazard mapping (left hand side) in Laplea district under present-day conditions (i.e. 3D area is between latitude 17° 44' 20" north and longitude 100° 03' 28" showing slope gradients in the mountainous areas)

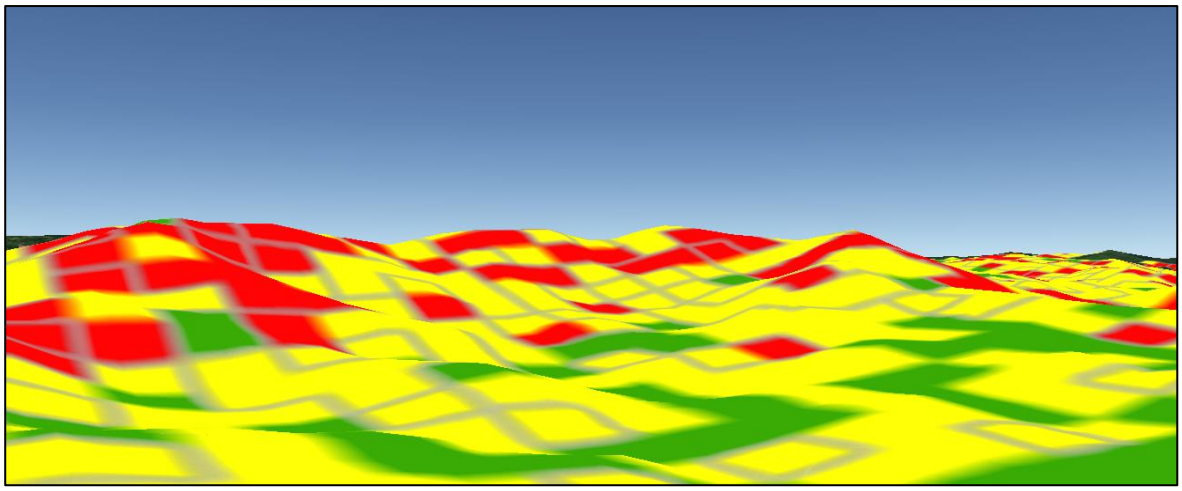

Figure 5.15 Three-dimensional representation of steep slope, low slope and flat areas showing between latitude 17° 44' 20" north and longitude 100° 03' 28" east in Laplea district

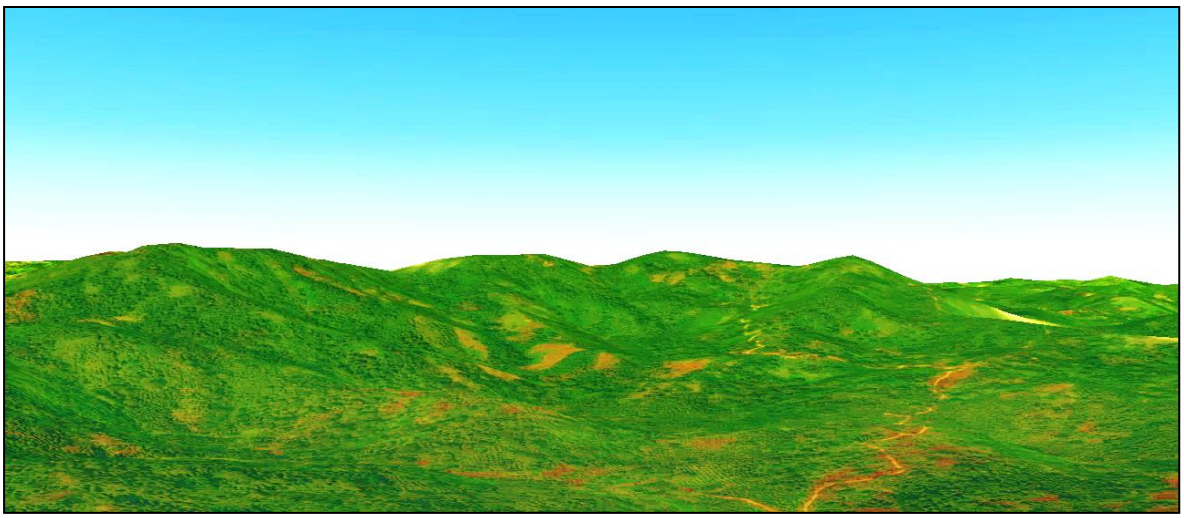

Figure 5.16 Three-dimensional representation of hilly and mountains showing by google earth showing the mixture of steep slopes, low slopes and flats between latitude 17° 44' 20" north and longitude 100° 03' 28" east in Laplea district

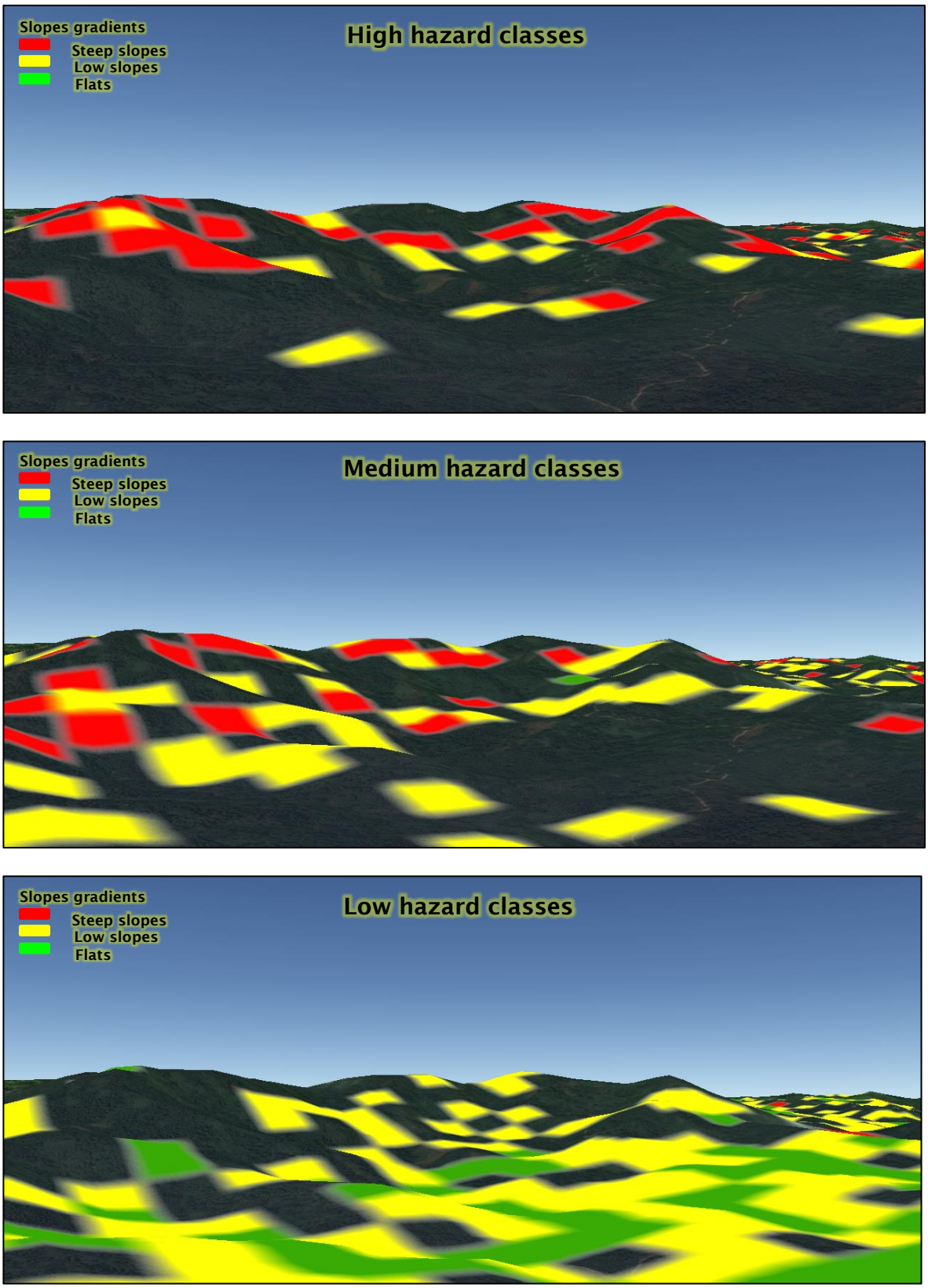

Figure 5.17 The comparison between steep slope, low slope and flat areas showing in the high, medium and low hazard classes in three-dimensional representation of hilly and mountainous areas in Laplea district

D) Nampat and Thongsaenkhun districts

The Nampat and Thonsaenkhun districts were under the same conditions of both soil and rainfall for analysis. The zonation of landslide risk in Thonsaenkhun and Nampat districts showed in a map (Fig 5.18 and Fig 5.22). In both districts, approximately 72-73.4% of steep slopes and 26.3-27.7 % of low slopes showed in high classes, about 23.8-26.4 % of steep slopes and approximately 70.2-72.5 % of low slopes were found in medium classes (Table 5.7 and Table 5.8). The probability of landslide occurred in steep slopes and low slopes (DWR, 2010). Steep slope areas are always on the top of mountains. Therefore, the high percentage of steep slope areas were found in high classes, while 26.3-27.7 % of low slope areas were found in high classes because low slope areas are mixed with steep slope areas on the top of mountains. In terms of medium classes, some areas of steep slope, that remain from the high classes, were found in medium classes. Most of low slope areas were found in medium classes, and most of flat were found in low classes. As for SINMAP parameters, the permeability values were quite high: 3.415E-04 cm/sec, including dimensionless cohesion value of 1.20 and the friction angle of 30.9^{o} were also high (Table 5.2). The rainfall values were quite low: 69.6 mm/24 hours (Fig 5.1). These four parameters corresponded with the sensitivity of permeability values (Section 4.2.2, Chapter 4). The zonation of landslide risk (km^2) was low, when compared other soil types.

Steep slope, low slope and flat areas were calculated by adding both 100% of high and medium class areas and 19.85% of low class areas in two districts. Therefore the zonation of landslide risk covered approximately 197 km^2 of steep slopes (by adding areas of high (107.1 km^2), medium (67.5 km^2) and low (22.4 km^2) and 379.2 km^2 of low slopes (by adding of high (38.4 km^2), medium (179.3 km^2) and low (161.5 km^2) and 9 km^2 of flat (by adding of high (0.5 km^2) and medium (8.5 km^2) in Nampat district (i.e. the zonation of landslide risk: 197+379.2+9 = 585.2 km^2) (Table 5.7). The three-dimensional representation of slope gradients and mountainous areas were shown in Fig 5.19 and Fig 5.20. Steep slopes, low slopes and flats presented in three hazard classes: high, medium and low as shown in Fig 5.21.

Approximately 50.9 km^2 of steep slopes (by adding of high (26.5 km^2), medium (19.0 km^2) and low (5.4 km^2), 172.6 km^2 of low slopes (by adding of high (10.2 km^2),

medium (58.0 km²) and low (104.4 km²) and 3.1 km² of flats (by adding of high (0.1 km²), medium (3.0 km²) in Thongsaenkhun district (i.e. the zonation of landslide risk: 50.9+172.6+3.1 = 226.6 km²) (Table 5.8). The three-dimensional representation of slope gradients and mountainous areas were shown in Fig 5.23 and Fig 5.24. Steep slopes, low slopes and flats presented in three hazard classes: high, medium and low as shown in Fig 5.25.

Nampat district	Hazard classes											
	High				Medium				Low			
	Slope gradient areas (km²)				Slope gradient areas (km²)				Slope gradient areas (km²)			
	steep slopes	low slopes	flats	total	steep slopes	low slopes	flats	total	steep slopes	low slopes	flats	total
	107.1	38.4	0.5	146	67.5	179.3	8.5	255.3	22.4	440.5	463.8	926.7
	73.4%	26.3%	0.3%	100%	26.4%	70.2%	3.3%	100%	2.5%	47.5%	50.0%	100%

Table 5.7 The relationship between the three hazard classes and three slope gradients, including the zonation of landslide risk (high, medium and low classes showing by steep slope, low slope and flat areas) in Nampat district under present-day conditions

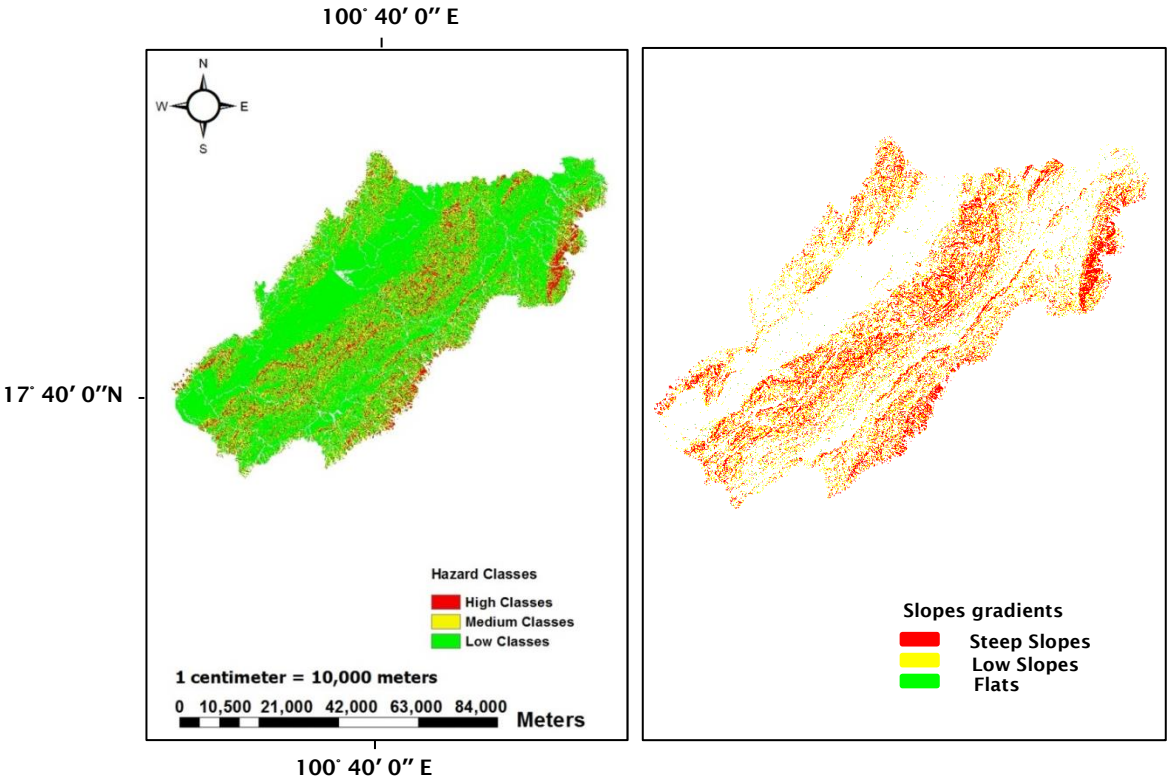

Figure 5.18 The comparison between steep slope, low slope and flat areas showing the zonation of landslide risk (right hand side) and landslide hazard mapping (left hand side) in Nampat district under present-day conditions (i.e. 3D area is between latitude 17° 44' 00" north and longitude 100° 55' 09" showing slope gradients in the mountainous areas)

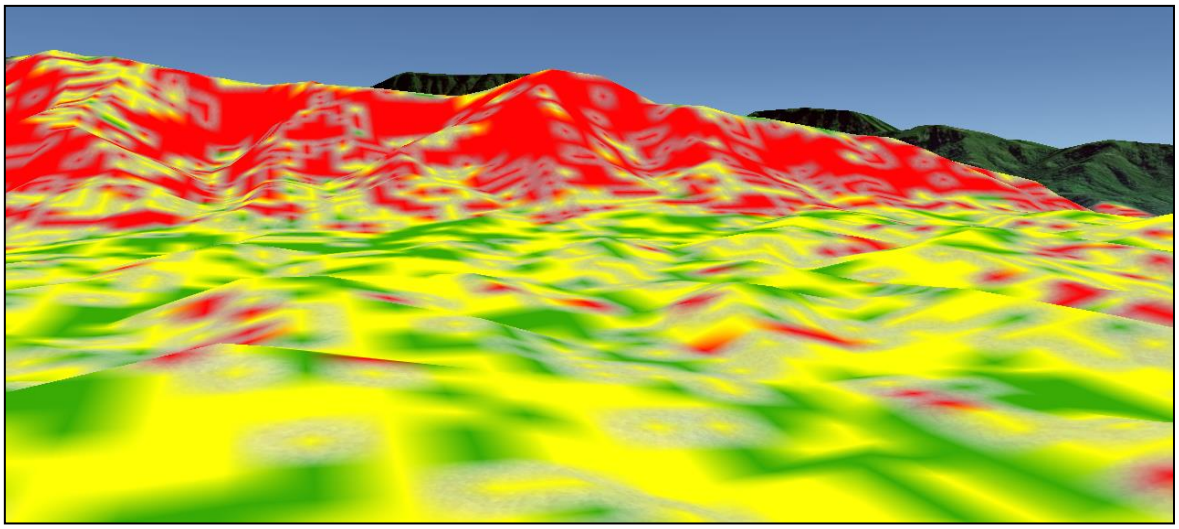

Figure 5.19 Three-dimensional representation of steep slope, low slope and flat areas showing between latitude 17° 44' 00" north and longitude 100° 55' 09" east in Nampat district

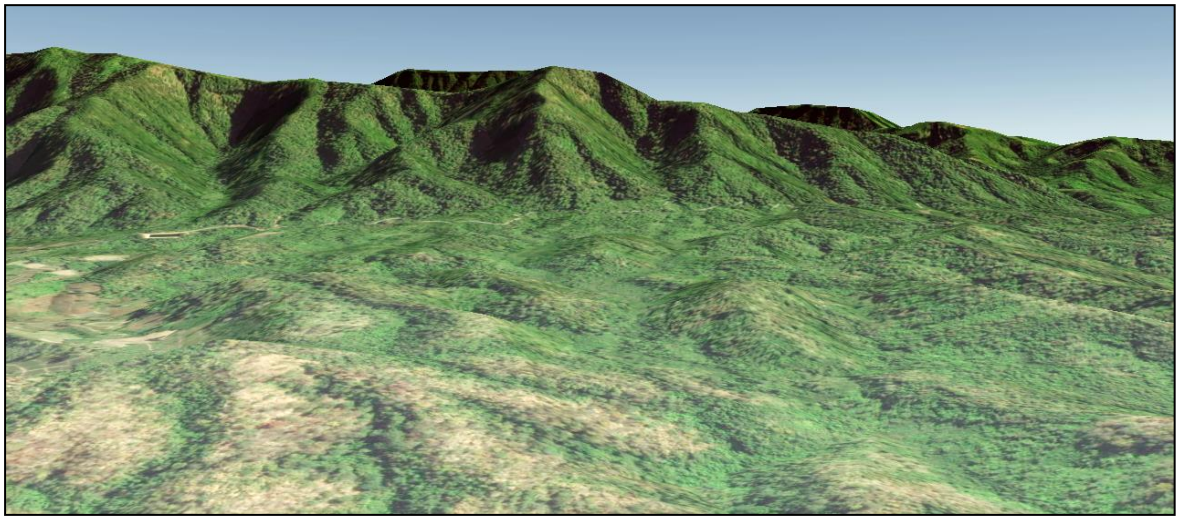

Figure 5.20 Three-dimensional representation of hilly and mountains by google earth showing the mixture of steep slopes, low slopes and flats between latitude 17° 44' 00" north and longitude 100° 55' 09" east in Nampat district

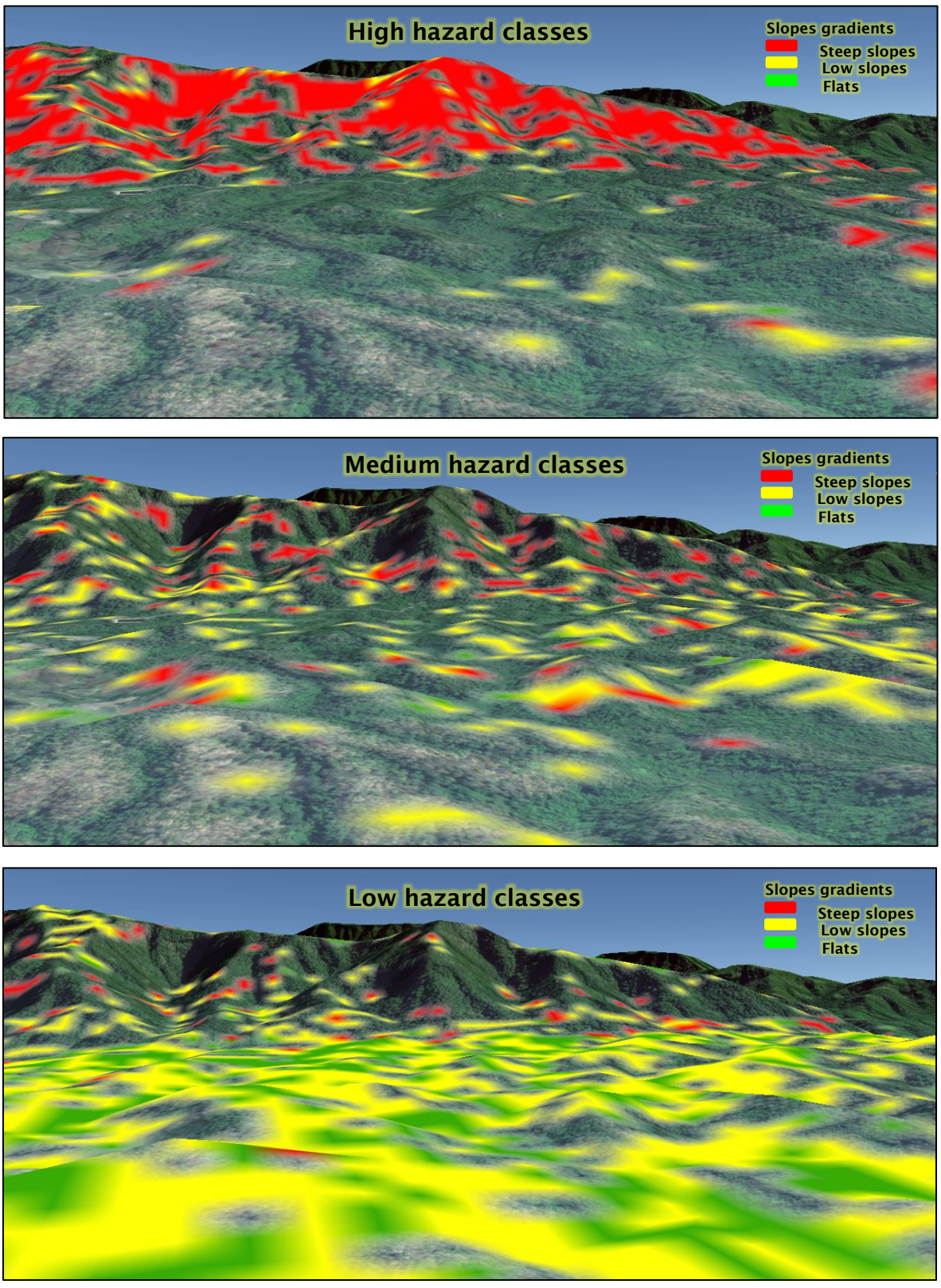

Figure 5.21 The comparison between steep slope, low slope and flat areas showing in the high, medium and low hazard classes in three-dimensional representation of hilly and mountainous areas in Nampat district

Thong saenkhun district	Hazard classes											
	High				Medium				Low			
	Slope gradient areas (km²)				Slope gradient areas (km²)				Slope gradient areas (km²)			
	steep slopes	low slopes	flats	total	steep slopes	low slopes	flats	total	steep slopes	low slopes	flats	total
	26.5	10.2	0.1	36.8	19.0	58.0	3.0	80.0	5.4	183.5	364.3	553.2
	72.0%	27.7%	0.3%	100%	23.8%	72.5%	3.8%	100%	1.0%	33.1%	65.9%	100%

Table 5.8 The relationship between the three hazard classes and three slope gradients, including the zonation of landslide risk (high, medium and low classes) showing by steep slope, low slope and flat areas in Thongsaenkhun district under present-day conditions

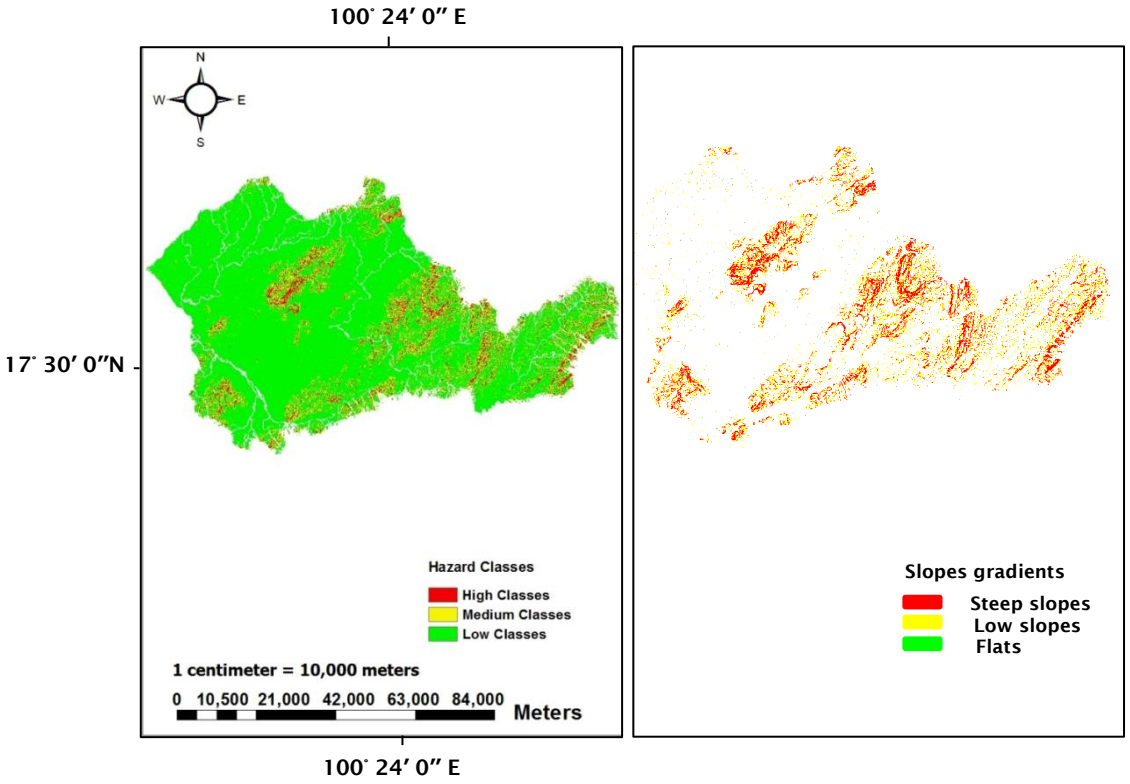

Figure 5.22 The comparison between steep slope, low slope and flat areas showing the zonation of landslide risk (right hand side) and landslide hazard mapping (left hand side) in Thongsaenkhun district under present-day conditions (i.e. 3D area is between latitude 17° 30' 18" north and longitude 100° 20' 04" showing slope gradients in the mountainous areas)

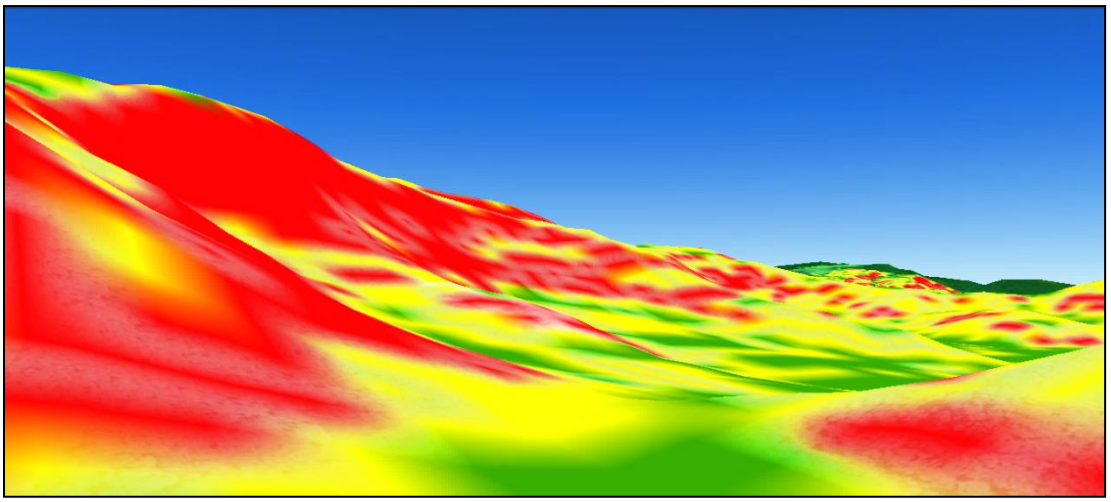

Figure 5.23 Three-dimensional representation of steep slope, low slope and flat areas showing between latitude 17° 30' 18" north and longitude 100° 20' 04" east in Thongsaenkhun district

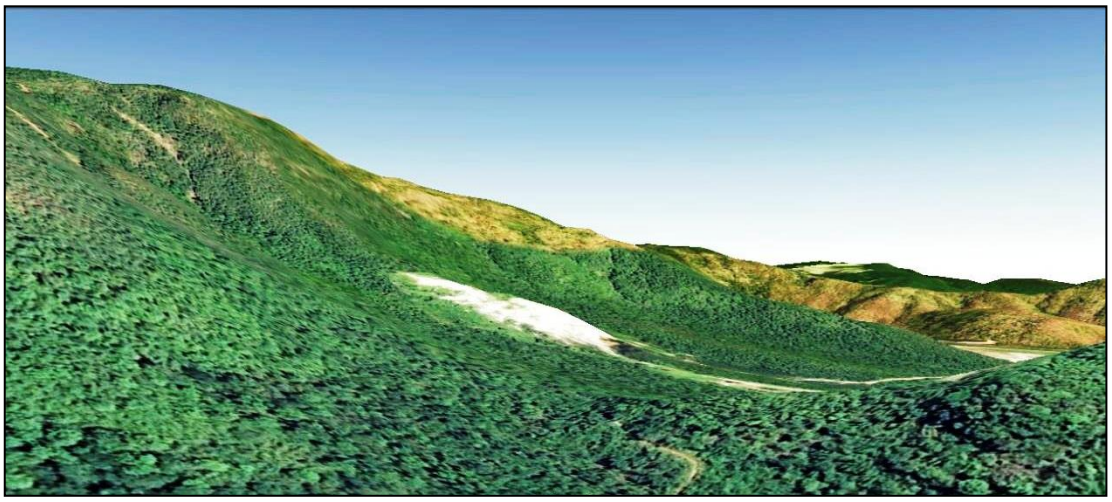

Figure 5.24 Three-dimensional representation of hilly and mountains by google earth showing the mixture of steep slopes, low slopes and flats between latitude 17° 30' 18" north and longitude 100° 20' 04" east in Thongsaenkhun district

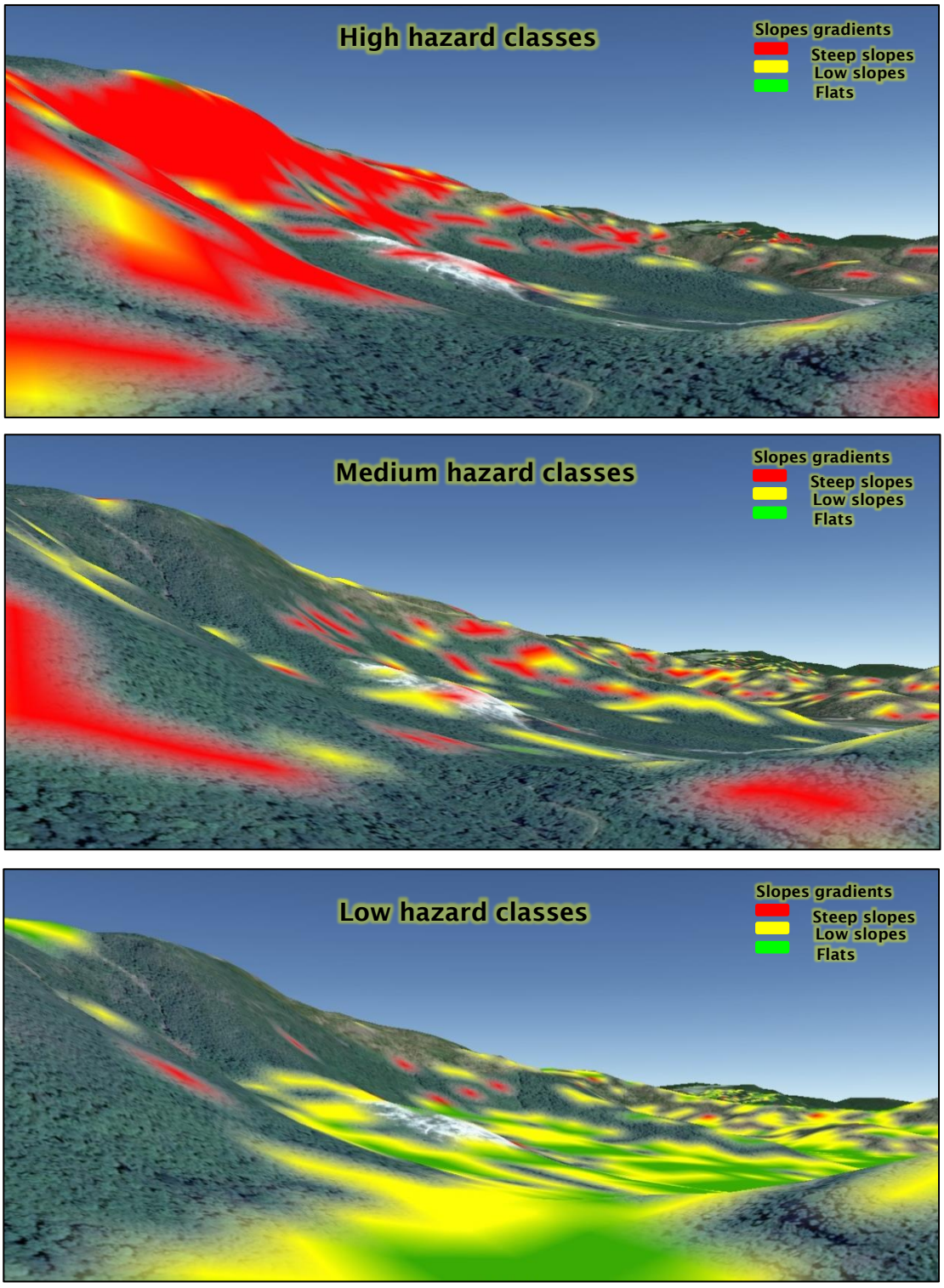

Figure 5.25 The comparison between steep slope, low slope and flat areas showing in the high, medium and low hazard classes in three-dimensional representation of hilly and mountainous areas in Thongsaenkhun district

e) Bankhok district

The landslide zonation risk covered in some parts of steep slope, low slope and flat areas in Bankhok district. The high classes covered 39.5 km^2 (86.8%) of steep slope and 6 km^2 (13.2%) of low slope areas, while the medium classes covered 52.7 km^2 30.8% of steep slope and 114.1 km^2 (66.6%) of low slope areas as shown in Table 5.9.

Hilly and mountainous terrain consists of steep slope and low slope areas, but the high classes (failure regions) obviously occurred in steep slope areas and the medium classes occurred in low slope areas. The high percentage of steep slope was found in the high classes areas, while the high percentage of low slope was found in the medium classes. The 362.4 km^2 (52.9%) of low slope areas was found in low class because low slope areas in this district were quite big and occurred around mountains, so low slope areas still showed in low classes. Approximately 300.1 km^2 (43.8%) of flat areas were found in low classes. As for the characteristic of soil (Table 5.2), clays were found in this district and linked with dimensionless cohesion values: 2.34 in Bankhok district, while dry sands (cohesionless) could not present for the lower values because clay is cohesive soil. Therefore, the lower values were 0.256 of dimensionless cohesion in clay (Srinil et al., 2001). In terms of land cover/land use, rubber plantations were found in this district, which were quite high in root strength values. So the dimensionless cohesion values were high, but the angle of friction and the permeability values was low: 24.62^o, 1.175E-06 cm/sec respectively. The rainfall values were the same as Nampat district: 69.6 mm/24 hours (Fig 5.1). The zonation of landslide was quite small in this district because of these parameters, especially high values of dimensionless cohesion and small values of permeability, which related to the sensitivity of SINMAP (Section 4.2.2, Chapter 4). Steep slope, low slope and flat areas were calculated by adding all areas of both high and medium classes and 19.85% of low class areas (zonation of landslide risk) and shown in a map (Fig 5.26). The zonation of landslide risk covered about 114.2 km^2 of steep slope areas (by adding of high (39.5 km^2), medium (52.7 km^2), low (22.0 km^2)) 234 km^2 of low slope areas (by adding of high (6.0 km^2), medium (114.1 km^2), low (113.9 km^2)) and 4.4 km^2 of flat areas (by adding of high (0 km^2), medium (4.4 km^2) (i.e. the zonation of landslide risk: 114.2+234+4.4 = 352.6 km^2) (Table 5.9). The three-dimensional representation of slope gradients and mountainous areas were shown in Fig 5.27 and Fig 5.28. Steep slopes, low slopes

and flats presented in three hazard classes: high, medium and low as shown in Fig 5.29.

Bankhok district	Hazard classes											
	High				Medium				Low			
	Slope gradient areas (km²)				Slope gradient areas (km²)				Slope gradient areas (km²)			
	steep slopes	low slopes	flats	total	steep slopes	low slopes	flats	total	steep slopes	low slopes	flats	total
	39.5	6.0	0	45.5	52.7	114.1	4.4	171.2	22.0	362.4	300.1	684.5
	86.8%	13.2%	0%	100%	30.8%	66.6%	2.6%	100%	3.2%	52.9%	43.8%	100%

Table 5.9 The relationship between the three hazard classes and three slope gradients, including the zonation of landslide risk (high, medium and low classes) showing by steep slope, low slope and flat areas in Bankhok district under present-day conditions

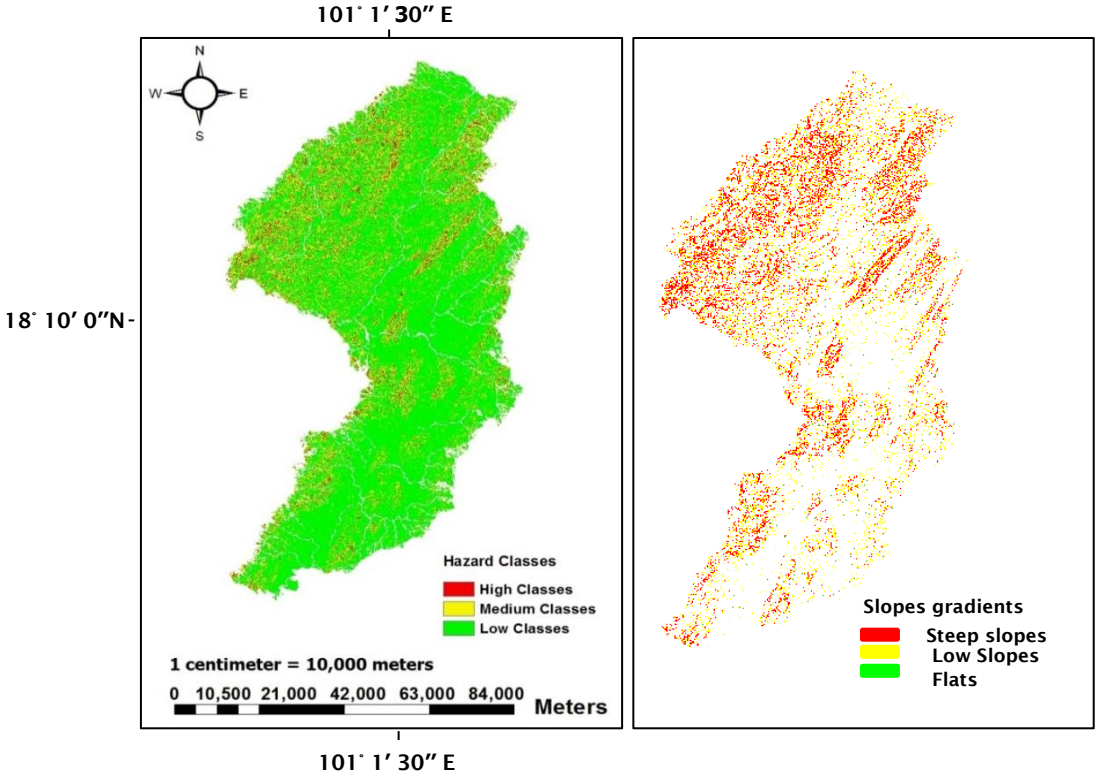

Figure 5.26 The comparison between steep slope, low slope and flat areas showing the zonation of landslide risk (right hand side) and landslide hazard mapping (left hand side) in Bankhok district under present-day conditions (i.e. 3D area is between latitude 18° 15' 48" north and longitude 101° 05' 44" showing slope gradients in the mountainous areas)

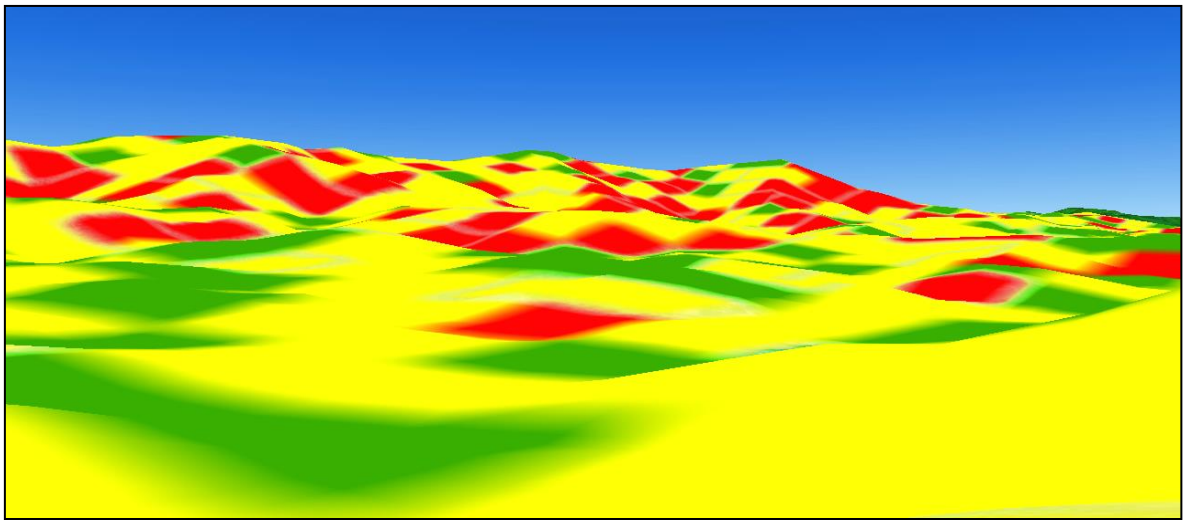

Figure 5.27 Three-dimensional representation of steep slope, low slope and flat areas showing between latitude 18° 15' 48" north and longitude 101° 05' 44" east in Bankhok district

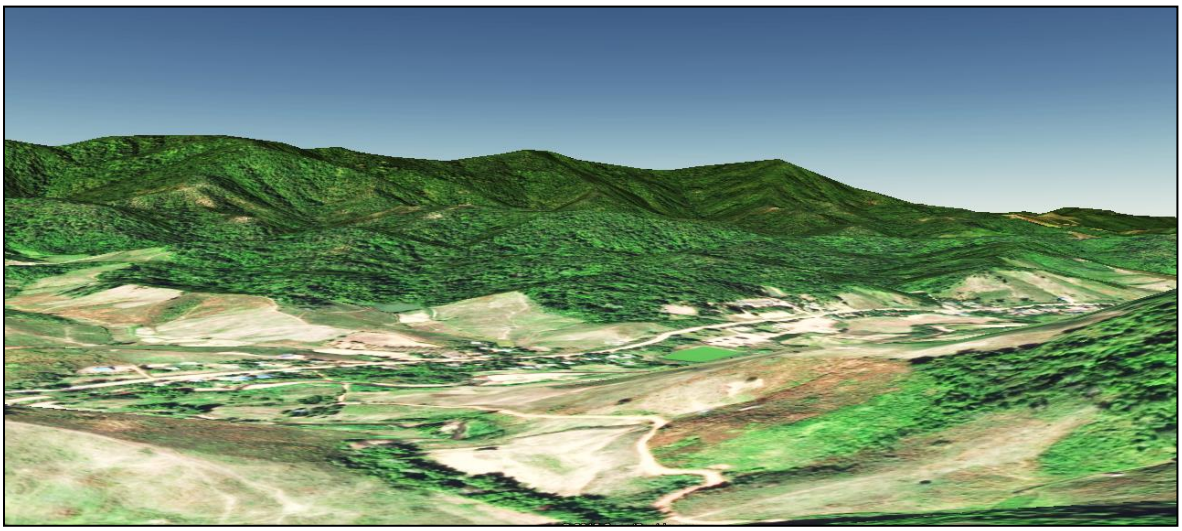

Figure 5.28 Three-dimensional presentation of hilly and mountains by google earth showing the mixture of steep slopes, low slopes and flats between latitude 18° 15' 48" north and longitude 101° 05' 44" east in Bankhok district

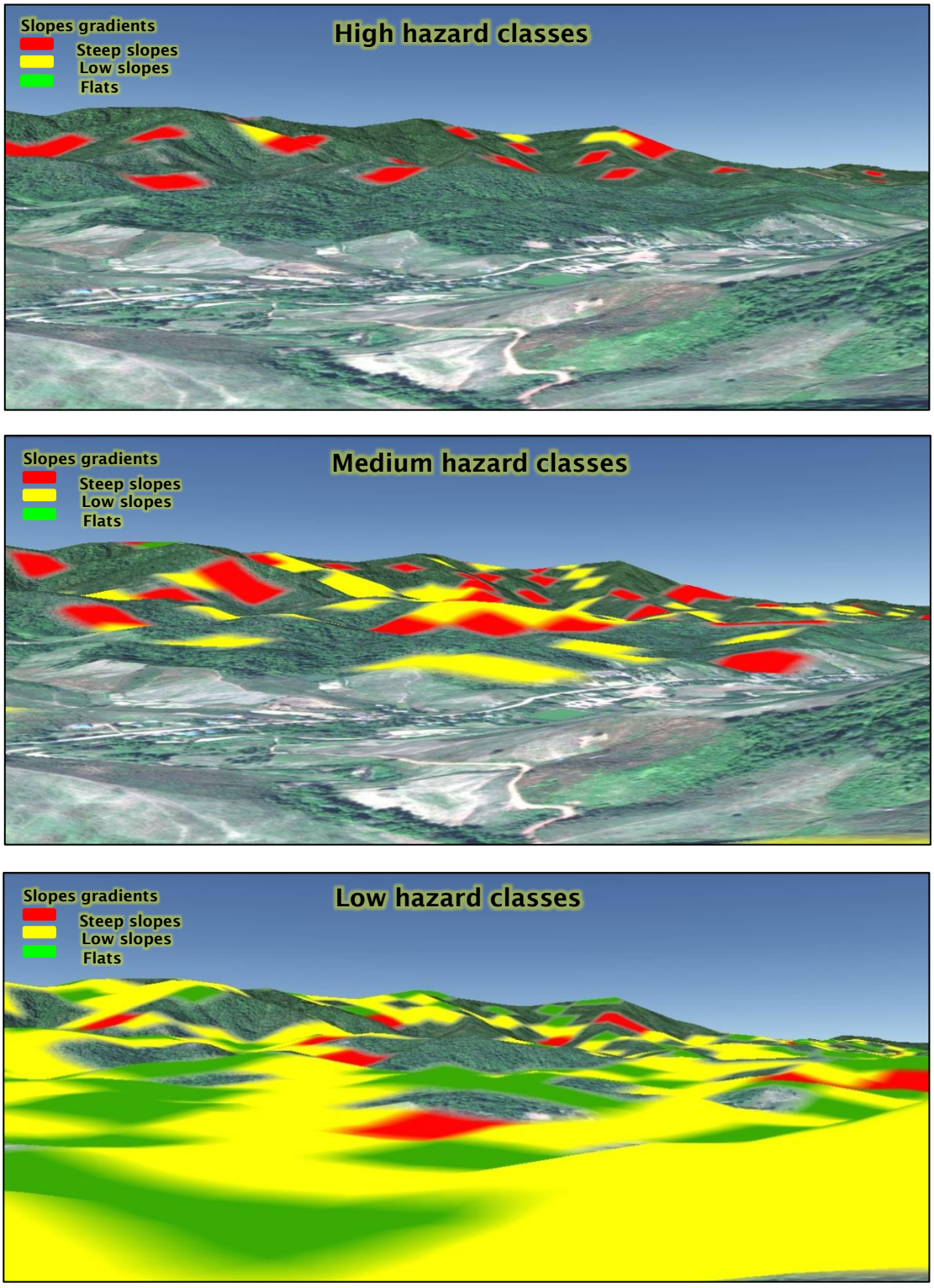

Figure 5.29 The comparison between steep slope, low slope and flat areas showing in the high, medium and low hazard classes in three-dimensional representation of hilly and mountainous areas in Bankhok district

f) Faktha district

In this district, the zonation of landslide risk covered both steep slopes and low slopes. Approximately 17.5 km^2 (90.2%) of steep slopes and 1.9 km^2 (9.8%) of low slopes were found in the high class areas, flats were not found in the high classes because flat areas were not found around the top of mountains. In terms of medium classes, 61.5 km^2 (59.7%) of steep slope areas still showed in this class because steep slope areas were big in this district, while about 41.3 km^2 (40.1%) of low slope areas presented in this class. Some parts of low slope areas presented in low classes. The 277.5 km^2 (59%) of low slope and 156.5 (33%) of flat areas presented in the low classes, while only 36.6 km^2 (7.8%) of steep slope was found in the low classes as given in Table 5.10 because some parts of steep slope areas occurred on the foot of the mountain, so this steep slope area showed in low classes. In terms of soil, clays were found in this district and linked with dimensionless cohesion values: 1.017 in Bankhok district, while dry sands (cohesionless) could not present for the lower values (Table 5.2). Therefore, the lower values were 0.256 of dimensionless cohesion because of clay (Srinil et al., 2001). In terms of land cover/land use, teaks were found in this district, which were quite high in root strength. The angle of friction values was quite low: 26.23°, while the permeability value was quite high: 8.187E-05 cm/sec, including low values of rainfall: 69.6 mm/24 hours (Fig 5.1). All SINMAP parameters were important, but lower values of dimensionless cohesion and permeability obviously affect the small area of zonation risk (Section 4.2, Chapter 4). Finally, the zonation of landslide risk in Faktha covered approximately 115.6 km^2 of steep slopes (by adding of high (17.5 km^2), medium (61.5 km^2) and low (36.6 km^2), 100 km^2 of low slopes (by adding of high (1.9 km^2), medium (41.3 km^2) and low (56.8 km^2) and only 0.2 km^2 of flats (by adding of high (0 km^2), medium (0.2 km^2) (i.e. the zonation of landslide risk: 115.6+100+0.2 = 215.8 km^2), and presented in a map (Fig 5.30). The three-dimensional representation of slope gradients and mountainous areas were shown in Fig 5.31 and Fig 5.32. Steep slopes, low slopes and flats presented in three hazard classes: high, medium and low as shown in Fig 5.33.

Faktha district	Hazard classes											
	High				Medium				Low			
	Slope gradient areas (km²)				Slope gradient areas (km²)				Slope gradient areas (km²)			
	steep slopes	low slopes	flats	total	steep slopes	low slopes	flats	total	steep slopes	low slopes	flats	total
	17.5	1.9	0	19.4	61.5	41.3	0.2	103	36.6	277.5	156.5	470.6
	90.2%	9.8%	0%	100%	59.7%	40.1%	0.2%	100%	7.8%	59.0%	33.3%	100%

Table 5.10 The relationship between the three hazard classes and three slope gradients, including the zonation of landslide risk (high, medium and low classes) showing by steep slope, low slope and flat areas in Faktha district under present-day conditions.

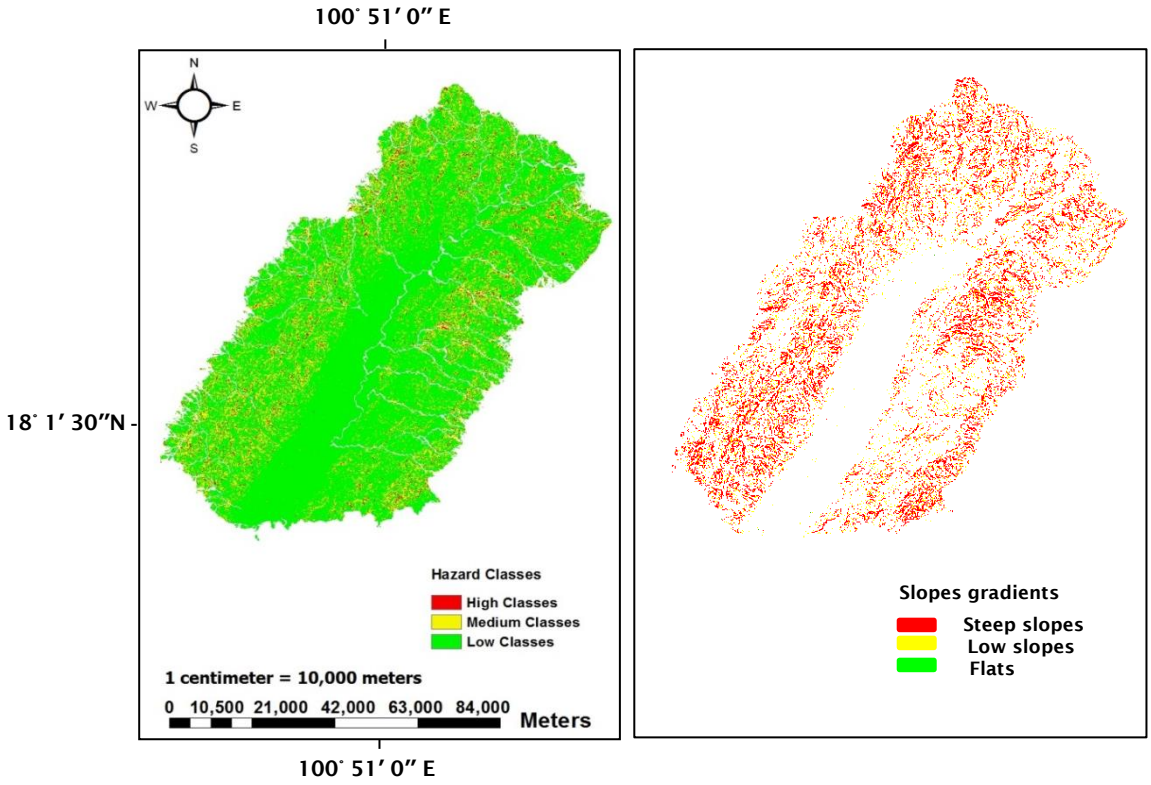

Figure 5.30 The comparison between steep slope, low slope and flat areas showing the zonation of landslide risk (right hand side) and landslide hazard mapping (left hand side) in Faktha district under present-day conditions (i.e. 3D area is between latitude 18° 03' 40" north and longitude 100° 52' 40" showing slope gradients in the mountainous areas)

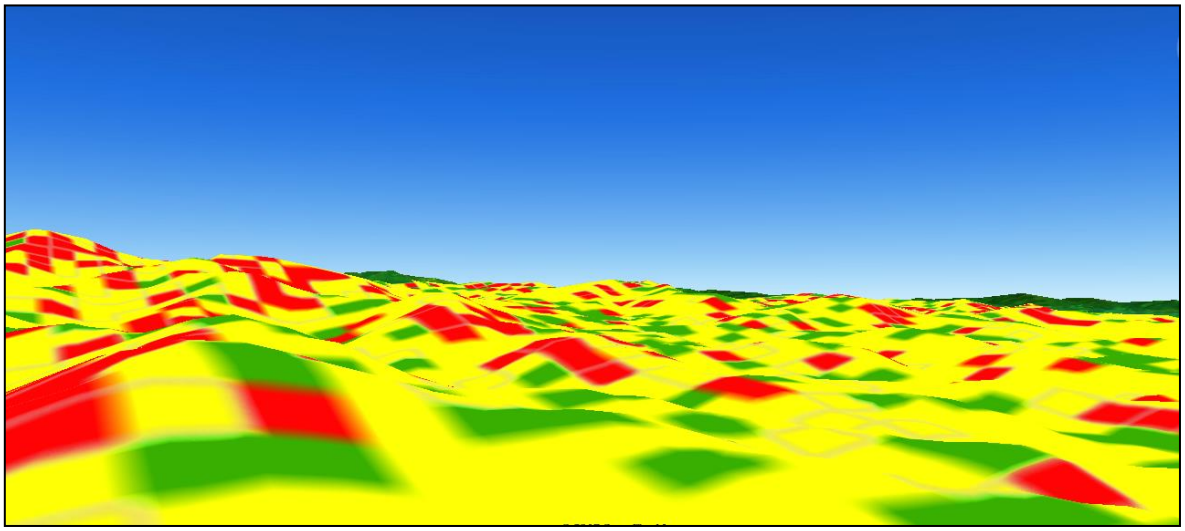

Figure 5.31 Three-dimensional representation of steep slope, low slope and flat areas showing between latitude 18° 03' 40" north and longitude 100° 52' 40" east in Faktha district

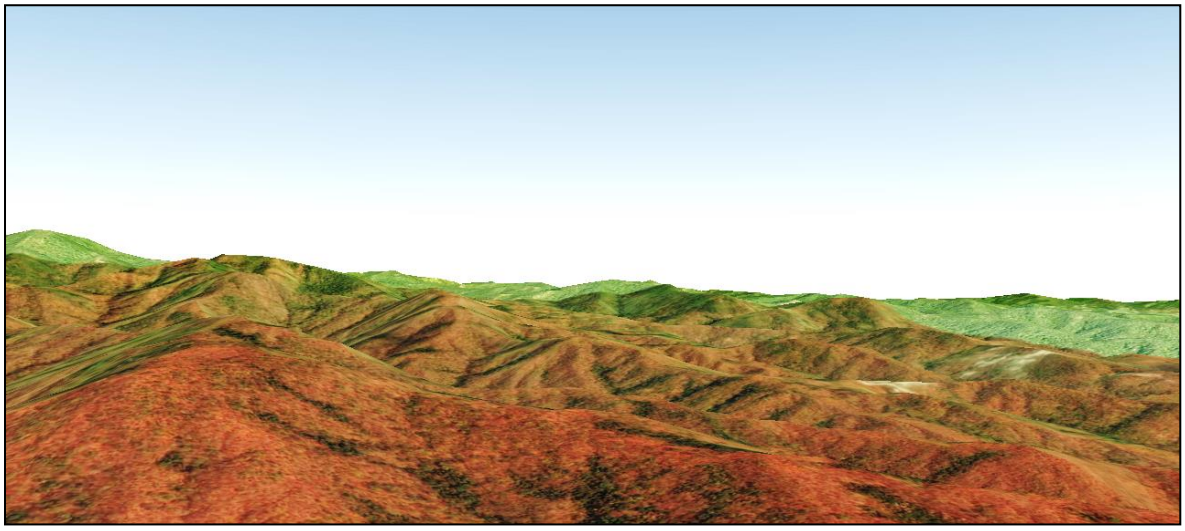

Figure 5.32 Three-dimensional representation of hilly and mountains by google earth showing the mixture of steep slopes, low slopes and flats between latitude 18° 03' 40" north and longitude 100° 52' 40" east in Faktha district

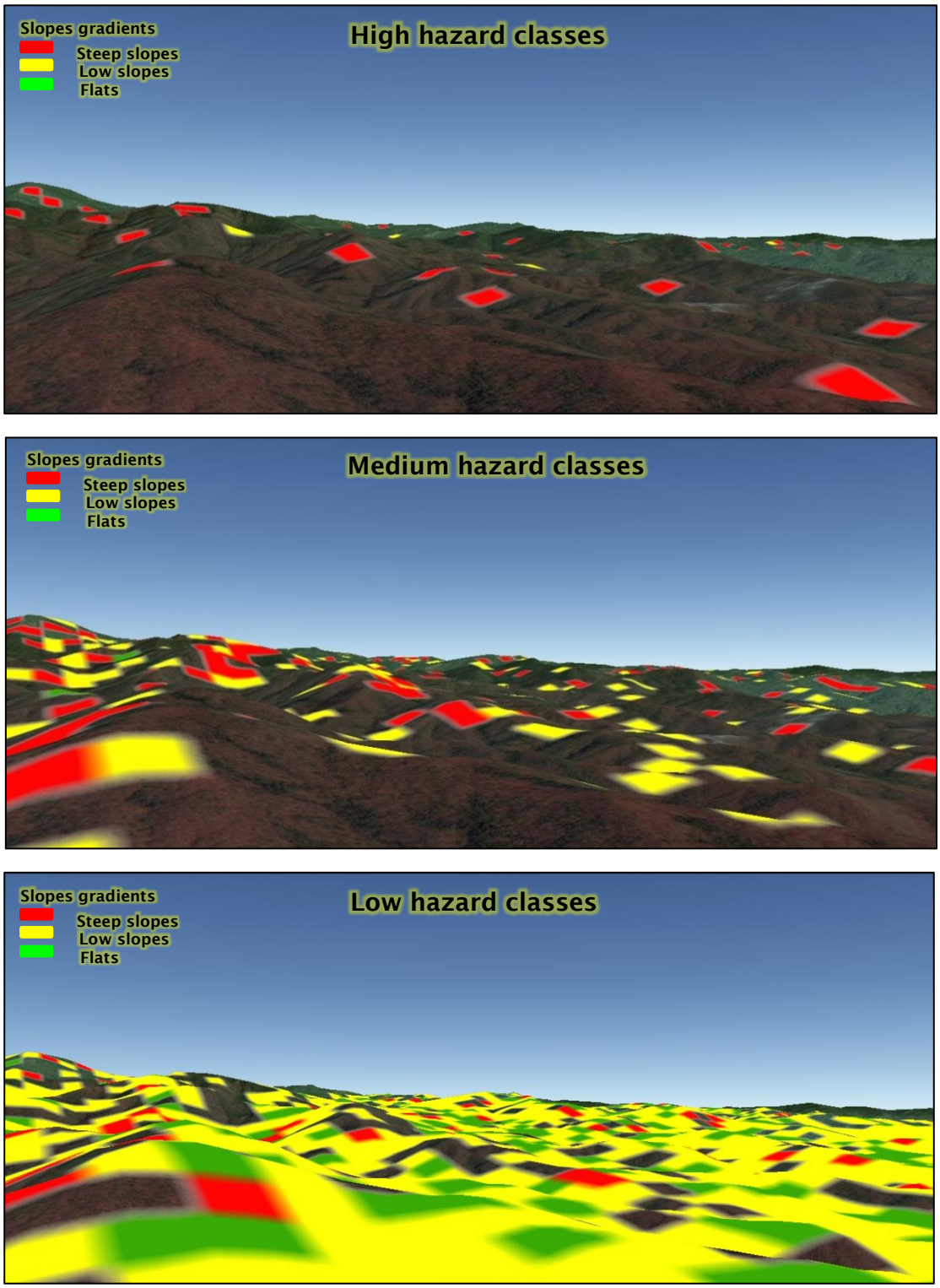

Figure 5.33 The comparison between steep slope, low slope and flat areas showing in the high, medium and low hazard classes in three-dimensional representation of hilly and mountainous areas in Faktha district

f) Tron and Phichai districts

In two districts, the zonation of landslide risk covered both steep slopes and low slopes. The zonation of landslide risk was the smallest in both Phichai and Tron districts, due to the steep slope and low slope areas being less than 1% and 10% in both district areas. Therefore, the zonation of landslide risk in both Phichai and Tron was negligible in this study. In terms of characteristic of soil (Table 5.2), the test pit location 2 of Laplea district was used for both districts because they border each other. Approximately 0–1.32 of dimensionless cohesion values and the friction angle of 32.23^{o} were quite high, while the permeability 2.918E-05 cm/sec and 69.6 mm/24 hours (Fig 5.1) of rainfall values were quite high. The zonation of risk was negligible in both districts because the steep slope and low slope areas were so small in both high (failure region) and medium (instability) classes, but most low slope areas were found in low classes. Therefore, the zonation of landslide risk in both Phichai and Tron was not considered in this study.

In Tron district, approximately 0.3 km^2 (60%) of steep slopes and 0.2 km^2 (40%) of low slopes were found in the high class areas. Flats were not found in the high classes because flat areas were not found around the top of mountains. In terms of medium classes, 0.2 km^2 (8.33%) of steep slope areas still showed in this class because some steep slope areas were found in the mountains, while about 1.9 km^2 (79.17%) of low slope areas presented in this class. Some parts of low slope areas presented in low classes. The 24.6 km^2 (8.56%) of low slope and 262.6 km^2 (91.40%) of flat areas presented in the low classes, while only 0.1 km^2 (0.03%) of steep slopes was found in the low classes as given in Table 5.11. The steep slope and low slope areas were so small in both high and medium classes, while most of low slope and flat areas presented in low classes. Both three hazard classes and three slope gradients were shown in two maps (Fig 5.34) and three-dimensional representation of slope gradients and mountainous areas were presented in Fig 5.35 and Fig. 5.36. Steep slopes, low slopes and flats presented in three hazards: high, medium and low as shown in Fig 5.37.

Tron district	Hazard classes											
	High				Medium				Low			
	Slope gradient areas (km^2)				Slope gradient areas (km^2)				Slope gradient areas (km^2)			
	steep slopes	low slopes	flats	total	steep slopes	low slopes	flats	total	steep slopes	low slopes	flats	total
	0.3	0.2	0	0.5	0.2	1.9	0.3	2.4	0.1	24.6	262.6	287.3
	60%	40%	0%	100%	8.33%	79.17%	12.5%	100%	0.03%	8.56%	91.40%	100%

Table 5.11 The relationship between the three hazard classes and three slope gradients, including the zonation of landslide risk (high, medium and low classes) showing steep slope, low slope and flat areas in Tron district under present-day condition.

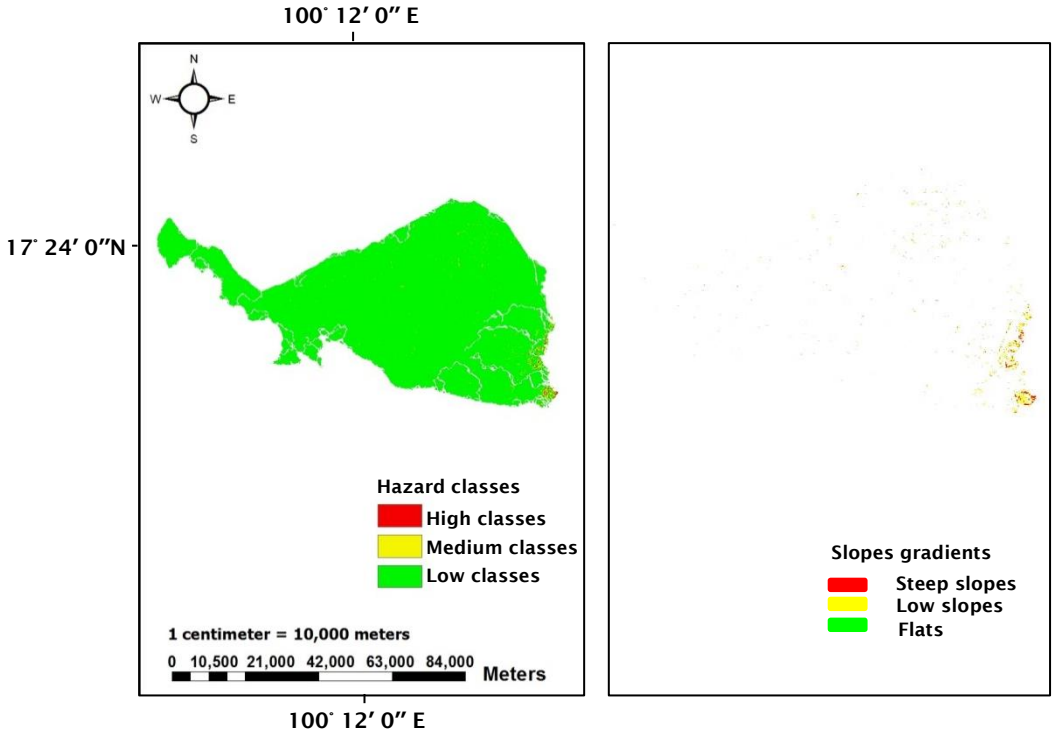

Figure 5.34 The comparison between steep slope, low slope and flat areas showing the zonation of landslide risk (right hand side) and landslide hazard mapping (left hand side) in Tron district under present-day conditions (i.e. 3D area is between latitude 17° 24' 05" north and longitude 100° 12' 17" showing slope gradients in the mountainous areas)

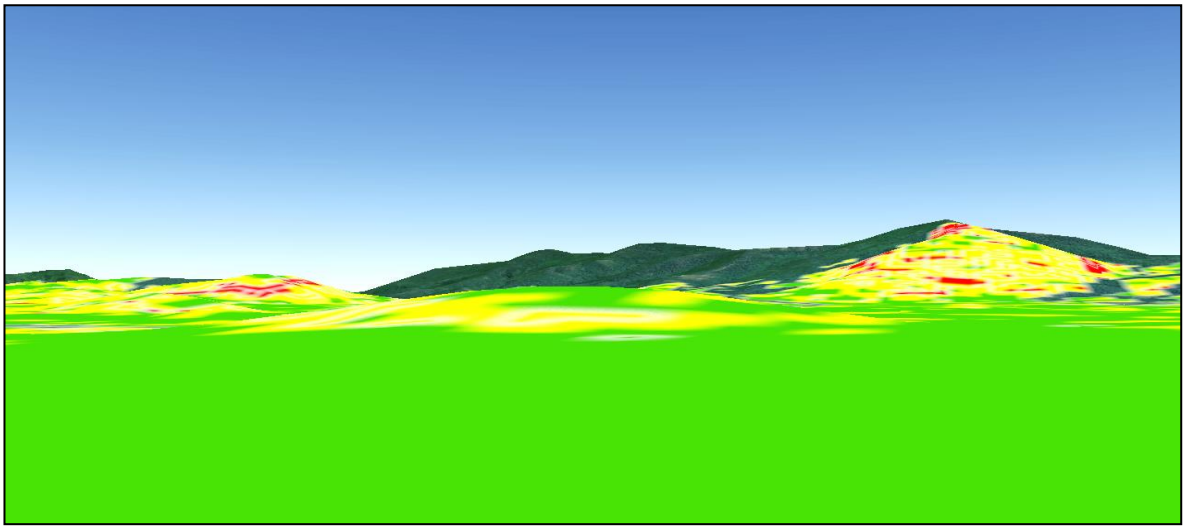

Figure 5.35 Three-dimensional representation of steep slope, low slope and flat areas showing between latitude 17° 24' 05" north and longitude 100° 12' 17" east in Tron district

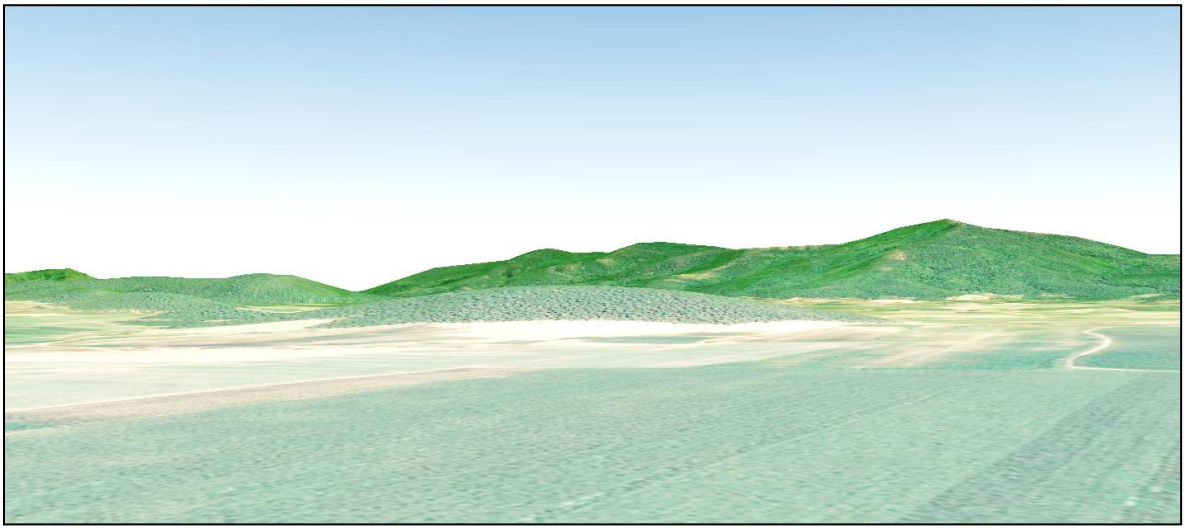

Figure 5.36 Three-dimensional representation of hilly and mountains by google earth showing the mixture of steep slopes, low slopes and flats between latitude 17° 24' 05" north and longitude 100° 12' 17" east in Tron district

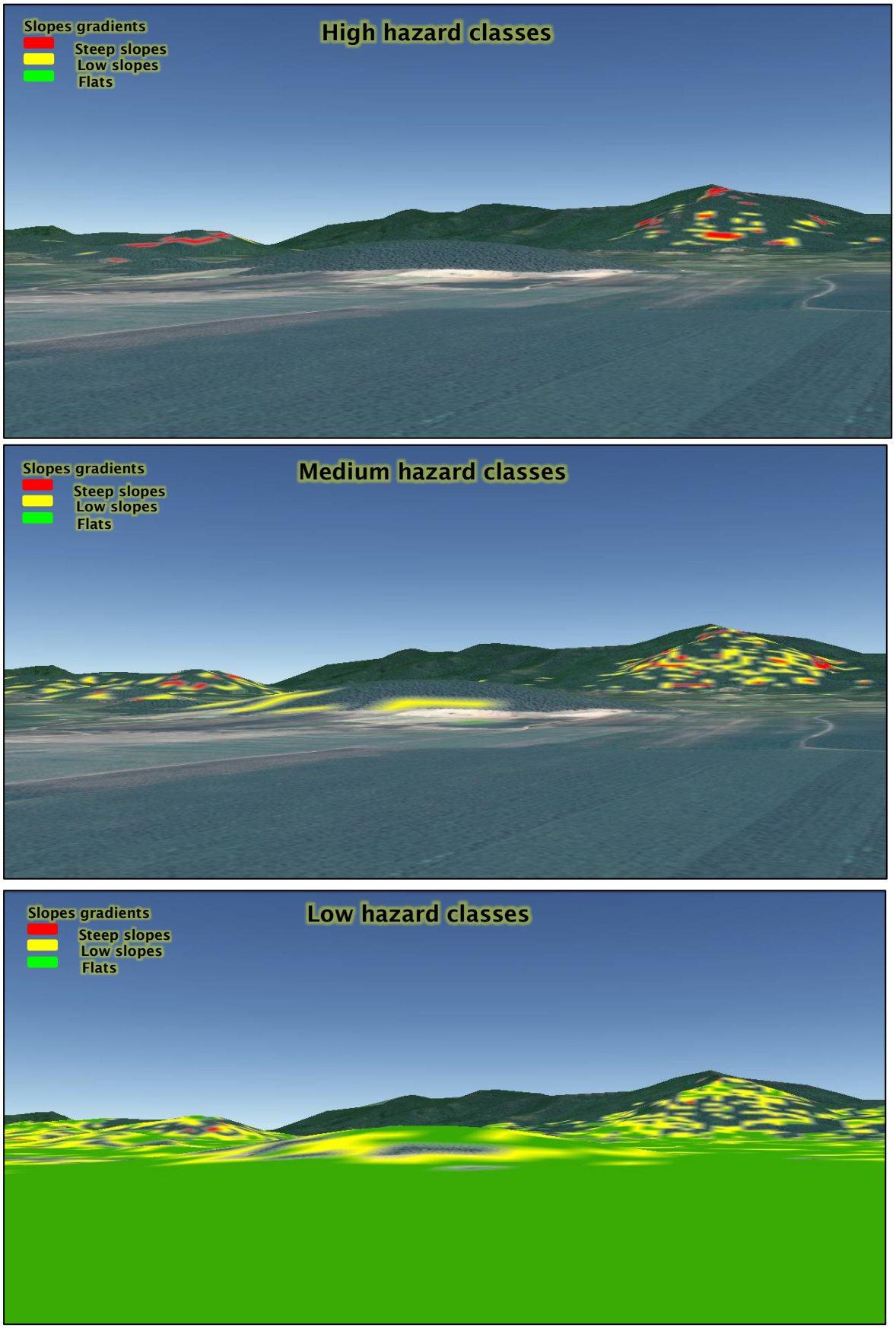

Figure 5.37 The comparison between steep slope, low slope and flat areas showing in the high, medium and low hazard classes in three-dimensional representation of hilly and mountainous areas in Tron district

In Phichai district, approximately 1.3 km^2 (61.9%) of steep slopes and 0.8 km^2 (38.1%) of low slopes were found in the high class areas, flats were not found in the high classes because flat areas were not found in the top of the mountains. In terms of medium classes, 1.2 km^2 (19.7%) of steep slope areas still showed in this class because some steep slope areas were found in the mountains, while about 4.5 km^2 (73.8%) of low slope areas presented in this class. On the other hand, most low slope areas presented in low classes. The 41.0 km^2 (6.33%) of low slope and 606.1 km^2 (93.64%) of flat areas presented in the low classes, while only 0.2 km^2 (0.03%) of steep slope was found in the low classes as given in Table 5.12. The steep slope and low slope areas were small in both high and medium classes, while most of low slope and flat areas presented in low classes. Both three hazard classes and three slope gradients were shown in two maps (Fig 5.38) and three-dimensional representation of slope gradients and mountainous areas were presented in Fig 5.39 and Fig. 5.40. Steep slopes, low slopes and flats presented in three hazards: high, medium and low as shown in Fig 5.41.

Phichai district	Hazard classes											
	High				Medium				Low			
	Slope gradient areas (km^2)				Slope gradient areas (km^2)				Slope gradient areas (km^2)			
	steep slopes	low slopes	flats	total	steep slopes	low slopes	flats	total	steep slopes	low slopes	flats	total
	1.3	0.8	0	2.1	1.2	4.5	0.4	6.1	0.2	41.0	606.1	647.3
	61.9%	38.1%	0%	100%	19.7%	73.8%	6.5%	100%	0.03%	6.33%	93.64%	100%

Table 5.12 The relationship between the three hazard classes and three slope gradients, including the zonation of landslide risk (high, medium and low classes) showing steep slope, low slope and flat areas in Phichai district under present-day conditions.

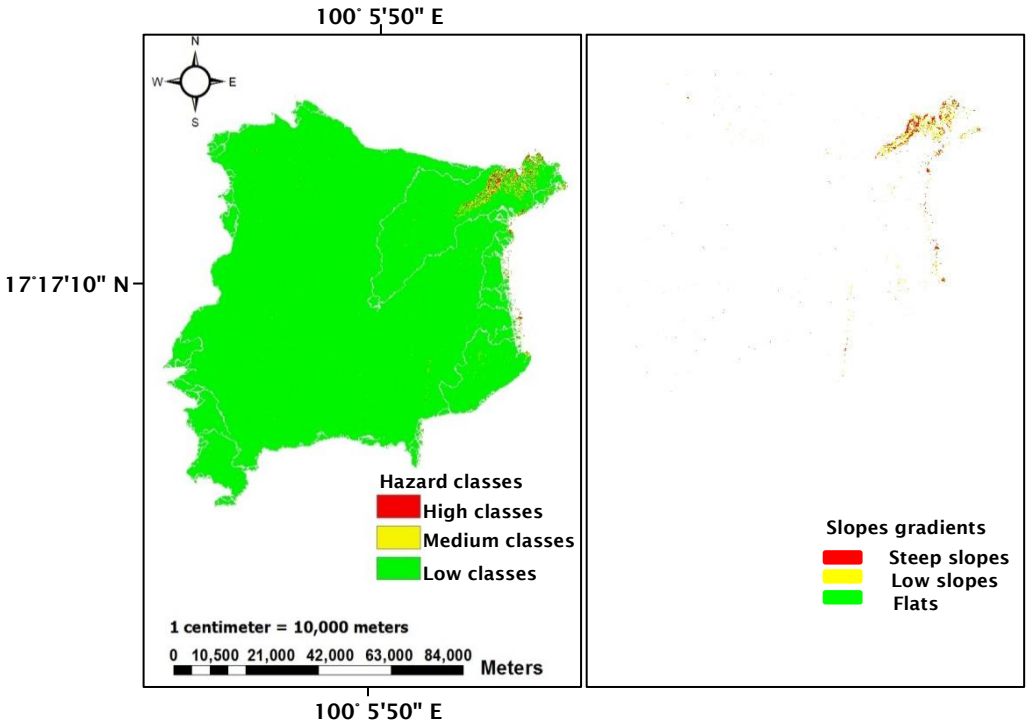

Figure 5.38 The comparison between steep slope, low slope and flat areas showing the zonation of landslide risk (right hand side) and landslide hazard mapping (left hand side) in Phichai district under present-day conditions (i.e. 3D area is between latitude 17° 21' 00" north and longitude 100° 13' 01" showing slope gradients in the mountainous areas)

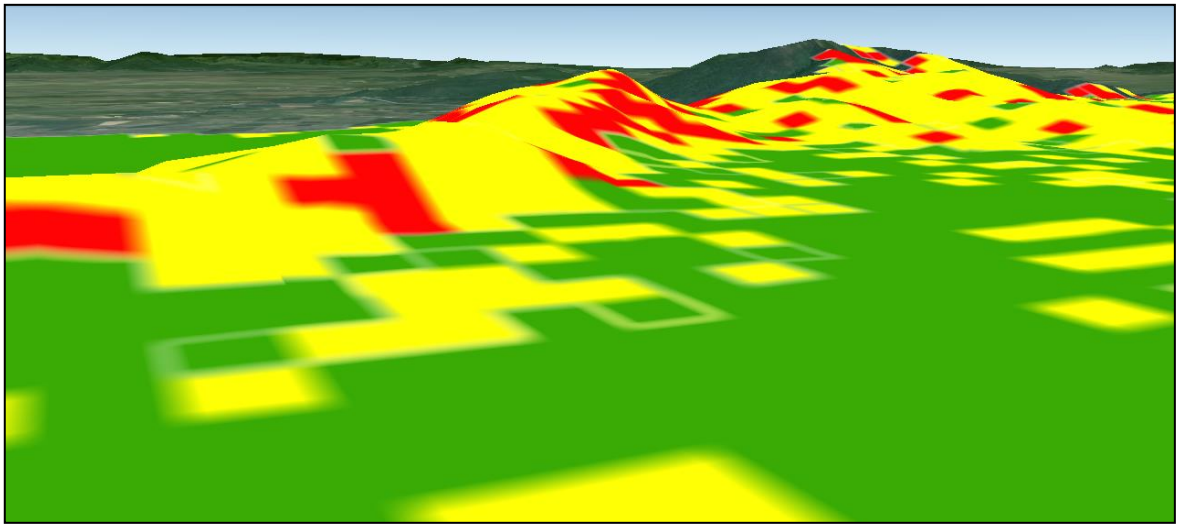

Figure 5.39 Three-dimensional representation of steep slope, low slope and flat areas showing between latitude 17° 21' 00" north and longitude 100° 13' 01" east in Phichai district

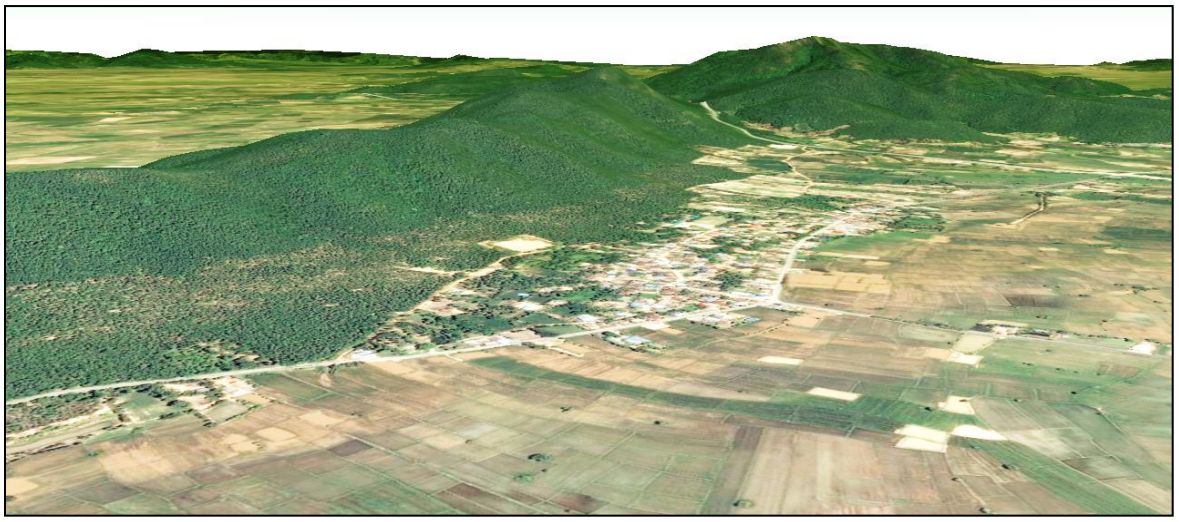

Figure 5.40 Three-dimensional representation of hilly and mountains by google earth showing the mixture of steep slopes, low slopes and flats between latitude 17° 21' 00" north and longitude 100° 13' 01" east in Phichai district

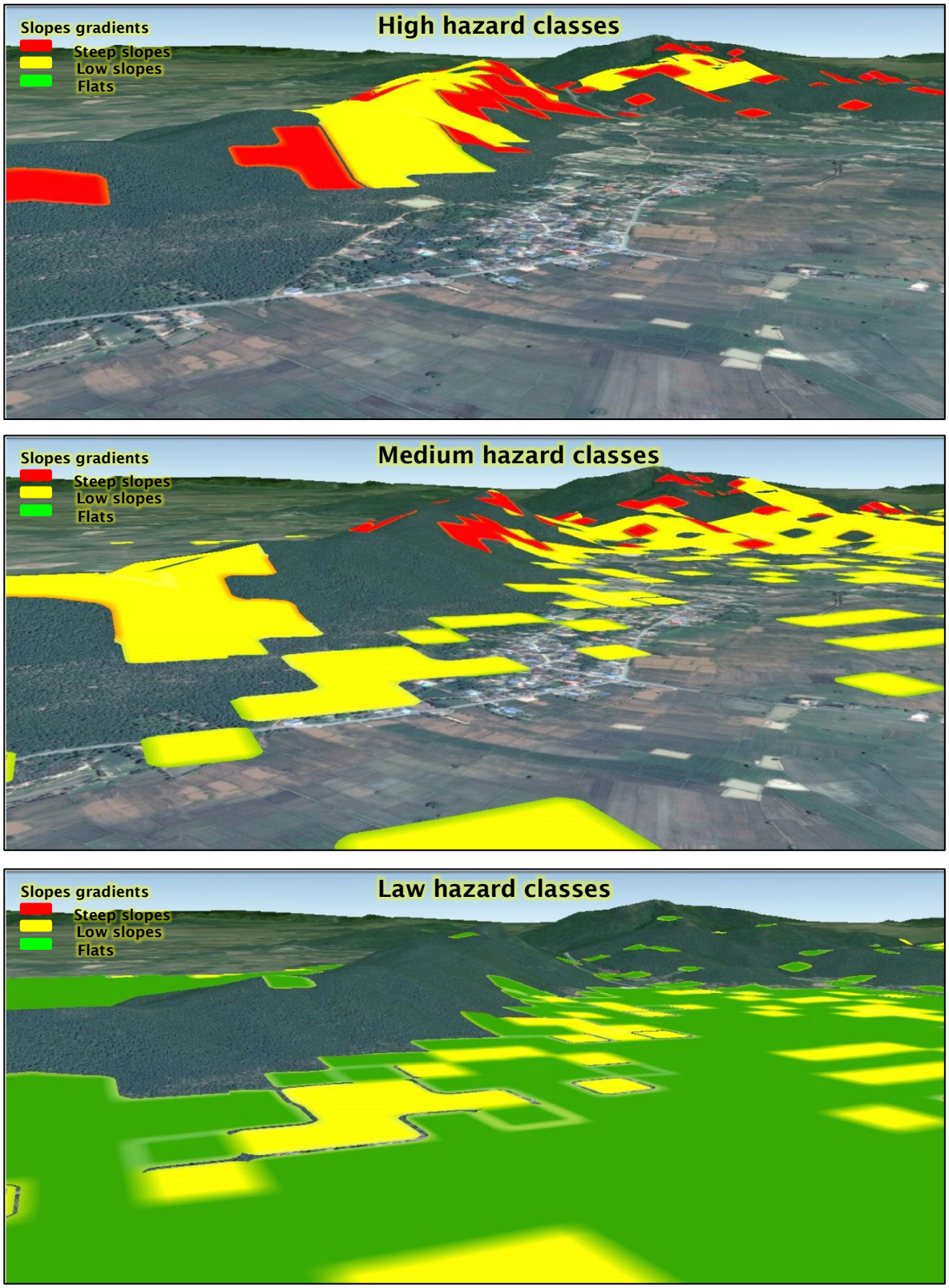

Figure 5.41 The comparison between steep slope, low slope and flat areas showing in the high, medium and low hazard classes in three-dimensional representation of hilly and mountainous areas in Phichai district

Finally, the zonation of landslide risk presented in steep slope, low slope and flat areas in each district. First most of steep slope areas occurred in high hazard classes, next it occurred in medium and low classes respectively. Some parts of steep slopes and low slopes remained showing in medium and low classes. Most of flats were found in low classes. The flow directions is to assign flow from each grid cell, either adjacent or diagonally, in the direction of the steepest downward slope. The increase of infiltrated rainfall related to the slope gradient, can increase the high hazard class areas. The infinite slope model is related to slope gradient length (Montgomery and Dietrich, 1994). Therefore, steep slopes were quite important for failure, instability also linked with low slopes. In addition, both hydrological and geotechnical data directly affected the zonation of landslide risk. For example, in Muang and in Faktha districts, the zonation of landslide risk was so different in both districts because geotechnical parameters (shear and root strength, permeability and angle friction) and hydrological parameter (rainfall) were also different.

The comparison between the zonation of landslide risk and hilly and mountainous areas in each district (by adding steep slope & low slope areas) are sorted descending from high zonation risk to low percentages as shown in Table 5.13. The zonation of landslide risk (km^2) was the highest in Muang district. The zonation of landslide risk covered 100% of all steep slope and low slope areas. The zonation of landslide risk in Thapla district is the second. The zonation of landslide risk covered 89.1% of steep slope and low slope areas. The Thonsaenkhun and Nampat districts were under the same conditions of both soil and rainfall for analysis. The zonation of landslide risk in Thonsaenkhun and Nampat districts covered both steep slopes and low slopes: 67.3% and 62.6% respectively. The 54.3% of landslide zonation risk covered both steep slope and low slope areas in Bankhok district. The Laplea district was the six highest: approximately 51.0% of the zonation of landslide risk was found in both steep slope and low slope areas. Finally, the zonation of landslide risk was the smallest in Faktha district: only 36.4% of sleep slope and low slope areas (Table 5.13). In both Tron and Phichai districts, the zonation of landslide risk was negligible in both districts because the steep slope and low slope areas were so small in both high (failure region) and medium (instability) classes, while most of low slope areas were found in low classes (safety areas).

District / Area (km^2)	Muang	Thapla	Thong saenkhun	Nampat	Bankhok	Laplae	Faktha
Total areas of hilly and mountains in each district (by adding steep slope & low slope areas (km^2)	264.4	1048.3	336.5	934.2	649.5	297.7	592.4
Zonation risk (100% both high & medium classes and 19.85% of low class areas) (km^2)	423.3	934.1	226.6	585.2	352.6	151.7	215.8
The percentages of zonation risk in hilly and mountainous areas (%)	100%	89.1%	67.3%	62.6%	54.3%	51.0%	36.4%

Table 5.13 The zonation of landslide risk is compared with the real areas of steep slope and low slope in each district and sorted descending from high zonation risk to low percentages

5.2 Landslide hazard mapping in future simulation

5.2.1 Assessment of climate change on the local scale

Over the period 1961-2099, the daily rainfall value predictors are generated by HadCM3 and CGCM2 in emission scenarios A2 and B2. The highest rise of carbon dioxide is presented for emission scenario A2, while emission scenario B2 is more ecologically friendly. Over the period 1961–1990, a daily rainfall (covering the baseline periods for all nine predicted variables) is obtained from the National Centre for Environmental Prediction (NCEP) re-analysis data (Kalnay et al., 1996).

a. SDSM calibration

The SDSM calibration process could be used to generate a time period of rainfall for accuracy. The start and end dates can be changed in the setting screen. The period 1961-1990 is the default dates of the baseline period of observed daily rainfall data. Over the period 1961-1990, the 100 member ensembles of synthetic rainfall time series and threshold 0.2 are indicated for the best condition because The gap between observed annual rainfall and modelled annual rainfall is small. The comparison between observed annual rainfall and modelled annual rainfall is presented in (Fig. 5.42) for nine rain stations in nine provinces. Over the 1961-2012 period, the gap between observed and modelled annual rainfall was approximately 3-10%. The gaps were small in 100 member ensembles, while the gap was bigger when the 10 member ensembles of synthetic rainfall time series were input. 100 member ensembles means that 100 rainfall values are averaged

for daily rainfall value, so 100 member ensembles are better than 10 member ensembles. The event threshold is specified to set the trace rainy days as dry days. Similarly 0.2 mm/day is set for the threshold of rainy days of SDSM software in this study.

The SDSM software is used for the prediction of annual rainfall in the future because it produces a small gap between the modelled and observed annual rainfall from 1961 to 2012. Another model type (seasonal, monthly) has a big gap between the modelled and observed annual rainfall from 1961 to 2012, including the year length consisting of 360 days in this SDSM version. It cannot show the exact season and month because of just covering 360 days per year. Therefore, the prediction of annual rainfall is more accurate by SDSM software.

As can be seen in Fig 5.42 it is found that the modelled and observed rainfall of quantile-quantile plot is the best correlation. This quantile plot demonstrates that lower modelled daily rainfalls (in black) are obtained in contrast to observed values, but modelled values climb to agree with higher values of the observed record (in blue: a 1:1 control line). Although modelled values between 2 and 6 mm/day do not reflect the observed values, elsewhere there is some agreement of the modelled (black) and observed (blue) rainfall is provided by the quantile plot, whilst the ensemble model values cover observed values. This representation of modelled rainfall data is the best one that can be achieved.

Another bar chart, the % wet day and maximum wet spell was presented for calibration time (1961-1990) as given in Fig 5.43. The modelled output and observed rainfall is nearly the same value in both the % wet day and the maximum wet spell in each month. These are presented because wetter days related to the critical period of wet weather, lead to the probability of landsliding (Beven and Kirkby, 1979)

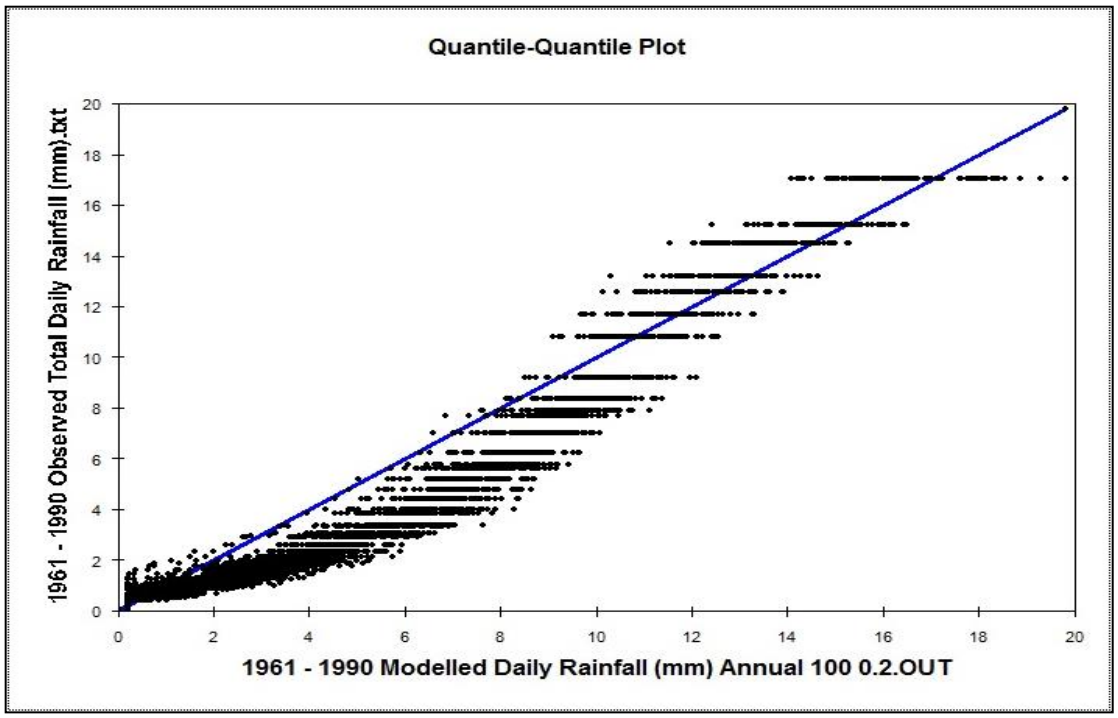

Figure 5.42 Quantile-Quantile plot of the modelled 100 member ensemble and observed rainfall

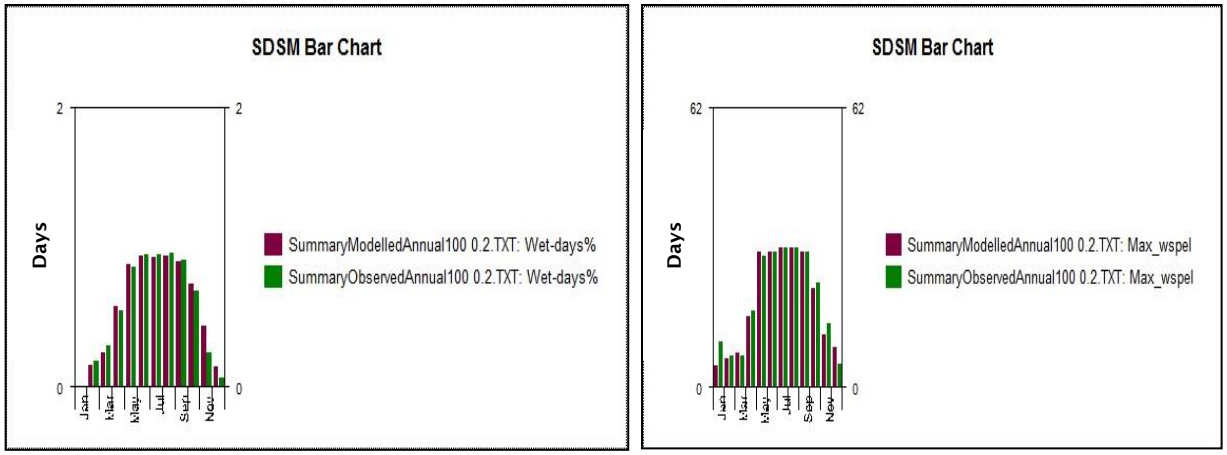

Figure 5.43 Time series plot of wet-day% and maximum wet spell, both modelled and observed rainfall

b. Southeast Asia START Regional Centre

The future climate was forecast by the Southeast Asia START Regional Centre for simulation scenario A2 and B2 in Thailand, which was also used in this study. The dataset describes a long period of climate conditions and represents the

changing of the greenhouse gas carbon dioxide. The database describes a long time period of climate conditions as it was found that the data cannot specify a specific year.

The START dataset was focused on a grid size of 20x20 km. In the present study, both latitude and longitude were indicated, covering nine provinces (Fig 3.10) and each province covering nine provinces: Uttaradit, Tak, Pisanulok, Khon Kean, Udontani, Lamprang, Petchaboon, Prea and Loei as given in Fig 3.12.

The prediction of daily rainfall is obtained by START from 1961 to 2099 under simulation scenario A2 and B2, which is only 360 days per year. In this study, the precipitation data (START) is downscaled from latitude 16° 26′ and 18° 37′ north and between longitude 98° 52′ and 103° 05′ east, which is the same areas as the SDSM.

c. Precipitation data

In this study, observed daily rainfall data (mm) covering nine central rain stations are obtained by future simulation from latitude 16° 26′ and 18° 37′ north and between longitude 98° 52′ and 103° 05′ east in SDSM software and START in nine provinces: Uttaradit, Tak, Pisanulok, Khon Kaen, Udontani, Lampang, Petchaboon, Phrae and Loei.

During the 1961 to 2012 period, the comparison between observed and modelled annual rainfall is compared, using the model as follows:

- The average of observed annual rainfall volumes during 1961-2012 and the annual modelled rainfall volumes, both SDSM in simulation scenario A2 and B2 and START in simulation scenario A2 and B2, during 1961 - 2099 are presented by a graph covering nine rain stations. Five lines are shown alongside each other in a graph (Fig 5.44). Both modelled annual rainfall of SDSMA2 and SDSMB2 in each three years are averaged: 1,341.1 mm and 1,334.8 mm from 1961 to 2012 respectively and annual rainfall of STARTA2 and STARTB2 in each three years are averaged: 1,381.2 mm and 1,335.2 mm from 1961 to 2012 respectively, while observed rainfall in each three years is averaged: 1289.2 mm from 1961 to 2012. The comparison between observed and modelled rainfall: SDSM and START presented approximately 3.78% and 5.35% difference from 1961 to 2012 respectively.

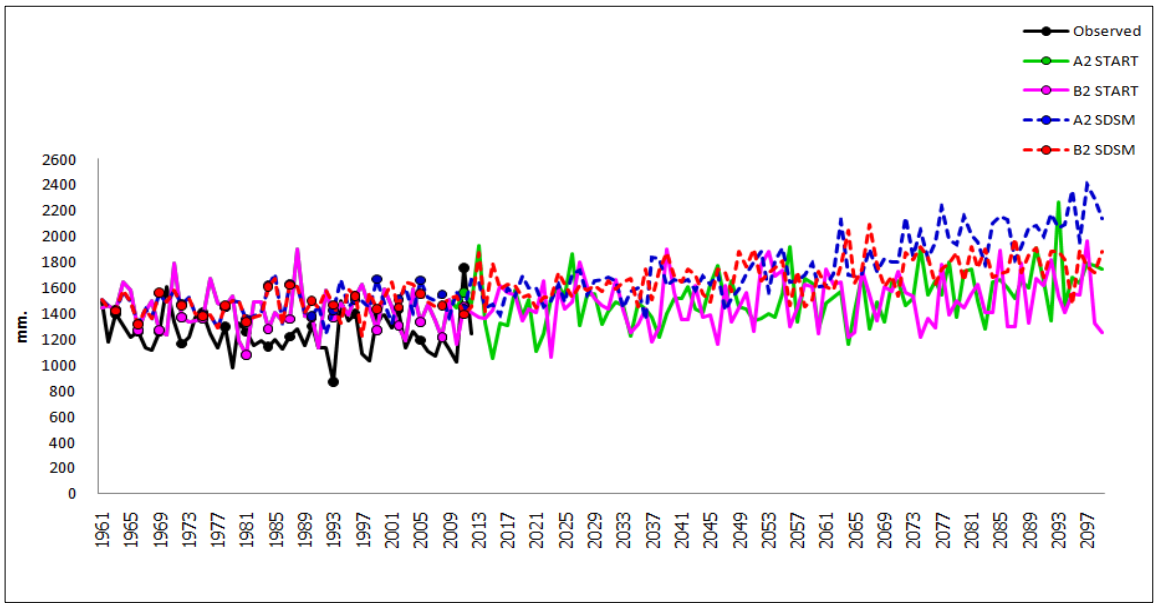

Figure 5.44 The observed annual rainfall during 1961-2012, and the predicted annual rainfall quantities, both START in scenario A2 and B2 and SDSM in scenario A2 and B2 (five lines in the graph), during 1961-2099 covering nine rain stations.

- The gap between observed annual rainfall volumes during 1961-2012 and modelled annual rainfall volumes, both START and SDSM, during 1961 - 2099 is presented by a graph for each rain station covering nine stations (nine graphs in Fig 5.45- Fig 5.53). The comparison between observed and modelled rainfall: SDSM and START presented approximately 10-15% of average difference from 1961 to 2012.

The annual precipitation of climate scenario A2 and B2 is used to predict rainfall conditions from 2013 to 2099 by graphs in both SDSM and START. As a result, the observed annual rainfall during 1961-2012, and the annual rainfall values, both START and SDSM, during 1961-2099 will be presented by nine graphs for each rain station in nine provinces: rain station 351201 (Uttaradit province), rain station 376201 (Tak province), rain station 378201 (Pisanulok province), rain station 381201(Khon Kaen province), rain station 354201 (Udontani province), rain station 328201 (Lampang province), rain station 379201 (Petchaboon province), rain station 330201 (Phrae province) and rain station 353201 (Loei province) as given in Figs 5.45- 5.53.

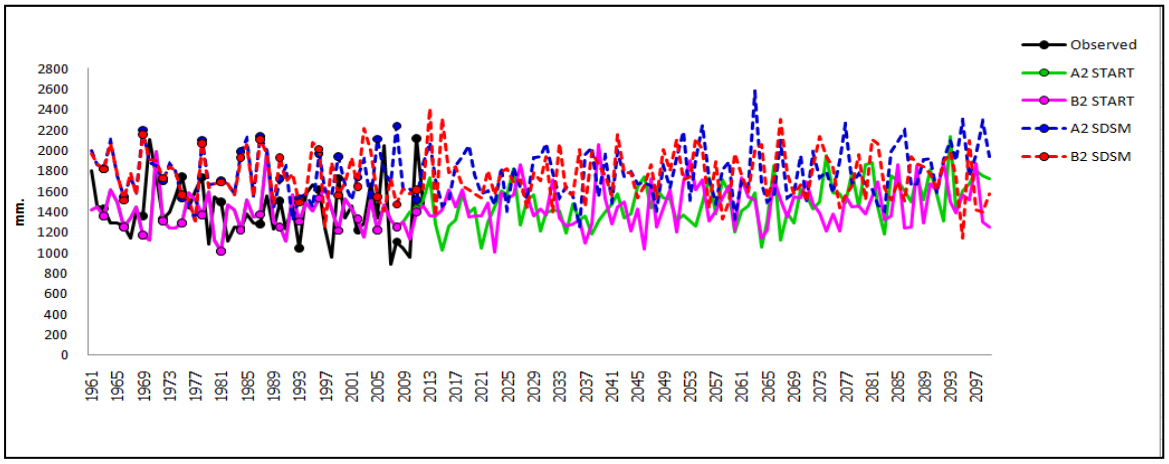

Figure 5.45 The observed annual rainfall during 1961-2012, and the predicted annual rainfall quantities, both START and SDSM in scenario A2 and B2 (five lines in the graph), during 1961-2099 covering rain station (351201) in Uttaradit province.

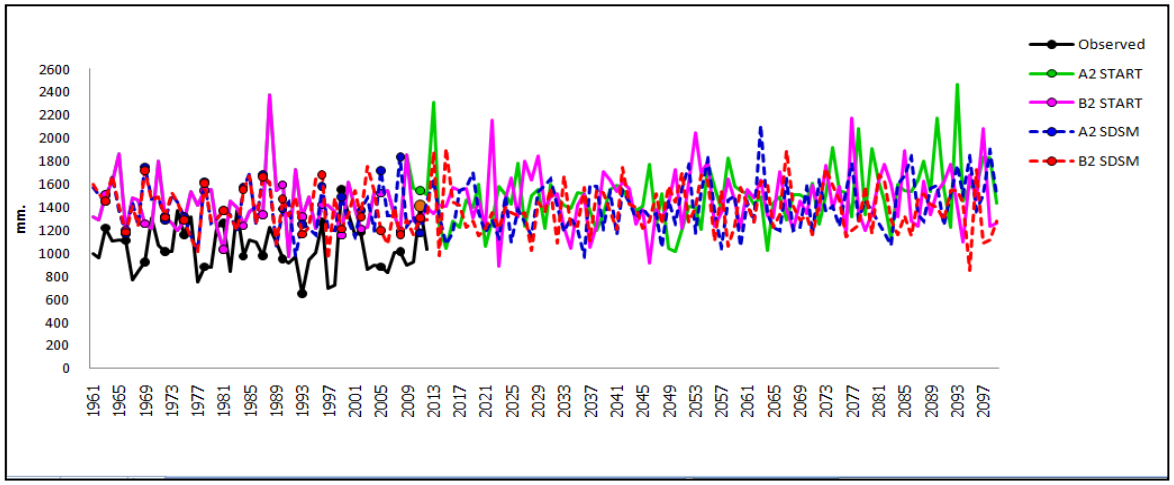

Figure 5.46 The observed annual rainfall during 1961-2012, and the predicted annual rainfall quantities, both START and SDSM in scenario A2 and B2 (five lines in the graph), during 1961-2099 covering rain station (376201) in Tak province.

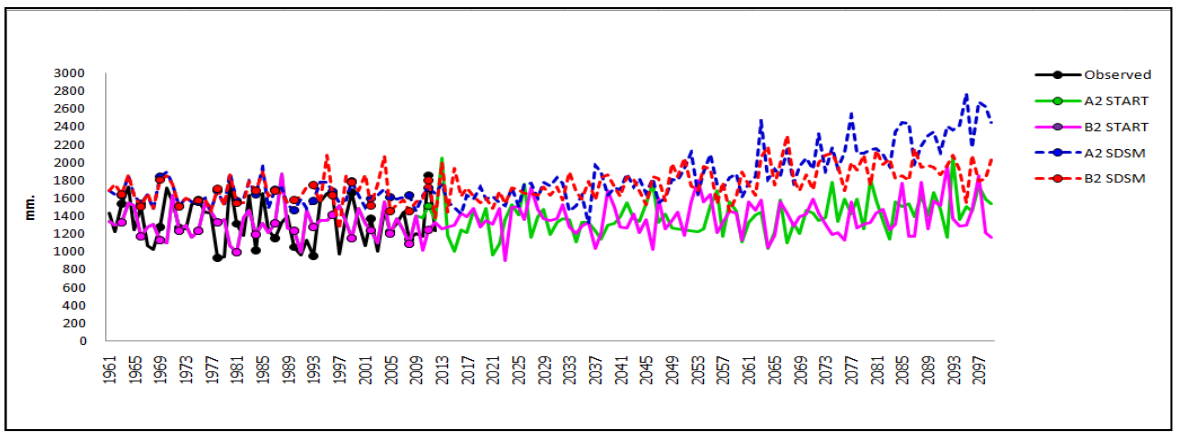

Figure 5.47 The observed annual rainfall during 1961-2012, and the predicted annual rainfall quantities, both START and SDSM in scenario A2 and B2 (five lines in the graph), during 1961-2099 covering rain station (378201) in Pisanulok province.

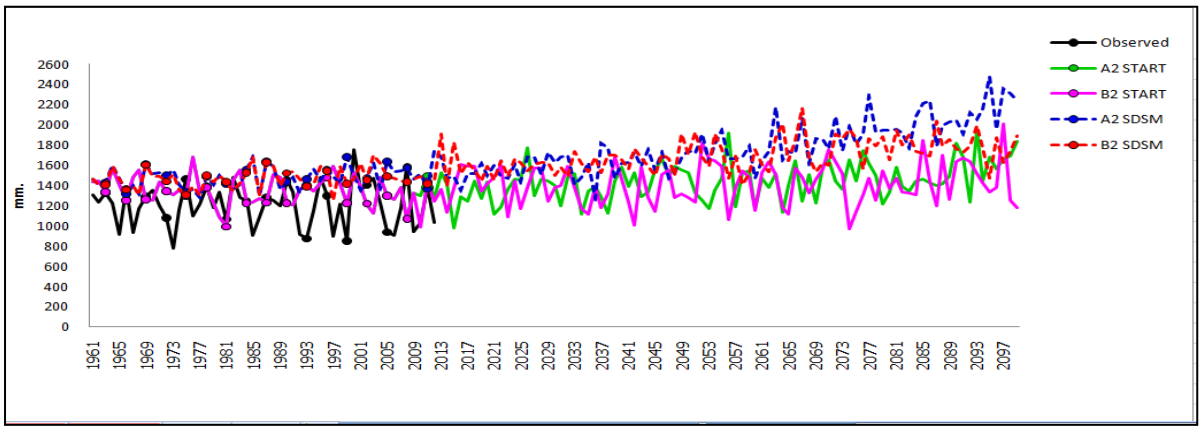

Figure 5.48 The observed annual rainfall during 1961-2012, and the predicted annual rainfall quantities, both START and SDSM in scenario A2 and B2 (five lines in the graph), during 1961-2099 covering rain station (381201) in Khon Kaen province.

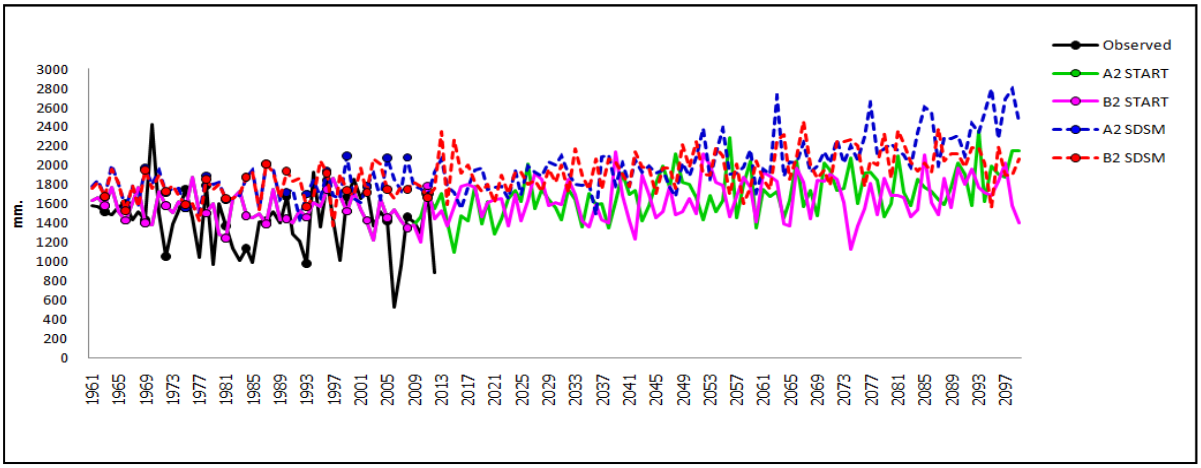

Figure 5.49 The observed annual rainfall during 1961-2012, and the predicted annual rainfall quantities, both START and SDSM in scenario A2 and B2 (five lines in the graph), during 1961-2099 covering rain station (354201) in Udontani province.

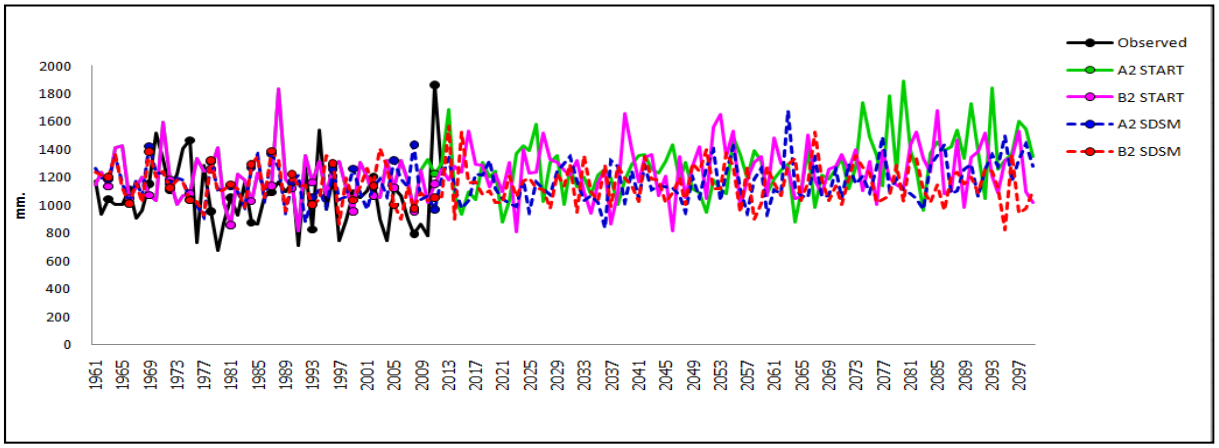

Figure 5.50 The observed annual rainfall during 1961-2012, and the predicted annual rainfall quantities, both START and SDSM in scenario A2 and B2 (five lines in the graph), during 1961-2099 covering rain station (328201) in Lampang province.

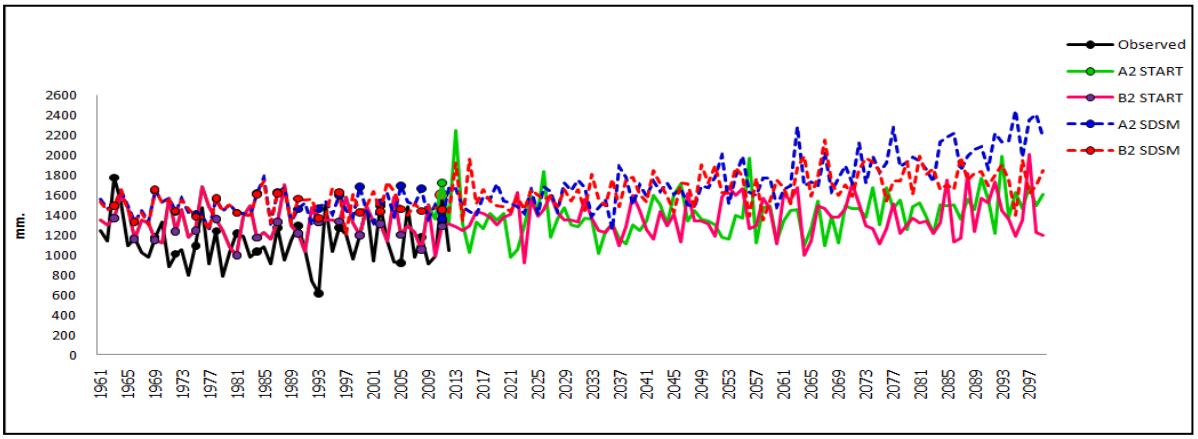

Figure 5.51 The observed annual rainfall during 1961-2012, and the predicted annual rainfall quantities, both START and SDSM in scenario A2 and B2 (five lines in the graph), during 1961-2099 covering rain station (379201) in Petchaboon province.

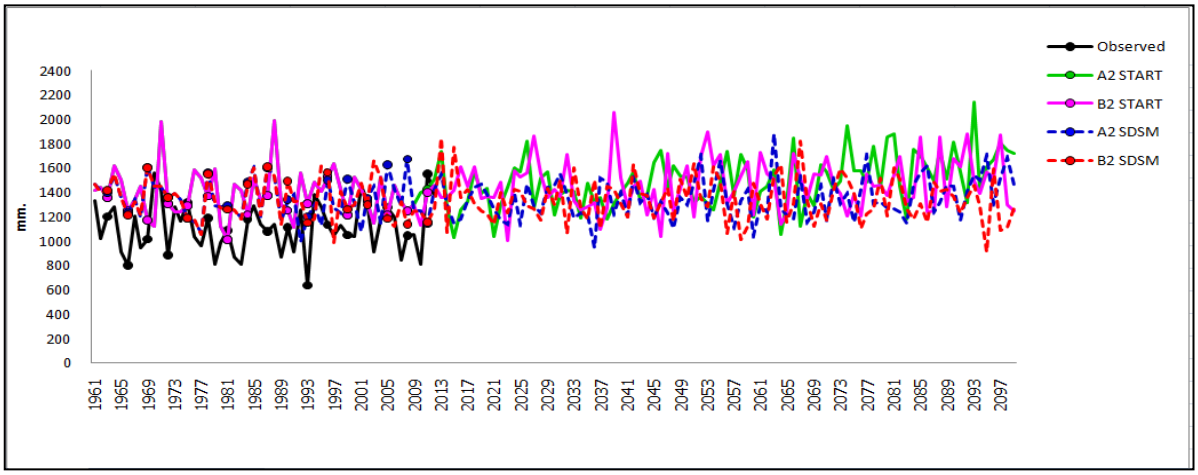

Figure 5.52 The observed annual rainfall during 1961-2012, and the predicted annual rainfall quantities, both START and SDSM in scenario A2 and B2 (five lines in the graph), during 1961-2099 covering rain station (330201) in Phrae province.

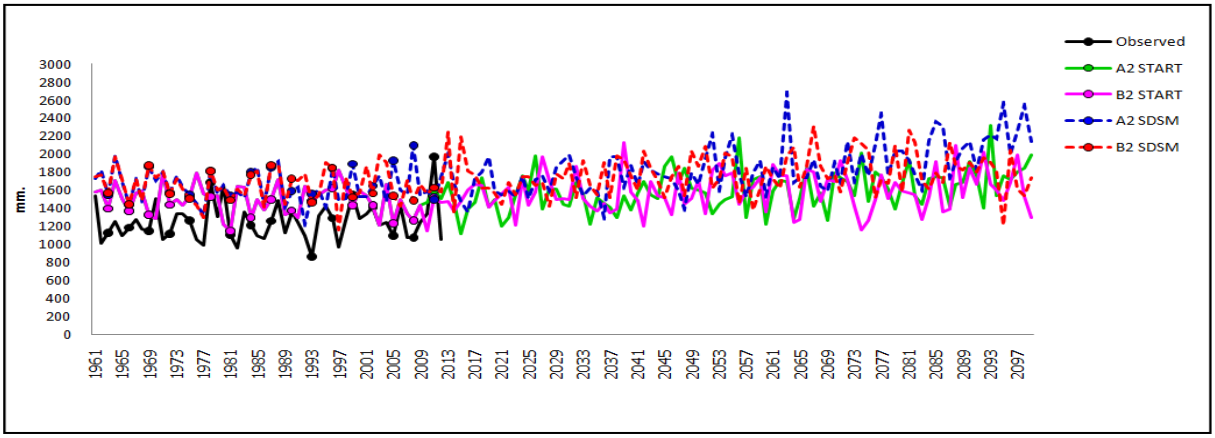

Figure 5.53 The observed annual rainfall during 1961-2012, and the predicted annual rainfall quantities, both START and SDSM in scenario A2 and B2 (five lines in the graph), during 1961-2099 covering rain station (353201) in Loei province.

The precipitation data, by START and SDSM, are described by a graph covering nine rain stations (one graph) (Fig 5.44) and a graph in each rain station covering nine rain stations (nine graphs)(Figs 5.45 – 5.53).

As a result, the percentages of the difference between the observed annual rainfall volumes during 1961-2012, the annual modelled rainfall volumes, both START and SDSM, during 1961-2099 are shown on a graph (Fig 5.44) covering nine rain stations and a graph in each rain station covering nine rain stations (nine graphs) and are small. Thus, this approach selects modelled annual rainfall volumes in each rain station in each province covering nine provinces: rain station 351201 (Uttaradit province), rain station 376201 (Tak province), rain station 378201 (Pisanulok province), rain station 381201(Khon Kaen province), rain station 354201 (Udontani province), rain station 328201 (Lampang province), rain station 379201 (Petchaboon province), rain station 330201(Phrae province) and rain station 353201 (Loei province). It is impossible for modelled annual rainfall to present the one value covering nine provinces.

5.2.2 Hydrological data

In the study, rainfall distribution is described by the calculation of nine rain stations covering the nine provinces of Uttaradit, Tak, Pisanulok, Khon Kaen, Udontani, Lampang, Petchaboon, Phrae and Loei, which correlate with the downscaling of the daily precipitation scenario in the future simulation from latitude 16° 26′ and 18° 37′ north and between longitude 98° 52′ and 103° 05′ east in SDSM software.

At the present calibration (1954-2012), in the nine central rain stations covering nine provinces, the mean annual rainfall was approximately 1,404.9 mm, 1,036.9 mm, 1,414.1 mm, 1,142.2 mm, 1,209.1 mm, 1,142.2 mm, 1,209.1 mm, 1,099.4 mm and 1,241.1 mm as in Uttaradit, Tak, Pisanulok, Khon Kaen, Udontani, Lampang, Petchaboon, Phrae and Loei respectively. In the future simulation (2013-2099), both emission scenario A2 and B2, increasing annual rainfall will appear, covering the nine provinces (Table 5.14 and Table 5.15). IPCC (2012) also confirms that annual precipitation will increase in the future in the northern mid-latitudes, which are associated with the northern and eastern parts of Thailand.

a) SDSM

The number of standard rainy hours from1981to 2010 (Section 3.8.1, Chapter 3) is used to calculate the average annual rainfall using the SDSM software for 2013-2099. The annual rainfall values for each rain station are calculated and shown in Table 5.12 for the rainfall values rate (mm/24 hours) for each rain station covering nine provinces. Although the gap by SDSM downscaling (covering nine provinces) between observed annual rainfall and modelled rainfall volumes is smaller, the modelled rainfall volumes for each rain station covering nine provinces are selected for rainfall calculation in the future (2013-2099). These rainfall values will be averaged by the interpolation approach and represented by the rainfall intensity rate on the map as show in Fig 5.54- Fig 5.55. The rainfall values (mm) in twenty-four hours are the key factor for landslide hazard analysis in the SINMAP software. The average three-hourly rainfall totals from 1981 to 2010 are used to calculate the standard of days of rain per year for each rain station covering nine provinces (Section 3.8.1, Chapter 3). The days of rain per year and annual rainfall were used to calculate rainfall in mm/24 hours as in Table 5.14.

Average rainfall 2013-2099	Uttaradit	Tak	Pisanulok	Khon Kaen	Udontani	Lampang	Petchaboon	Phrae	Loei
A2 (annual rainfall)	2820	1408.7	1914.1	1774.6	2063	1173.2	1777.1	1350.8	1852.8
B2 (annual rainfall)	2794.9	1383.8	1803.4	1696.3	1980.3	1156.9	1689.5	1342.2	1783.4
Days rain per a year	19	18	19	15	18	16	20	18	18
A2 (mm./24 hours)	148.4	78.3	100.7	118.31	114.6	73.3	88.85	74.1	102.9
B2 (mm./24 hours)	147.1	76.9	94.9	113.09	110.2	72.3	84.47	73.6	99.1

Table 5.14 The modelled annual rainfall and rainfall rate (mm/24 hours) in scenario A2 and B2 by SDSM

In the SDSM software, the rainfall values rate (mm/24 hours) of 140.9 mm/24 hours in Muang, Laplea and Tron districts, 110.8 –125.9 mm/24 hours in Phichai and Thongsaenkhun districts, 110.8 mm/24 hours in Nampat districts, 95.8 –110.8 mm./24 hours in Thapla district, 95.8 mm/24 hours in Bankhok and Faktha districts are presented by scenario A2 (Fig 5.54) and 139.6 mm/24 hours both Muang, Laplea and Tron districts, 109.7–124.6 mm/24 hours in Phichai and Thongsaenkhun districts, 109.7 mm/24 hours in Nampat districts, 94.7– 109.7 mm/24 hours in Thapla district, 94.7 mm/24 hours in Bankhok and Faktha districts are presented by scenario B2 (Fig 5.55).

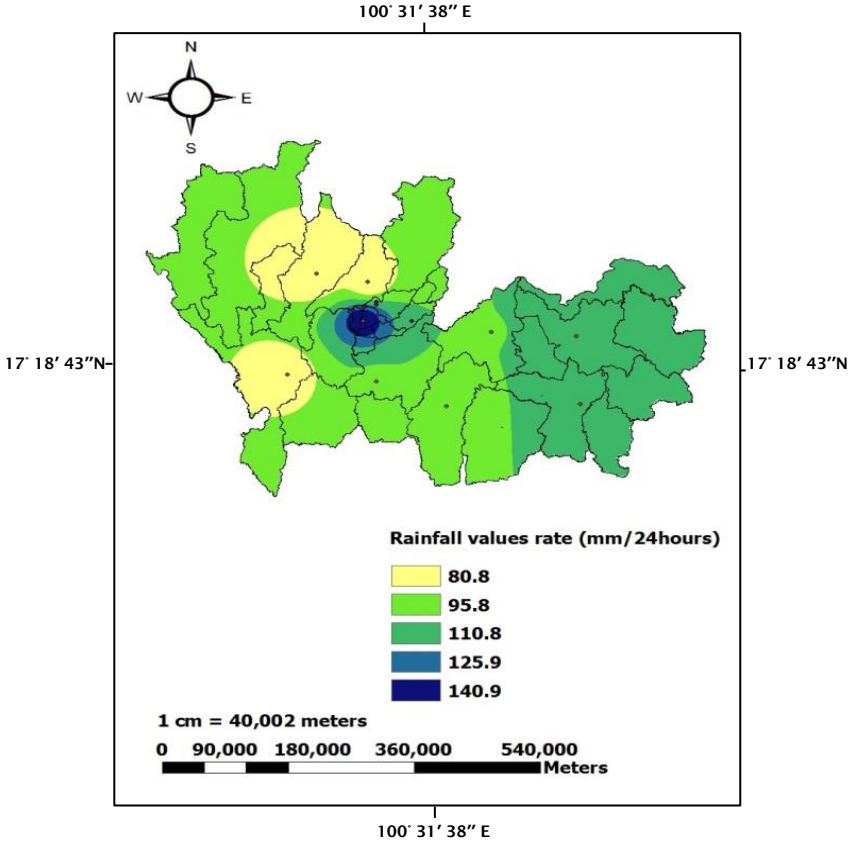

Figure 5.54 The interpolated map scenario A2 by SDSM

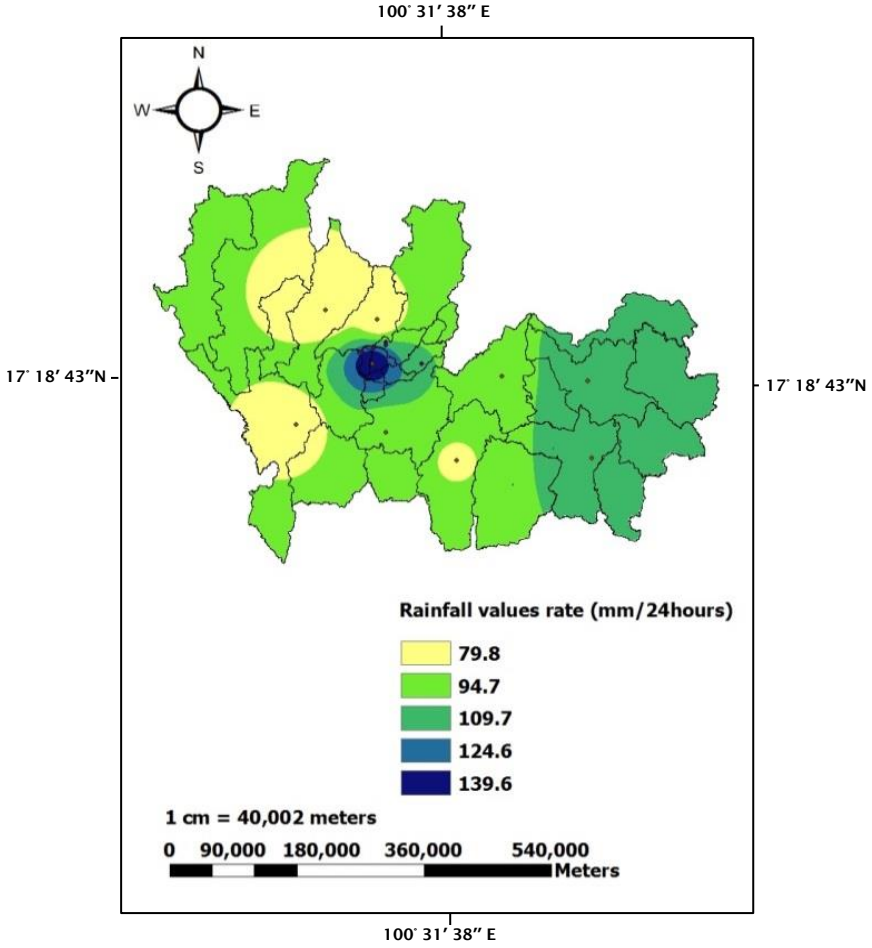

Figure 5.55 The interpolated map scenario B2 by SDSM

b) START

Daily rainfall data, only 360 days per a year, were verified by START from 1961 to 2099 under simulation scenario A2 and B2. This study of modelled rainfall (START) is correlated with the modelled rainfall (SDSM) by graphs of annual rainfall during the 2013-2099 period, whereas observed annual rainfall was described by graphs during 1961-2012 (Fig 5.56-Fig 5.57). In terms of modelled rainfall by START, the standard of hours rainfall from 1981-2010 (Section 3.8.1, Chapter 3) was used to calculate the rainfall rate (mm/24 hours) in the period 2013-2099 in each rain station as shown in Table 5.15. Then the interpolation approach is represented by the rainfall distribution on the map, as shown in Fig 5.56-Fig 5.57.

Average rainfall 2013-2099	Uttaradit	Tak	Pisanulok	Khon Kaen	Udontani	Lampang	Petcha boon	Phrae	Loei
A2 (annual rainfall)	2320.9	1494.1	1392.1	1441.2	1712.2	1278.4	1401.5	1490.4	1602.7
B2 (annual rainfall)	2291.6	1474.3	1377.3	1412.6	1663.7	1253.5	1383.7	1465.1	1586.5
Days rain per a year	19	18	19	15	18	16	20	18	18
A2(mm./24 hours)	122.1	83	73.3	96.1	95.1	79.9	70.1	81.9	89
B2 (mm./24 hours)	120.6	81.9	72.5	94.2	92.4	78.4	69.2	80.7	88.1

Table 5.15 The modelled annual rainfall and rainfall rate in scenario A2 and B2 by START

The rainfall values rate (mm/24 hours) of START are presented in each district. The rainfall values rate (mm/24 hours) of 116.9 mm/24 hours in Muang, Laplea and Tron districts, 96.1−106.5 mm/24 hours in Phichai and Thongsaenkhun districts, 96.1 mm/24 hours in Thapla and Nampat districts, 85.7− 96.1 mm./24 hours in Faktha district and 85.7 mm/24 hours in Bankhok district, are presented by scenario A2 (Fig 5.56) and 115.4 mm/24 hours both Muang, Laplea and Tron districts, 94.8 − 105.2 mm/24 hours in Phichai and Thongsaenkhun districts, 94.8 mm/24 hours in Thapla and Nampat districts, 84.6 − 94.8 mm/24 hours in Faktha district and 84.6 mm/24 hours in Bankhok district are presented by scenario B2 (Fig 5.57) for the SINMAP calculation.

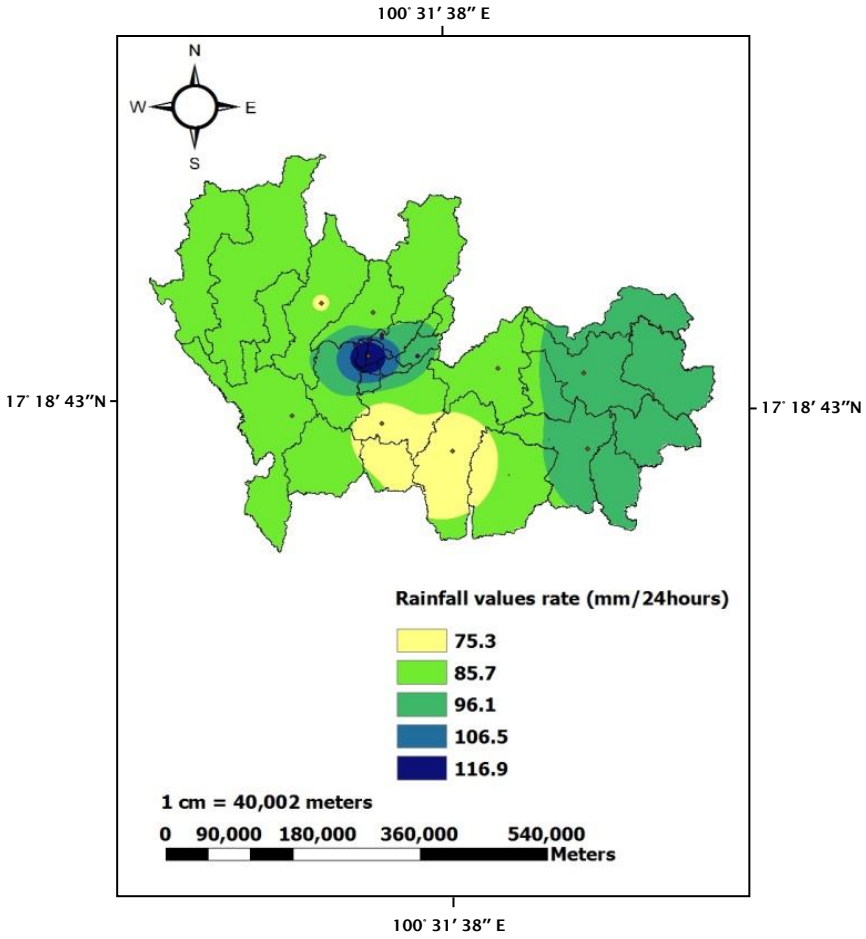

Figure 5.56 The interpolated map scenario A2 by START

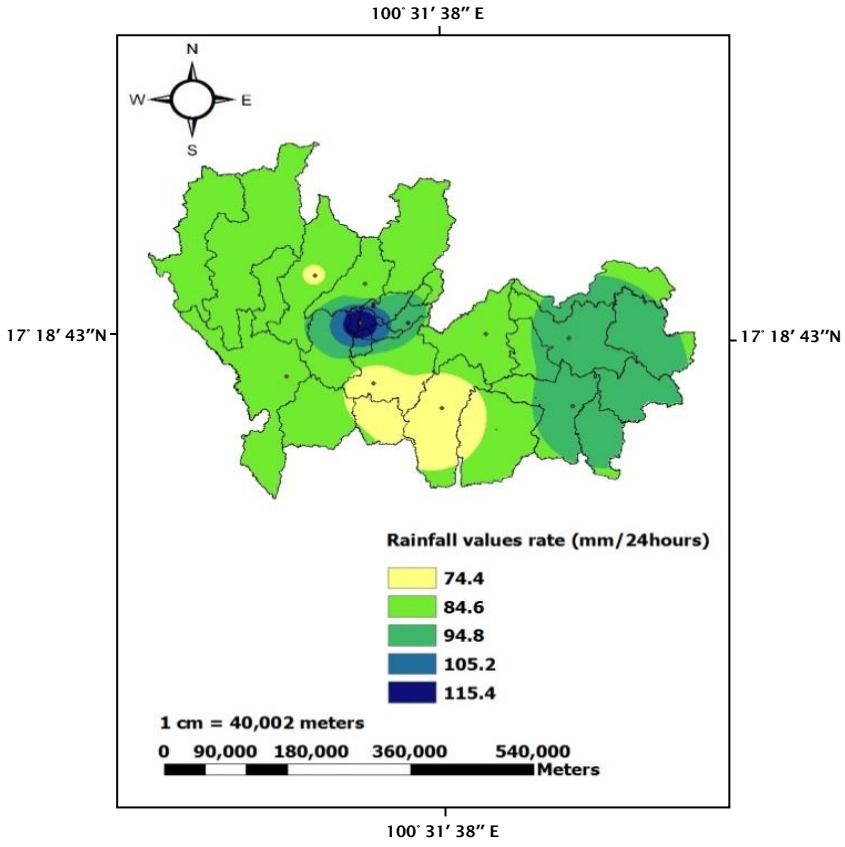

Figure 5.57 The interpolated map scenario B2 by START

The result of rainfall prediction in the future simulation in scenario A2 and B2 both SDSM and START, increases in the same direction. The IPCC (2012) insists that extreme weather conditions, rapidly growing in the future, will lead to changed rainfall, both in intensity and seasonality. Therefore, the annual precipitation will be increased to approximately 100-300 mm. over the northern part of the hemisphere that covers Thailand.

The trend of rainfall increases in every province, especially in Uttaradit province. Therefore, the intense rainfall is found in Uttaradit province, which is presented by the interpolation map. As a result, the predicted rainfall will increase in four simulations: scenario A2 and B2 by SDSM (Table 5.14), scenario A2 and B2 by START (Table 5.15).

5.2.3 Landslide hazard mapping

In the future simulation, geotechnical data are described by soil depth, cohesive soil, angle friction, permeability and soil density values in each district, covering the nine districts of Muang (TP1), Laplea (TP2), Thapla (TP3), Nampat (TP5), Bankhok (TP6), Faktha (TP7), both Tron and Phichai (TP2) and Thongsaenkhun (TP5) for the SINMAP calculation. This calculation is the same as at the present-day conditions (1954-2012).

The rainfall values rate (mm/24 hours) will be used to analyse the nine districts in Uttaradit province by interpolation, the average and intense rainfall values presented in the interpolated map in scenarioA2 and B2 by both SDSM and START (Fig 5.54 – Fig 5.57). The rainfall values rate, in Uttaradit province, is selected for SINMAP software in the boundary of the nine districts of Muang, Laplea, Thapla, Nampat, Bankhok, Faktha, Thongsaengkhun, Phichai and Tron. The description of landslide hazard classes was calculated into high, medium, and low in Uttaradit province.

In the future simulation (2013-2099) by SDSM software, the landslide hazard mappings presented in high (red), medium (yellow) and low (green) hazard classes in nine districts in Uttaradit province as shown in Fig 5.58 and Fig 5.59. Both the simulation scenario A2 and B2, three (high (red), medium (yellow) and low (green)) hazard class areas (km^2) and also total area of all districts (purple) are nearly the same, as given in Fig 5.60 and Fig 5.61.

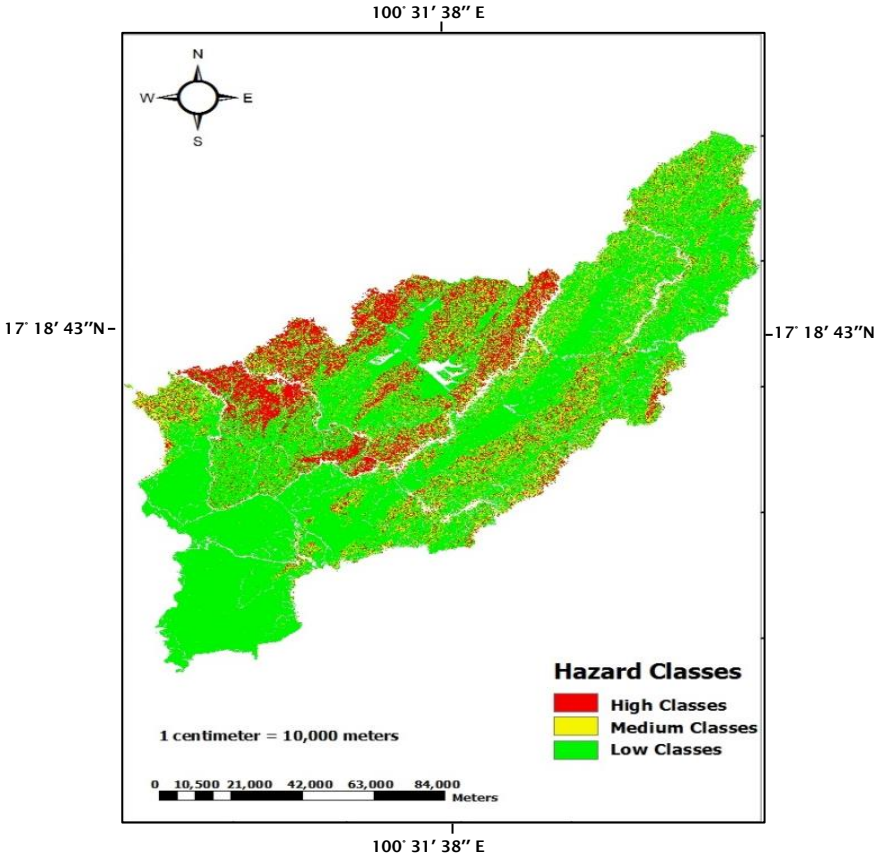

Figure 5.58 The landslide hazard mapping scenario A2 by SDSM

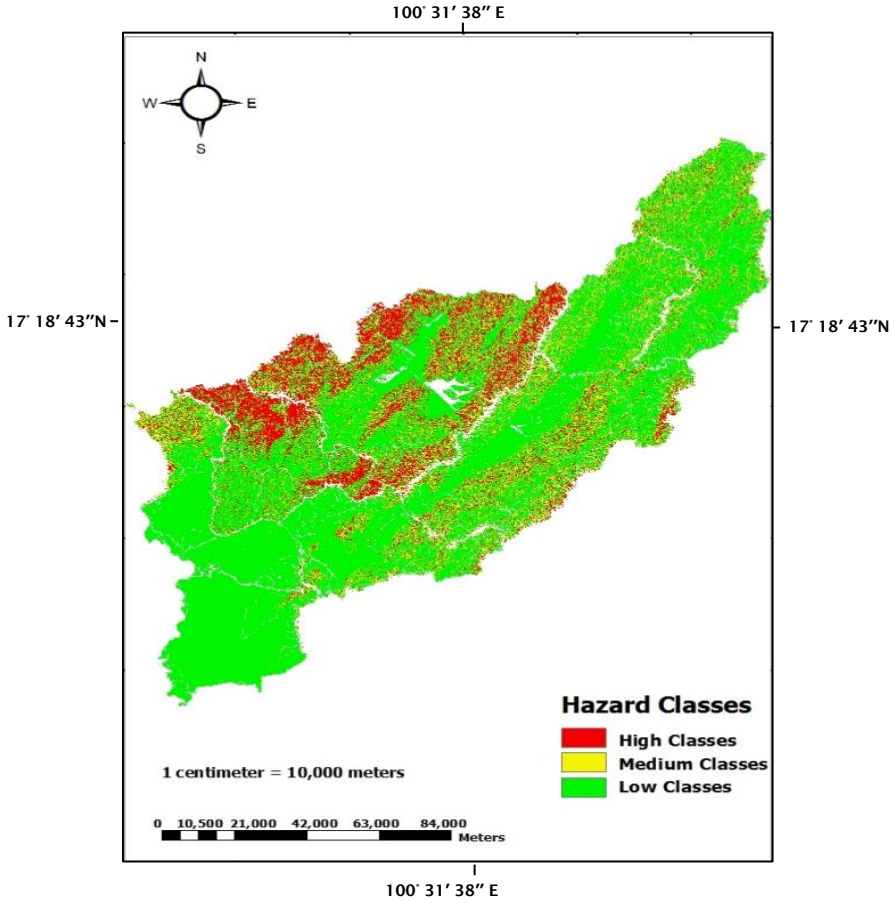

Figure 5.59 The landslide hazard mapping scenario B2 by SDSM

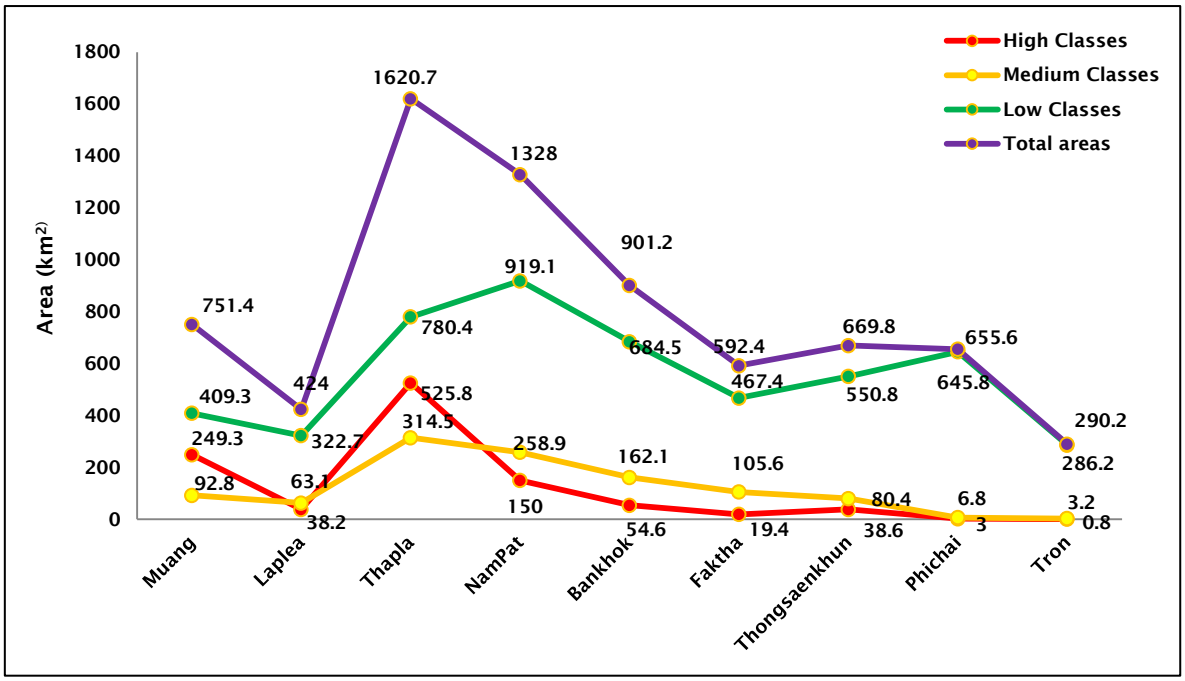

Figure 5.60 The landslide hazard mapping areas (km²) emission scenario A2 by SDSM

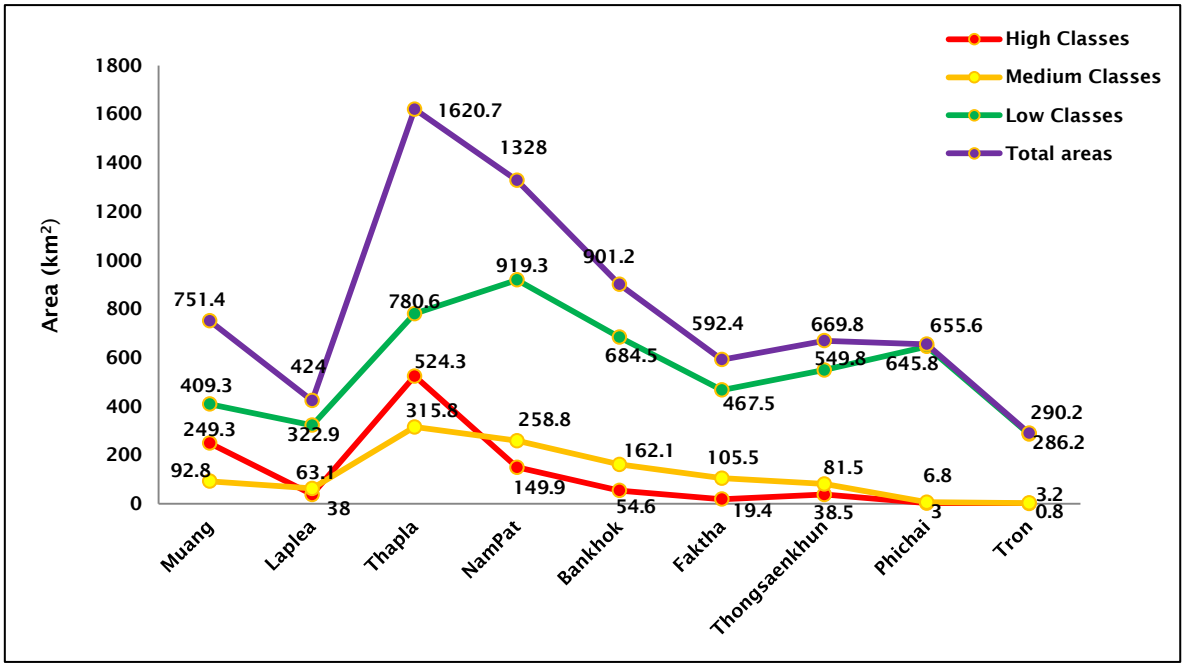

Figure 5.61 The landslide hazard mapping areas (km²) emission scenario B2 by SDSM

Then, the landslide hazard mappings by START (Fig 5.62 and Fig 5.63) are compared with the landslide hazard mappings of SDSM in both scenario A2 and B2. As a result, three hazard class areas (km²) are high, medium and low in each district and also total area of all districts in Uttaradit province as given in Fig 5.64

and Fig 5.65. These three levels of hazard classes are nearly the same direction in scenario A2 and B2.

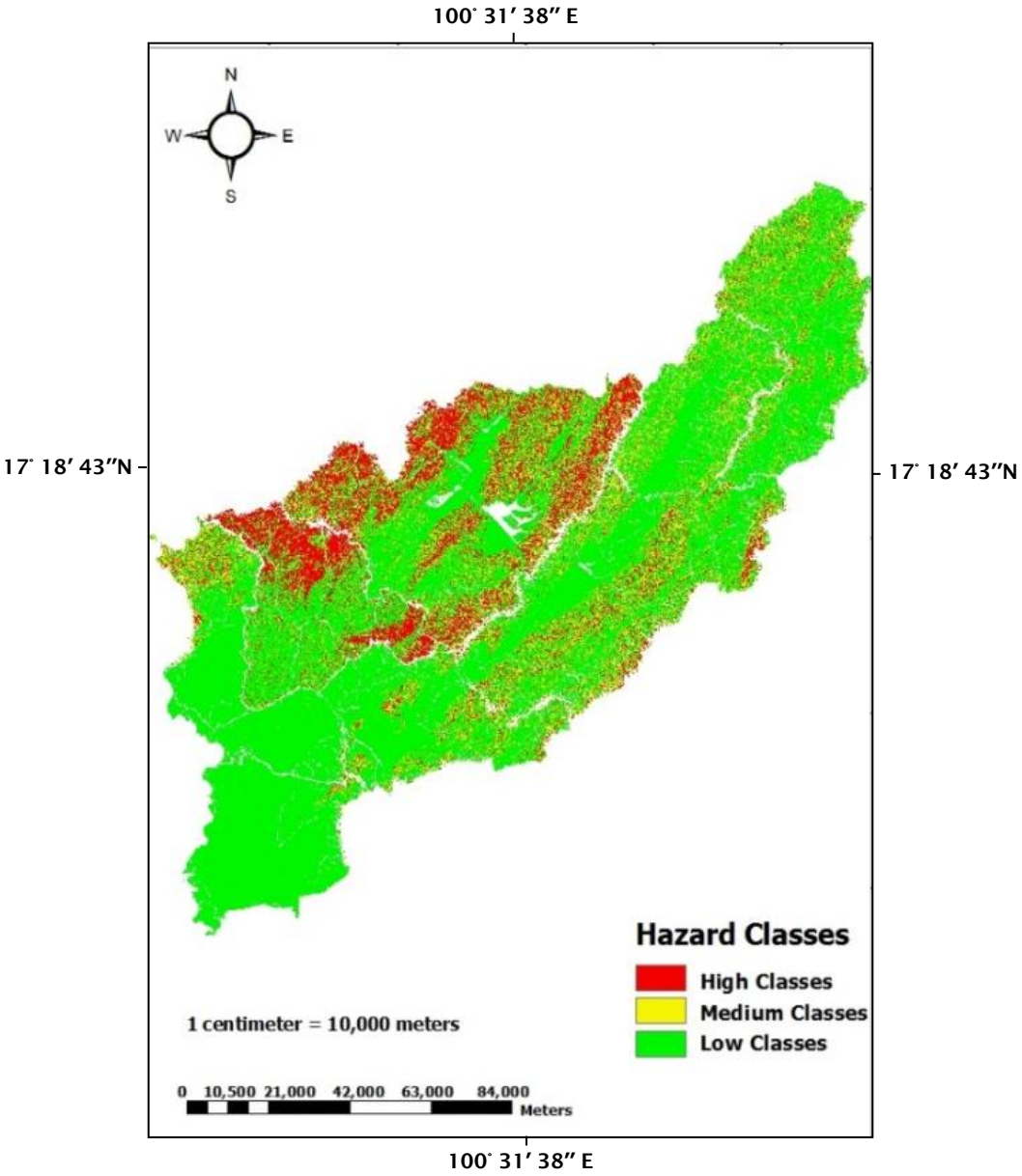

Figure 5.62 The landslide hazard mapping scenario A2 by START

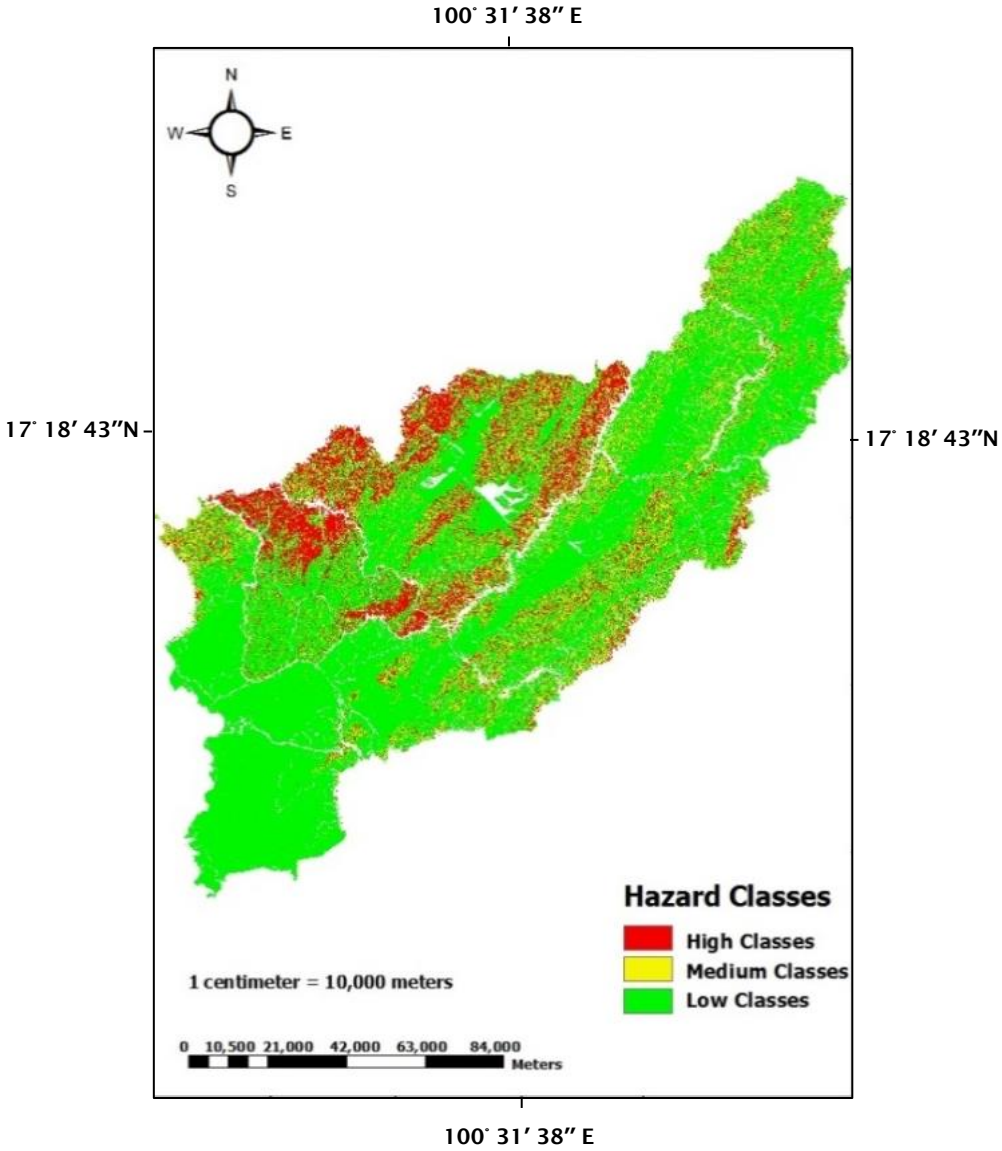

Figure 5.63 The landslide hazard mapping scenario B2 by START

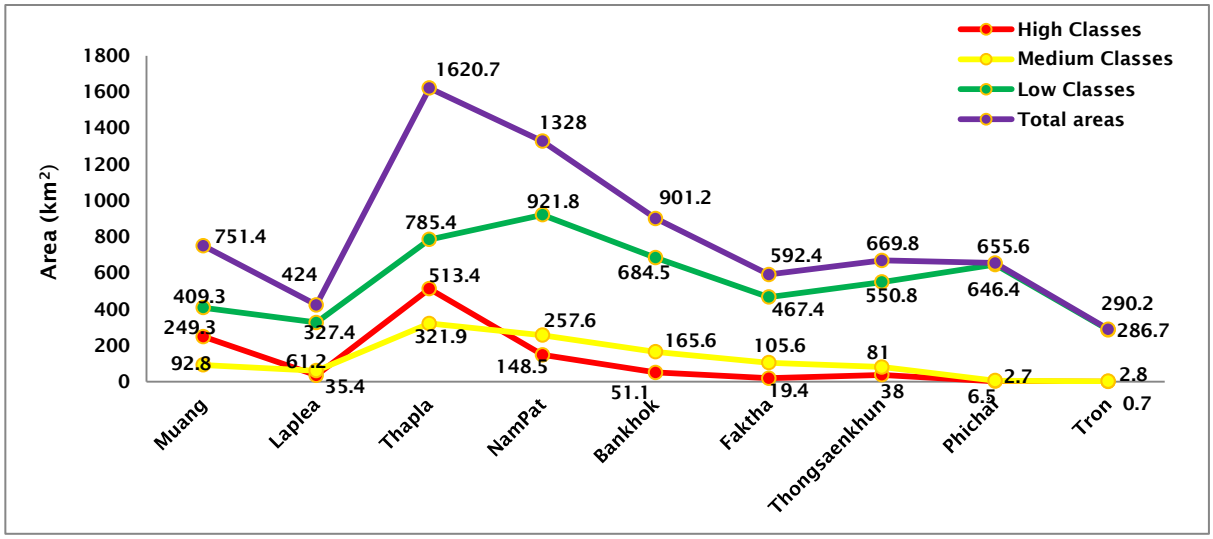

Figure 5.64 The landslide hazard mapping areas (km^2) emission scenario A2 by START

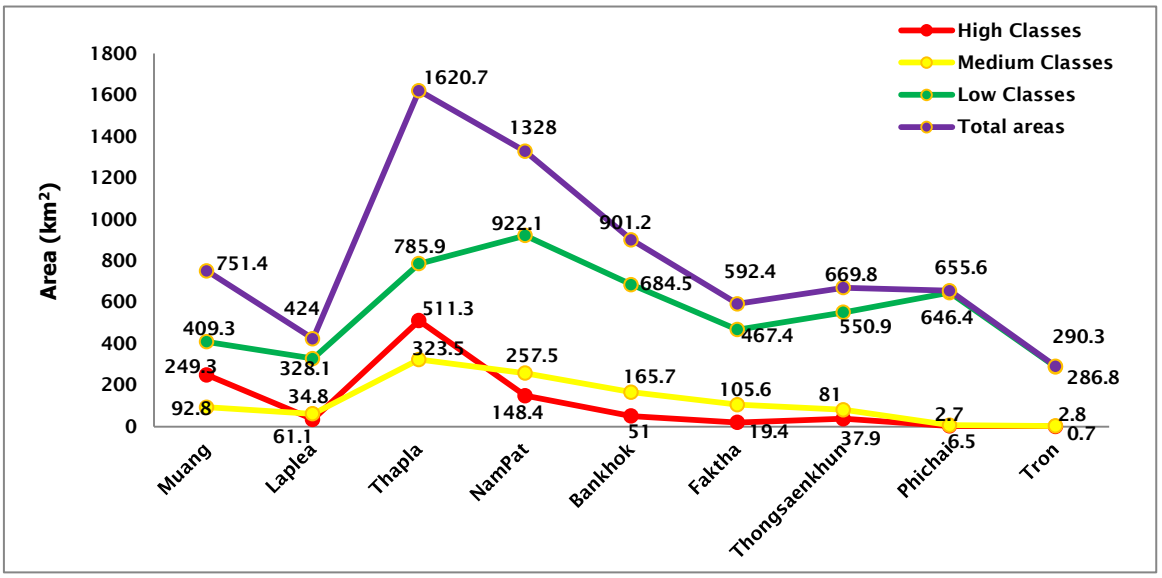

Figure 5.65 The landslide hazard mapping areas (km²) emission scenario B2 by START

5.2.4 The comparison between zonation of landslide risk under the present-day conditions and future simulation scenario A2 and B2

The pervious result has shown that the zonation of landslide risk (km²) is calculated by adding all areas of high and medium classes and 19.85% of low class areas. The average annual rainfall in all nine provinces is presented: 1,213.3 mm of present-day conditions (Section 3.8.1, Chaptor3), 1,792.7 mm of SDSMA2 and 1,736.7 mm of SDSMB2 (Table 5.14), 1,570.4 mm of STARTA2 and 1,545.4 mm of STARTB2 (Table 5.15) respectively. For the future (2013-2099) the annual rainfall values in the future simulation are higher than under present-day conditions, which are calculated in mm/24 hours unit in every district in Uttaradit province. Therefore, in both SDSM and START, the annual rainfall will be increased to approximately 300-500 mm covering the northern and north-eastern part of Thailand, while the IPCC (2012) also presents that the annual precipitation will be increased to approximately 100-300 mm over the northern part of the hemisphere that covers Thailand.

The comparison between the zonation of landslide risk (km²), by adding all areas of high and medium classes and 19.85% of low classes and rainfall values in the future simulation scenario A2 and B2 is clearly higher than under present-day conditions in six districts: Muang, Laplea, Thapla, Nampat, Faktha, Thongsaenkhun, while the zonation of landslide risk is nearly the same in Bankhok districts between under the present-day conditions and in the future

simulation (Table 5.16). The relationship between the three hazard classes and three slope gradients were presented for each district. The zonation of landslide risk was negligible in both Phichai and Tron, due to the hilly terrain: steep slope and low slope areas, being less than 11% in all district areas. Therefore, the zonation of landslide risk in both Phichai and Tron was not considered in this study. The zonation of landslide risk presented in all areas of high and medium classes and 19.85% of low class areas and also classified in steep slope, low slope and flat areas in seven districts: Muang, Thapla, Laplea, Nampat, Thongsaenkhun, Faktha and Bankhok as follows:

rainfall value (mm/24 hours) / The zonation of landslide risk (km^2)		Muang	Laplea	Thapla	Nampat	Thongsaen khun	Bankhok	Faktha
Present-day condition	Rainfall values	73.7	73.7	65.5-69.6	69.6	69.6	69.6	69.6
	Landslide risk	423.3	151.7	934.1	585.2	226.6	352.5	215.8
A2 (SDSM)	Rainfall values	140.9	140.9	95.8-110.8	110.8	110.8-125.9	95.8	95.8
	Landslide risk	423.3	165.2	995.2	591.4	228.2	352.6	217.8
B2 (SDSM)	Rainfall values	139.6	139.6	94.7-109.7	109.7	109.7-124.6	94.7	94.7
	Landslide risk	423.3	165.2	995.0	591.2	229.1	352.6	217.7
A2 (START)	Rainfall values	116.9	116.9	96.1	96.1	96.1-106.5	85.7	85.7-96.1
	Landslide risk	423.3	161.6	991.2	589.1	228.3	352.6	217.8
B2 (START)	Rainfall values	115.4	115.4	94.8	94.8	94.8-105.2	84.6	84.6-94.8
	Landslide risk	423.3	161.0	990.8	588.9	228.2	352.6	217.8

Table 5.16 The rainfall values and the zonation of landslide risk both the present-day conditions and in the future simulation

The zonation of landslide risk (km^2) is presented nearly the same in four simulations: SDSMA2, SDSMB2, STARTA2 and STARTB2. Therefore, only the zonation of landslide risk in the future simulation (SDSMA2) is compared with the present-day conditions, showing by slope gradient areas: steep slopes, low slopes and flats and percentages. Steep slope, low slope and flat areas are calculated by adding 100% of high and medium class and 19.85% of low class areas in each district as follows:

a) Muang district

In Muang district, the zonation of landslide risk (km^2) is the highest in Uttaradit province. The highest rainfall value occurs in both Muang district as 140.9 mm/24 hours in the future simulation scenario A2 (Table 5.16).The increase in high class (failure regions) areas is clearly shown on the map (Fig 5.66), but the failure region in the future simulation is higher than under the present-day conditions. The 35.8 km^2 of steep slope areas are the same between present-day conditions and future simulation, while both the increase of low slope and flat areas in high classes presented: 149.3 km^2 and 64.2 km^2 (Table 5.4 and Table 5.17). First the high classes cover all areas of steep slopes (41.7 km^2) (Fig 5.5), next it will cover low slope and flat areas respectively.

In Muang district, the zonation of landslide risk presented in a map (Fig 5.6). Steep slope, low slope and flat areas were calculated by adding 100% of high & medium classes and 19.85% of low class areas (zonation of landslide risk), covered approximately 36.5 km^2 of steep slopes (by adding of high (35.8 km^2), medium (0.3 km^2) and low (0.4 km^2) classes), 222.7 km^2 of low slopes (by adding of high (149.3 km^2), medium (19.3 km^2) and low (35 km^2) classes) and 183.2 km^2 of flats (by adding of high (64.2 km^2), medium (73.2 km^2) and low (45.8 km^2) classes (i.e. the zonation of landslide risk in the future: 36.5+222.7+183.2 = 442.4 km^2) as shown in Table 5.17.

Finally, the zonation of landslide risk in the future will cover 36.5 km^2 of steep slopes, 222.7 km^2 of low slopes and 183.2 km^2 of flat areas i.e. the same as present-day conditions. On the other hand, low slope areas will increase from 124 km^2 to 149.3 km^2 and flat areas will increase from 9.4 km^2 to 64.2 km^2 in high hazard classes: failure regions, while low slope and flat areas decrease in medium classes (Table 5.4 and Table 5.17).

Muang district	Hazard classes											
	High				Medium				Low			
	Slope gradient areas (km^2)				Slope gradient areas (km^2)				Slope gradient areas (km^2)			
	steep slopes	low slopes	flats	total	Steep slopes	low slopes	flats	total	Steep slopes	low slopes	flats	total
	35.8	149.3	64.2	249.3	0.3	19.3	73.2	92.8	0.4	35	373.8	409.2
	14.4%	59.9%	25.8%	100%	0.30%	20.8%	78.9%	100%	0.10%	8.60%	91.3%	100%

Table 5.17 The relationship between the three hazard classes and three slope gradients, including the zonation of landslide risk (high, medium and low classes) in the future simulation in Muang district

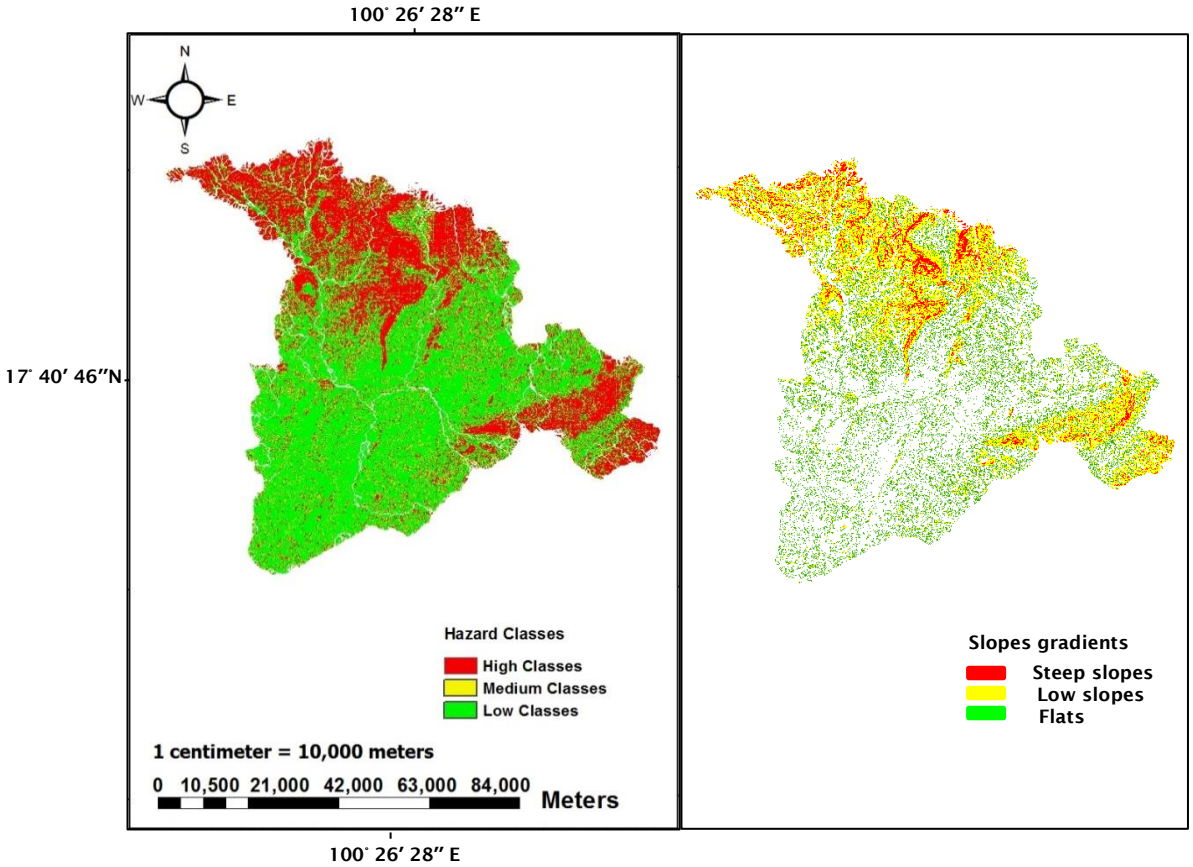

Figure 5.66 The comparison between steep slope, low slope and flat areas showing in the zonation of landslide risk (right hand side) and landslide hazard mapping (left hand side) in future simulation in Muang district

b) Thapla district

In Thapla district, the rainfall values are 95.8 – 110.8 mm/24 hours in the future simulation scenario A2 (Table 5.16), which higher than present-day conditions.

In Thapla district, the increasing of high class (failure regions) areas are obviously shown on the map (Fig 5.67). The high classes covered 169.4 km^2 of steep slope and 351.2 km^2 of low slope areas, both areas will increase in the future as shown in a map. On the other hand, the medium classes, which covered 3.8 km^2 of steep slope, 252 km^2 of low slope and 58.7 km^2 of flat areas decrease and all slope gradient areas (steep slopes, low slopes and flats) of low classes also decrease when compared with present-day conditions. Eventually, the rainfall values will increase in this district. The steep slope and low slope areas in the high classes will increase, while steep slope and low slope areas in the medium and low classes will decrease. It means that the high class areas will increase, when the medium and low class areas decrease. The increasing rainfall lead to the situation of instability (medium classes), becoming failure regions (high classes) and the

situation of safety areas (low classes), becoming instability (medium classes). Finally, in Thapla district, the zonation of landslide risk in the future will cover 178.4 km^2 of steep slope areas (by adding of high (169.4 km^2), medium (3.8 km^2) and low (5.2 km^2) classes), while 178.4 km^2 of steep slopes (by adding of high (163.8 km^2), medium (9.2 km^2) and low (5.4 km^2) classes) present under present-day conditions (Table 5.5). The low slope areas will increase from 717.5 km^2 of low slopes (by adding of high (256.6 km^2), medium (296.3 km^2) and low (164.6 km^2) classes) to 752.9 km^2 (by adding of high (351.2 km^2), medium (252 km^2) and low (149.7 km^2). The flat areas will increase from 38.2 km^2 (by adding both high (3.4 km^2), medium (34.8 km^2) to 63.9 km^2 (by adding both high (5.2 km^2), medium (58.7 km^2) (i.e. the zonation of landslide risk in the future: 178.4+752.9+63.9 = 995.2 km^2) as given in Table 5.18. All slope gradients of zonation risk in future simulation are higher than at the present-day conditions.

	Hazard classes											
	High				Medium				Low			
	Slope gradient areas (km^2)				Slope gradient areas (km^2)				Slope gradient areas (km^2)			
Thapla district	steep slopes	low slopes	flats	total	steep slopes	low slopes	flats	total	steep slopes	low slopes	flats	total
	169.4	351.2	5.2	525.8	3.8	252	58.7	314.5	5.2	193.3	581.9	780.4
	32.2%	66.8%	1.0%	100%	1.2%	80.1%	18.7%	100%	0.7%	24.8%	74.6%	100%

Table 5.18 The relationship between the three hazard classes and three slope gradients, including the zonation of landslide risk (high, medium and low classes) in the future simulation in Thapla district

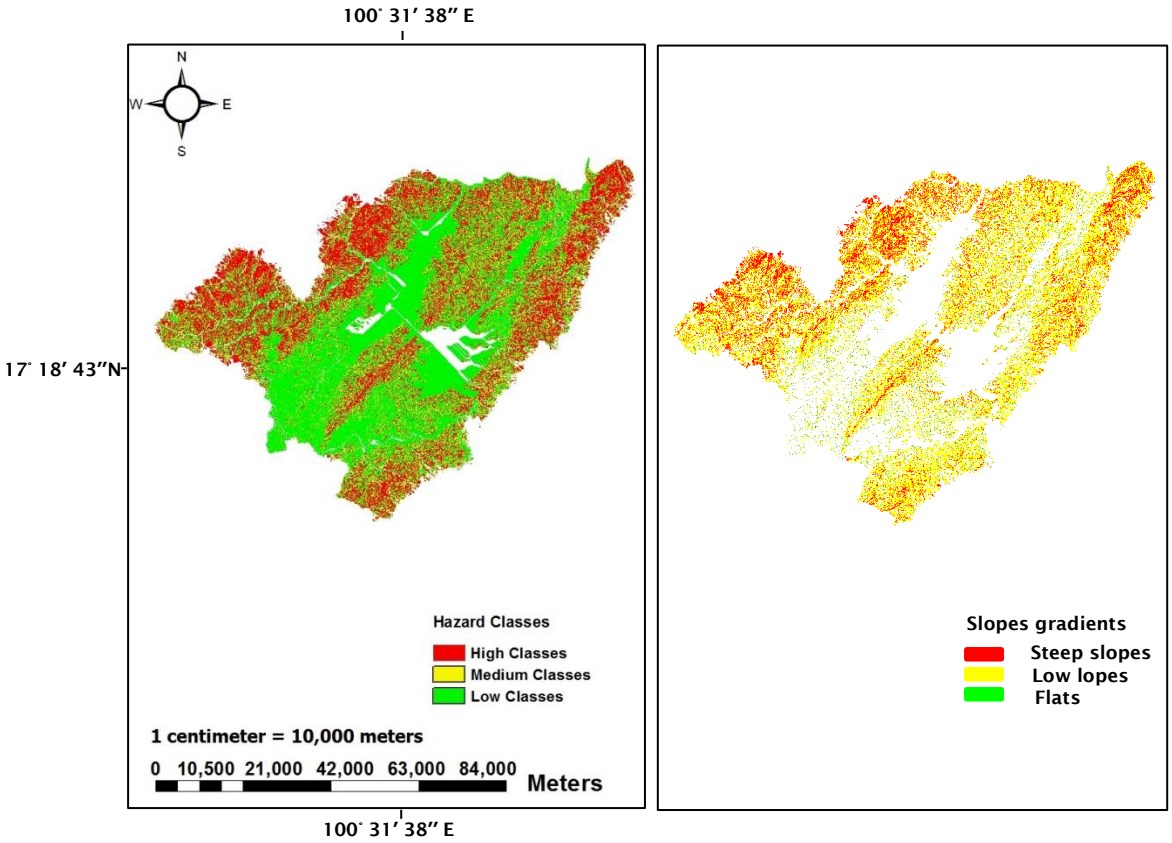

Figure 5.67 The comparison between steep slope, low slope and flat areas showing in the zonation of landslide risk (right hand side) and landslide hazard mapping (left hand side) in future simulation in Thapla district

c) Laplea district

The highest rainfall value occurs in Laplea districts as 140.9 mm/24 hours in the future simulation scenario A2 (Table 5.16). In Table 5.19, approximately 23.6 km^2 of steep slope and 14.4 km^2 of low slope areas showed in the high classes, while 13 km^2 of steep slope and 47.8 km^2 of low slope areas are also found in the medium classes. The steep slope and low slope areas in the high classes will increase in the future, while in the medium classes, steep slope areas will decrease and low slope areas increase as given in Fig 5.68. The increasing of rainfall leads to both steep slope and low slope area increase in high classes, then steep slope areas decrease in the medium classes. But low slope areas increase in the medium classes because all slope gradients (steep slopes, low slopes and flats) decrease in the low classes.

In Laplea district, the increasing rainfall values from 73.7 to 140.9 mm/24 hours (Table 5.16) leads to the situation of instability (medium classes) becoming failure regions (high classes) in steep slope areas, while some parts of flat areas in low classes will become destabilised in medium classes. In Laplea district, the zonation of landslide risk in the future will increase from 38.8 km^2 (by adding of high (19.2 km^2), medium (15.9 km^2) and low (3.7 km^2)) to 38.7 km^2 of steep slope areas (by adding of high (23.6 km^2), medium (13 km^2) and low (2.1 km^2)) and low slope areas will increase from 113.2 km^2 (by adding of high (9.3 km^2), medium (40.6 km^2) and low (63.3 km^2)) to 124.1 km^2 (by adding of high (14.4 km^2), medium (47.8 km^2) and low (61.9 km^2)). The flat areas will increase from 1.7 km^2 (by adding of high (0.1 km^2), medium (1.6 km^2) to 2.4 km^2 (by adding of high (0.2 km^2), medium (2.2 km^2) respectively (i.e. the zonation of landslide risk in the future: 38.7+124.1+2.4 = 165.2 km^2) (Table 5.6 and Table 5.19).

	Hazard classes											
	High				Medium				Low			
	Slope gradient areas (km^2)				Slope gradient areas (km^2)				Slope gradient areas (km^2)			
Laplea district	steep slopes	low slopes	flats	total	steep slope	low slopes	flats	total	steep slopes	low slopes	flats	total
	23.6	14.4	0.2	38.2	13	47.8	2.2	63.1	2.1	72.4	248.2	322.7
	61.8%	37.7%	0.5%	100%	20.6%	75.8%	3.5%	100%	0.7%	22.4%	76.9%	100%

Table 5.19 The relationship between the three hazard classes and three slope gradients, including the zonation of landslide risk (high, medium and low classes) in the future simulation in Laplea district

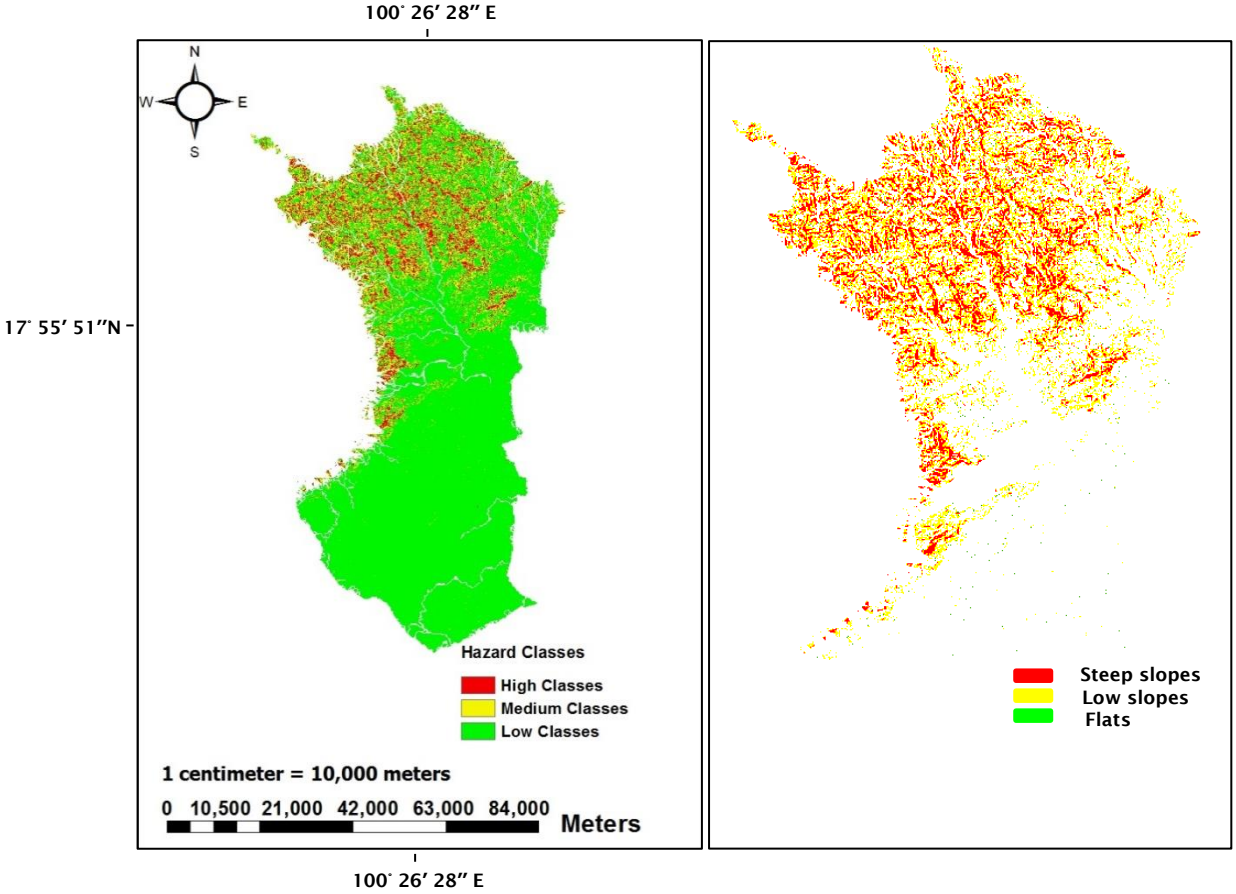

Figure 5.68 The comparison between steep slope, low slope and flat areas showing in the zonation of landslide risk (right hand side) and landslide hazard mapping (left hand side) in future simulation in Laplea district

Finally, as for Muang, Laplea and Thapla districts, 4.006E-6, 2.918E-5 and 6.081E-6 of the permeability values are presented, and 1E-6 and 1E-5 are classified in an impervious soil group (Pack et al., 1948). This is linked with the sensitivity of permeability output of 1E-6, which is high in the high hazard class areas. The highest rainfall value occurs in both Muang and Laplea districts as 140.9 mm/24 hours in scenario A2. In Thapla district, the rainfall values are 95.8 – 110.8 mm/24 hours in scenario A2 (Table 5.16). The increase of rainfall values is sensitive, with permeability values leading to an increase of steep slope and low slope areas in the high classes.

D) Nampat and Thongsaenkhun districts

110.8 –125.9 mm/24 hours of rainfall values present in Thongsaenkhun district, while 110.8 mm/24 hours of rainfall values show in Nampat districts. Then,

Nampat and Thongsaenkhun districts present nearly the same in zonation of landslide risk as shown in a map (Fig 5.69 and Fig 5.70). The increased high hazard classes (km^2) are less, compared with present-day conditions. The comparison between Table 5.7 and Table 5.20, the 108.5km^2 of steep slope and 40.9 km^2 of low slope areas will increase in the high classes and 66.9 km^2 of steep slope and 182.7 km^2 of low slope areas will decrease in medium classes in the future, while all slope gradient areas (steep slopes, low slopes and flats) of low classes will decrease in Nampat district. All steep slope and low slope areas in high classes will increase in the future, while all steep slope and low slope areas will also decrease in medium classes in Thongsaenkhun district.

Finally, increased rainfall in both districts leads to an increase of failure regions (high classes), while instability (medium classes) and safety areas (low classes) decrease. In Nampat district, the increasing of zonation risk in the future is small, while the 197 km^2 to 197 km^2 of steep slope areas i.e. nearly the same as present-day conditions. Approximately 197 km^2 of steep slope areas (by adding areas of high (108.6 km^2), medium (66.9 km^2) and low (21.5 km^2) in the future and 197 km^2 of steep slopes (by adding areas of high (107.1 km^2), medium (67.5 km^2) and low (22.4 km^2) under present-day conditions are presented as shown in Table 5.7 and Table 5.20.

On the other hand, low slope areas will increase from 379.2 km^2 (by adding of high (38.4 km^2), medium (179.3 km^2) and low (161.5 km^2) to 384.5 km^2 (by adding of high (40.9 km^2), medium (182.7 km^2) and low (160.9 km^2). Flat areas will increase from 9.0 km^2 (by adding of high (0.5 km^2) and medium (8.5 km^2) to 9.9 km^2 (by adding of high (0.6 km^2) and medium (9.3 km^2) respectively (i.e. the zonation of landslide risk in the future: 197+384.5+9.9 = 591.4 km^2) (Table 5.7 and Table 5.20).

In Thongsaenkhun district, the zonation of landslide risk in the future, will cover from 50.9 km^2 of steep slopes (by adding of high (26.5 km^2), medium (19.0 km^2) and low (5.4 km^2), while 50.9 km^2 of steep slope areas (by adding of high (27.1 km^2), medium (18.6 km^2) and low (5.2 km^2) i.e. nearly the same as present-day conditions, but low slope areas will increase from 172.6 km^2 of low slopes (by adding of high (10.2 km^2), medium (58.0 km^2) and low (104.4 km^2) to 173.8 km^2 of low slopes (by adding of high (11.3 km^2), medium (58.4 km^2) and low (104.1 km^2). The flat areas will increase from 3.1 km^2 (by adding of high (0.1 km^2), medium (3.0 km^2) to 3.5 km^2 (by adding of high (0.2 km^2), medium (3.3 km^2) respectively

(i.e. the zonation of landslide risk in the future: 50.9+173.8+3.5 = 228.2 km^2) (Table 5.8 and Table 5.21).

Nampat district	Hazard classes											
	High				Medium				Low			
	Slope gradient areas (km^2)				Slope gradient areas (km^2)				Slope gradient areas (km^2)			
	steep slopes	low slopes	flats	total	steep slopes	low slopes	flats	total	steep slopes	low slopes	flats	total
	108.6	40.9	0.6	150	66.9	182.7	9.3	258.9	21.5	434.7	462.9	919.1
	72.3%	27.3%	0.4%	100%	25.8%	70.6%	3.6%	100%	2.3%	47.3%	50.4%	100%

Table 5.20 The relationship between the three hazard classes and three slope gradients, including the zonation of landslide risk (high, medium and low classes) in the future simulation in Nampat district

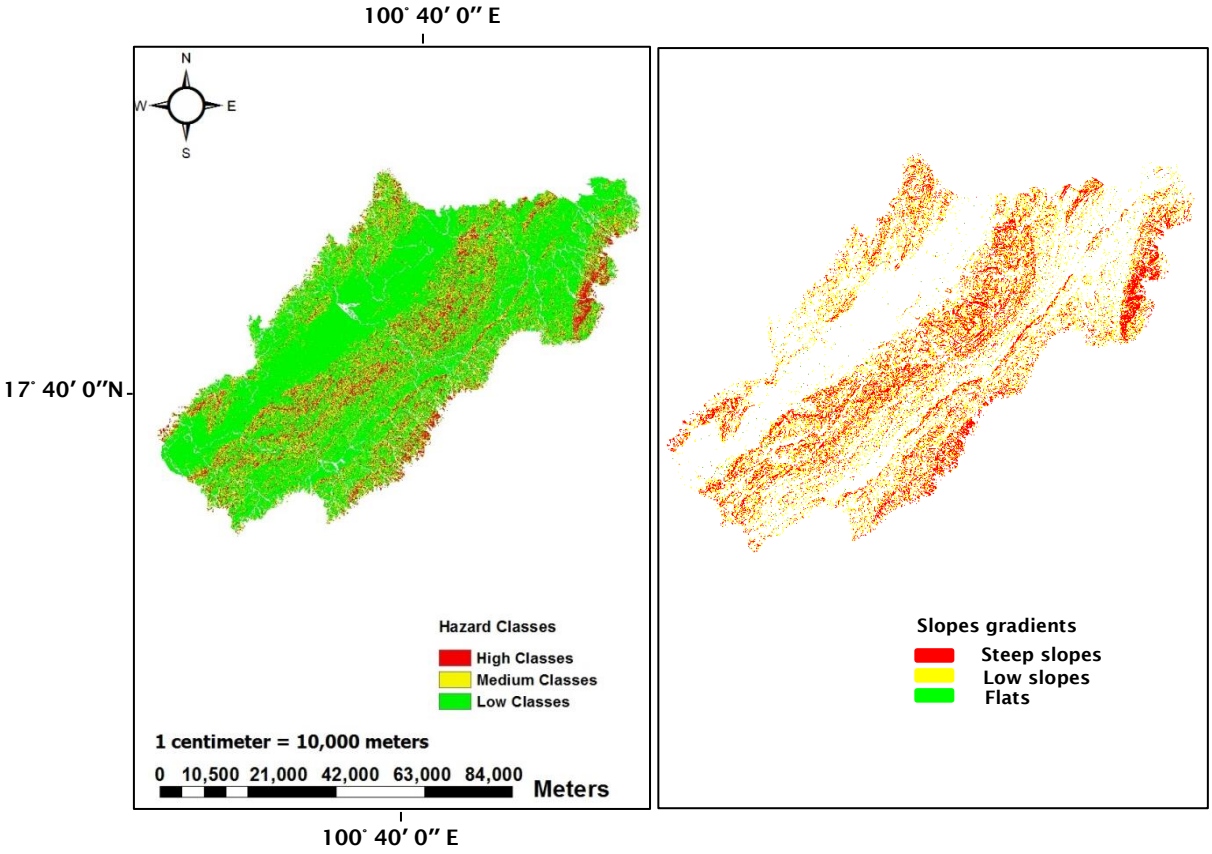

Figure 5.69 The comparison between steep slope, low slope and flat areas showing in the zonation of landslide risk (right hand side) and landslide hazard mapping (left hand side) in future simulation in Nampat district

Thong saenkhun district	Hazard classes											
	High				Medium				Low			
	Slope gradient areas (km^2)				Slope gradient areas (km^2)				Slope gradient areas (km^2)			
	steep slopes	low slopes	flats	total	steep slopes	low slopes	flats	total	steep slopes	low slopes	flats	total
	27.1	11.3	0.2	38.6	18.6	58.4	3.3	80.3	5.2	181.8	363.9	550.8
	70.2%	29.3%	0.5%	100%	23.2%	72.7%	4.1%	100%	0.9%	33.0%	66.1%	100%

Table 5.21 The relationship between the three hazard classes and three slope gradients, including the zonation of landslide risk (high, medium and low classes) in the future simulation in Thongsaenkhun district

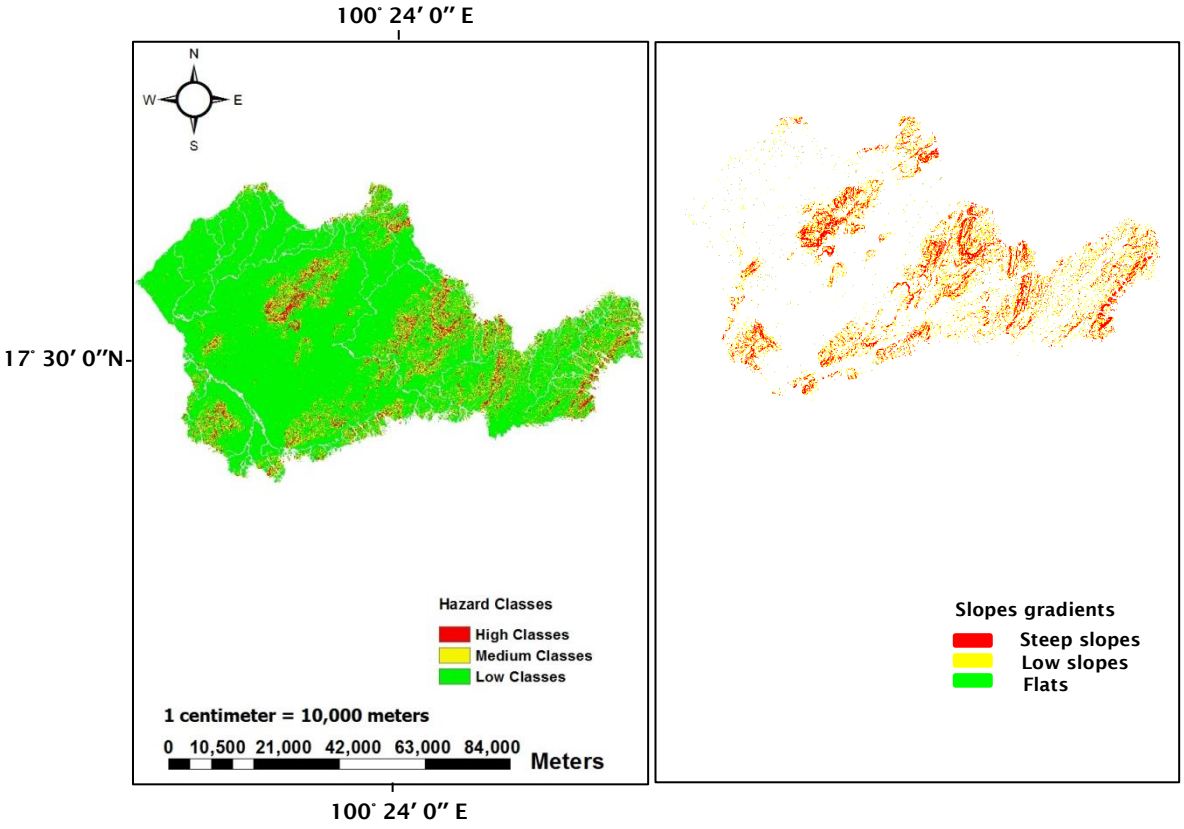

Figure 5.70 The comparison between steep slope, low slope and flat areas showing in the zonation of landslide risk (right hand side) and landslide hazard mapping (left hand side) in future simulation in Thongsaenkhun district

In Nampat and Thongsaenkhun districts, the increased zonation of landslide risk (km^2) is less, compared with present-day conditions. The characteristic of the soil is sand (TP5) and 3.415E-4 of permeability values, which affect both high and medium class areas (Section 4.2.3, Chapter 4), are described in Nampat and

Thongsaenkhun districts. As a result, the permeability values affect the zonation of landslide risk in these two districts.

e) Bankhok district

The increase of rainfall values, both Bankhok: 95.8 mm/24 hours by scenario A2 is lower than other districts. The high class areas, which covered 41.9 km^2 of steep slope and 12.6 km^2 of low slope areas will increase in the future, while the medium classes, which covered 50.3 km^2 of steep slope and 107.5 km^2 of low slope areas will decrease. All slope gradients (steep slopes, low slopes and flats) are the same in the low classes (Table 5.9 and Table 5.22).

Eventually, the increased rainfall values will be low in this district. The steep slope and low slope areas in the high classes will increase, while steep slope and low slope areas in the medium classes will decrease. The increasing rainfall will lead to the situation of instability (medium classes) becoming failure regions (high classes), while safety areas are the same as present-day conditions. Therefore, the zonation of landslide risk is shown in a map (Fig 5.71) and is nearly the same in present-day conditions: 114.2 km^2 of steep slope areas (by adding of high (41.9 km^2), medium (50.3 km^2), low (22.0 km^2)), 234 km^2 of low slope areas (by adding of high (12.6 km^2), medium (107.5 km^2), low (113.9 km^2)) and 4.4 km^2 flat areas (by adding of high (0.1 km^2), medium (4.3 km^2) respectively (Table 5.22) (i.e. the zonation of landslide risk in the future: 114.2+234+4.4 = 352.6 km^2).

Bankhok district	Hazard classes											
	High				Medium				Low			
	Slope gradient areas (km^2)				Slope gradient areas (km^2)				Slope gradient areas (km^2)			
	steep slopes	low slopes	flats	total	steep slopes	low slopes	flats	total	steep slopes	low slopes	flats	total
	41.9	12.6	0.1	54.6	50.3	107.5	4.3	162.1	22	362.4	300.1	684.5
	76.7%	23.1%	0.2%	100%	31.0%	66.3%	2.7%	100%	3.2%	52.9%	43.8%	100%

Table 5.22 The relationship between the three hazard classes and three slope gradients, including the zonation of landslide risk (high, medium and low classes) in the future simulation in Bankhok district

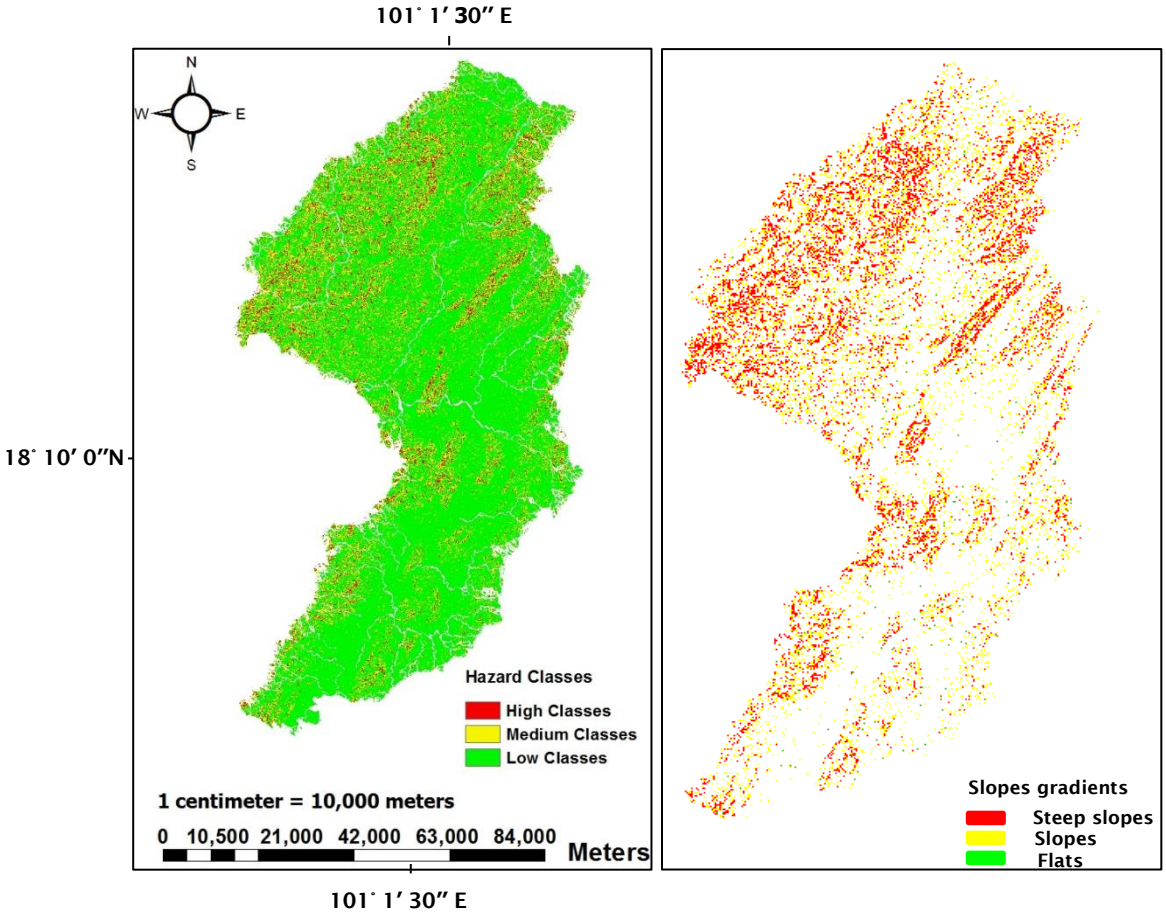

Figure 5.71 The comparison between steep slope and slope areas showing in the zonation of landslide risk (right hand side) and landslide hazard mapping (left hand side) in future simulation in Bankhok district

f) Faktha district

The increase of rainfall values, in Faktha districts: 95.8 mm/24 hours by scenario A2 is the same in Bankhok district. The steep slope areas will increase from 17.5 km^2 to 18 km^2, while the low slope areas decrease from 1.9 km^2 to 1.4 km^2 in the high class areas, flats are not found in the high classes (Table 5.10 and Table 5.23). The steep slope areas increase, but low slope areas decrease because increased rainfall in the future lead to an increase of steep slope areas. On the other hand, all slope gradient areas in the low classes will decrease. The zonation of landslide risk (Fig 5.72) in the future covers steep slope, low slope and flat areas: 115.6 km^2 of steep slopes (by adding of high (18 km^2), medium (62 km^2) and low (35.6 km^2), 101.9 km^2 of low slopes (by adding of high (1.4 km^2), medium (43.3 km^2) and low (57.2 km^2) and only 0.3 km^2 of flats (by adding of high (0 km^2), medium (0.3 km^2) respectively (Table 5.23), while the zonation of landslide risk in present-day

conditions covers steep slope, low slope and flat areas: 115.6 km^2, 43.2 km^2 and 0.2 km^2 respectively (Table 5.10) (i.e. the zonation of landslide risk in the future: 115.6+101.9+0.3 = 217.8 km^2).

Faktha district	Hazard classes											
	High				Medium				Low			
	Slope gradient areas (km^2)				Slope gradient areas (km^2)				Slope gradient areas (km^2)			
	steep slopes	low slopes	flats	total	steep slopes	low slopes	flats	total	steep slopes	low slopes	flats	total
	18	1.4	0	19.4	62	43.3	0.3	105.6	35.6	275.5	156.4	467.5
	92.8%	7.2%	0%	100%	58.7%	41.0%	0.3%	100%	7.6%	58.9%	33.5%	100%

Table 5.23 The relationship between the three hazard classes and three slope gradients, including the zonation of landslide risk (high, medium and low classes) in the future simulation in Faktha district

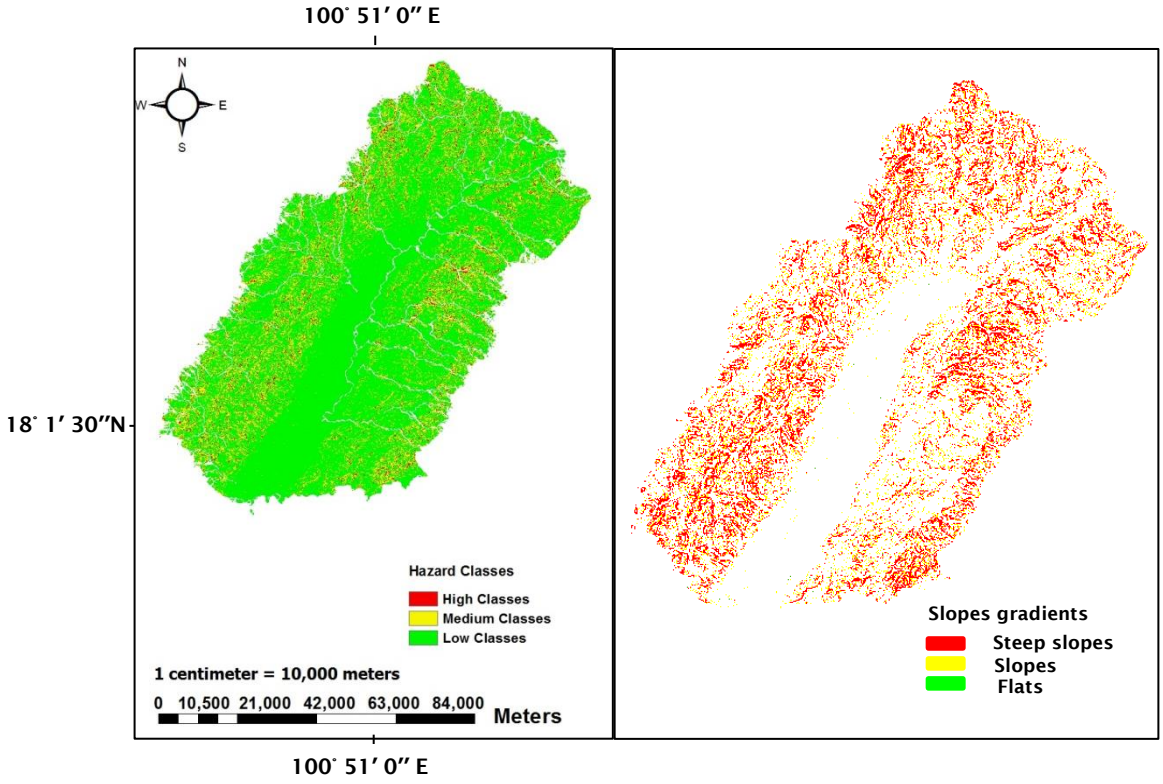

Figure 5.72 The comparison between steep slope and slope areas showing in the zonation of landslide risk (right hand side) and landslide hazard mapping (left hand side) in future simulation in Faktha district

Finally, the increase of rainfall values, both Bankhok and Faktha districts: 95.8 mm/24 hours by scenario A2 are lower than other districts (Table 5.14). Although the permeability values are 1.175-E06 in Faktha district and 8.187-E05 in Bankhok district, including rainfall value rates, the increase of the zonation of risk (km^2) is also small. Clays and both teak and rubber plantations present in two districts: Bankhok and Faktha, so that the high value of dimensionless cohesion is obtained in both districts. As a result, an increase in the zonation risk (km^2) is small in Bankhok and Faktha districts, due to the dimensionless cohesion value.

f) Tron and Phichai districts

The increase of rainfall value will present in both Tron and Phichai districts: 140.9 and 110.8 – 125.9 mm/24 hours in scenario A2. In Tron district, the steep slope areas are nearly the same between under present-day conditions and future simulation, while the low slope areas increase from 0.2 km^2 to 0.5 km^2 in the high class areas, flats are not found in the high classes (Table 5.11 and Table 5.24). Similarly, the low slope areas also increase from 1.9 km^2 to 2.4 km^2 in the medium class areas, but the low slope areas decrease from 24.6 km^2 to 23.8 km^2 in the low classes. Both hazard and slope gradient map presented in Fig 5.73.

The steep slope areas are so small in this district that why the steep slope areas are the same between under present-day conditions and future simulation, while low slope areas increase because increased rainfall in the future lead to an increase of low slope areas. Although, the low slope areas will increase in the future, but it is negligible. Most of flat areas are presented in the low classes, while the steep slope and low slope areas are so small in both high (failure region) and medium (instability) classes. Therefore, the zonation risk was negligible in this district.

In Phichai district, the steep slope areas increase from 1.3 km^2 to 1.6 km^2 and the low slope also increase from 0.8 km^2 to 1.3 km^2 in the high classes, while the steep slope areas decrease from 1.2 km^2 to 1.0 km^2 and the low slope increase from 4.5 km^2 to 5.3 km^2 in the medium classes between under present-day conditions and future simulation. Both hazard and slope gradient map presented in Fig 5.74. All slope gradient areas in the low classes decrease (Table 5.12 and Table 5.25). Finally, most of flat areas are presented in the low classes, while the steep slope and low slope areas are so small in both high (failure region) and

medium (instability) classes. Therefore, the zonation risk is also negligible in this district.

Tron district	Hazard classes											
	High				Medium				Low			
	Slope gradient areas (km²)				Slope gradient areas (km²)				Slope gradient areas (km²)			
	steep slopes	low slopes	flats	total	steep slopes	low slopes	flats	total	steep slopes	low slopes	flats	total
	0.3	0.5	0	0.5	0.2	2.4	0.6	2.4	0.1	23.8	262.3	287.3
	37.5%	62.5%	0%	100%	6.3%	75.0%	18.8%	100%	0.03%	8.56%	91.40%	100%

Table 5.24 The relationship between the three hazard classes and three slope gradients, including the zonation of landslide risk (high, medium and low classes) showing by steep slope, low slope and flat areas in the future simulation in Tron district.

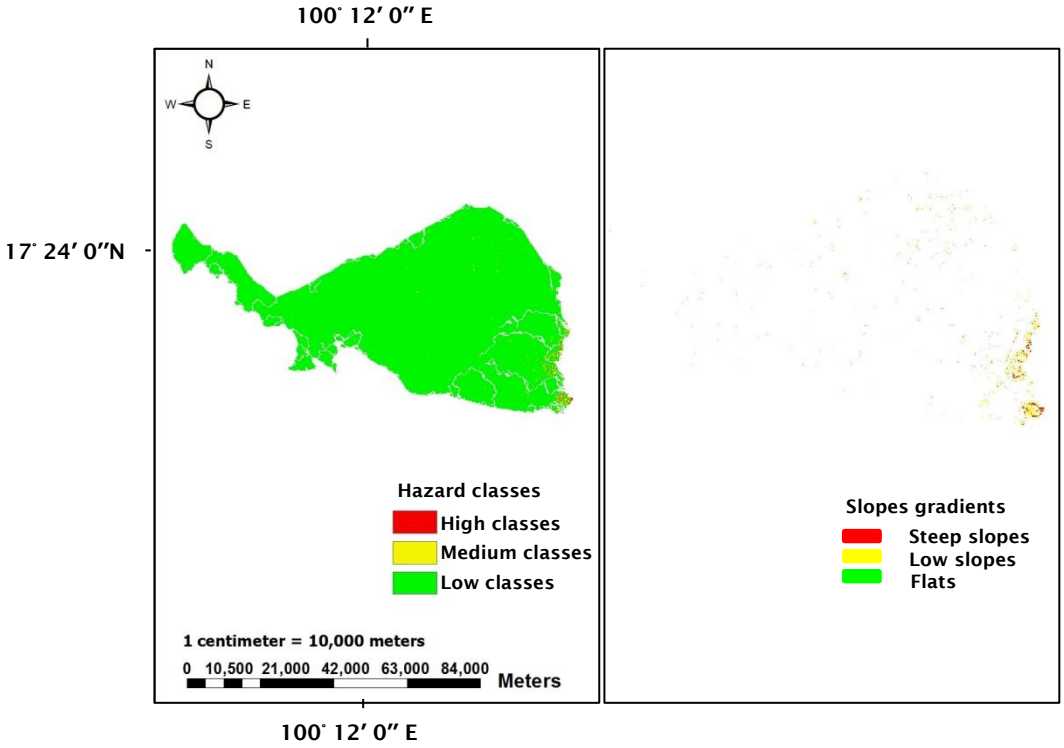

Figure 5.73 The comparison between steep slope, low slope and flat areas showing in the zonation of landslide risk (right hand side) and landslide hazard mapping (left hand side) in the future simulation in Tron district

Phichai district	Hazard classes											
	High				Medium				Low			
	Slope gradient areas (km^2)				Slope gradient areas (km^2)				Slope gradient areas (km^2)			
	steep slopes	low slopes	flats	total	steep slopes	low slopes	flats	total	steep slopes	low slopes	flats	total
	1.6	1.3	0	2.1	1.0	5.3	0.6	6.1	0.1	39.7	605.9	647.3
	55.2%	44.8%	0%	100%	14.0%	77.9%	4.1%	100%	0.1%	6.1%	93.8%	100%

Table 5.25 The relationship between the three hazard classes and three slope gradients, including the zonation of landslide risk (high, medium and low classes) showing by steep slope, low slope and flat areas in the future simulation in Phichai district.

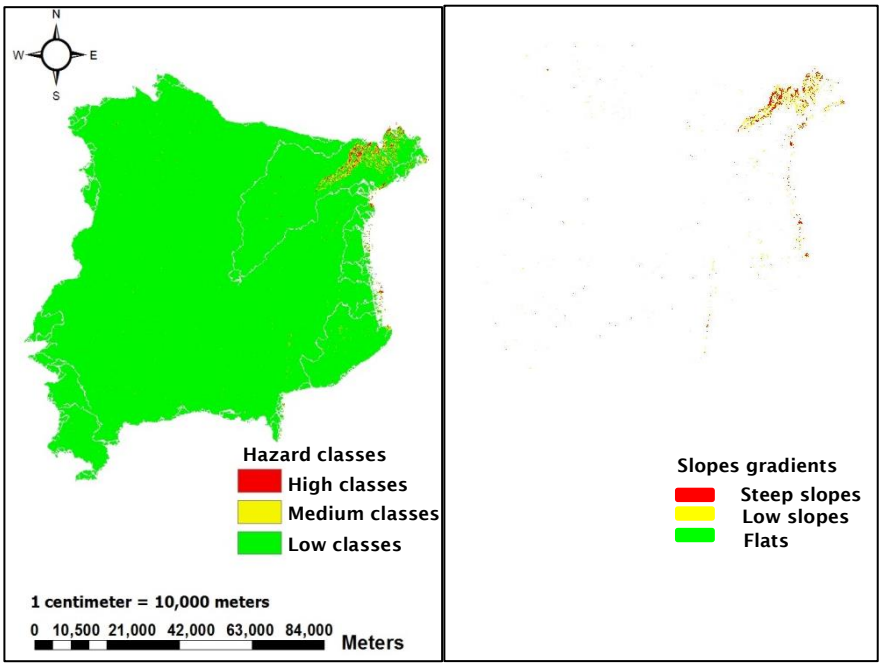

Figure 5.74 The comparison between steep slope, low slope and flat areas showing in the zonation of landslide risk (right hand side) and landslide hazard mapping (left hand side) in the future simulation in Phichai district

5.2.5 The slope gradients in zonation of landslide risk in the future

The zonation of landslide risk between present-day conditions and future simulation present in steep slope, low slope and flat areas in each district. In the future, first most of steep slope and low slope areas occur in high hazard classes, and then it will occur in medium and low classes respectively. Some parts of steep slopes and low slopes remained showing in medium and low classes. Most of flats were found in low classes. The high class areas will increase, while the medium

and low class areas decrease when rainfall increase. Therefore, the increasing rainfall lead to the situation of instability (medium classes), becoming failure regions (high classes) and the situation of safety areas (low classes), becoming instability (medium classes). Therefore, rainfall is quite important for failure in steep slope and low slope areas.

In the literature review, slope gradients affect the probability of landslide occurrences: in these results, the probability of landslide is more than 70% when slope gradients are more than 35°, while the probability of landslide is between 50% and 70% with slope gradients of 26.7° - 35°. The probability of landslide is between 30% and 50% on slope gradients of 16.7° - 26.7°. The probability of landslide is between 15% and 30% on slope gradients of 8.5° - 16.7°, while the probability of landslide impacts is between 0% and 15% on slope gradients of 0° - 8.5° (DWR, 2010).

The comparison between the zonation of landslide risk and hilly and mountainous areas in each district (by adding steep slope & low slope areas) are sorted descending from high zonation risk to low percentages as shown in Table 5.4. The zonation of landslide risk (km^2) is the highest in Muang district. The zonation of landslide risk covers all steep slope and low slope areas, and also covered some flat areas (approximately 67.3% of all flat areas). The zonation of landslide risk in Thapla district is the second. The zonation of landslide risk covered 94.9% of steep slope and low slope areas. The Thonsaenkhun and Nampat districts are under the same conditions of both soil and rainfall for analysis. The zonation of landslide risk in Thonsaenkhun and Nampat districts cover both steep slopes and low slopes: 67.8% and 63.3% respectively. The 54.3% of landslide zonation risk cover both steep slope and low slope areas in Bankhok district (Table 5.4). Laplea district is the six highest: approximately 55.5% of the zonation of landslide risk is found in both steep slope and low slope areas. The zonation of landslide risk is the smallest in Faktha district: only 36.8% of sleep slope and low slope areas (Table 5.26). Finally, the zonation of landslide risk will increase in the future in six districts: Muang, Thapla, Laplea, Nampat, Thongsaenkhun and Faktha, exception of Bankhok district. The increasing of rainfall directly affects the high hazard class areas. First the high risk covers the areas of steep slope and then it will cover low slopes and flats respectively. The flow directions is to assign flow from each grid cell, either adjacent or diagonally, in the direction of the steepest downward slope. Thus, the increase of infiltrated rainfall related to the slope

gradient, can increase the high hazard class areas. The infinite slope model is related to slope gradient length (Montgomery and Dietrich, 1994).

District / Area (km^2)	Muang	Thapla	Thong saenkhun	Nampat	Bankhok	Laplae	Faktha
Total areas of hilly and mountains in each district (by adding steep slope & low slope areas)	264.4	1048.3	336.5	934.2	649.5	297.7	592.4
Zonation risk under present-day conditions	423.3	934.1	226.6	585.2	352.5	151.7	215.8
The percentages of zonation risk in hilly and mountainous areas (present-day conditions)	100%	89.1%	67.3%	62.6%	54.3%	51%	36.4%
Zonation risk in the future simulation	423.3	995.2	228.2	591.4	352.6	165.2	217.8
The percentages of zonation risk in hilly and mountainous areas (in the future simulation)	100%	94.9%	67.8%	63.3%	54.3%	55.5%	36.8%

Table 5.26 The zonation of landslide risk is compared with the real areas of steep slope and low slope in each district and sorted descending from high zonation risk to low percentages between present-day conditions and future simulation

5.2.6 The rainfall trend, both SDSM and START, in Thapla district

In Thapla district, the comparison of high hazard classes is quite high between the present-day conditions and the future simulation, both in scenario A2 and B2. So, the rainfall distribution is calculated by the interpolation of nine rain stations covering the nine provinces of Uttaradit, Tak, Pisanulok, Khon Kaen, Udontani, Lampang, Petchaboon, Phrae and Loei every five years from 2013 to 2099, in both SDSM software and START in Appendix 1-2. The years of 2013, 2018, 2023, 2028, 2033, 2038, 2043, 2048, 2053, 2058, 2063, 2068, 2073, 2078, 2083, 2088, 2093 and 2099 present both the trend of the rainfall values and the high hazard classes in Thapla district.

The number of standard rainy hours from1981 to 2010 (Section 3.8.1, Chapter 3) is used to calculate for mm/24 hours. Then, the interpolation is used to calculate the rainfall values in Thapla district. These rainfall values will be averaged by the

Interpolation approach and represented by the rainfall intense rate as shown in Table 5.27, the interpolation maps in four simulation scenarios (SDSMA2, SDSMB2, STARTA2 and STARTB2) every five years from 2013 to 2099 as shown in Appendix 3 – 74.

Year	Rainfall rate (mm/24 hours)			
	SDSM		START	
	A2	B2	A2	B2
2013	96-102.3	**116.7**	98.6	74.8
2018	95.4-102	81.7	87.6	91.2
2023	76.3	79.4	80.9	58
2028	80.2	77.2	85.8	85-91.4
2033	79	98.9-106	81.2	73-78
2038	95.1-103	94-101	67.1	73.1
2043	85-92	89.2	73.6-76.7	85
2048	76	77.5	90.5	69.4
2053	82.3	84.4	72.2	**108**
2058	89.1	71.2	96.1	88
2063	**123-132.3**	98.5-107.4	90	83.4-88
2068	82	88.8	76-82	75.3
2073	90	100.7-108.6	80.2-86	79.3
2078	93	87.9	100.4	79
2083	82.7	92	65.6	77.5
2088	94.4	94	95.4	101
2093	106	99.7	**122**	84
2099	107.7	91.7	96.6	67.2-71

Table 5.27 The rainfall rate (mm/24 hours) in Thapla district in Uttaradit province

The high hazard class areas (km^2), every five years from 2013 to 2099, are higher than at the present time. The high hazard class areas relate to the rainfall rate. The high hazard class areas are linked with the slope gradient both 25^o – 65^o and 25^o – 10^o.

In SDSM, the high hazard class areas of 563 km^2 are the highest in 2063, but 445.2 km^2 is the lowest in 2048 by scenario A2 (Fig 5.75). The high hazard class areas of 537.5 km^2 are the highest in 2013, while 429.9 km^2 is the lowest in 2058 by scenario B2 (Fig 5.76).

In START, the high hazard class areas of 547 km^2 are the highest in 2093, but 411.5 km^2 is the lowest in 2083 in scenario A2 (Fig 5.77). The high hazard class

areas of 521.6 km² are the highest in 2053, while 388.2 km² is the lowest in 2023 in scenario B2 (Fig 5.78).

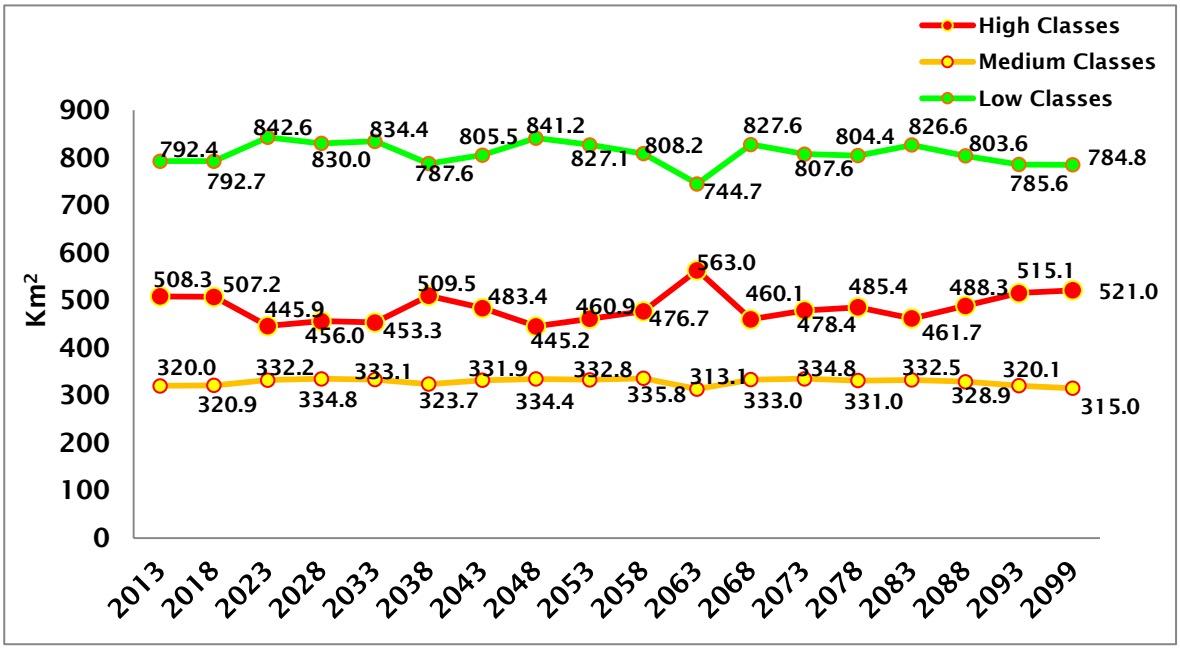

Figure 5.75 The high hazard classes of SDSMA2 in Thapla district every five years from 2013 to 2099

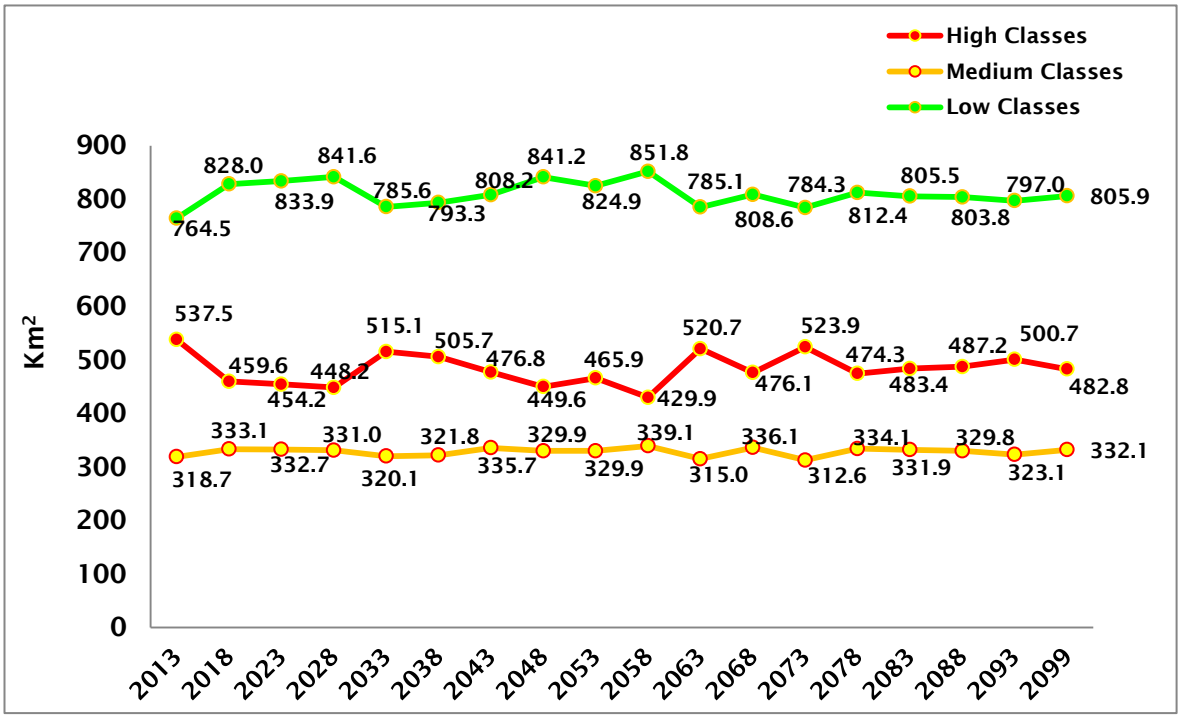

Figure 5.76 The high hazard classes of SDSMB2 in Thapla district every five years from 2013 to 2099

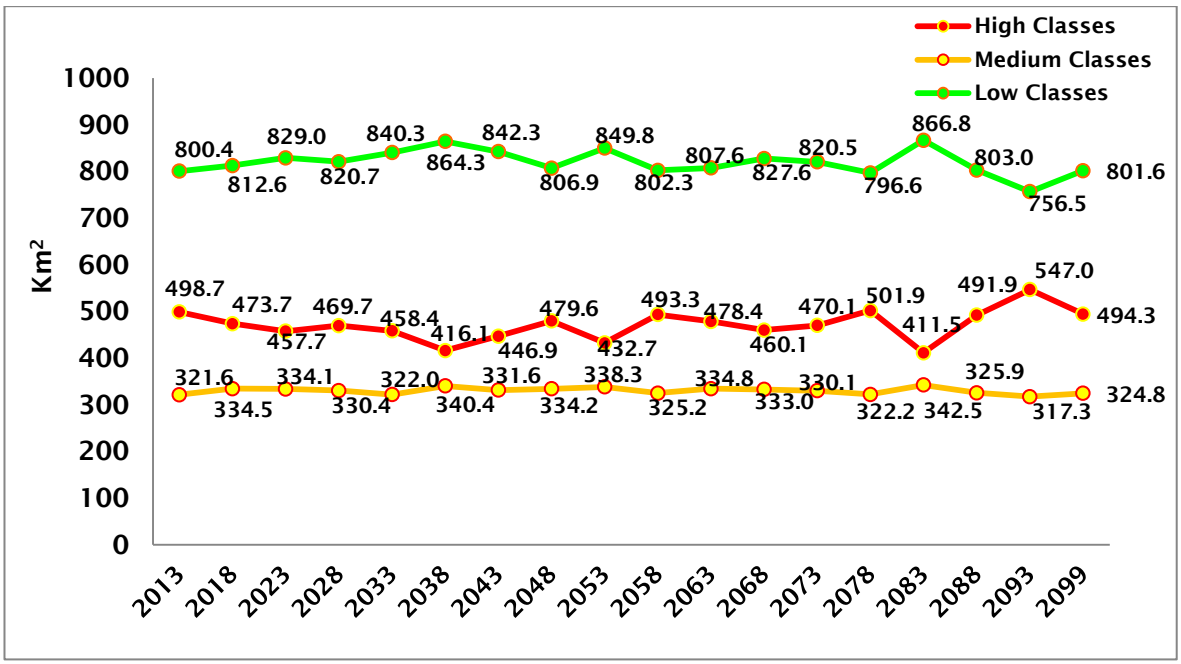

Figure 5.77 The high hazard classes of STARTA2 in Thapla district every five year from 2013 to 2099

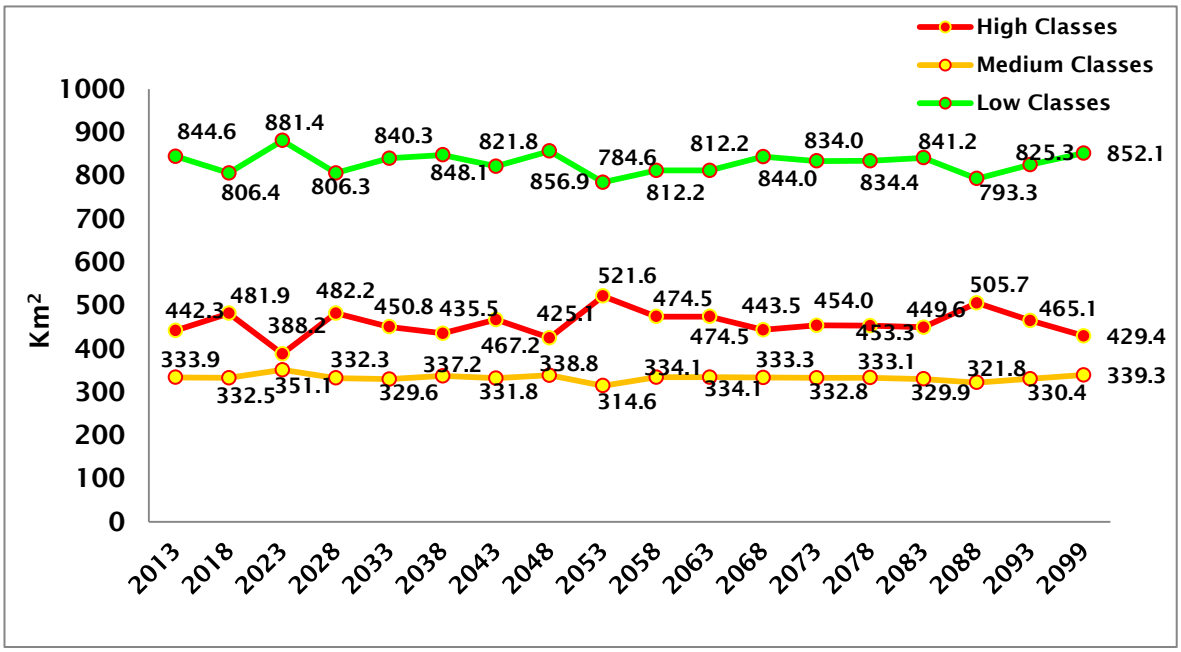

Figure 5.78 The high hazard classes of STARTB2 in Thapla district every five year from 2013 to 2099

Based on the results obtained in Chapter 5, this section will show the correlation between three hazard class areas and rainfall conditions in Thapla district each five years from 2013 to 2099. Regression analysis is used to show the correlation in terms of linear regression. As described in the chart, the regression

of relationship between three hazard class areas and rainfall values are presented in four simulations: SDSMA2, SDSMB2, STARTA2 and STARTB2.

It can be seen from Fig 5.79 that the trend of the four simulations is similar among all regressions between the high hazard classes and rainfall values. The values of correlation coefficient for the four simulations: SDSMA2, SDSMB2, STARTA2 and STARTB2 are: simulation scenarios A2 and B2 (SDSM) have a regression r^2=0.984 and r^2=0.980 and both are approximately 98%. In addition, the simulation scenarios A2 and B2 (START) have a regression r^2=0.980 and r^2=0.982 and both are also approximately 98%.

On the other hand, the trend of the four simulations among all regressions between the medium and low hazard classes and rainfall values are negative (Fig 5.80 and Fig 5.81). The values of correlation coefficient for the four simulations in the medium classes: SDSMA2, SDSMB2, STARTA2 and STARTB2 are: simulation scenarios A2 and B2 (SDSM) have a regression r^2=0.7998 and r^2=0.646 and both scenarios A2 and B2 (START) have a regression r^2=0.6917 and r^2=0.7795 and all four scenarios are approximately 64% - 78%. The values of correlation coefficient for the four simulations in the low classes have only one regression r^2=0.97 and are approximately 97%.

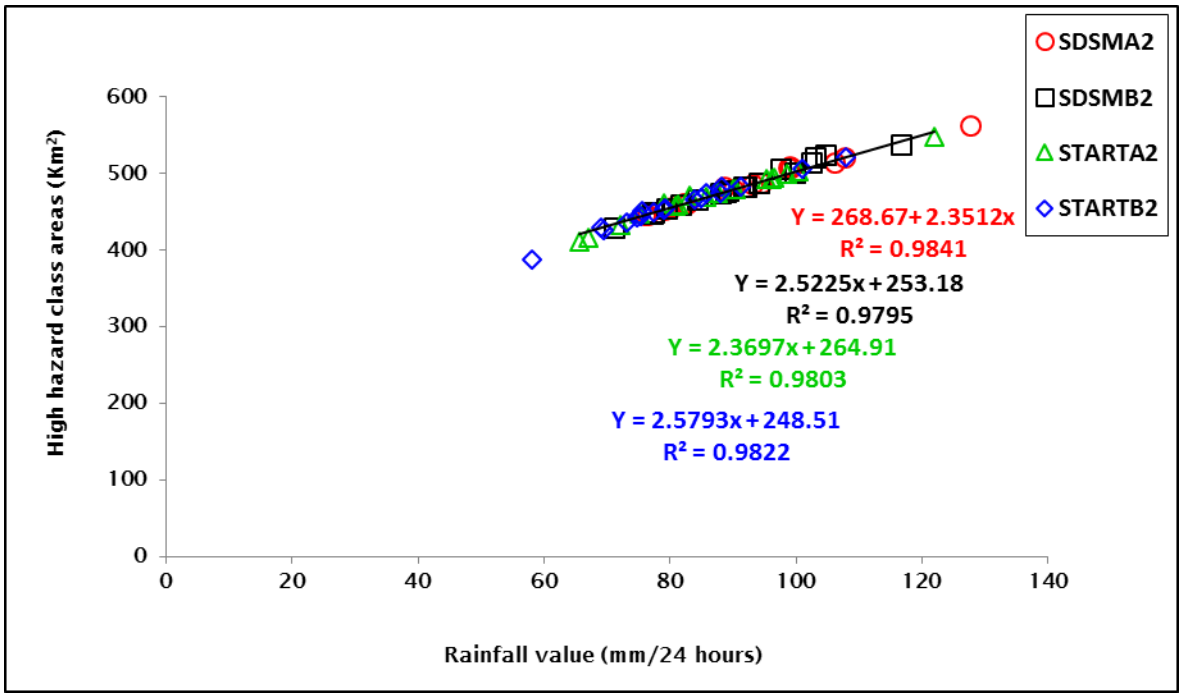

Figure 5.79 The regression of high class areas and rainfall value by SDSMA2

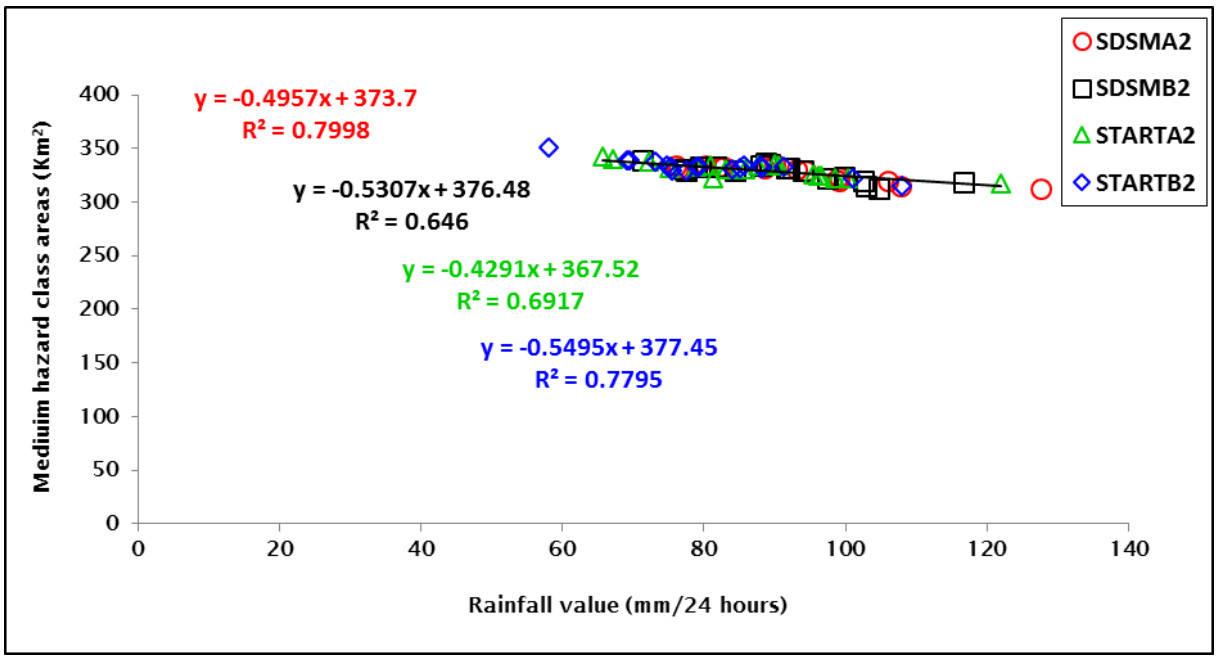

Figure 5.80 The regression of medium class areas and rainfall values by SDSMA2

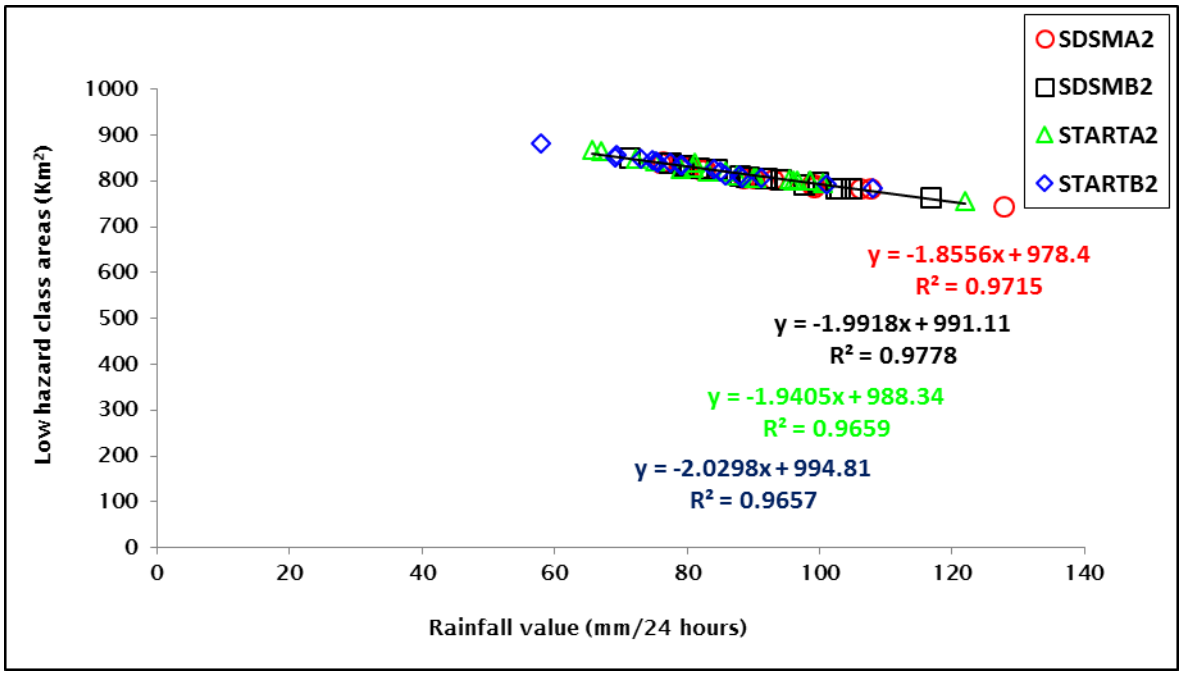

Figure 5.81 The regression of low class areas and rainfall values by SDSMA2

One of the reasons why the correlation is nearly the same in the four simulation scenarios, and the correlation coefficient for the four simulations is so high is because both the high hazard classes and rainfall values are variable in the same area (Thapla district) and the geotechnical soils are the same. The relationship

between the high hazard classes and rainfall values are correlated the correlation of regression in four simulations: SDSMA2, SDSMB2, STARTA2 and STARTB2. On the other hand, the correlation is also the same in the four simulation scenarios in both medium and high classes, and the correlation coefficient for the four simulations is negative because rainfall values directly increase the high hazard class areas (failure regions), so the medium and the low hazard classes decrease. The increasing rainfall leads to the situation of instability (medium classes), becoming failure regions (high classes) and the situation of safety areas (low classes), becoming unstable (medium classes). For this reason, the values of correlation coefficient for the four simulations in the medium classes are only about 64% - 78%, while the high and low classes are approximately 98% and 97%.

Finally, the comparison of landslide risk and rainfall under present-day conditions and in the future simulation increases, showing in each district in the Uttaradit province. The zonation of landslide risk is nearly the same between the present and in the future simulation. On the other hand, the increase of rainfall in the future will increase the high hazard class areas (failure regions), especially in steep slope areas, while the medium and low hazard class areas will decrease. Some areas of medium and low hazard classes become the high hazard class areas in steep slopes, low slopes and flat areas respectively. Thus, the increase of rainfall directly relates to the increase of landslide risk (failure region) in each district, while characteristics of soil (cohesive soil and permeability) also affect the risk areas.

CHAPTER 6 DISCUSSION

In the previous chapter, the landslide risk assessment has been analysed through three simulations for present-day conditions (1954 – 2012) and future simulation scenarios A2 and B2 (2013 – 2099) in nine districts in Uttaradit province using the SINMAP model. This chapter will discuss the result of quantitative SINMAP output, including the dominant parameters affecting SINMAP. The relationship between rainfall values and landslide hazard is analysed for risk assessment, in terms of the zonation of landslide risk areas (km^2). In addition, the results are obtained from the comparison between the zonation of landslide risk under present-day conditions and future simulation.

6.1 SINMAP processes in Uttaradit province

6.1.1 SINMAP and Quantitative analysis

The high hazard class area (failure region) was compared with the landslide scar in tambon Maephun in Laplea district and in tambon Namman in Thapla district.

The high hazard class area (failure region) and the landslide scar were very different. Both were discussed.

The failure region covered more area than just the landslide scar. For example, both landslide scar areas and the failure region in the two tambons were compared (tambon Maephun in Laplea district and in tambon Namman in Thapla district) as follows:

The failure region in tambon Maephun in Laplea district is about 41.04 km^2, while the landslide scar is approximately 26.8 km^2. In tambbon Namman in Thapla district, the failure region is approximately 139.8 km^2, while the landslide scar is only approximately 13.1 km^2 (Section 4.1.1, Chapter 4). The difference between the failure region and the landslide scar are shown as in Table 6.1.

Study areas	High hazard class areas (failure region) (km^2)	The landslide scar (km^2)	Different areas of zonation of landslide risk and landslide scar (km^2)
Tambon Maephun	41.04	26.8	14.24
Tambon Namman	139.8	13.1	126.7

Table 6.1 The different percentages between the zonation of landslide risk and the landslide scar in two tambons: Maephun and Namman

All three slope gradients and hazard classes throughout risky areas are higher than the landslide scars (Section 4.1.1, Chapter 4). The rainfall was unevenly distributed and orographically enhanced and the spatial distribution did not account for the real situation (landslide scar). The risky areas are linked with only one rainfall value (i.e. the rainfall value referred to by the landslide occurrences in 2006, in Laplea district, as 330 mm) (DMR, 2011a).

According to SINMAP, one rainfall value was calculated throughout all the tambons in Laplea district (i.e. all areas of tambons in each district have the same rainfall value). So, slope gradients and rainfall was a key to calculate the failure regions, instability and safety areas. The infinite slope model is related to slope gradient length (Montgomery and Dietrich, 1994). The flow distance is actually along the slope, and steep slopes give rise to landslides. Thus, the increase of infiltrated rainfall is related to the slope gradient and can increase the high hazard class areas (failure region). This method was implemented with software based on grid-based data structures. The accuracy of the output depended on the accuracy of the digital elevation model (DEM) data input. Therefore, the accuracy of DEM was important in this analysis. In this study, the DEM grid in 30 metres resolution was used and calculated by 30 metres on the ground. The output of SINMAP was mapped and defined for the areas of potential terrain instability.

The zonation of landside risk should be compared with the areas of slope gradient. The result shows that the zonation of landslide risk and slope gradient areas is linked to each other. The zonation of landslide risk is calculated by adding 100% of both high and medium hazard classes and 19.85% of low hazard class, while slope gradients are also calculated by adding 100% of both steep and low slope areas and 19.85% of flat areas. Both the zonation of landslide risk and slope gradients presented in tambon Maephun in Laplea district: 88.6 km^2 and 109.8 km^2 respectively and in tambon Namman in Thapla district: 180.1 km^2 and 210.4 km^2. Therefore, the percentage of risk is 80.7% in tambon Maephun in

Laplea district and 85.6% in tambon Namman in Thapla district. It means that the SINMAP output (the zonation of landslide risk) is linked with the slope gradients in both tambon Maephun in Laplea district and in tambon Namman in Thapla district.

Finally, the failure region was bigger than the landslide scar because the rainfall occurred on some parts of the mountains in the past, while the zonation of landslide risk and slope gradient areas were linked with each other. In terms of hydrological data, the upslope area per unit contour length (m^2/m) is developed for the hydrological model. The theoretical SINMAP is based on the infinite slope stability together with the topographically based wetness index. The equilibrium of lateral discharge in each pixel point shows a steady state recharge R (mm/day), so the rainfall value (mm/day) is calculated for all areas (i.e. all areas of tambons in each district have the same rainfall value). As for rainfall in the future, there are four rainfall causes in Thailand as shown in the Literature Review: orographic rain, monsoon rain, convective rain and cyclonic rain. All four causes of rainfall are likely to occur in any of the tambons in each district. So, in this study, the covering of rainfall distribution in all areas is good to predict landslide risk areas in the future.

According to the observations of Lan et al.(2004), lithology, structure, slope angle, slope aspect, elevation and the length of the fault influence Stability Index Mapping. The spatial database of the landslides in the Xiaojiang watershed in China is evaluated by techniques of GIS in terms of the susceptibility maps. The landslide factors are classified and calculated by the Certainty Factor model (CF) values for the hazard class of landslide zonation. In addition, the comparisons of the threshold precipitation values are still identified by the instability classes of the landslide hazard map.

6.1.2 Dominant parameters of SINMAP

Six parameters of the SINMAP model were discussed in Chapter 4: dimensionless cohesion, angle friction, permeability, soil depth, rainfall, and slope gradients, but only two dominant parameters: slope gradients and rainfall and three important parameters: dimensionless cohesion, angle friction and permeability. These five parameters will be discussed in this chapter.

a) The dominant parameters: slope gradients and rainfall

Three slope gradients: steep slopes, low slopes and flats are related to three hazard classes: high, medium and low. Increase of rainfall from 50 to 300 mm/24 hours (Section 4.2.3, Chapter4) is dominant for increasing the high hazard classes on three slope gradients: steep slopes, low slopes and flats. Then, the areas of steep slope decrease, while low slope and flat areas increase in the medium hazard classes. All three slope gradient areas decrease in the low hazard classes. First the high hazard class areas occurred in steep slope areas, and then in low slope and flat areas respectively, when high class areas increased. The medium class areas occurred in the steep slope, low slope and flat areas that remained from the high classes. When the high class areas increased, the high class areas covered some parts of medium class areas. The medium class areas covered some parts of low class areas, and then low class areas decreased. The failure region increases in all three slope gradient areas: steep slope, low slope and flat areas when rainfall increases from 50 to 300 mm/24 hours, as shown in Table 6.2. Approximately 71.4% of steep slope areas, while 28.4% of low slope areas and 2.32% of flat areas present for failure regions when 300 mm/24 hours of rainfall occurs. On the other hand, approximately 46.3% of steep slope areas, while 10.3% of low slope areas and 0.90% of flat areas present for failure regions when 50 mm/24 hours of rainfall occurs. Thus, increase of rainfall directly affects the failure region in slope gradient areas, as shown in Table 6.2.

Rainfall (mm/24 hours)	High hazard class areas (failure region)					
	Steep slope areas (km^2)	Steep slope areas in Thapla district(km^2)	Low slope areas (km^2)	Low slope areas in Thapla district (km^2)	Flat areas (km^2)	Flat areas in Thapla district (km^2)
50	92.3 (46.3%)	199.3(100%)	87.7 (10.3%)	849 (100%)	6.5 (0.90%)	722.9 (100%)
100	108.6 (54.5%)		121 (14.2%)		8.3 (1.15%)	
150	121.4 (60.9%)		153.2 (18.0%)		10.0 (1.39%)	
200	131 (65.7%)		184.7 (21.7%)		12.2 (1.68%)	
250	137.8 (69.1%)		214.2 (25.2%)		14.4 (1.20%)	
300	142.4 (71.4%)		240.9 (28.4%)		16.8 (2.32%)	

Table 6.2 The failure regions in three slope gradients: steep slopes, low slopes and flats, increasing rainfall value from 50 to 300 mm/24 hours

The Literature Review described that slope gradients and rainfall are the most important factor for landslides (DWR, 2010). The gradient of a slope has an effect on the probability of landslide occurrences. Slope gradient stabilities are

divided into five levels: the possibility of landslide is more than 70% is on 35° slope angles, between 50% and 70% on 26.7° - 35° slope gradients, 30 - 50% on 16.7° - 26.7° slope gradients, 15 - 30% on 8.5° -16.7° slope gradients and 0-15% on 0° - 8.5° slope gradients (DWR, 2010).

As for SINMAP, the majority of SINMAP theory is computed in terms of stability index and saturation (wetness index). Additionally, the digital elevation model (DEM) grid data and the topographic pit filling are manipulated by calculating slopes, determining flow directions, and defining the area draining to a specific point. The SINMAP theory specifies the upslope area per contour length unit and has been developed by Beven and Kirkby (1979). The mechanism of saturation form determines both the increase of soil moisture and surface saturation area relevant to the convergent hollow area (Montgomery and Dietrich, 1994). Based on wetness, the assumption of shallow lateral subsurface flow along the topographic gradient, including the lateral discharge, is the balance of a steady state discharge.

Then, the simplest method for specifying flow directions is to assign flow from each grid cell, either adjacent or diagonally, in the direction of the steepest downward slope. Thus, the increase of infiltrated rainfall related to the slope gradient, can increase the number of high hazard class areas. The increase of the slope angle leads to an increase in the driving force, which affects the resisting force. Then, a potential failure surface might occur on the slope. In addition, soil cohesion also affects shallow landslides (Sidle and Ochiai, 2006).

The infinite slope model is related to slope gradient length (Montgomery and Dietrich, 1994). Therefore, in this study, the failure regions are strongly related to steep slope areas, while the instabilities and the safety areas obviously increase in both low slope and flat areas. During prolonged rainfall (50 – 300 mm/24 hours), approximately 28.3% - 32.4% of low slope areas presents for instability (Table 6.3), while approximately 33.0% - 55.1% of low slope areas presents for safety areas (Table 6.4). The 78.3% - 84.5% of flat areas is shown for safety areas (Table 6.4). Thus, all three ranges of slope gradients directly affect the three hazard classes in the SINMAP model.

Rainfall (mm/24 hours)	Medium hazard class areas (instability region)					
	Steep slope areas (km^2)	Steep slope areas in Thapla district(km^2)	Low slope areas (km^2)	Low slope areas in Thapla district (km^2)	Flat areas (km^2)	Flat areas in Thapla district (km^2)
50	58.5 (29.4%)	199.3(100%)	240.2 (28.3%)	849 (100%)	29.7 (4.1%)	722.9 (100%)
100	49.3 (24.7%)		266.1 (31.3%)		37.3 (5.2%)	
150	40.0 (20.0%)		277.7 (32.7%)		43.4 (6.0%)	
200	32.2 (16.2%)		281.3 (33.1%)		50.1 (6.9%)	
250	26.5 (13.3%)		282.0 (33.2%)		58.6 (8.1%)	
300	22.4 (11.2%)		275.3 (32.4%)		64.5 (8.9%)	

Table 6.3 The instability regions in three slope gradients: steep slopes, low slopes and flats, increasing rainfall value from 50 to 300 mm/24 hours

Rainfall (mm/24 hours)	Low hazard class areas (safety area)					
	Steep slope areas (km^2)	Steep slope areas in Thapla district(km^2)	Low slope areas (km^2)	Low slope areas in Thapla district (km^2)	Flat areas (km^2)	Flats areas in Thapla district (km^2)
50	27.9 (14.0%)	199.3(100%)	468.2 (55.1%)	849 (100%)	611.0 (84.5%)	722.9 (100%)
100	20.8 (10.5%)		409.0 (48.2%)		601.6 (83.2%)	
150	17.3 (8.7%)		365.2 (43.0%)		593.8 (82.1%)	
200	15.5 (7.8%)		330.2 (38.9%)		583.9 (80.9%)	
250	14.5 (7.3%)		299.9 (35.3%)		574.3 (79.4%)	
300	14.0 (7.0%)		279.9 (33.0%)		565.9 (78.3%)	

Table 6.4 The safety areas in three slope gradients: steep slopes, low slopes and flats, increasing rainfall value from 50 to 300 mm/24 hours

Finally, the mechanism of rainfall and slope gradients is the main factor to scope the risky areas on hilly and mountainous terrain. In addition, the slope stability and rainfall induced slope failure were discovered by Collins (2004). The infiltration was developed for failure regions, including the combination of the soil geometry, soil strength and infiltration parameters. Rainfall induced slope failure is determined by both one dimensional flow modelling and infinite slope analysis. So the relationship between soil and rainfall are main cause of failure on slopes.

Another study in Zhejiang Province in China discovered the relationship between the landslide zonation and rainfall via a statistic approach, including analysing many factors in respect of landslide occurrence: topography, geological

structure, lithology, as well as slope instability and critical daily rainfall. Thus, rainfall-infiltrated slope failure indicates that several factors affect stability on slopes (Zhang et al., 2011).

In terms of intensity of landslide occurrence, the semi-quantitative analysis of regional landslide hazard is used to prove spatial landslide prediction. The information is considered from the history of landslide occurrence to show the relation between five environmental factors, such as slope gradient, lithological formation, faults distribution, water system, land-use type, and two triggering factors, such as the annual number of rainstorm days and human activities. These are seven factors to incorporate on a map in the scale 1: 100,000 to create either a quantitative information map or a GIS analysis function. The effective rainfall (≥300 mm) has influenced large and moderate landslides in high hazard areas. Then, it is divided into three levels of hazard: low, moderate and high, taking into consideration rainfall intensity and effective rainfall. In this case, the effective rainfall is compared in low, medium and high hazard classes in large and moderate landslides: 0-200 mm, 200-300 and ≥300 mm respectively. While, the effective rainfall is divided into hazard levels of rainfall in small landslides: low, medium and high as 0-150, 150 -250 mm and ≥250 mm respectively. Finally, rainfall values are given that were related to slope failures. Thus the low, medium and high hazard categories were defined for large and moderate landslides: 0-200 mm, 200-300 and ≥300 mm respectively (Zhang et al., 2011).

b) Geotechnical data: shear strength, angle of friction and permeability

The behaviour of three parameters: shear strength, angle of friction and permeability are inked each other in this result (Section 4.2.2 Chapter 4). Thus, these three parameters are important for landslide analysis as follows;

- Dimensionless cohesion and angle of friction

In addition, the behaviour of dimensionless cohesion values (shear strength & root strength) directly affected the low hazard classes (safety area). Increased dimensionless cohesion ranges could reduce high (failure region) and medium (instability) class areas in hilly and mountainous areas, becoming low hazard class areas (safe). The dimensionless cohesion values of 0.5 – 1.0 present for safe areas (low hazard classes) in the hilly and mountainous terrains (Section 4.2.2, Chapter4). Three hazard class areas: high, medium and low of three ranges of

dimensionless cohesion: 0 – 0.125, 0.125 – 0.5 and 0.5 – 1.0 are shown in three slope gradient areas: steep slope, low slope and flat. The failure region decreases in three slope gradient areas: steep slope, low slope and flat from 0 – 0.125 Kpa to 0.5 – 1.0 Kpa of dimensionless cohesion, but the safety area increases in all three slope gradient areas, as shown in Table 6.5 and Table 6.6. The percentage of failure region decreases in steep slope areas: 64.5%, 32.1% and 10.6%, but the safety area increases both in low slope and flat areas: 46.4%, 70.4%, 85.5% and 86.7%, 88.9%, 89.3% respectively.

District	Dimensionless cohesion	High hazard class areas (failure region)					
Thapla		Steep slope areas (km^2)	Steep slope areas in Thapla district (km^2)	Low slope areas (km^2)	Low slope areas in Thapla district (km^2)	Flat areas (km^2)	Flats areas in Thapla district (km^2)
	0 – 0.125	128.6 (64.5%)	199.3 (100%)	106.8 (12.6%)	849 (100%)	0.003 (0.0004%)	722.9 (100%)
	0.125 – 0.5	63.9 (32.1%)		18.0 (2.12%)		0.025 (0.003%)	
	0.5 – 1.0	21.1 (10.6%)		1.6 (0.19%)		1.1 (0.15%)	

Table 6.5 The failure regions in three slope gradients: steep slopes, low slopes and flats in Thapla district from 0 – 0.125 Kpa to 0.5 – 1.0 Kpa of dimensionless cohesion

District	Dimensionless cohesion	Low hazard class areas (safety area)					
Thapla		Steep slope areas (km^2)	Steep slope areas in Thapla district (km^2)	Low slope areas (km^2)	Low slope areas in Thapla district (km^2)	Flat areas (km^2)	Flats areas in Thapla district (km^2)
	0 – 0.125	9.4 (4.72%)	199.3 (100%)	393.8 (46.4%)	849 (100%)	627.1 (86.7%)	722.9 (100%)
	0.125 – 0.5	25.2 (12.6%)		598.1 (70.4%)		643.0 (88.9%)	
	0.5 – 1.0	61.0 (30.6%)		725.6 (85.5%)		645.4 (89.3%)	

Table 6.6 The safety areas in three slope gradients: steep slopes, low slopes and flats in Thapla district from 0 – 0.125 Kpa to 0.5 – 1.0 Kpa of dimensionless cohesion

It means that both shear and root strengths are significant parameters in identifying safety areas with SINMAP software, since the SINMAP theoretical basis identifies the infinite plane slope stability model with wetness (pore pressures),

obtained from a topographically based steady state model of hydrology. Digital elevation model (DEM) methods are also used to define the important input information. Debris flow source areas are strongly controlled by surface topography through shallow subsurface flow convergence. Increased soil saturation and increased pore pressures affect shear strength reduction (Montgomery and Dietrich,1994). Then, the soil moisture reduces the effective normal stress, the friction angle being related to the shear strength. The cohesion (soil & root) is retained in the slope stability model. The behaviour of dimensionless cohesion is sensitive for three hazard classes. The high and medium class areas decrease, but low class areas increase when dimensionless cohesion ranges increase. Another study, Ray (2010) found that with the increase in unsaturated zone moisture of the soil layer, the groundwater table will be near the surface and the highly susceptible area will be increased.

For angle of friction, the increasing of angle of friction can reduce the high and medium hazard class areas (failure regions and instability), showing the same behaviour as in dimensionless cohesion values (Section 4.2.2, Chapter4). The high range of the angle of friction can reduce the high and medium hazard class areas because the angle of friction parameter is a part of the dimensionless cohesion parameter.

Eventually, the high value of dimensionless cohesion and angle of friction ranges lead to the small areas of high and medium classes, covering only steep slope and some parts of low slope areas, while low class areas (safety area) cover higher areas of low slope and flat areas.

For example, in the field observation in Thapla district, shallow roots of annual crops in agricultural areas (1.1014 kpa of root strength value) and bare land (0 kpa of root strength value) are found in land cover/land use areas (Section 3.2.1, Chapter 3). So both with root and without root strength present in Thapla district under present-day conditions and in the future simulation, as shown in Table 6.7. On the other hand, with roots of both in the horticultural area (slash-and-burn agriculture, annual crops and galangal oil) and teak (semi-natural and forest plantation (mainly teak) on the mountain areas (1.1014 - 2.9417 kpa of root strength value) cover all areas of land cover/land use areas, with root strength present in Thapla district under present-day conditions and in the future simulation. Approximately 82.8% of steep slope areas, 30.2% of low slope areas

and 0.47% of flat areas present for failure regions both with root and without roots under present-day conditions, while approximately 55.9% of steep slope areas, 6.52% of low slope areas and 0.01% of flat areas present for failure regions with roots in all areas under present-day condition (Table 6.7).

In the future simulation, approximately 85.0% of steep slope areas, 41.4% of low slope areas and 0.72% of flat areas present for failure regions, both with root and without roots, while approximately 68.5% of steep slope areas, 10.3% of low slope areas and 0.01% of flat areas present for failure regions with roots in all areas (Table 6.7).

Therefore, the failure regions (km^2) on three slope gradients: steep slopes, low slopes and flats can be reduced on slopes because roots cover all areas of hilly terrain.

District	Rainfall values (mm/24 hours)	High hazard class areas (failure region)					
		Steep slope areas (km^2)	Steep slope areas in Thapla district(km^2)	Low slope areas (km^2)	Low slope areas in Thapla district (km^2)	Flat areas (km^2)	Flats areas in Thapla district (km^2)
Thapla (with root) under present-day condition	65.5-69.6	111.4 (55.9%)	199.3(100%)	55.4 (6.52%)	849 (100%)	0.09 0.01%)	722.9 (100%)
Thapla (without root-with root) under present-day condition		163.8 (82.8%)		256.6 (30.2%)		3.4 (0.47%)	
Thapla (with root) in the future	95.8-110.8	136.5 (68.5%)		87.4 (10.3%)		0.10 (0.01%)	
Thapla (without root-with root) in the future		169.4 (85.0%)		351.2 (41.4%)		5.2(0.72%)	

Table 6.7 The failure regions in three slope gradients: steep slopes, low slopes and flats in Thapla district both with root and without root-with root under present-day conditions and in the future

Forze (2012) presented that forests and non-forests are compared for three hazard class areas: high, medium and low in Mae Hong Son province in the northern part of Thailand. The high hazard class areas (failure region) reduce in the forest regions, while the high hazard class areas (failure region) increase in non-forest regions. High value of root strength (7 Kpa) is used for calculation because forests are found in Mae Hong Son province. It confirms that large trees (deep root) are important to reduce the risky areas.

- Permeability

Another parameter, permeability is also significant. The high values of high hazard classes will show in small values of permeability, especially E-06 and E-07 (cm/sec) of permeability. Both E-06 and E-07 (cm/sec) present the high level of high hazard classes, which indicate the maximum of high hazard classes. The high hazard class areas (failure region) obviously increase, while the low hazard class areas (safety area) decrease from E-04 to E-07 (cm/sec) (Section 4.2.3, Chapter 4).

The theoretical basis of permeability values depends on numerous factors: particle size distribution, particle shape and texture, mineral composition, voids ratio, degree of saturation, soil fabric, nature of fluid, type of flow and temperature. The permeability values are classified into five levels: high (greater than E-03), medium (E-03-E-05), low (E-05-E-07), very low (E-07-E-09) and practically impermeable (less than E-09) (Pack et al., 1948). In this study, the permeability values vary between medium and low levels (E-04-E-07) from geotechnical laboratory, which cover seven test pit locations. Both E-06 and E-07 (cm/sec) of permeability value presented the higher failure regions (Section 4.2.2, Chapter4).

For example, the 4.006E-06 (cm/sec) of permeability value in Muang district shows approximately 169.2 km^2 of the high hazard class areas, which occurs in 35.8 km^2 (85.8%) of steep slope, 124 km^2 (55.7%) of low slope and 9.4 km^2 (1.72%) of flat areas. On the other hand, 3.415E-04 (cm/sec) of permeability value in Nampat district shows approximately 146.0 km^2 of the high hazard class areas, which occurs in 107.1 km^2 (48.4%) of steep slope, 38.4 km^2 (5.38%) of low slope and 0.5 km^2 (0.09%) of flat areas (Table 6.8). The failure regions in Muang district occur in three slope gradient areas is bigger than in Nampat district. The dimensionless cohesion value in Muang and Nampat districts present: 1.048 and 1.20 Kpa respectively. Both values are nearly the same, so the failure regions in both districts are different because of the permeability value.

District	High hazard class areas (failure region)			All areas in district		
	Steep slope areas (km^2)	Low slope areas (km^2)	Flat areas(km^2)	Steep slope areas(km^2)	Low slope areas(km^2)	Flat areas(km^2)
Muang	35.8 (85.8%)	124(55.7%)	9.4(1.72%)	41.7 (100%)	222.7(100%)	544.1(100%)
Nampat	107.1(48.4%)	38.4(5.38%)	0.5(0.09%)	221.1(100%)	713.1(100%)	516.9(100%)

Table 6.8 the comparison between failure regions in Muang and Nampat districts under the present-day conditions

In addition, the failure regions in both districts are compared with each other in the future. The rainfall value in simulation scenario SDSMA2 is considered in Muang and Nampat districts: 140.9 and 110.8 mm/24 hours, as shown in Section 5.2.4, Chapter5. The permeability value in the future is the same as in present-day conditions: 4.006E-06 (cm/sec) in Muang district and 3.415E-04 (cm/sec) in Nampat district. The bigger failure regions are shown in Maung and Nampat districts: 249.3 km^2 and 150 km^2 because rainfall will increase in the future. The failure regions are shown in three slope gradient areas: steep slope, low slope and flat (Table 6.9).

District	High hazard class areas (failure region)			All areas in district		
	Steep slope areas (km^2)	Low slope areas (km^2)	Flat areas(km^2)	Steep slope areas(km^2)	Low slope areas(km^2)	Flat areas(km^2)
Muang	35.8 (85.8%)	149.3(67.0%)	64.2(11.8%)	41.7 (100%)	222.7(100%)	544.1(100%)
Nampat	108.6(49.1%)	40.9(5.73%)	0.6(0.11%)	221.1(100%)	713.1(100%)	516.9(100%)

Table 6.9 the comparison between failure region of Muang and Nampat districts in the future simulation

From above it is clear that bigger failure region in Muang district covers both low slope and flat areas, while the larger failure region in Nampat district is very small, covering steep slope, low slope and flat areas, comparing present-day conditions and future simulation.

In this case, the effect of low value of permeability (E-06) in the failure regions on slope gradients is higher than the medium value of permeability (E-04). The increase of rainfall in low value of permeability of soil leads to an increase of failure regions in slope gradient areas.

In addition, the permeability of both with root and without root strength is considered for the failure regions. Table 6.6 presents that the failure region is the same both with root and without root strength under present-day conditions and

in the future simulation. Approximately E-06 (cm/sec) of permeability presents in Thapla district (Section 5.1.2, Chapter5), while the failure region is the same in all four simulations: with roots & without roots both under present-day conditions and in the future simulation. It means that with or without roots does not affect the failure regions on slopes with in the same permeability. The infiltrated rainfall is presented by the wetness index.

The wetness index is used to present the ratio of the saturated soil thickness above the failure plane and the total depth of the soil above the failure plane. Therefore, approximately E-06 (cm/sec) of the permeability values, in Muang district, leads to increased failure regions on three slope gradients. This permeability value is classified for low level of permeability.

In terms of SINMAP, an upslope area per unit contour length (m^2/m) is developed for hydrological model (Bven and Kirkby, 1979). The higher soil moisture or the trend of areas of surface saturation occurs in convergent hollow areas. The literal discharge (R) (m/hr)/the soil transmissivity (T) (m^2/hr) define the relative depth of the perched water table within the soil layer. The wetness index model (Section 3.3.6, Chapter 3) quantifies the relative wetness in terms of assumed steady state recharge relative to the soil's capacity for lateral drainage of water. The pore water pressure is computed by assuming a hydrologic steady state with the depth of saturated soil computed by the upslope area per contour length unit. This concept may be useful for establishing field estimates of R/T through the field identification of the limits of surface saturation. Therefore, impermeable soil (low permeability (cm/sec)) affects the high hazard class areas (failure regions). Among these factors, the permeability is a very important parameter in seepage and stability problems involving unsaturated soils. This mechanism of the trigger failure on a slope during rainfall infiltration and loss of suction, when propagation of the wetting front and the water increase, produces a positive pore water pressure and a shallow failure.

Also in Tsaparas (2002) in Hong Kong, the stability of unsaturated soil during the rainfall period, the saturated coefficient of permeability in the case of water and the effect of rainfall pattern in the seepage under saturated soil slopes were tested in the laboratory. Seepage under slope gradients is important for the saturated coefficient of permeability in the case of water. Seepage analysis is considered for stability analysis under unsaturated slopes when slope failure

occurs under heavy rainfall. The 70 mm/one hour of rainfall intensity indicates landslide occurrence in Hong Kong. So three parameters of stability: climatic conditions, characteristic of soil and infiltration are shown in this study. These parameters are the key conditions for slopes together with the saturated coefficient of permeability that affect the stability on slopes. Finally, the coefficient of permeability in different simulations in the case of water can control the infiltration on slopes. The permeability of soil is low (ks =E-06 – E-07 (m/s)), the pore water pressure increases until the end of the wet period. Thus, the permeability of soil is an important parameter for stability analysis.

Therefore, the infiltrated water has a significant role in the shear strength of residual soil. The shear strength varies with the degree of saturation. The relationship between the shear strength of soil and the API was considered by Soralump (2010). As the saturation of soil increased, then the shear strength dramatically dropped, finally the shear strength became stable, after 90% of soil saturation (Soralump et al., 2010).

In addition, the infinite slope stability relates to the slope length. Only 10% increase of soil saturation might be a cause of unstable regions on hill slopes. It means that wet soil is a more unstable slope than dry soil (Ram et al., 2010). Ohtsu (2012) described that the API is used to consider the trigger for slope failure. The variation of pore water pressure is found by the API to be about 1.5 metres of depth on a plane and is about 2.5 metres of depth on a slope. This is used to test for the trigger of slope failure. During the intense rainfall period, the correlation between the interval rainfalls is recorded for one day and ten days, together with the pore water pressure. When unsaturation occurs, the pore water pressure is slightly changed, but when saturation occurs, the pore water pressure strongly increases. It means that the antecedent rainfall affects the pore water pressure.

c) The quality of SINMAP in Uttaradit province

Both qualitative SINMAP analysis and dominant parameters of SINMAP are considered to show the quality of SINMAP. The zonation of landslide risk is calculated by three hazard classes because it is linked with the landslide scar, while the zonation of landslide risk is much bigger than the landslide scar. The percentage of landslide zonation risk found in hilly terrains (three slope gradients) in tambon Maephun in Laplea district and tambon Namman in Thapla

district are 80.7% and 85.6%, while rainfall is calculated throughout all tambons. Both percentages confirm that SINMAP is precise to identify the zonation of landslide risk in hilly and mountainous areas. As for dominant parameters, rainfall and slope gradients are factors for landslide occurrence, while dimensionless cohesion and permeability are also important. These parameters can be applied to assess community planning in hilly environments, especially dimensionless cohesion. Higher dimensionless cohesion (both cohesive soil and root) can reduce the failure regions in slope gradient areas. Although, in this study, the failure regions on slope gradients are the same in both with roots and without roots in Thapla district, since the upper and lower values of dimensionless cohesion are used for SINMAP parameters. So non-cohesive soil (dry sand and bare lands) and cohesive soil present for Thapla district. Another reason, most of land cover/land use is in agricultural areas (Section 3.2.1, Chapter3), so the cohesive root has a small value. Thus, the failure regions cannot be reduced in Thapla district.

In this study, this result considers that cohesive roots are important in reducing the failure regions on slope gradients, especially deep roots. Shallow roots cannot reduce the failure region. In addition, large trees or forests should be found in all areas, not only on some parts of the mountains.

In addition, the output of SINMAP is applied for quantitative risk assessment of landslides in Uttaradit province. The landslide risk assessment is considered for land use planning in hilly terrains. All slope gradients: steep slopes, low slopes and flats are classified in three levels: high, medium and low, in this study, in nine districts in Uttaradit province. The risk assessment is determined in local areas to define the significance of landslide hazard. The assessed risk in the local areas can be applied to reduce the high risk in hilly and mountainous terrain. This approach in landslide risk assessment can be used for risk assessment.

6.1.3 The wider implication of another SINMAP research

There have been four studies in four countries which have used the SINMAP procedure. First of all, according to the observation of Fowze et al. (2012), the mechanism of the stability is changed on a slope because of rainfall. There are four steps to predict the stability on a slope as follows: 1) the reduction of shear strength of soil when soil moisture increases. 2) The permeability of residual soil is unsaturated under base rock layer. 3) The expectation of a failure region is

controlled by soil types, thickness and slope gradients; 4) The initial saturation will occur, and 5) Retention of water is absorbed by land cover. In addition, the SINMAP model has been used for landslide mitigation on slope gradients in Mae Hong Son province in the northern part of Thailand. Forest and non-forest regions are compared for three hazard class areas: high, medium and low. The high hazard class areas (failure region) reduce in forest regions, while the high hazard class areas (failure region) increase in non-forest regions. On the other hand, Fowzes study, it does not classify or calculate slope gradient areas in hilly and mountainous areas.

Secondly, the Stability Index Mapping (SINMAP) model, which was developed by the State of British Columbia coordinating with the Canadian government, uses the Geographic Information System (Arc view version) for landslide prone areas analysis. The potential of shallow landsliding is presented by National Forest and Transportation Management. The slope stability index is based on the 30 metres resolution of the Digital Elevation Model (DEM). In this study, six classes of stability index are presented by areas (km^2) and percentages of a region, then, classified into three levels: moderate to high, low to moderate and none to low. The landslide-prone areas are based on five main factors: the history of landslides, the characteristic of the soil, ground slope, contributing drainage areas and vegetation (root strength) (Michael and Dixon, 1998).

Thirdly, Acharya et al. (2006) presented the slope stability analysis covering 409 km^2 of the Himalayas in the northern part of Rasuwa district in Nepal. Landslides often occur in the rainy season. In this study, SINMAP software was used on GIS Arc View 8.1. In terms of digital data, the spatial soil types, DEM, land-use and vegetation are used to compute the slope stability factor. The combination of hydrological data and slope angle are calculated, the wetness of soil depended on during the extreme rainfall period and the slope angle of a DEM. The Digital Elevation Model presented the slope ranges between 0^o and 64^o on the Himalayan mountains. The increase of saturated groundwater flows correlated with slope failure regions. The scenario of dry soil, half and fully-saturated soil are used to increase the wetness of soil from dry to a saturated condition, the safety factor decreases but it depends on the slope angle. Then, the scenarios of the extreme daily rainfall events in both a 1 year and 10 year return period are compared to the percentage of slope stability classes. There is a small difference in saturated conditions. As a result, the impact of storm events are overestimated by saturated

and non-saturated (dry sand) conditions. It easily becomes an unstable class in saturated conditions under a steep slope of more than 30°. The agricultural areas or areas of deforestation are also dominant in association with slope failure during the monsoon season.

Fourthly, the relationship between Stability Index Mapping (SINMAP) and the Frequency Ratio model (FR) as a simple method (logistic regression& neural network) are two main factors in the causes of slide: ground water pressures and toe erosion. Yilmaz (2009) found that indicated the relationship between landslide factors and landslide occurrence location to create the susceptibility classes in the landslide susceptibility maps. There are several factors to consider in this case, such as the distance from drainage systems, faults and roads, slope angle and aspect, topographic elevation, topographical wetness index and vegetation cover, including rainfall which is a main factor in identifying landslide susceptibility. The quality of this model is tested for validation under the statistical frequency ratio (FR) model.

Finally, the previous four studies of SINMAP confirm that the stability of three hazard class areas to identify the risky areas, while rainfall and slope gradients are dominant, including characteristic of soil.

In addition, the zonation of landslide risk (km^2) on slope gradients is useful for land use planning. In this study, the output of SINMAP is classified in three hazard classes in three slope gradient areas and shows the risk areas (km^2) on slope gradients, while other research did not show the areas in three steps of slope gradients. So, the output of SINMAP, in this study, can be applied for quantitative risk assessment of landslide in Uttaradit province. The landslide risk assessment is considered for land use planning in hilly terrains. All slope gradients: steep slopes, low slopes and flats are classified in three levels: high, medium and low. For example, in tambon Maephun in Laplea district, the risk assessment is determined for the risk levels in local areas to define the significance of landslide hazard. The high risk areas are shown in each district (Section 5.1.3, Chapter 5).

Finally, the risk areas should be preserved for land use planning in order to reduce the high risk in hilly and mountainous terrain. In addition, the approach of landslide risk assessment is used for risk assessment throughout the world. For example, in Hong Kong, the landslide risk in hilly terrain is determined using the

qualitative risk assessment to design the mitigation measures and protection guideline, especially in high risk areas. In Australia, landslide risk assessment is important for the procedure of land development, including assessing community planning in hilly environments (Lee et al., 2014).

6.2 The comparison of rainfall under present-day conditions and in the future simulation in Uttaradit province

In the previous chapter, the downscaled Global Climate Model (GCM) output was required for the scenario simulation of future climate change. The temporal and spatial resolution time series of precipitation are provided by the Statisitical DownScaling Model (SDSM) (Wilby et al., 2007). The large scale atmospheric predictor was used to downscale in the local areas by the weather generator downscaling tool. Over the period 1961-2099, the daily predictor values are generated by HadCM3 and CGCM2 under simulation scenario A2 and B2. The calibration model of SDSM for precipitation was provided, using observed record from 1961 to 1990 from the National Centre for Environmental Prediction (NCEP) analysis data (Kalnay et al., 1996). The variations in the NCEP observed climate records were used in the statistical model. In START, the future climate projection is simulated for future climate at 20x20 km of grid resolution in the mainland of Southeast Asia, using the baseline during the 1960-1999 periods. Over the period 2010-2099, the daily predictor values are generated by PRECIS (Providing Regional Climates for Impacts Studies) regional climate model and GCM (Global Circulation Model), ECHAM4 dataset as initial data for calculation under simulation scenario A2 and B2. Both SDSM and START will be discussed as below:

6.2.1 SDSM and START processes

The results of SDSM version 4.2 were limited because they were downscaled in a square box that covers all nine provinces from latitude 16° 26′ and 18° 37′ north and between longitude 98° 52′ and 103° 05′ east (Fig 3.10). The start and end dates can be changed in the setting screen. The period 1961-1990 is the default dates of the baseline period of observed daily rainfall data. The observed daily rainfall (predictant) was used from a rain station in each province: 351201 (Uttaradit province), rain station 376201 (Tak province), rain station 378201 (Pisanulok province), rain station 381201(Khon Kaen province), rain station

354201 (Udontani province), rain station 328201 (Lampang province), rain station 379201 (Petchaboon province), rain station 330201(Phare province) and rain station 353201 (Loei province). This version cannot be downscaled in each province and to specific latitudes and longitudes. So, the result of SDSM may have an error.

The results of START were downscaled in latitudes and longitudes that covers all nine provinces, from latitude 16° 26′ and 18° 37′ north and between longitude 98° 52′ and 103° 05′ east, and the observed rainfall (predictant) was downscaled in latitude and longitude from a rain station in each province: 351201 (Uttaradit province), rain station 376201 (Tak province), rain station 378201 (Pisanulok province), rain station 381201(Khon Kaen province), rain station 354201 (Udontani province), rain station 328201 (Lampang province), rain station 379201 (Petchaboon province), rain station 330201(Phare province) and rain station 353201 (Loei province).

Five lines are shown alongside each other in Fig 6.1. Both modelled annual rainfall of SDSMA2 and SDSMB2 and annual rainfall of STARTA2 and STARTB2 in each three years were averaged from 1961 to 2012, while observed annual rainfall in each three years was averaged in nine provinces: Uttaradit, Tak, Pisanulok, Khon Kaen, Udontani, Lampang, Petchaboon, Phare and Loei. The average annual modelled and observed rainfall was used to calculate the rainfall rate (mm/24 hours). The number of wet days (here defined as the number of standard rainy hours from 1981 to 2010) was used to calculate wet days per year in the annual rainfall values in each province from 1961 to 2012. The comparison between averages observed and modelled rainfall (mm/24 hours): SDSM and START from 1961 to 2012 are shown in Fig 6.1. The average modelled rainfall (mm/24 hours) in scenario A2 and B2 were nearly the same in both SDSM and START from 1961 to 2012.

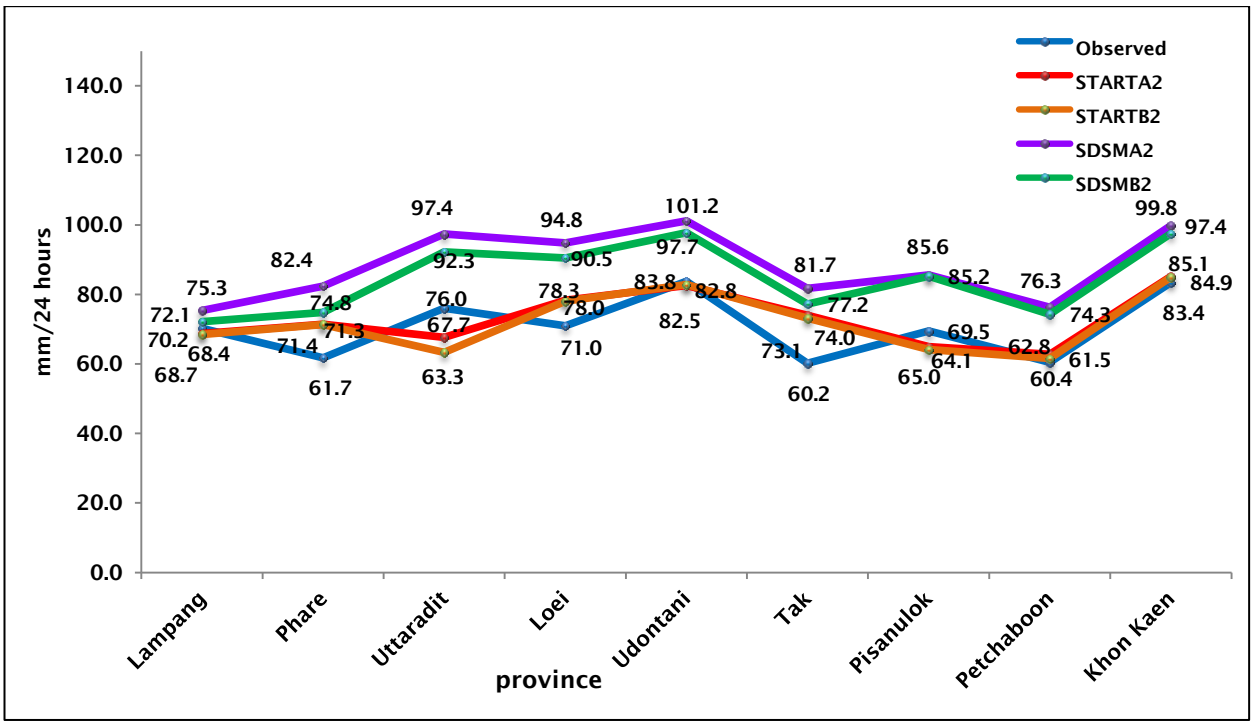

Figure 6.1 The comparison between observed and modelled rainfall values (mm/24 hours): SDSM and START from 1961 to 2012

In both results, the gap between modelled and observed rainfall by START was smaller than by SDSM from 1961 to 2012 in all nine rain stations in the nine provinces, since SDSM version 4.2 could not specify the latitudes and the longitudes. There could be an error in the result of SDSM, due to this version being unable to downscale in each province. Thus, the error of SDSM was higher than the error of START. The gap between average observed and modelled rainfall (START) was better than SDSM from 1961 to 2012, while the correlation coefficient of both observed and modelled rainfall from SDSMA2 and SDSMB2: 84.2% and 87.6% was better than from STARTA2 and STARTB2: 66% and 60.4%. However, both results were in the same direction and linked with the IPCC (2007).

6.2.2 The rainfall trend in the future

The trend of annual rainfall in the future simulation from 2013 to 2099 both SDSM and START in scenario A2 and B2 increasingly fluctuates, and the observed annual rainfall from 1954 to 2012 also fluctuates. Approximately 300-500 mm of average annual rainfall increased in both SDSM and START in scenario A2 and B2. According to the IPCC (2007), the climate conditions are predicted in the future for several decades. The average annual rainfall will increase about 300 mm in the future (2013-2099). Thus, the results of both SDSM and START are almost in

the same direction as the IPCC (2007). Modelling has developed rapidly over the recent decade (Houghton, 2009). There are numerous published maps to show the prediction of precipitation and temperature in the future (World Bank, 2010). Over the decades in the twentieth century, observed change in rainfall has been responding to anthropogenic activity. The result of aerosol concentration and greenhouse gases have increased, linked with human activity. By the end of the twenty-first century, these phenomena will lead to increased rainfall (Turner et al., 2012). The IPCC (2012) insists that extreme weather conditions rapidly growing in the future will lead to changed rainfall, both in intensity and seasonality.

In addition, both the SDSM and START results, in this study, the SRES scenario series comprise two scenario storylines: A2 and B2. The SRES scenario of the A2 storyline describes the development of economic growth and technological change on local and regional levels. On the other hand, the scenario of the B2 storyline is in the local situation, in economic, social and environmental sustainability, including environmental protection and social equity (Houghton, 2009). The output of SDSM, both scenarios A2 and B2, are nearly in the same direction as START, but average annual rainfall values in scenario A2 are higher than scenario B2 both SDSM and START.

DWR (2014) presents that the trend of rainfall in the future is also predicted in seven river basins in the northern part of Thailand by the PRECIS model in simulation scenarios A2 and B2. As a result, the trend of rainfall in all seven river basins in the future (2012-2069) will increase, when compared with the trend of rainfall at the present time (1980-2011). The rainfall values are related to the antecedent precipitation index (API) on slopes. The infinite slope stability and factor of safety are specified, including soil moisture of 90% saturated soil. The zonation of landslide risk is focused on each river basin and shown in the landslide hazard mapping. Nan river basin is one of seven basins, which flows though Uttaradit province. Thus, rainfall-induced landslides will occur in Uttaradit province in the future (DWR, 2014).

The highest rainfall prediction is presented in simulation scenario A2 in 2024 and 2035, and the zonation of landslide risk will increase in these two years. The highest rainfall of simulation scenario B2 is shown in 2033, so the zonation of landslide risk increases in this year (DWR, 2014).

6.3 The comparison of zonation of landslide risk under present-day conditions and in the future simulation in Uttaradit province

The zonation of landslide risk focuses on all areas of high and medium hazard classes and 19.85% of low hazard classes in nine districts: Muang, Laplea, Thapla, Nampat, Bankhok, Faktha, Thongsaenkhun, Phichai and Tron. The comparison between the zonation of landslide risk (km^2), by adding all areas of high and medium classes and 19.85% of low classes and rainfall values in the future simulation scenarios A2 (SDSM) is obviously higher than under present-day conditions in Thapla district, while the zonation of landslide risk is nearly the same in Bankhok districts between the present-day conditions and future simulation (Table 5.16). Both districts will be discussed as follows:

In Thapla district, the increasing of high class (failure regions) areas are presented, while the steep slope and low slope areas in the high hazard classes will increase in the future. On the other hand, the medium classes, in steep slope, low slope and flat areas decrease and all slope gradient areas (steep slopes, low slopes and flats) of low classes also decrease when compared with present-day conditions. The increasing rainfall values are presented for this district. It shows that the high class areas will increase, when the medium and low class areas decrease. The increasing rainfall leads to the situation of instability (medium classes), becoming failure regions (high classes) and the situation of safety areas (low classes), becoming unstable (medium classes). The higher percentages of failure regions cover the steep slope, low slope and flat areas: 2.8%, 11.2% and 0.25% under present-day conditions and in the future simulation as show in Table 6.10. The higher percentages of instability regions cover only in flat areas: 8.1%, but the lower percentages cover in steep slope and low slope areas: 5.4%, 5.2% under present-day conditions and in the future simulation as show in Table 6.11. The lower percentages of safety areas cover in steep slope, low slope and flat areas: 0.1%, 5.9% and 3.5% under present-day conditions and in the future simulation as show in Table 6.12.

District	Condition	Hazard class areas (failure region)					
		Steep slope areas (km^2)	Steep slope areas in Thapla district (km^2)	Low slope areas (km^2)	Low slope areas in Thapla district (km^2)	Flat areas (km^2)	Flats areas in Thapla district (km^2)
Thapla	Present-day conditions	163.8 (82.2%)	199.3 (100%)	256.6 (30.2%)	849 (100%)	3.4 (0.47%)	722.9 (100%)
	Future simulation	169.4 (85.0%)		351.2 (41.4%)		5.2 (0.72%)	
	Different risk areas	5.60 (2.8%)		94.6 (11.2%)		1.8 (0.25%)	

Table 6.10 The failure regions in three slope gradient areas: steep slope, low slope and flat under present-day conditions and in the future simulation in Thapla district

District	Condition	Medium hazard class areas (instability region)					
		Steep slope areas (km^2)	Steep slope areas in Thapla district (km^2)	Low slope areas (km^2)	Low slope areas in Thapla district (km^2)	Flat areas (km^2)	Flats areas in Thapla district (km^2)
Thapla	Present-day conditions	9.2 (4.6%)	199.3 (100%)	296.3 (34.9%)	849 (100%)	34.8 (4.8%)	722.9 (100%)
	Future simulation	3.8 (1.9%)		252 (29.7%)		58.7 (8.1%)	
	Different risk areas	-5.4 (-2.7%)		-44.3 (-5.2%)		23.9 (3.3%)	

Table 6.11 The instability regions in three slope gradient areas: steep slope, low slope and flat under present-day conditions and in the future simulation in Thapla district

District	Condition	Low hazard class areas (safety areas)					
		Steep slope areas (km^2)	Steep slope areas in Thapla district (km^2)	Low slope areas (km^2)	Low slope areas in Thapla district (km^2)	Flat areas (km^2)	Flats areas in Thapla district (km^2)
Thapla	Present-day conditions	5.4 (2.7%)	199.3 (100%)	243.7 (28.7%)	849 (100%)	607.6 (84.0%)	722.9 (100%)
	Future simulation	5.2 (2.6%)		193.3 (22.8%)		581.9 (80.5%)	
	Different risk areas	-0.2 (-0.1%)		-50.4 (-5.9%)		-25.7 (-3.5%)	

Table 6.12 The safety areas in three slope gradient areas: steep slope, low slope and flat under present-day conditions and in the future simulation in Thapla district

On the other hand, the increased rainfall values will be low in Bankhok district. The steep slope and low slope areas in the high classes will increase, while steep slope and low slope areas in the medium classes will decrease. The increasing rainfall will lead to the situation of instability (medium classes) becoming failure regions (high classes), while safety areas are the same as present-day conditions. However, the zonation of landslide risk between present-day conditions and future simulation is nearly the same.

The higher percentages of failure regions cover in steep slope, low slope and flat areas: 1.2%, 0.78 and 0.01% under present-day conditions and in the future simulation as show in Table 6.13. On the other hand, the lower percentages of instability regions cover in steep slope, low slope and flat areas: 1.2%, 0.70% and 0.01% under present-day conditions and in the future simulation (Table 6.14). The percentages of safety areas are the same in all three slope gradients both under present-day conditions and in the future simulation as shown in Table 6.15.

District	Condition	High hard class areas (failure region)					
		Steep slope areas (km^2)	Steep slope areas in Thapla district (km^2)	Low slope areas (km^2)	Low slope areas in Thapla district (km^2)	Flat areas (km^2)	Flats areas in Thapla district (km^2)
Bankhok	Present-day conditions	39.5 (19.8%)	199.3 (100%)	6.0 (0.70%)	849 (100%)	0 (0%)	722.9 (100%)
	Future simulation	41.9 (21.0%)		12.6 (1.48%)		0.1 (0.01%)	
	Different risk areas	2.4 (1.2%)		6.6 (0.78%)		0.1 (0.01%)	

Table 6.13 The failure regions in three slope gradient areas: steep slope, low slope and flat under present-day conditions and in the future simulation in Bankhok district

District	Condition	Medium hazard class areas (instability region)					
		Steep slope areas (km^2)	Steep slope areas in Thapla district (km^2)	Low slope areas (km^2)	Low slope areas in Thapla district (km^2)	Flat areas (km^2)	Flats areas in Thapla district (km^2)
Bankhok	Present-day conditions	52.7 (26.4%)	199.3 (100%)	114.1 (13.4%)	849 (100%)	4.4 (0.60%)	722.9 (100%)
	Future simulation	50.3 (25.2%)		107.5 (12.7%)		4.3 (0.59%)	
	Different risk areas	-2.4 (-1.2%)		-6.60 (-0.70%)		-0.1 (-0.01%)	

Table 6.14 The instability regions in three slope gradient areas: steep slope, low slope and flat under present-day conditions and in the future simulation in Bankhok district

District	Condition	Low hazard class areas (safety areas)					
		Steep slope areas (km^2)	Steep slope areas in Thapla district (km^2)	Low slope areas (km^2)	Low slope areas in Thapla district (km^2)	Flat areas (km^2)	Flats areas in Thapla district (km^2)
Bankhok	Present-day conditions	22.0 (11.0%)	199.3 (100%)	362.4 (42.7%)	849 (100%)	300.1 (41.5%)	722.9 (100%)
	Future simulation	22.0 (11.0%)		362.4 (42.7%)		300.1 (41.5%)	
	Different risk areas	0 (0%)		0 (0%)		0 (0%)	

Table 6.15 The safety areas in three slope gradient areas: steep slope, low slope and flat under present-day conditions and in the future simulation in Bankhok district

Finally, the big difference of zonation of landslide risk in Thapla district shows that increasing rainfall leads to the situation of instability (medium classes), becoming failure regions (high classes) and the situation of safety areas (low classes), becoming unstable (medium classes), while the small difference of zonation of landslide risk in Bankhok district shows that the increasing rainfall will lead to the situation of instability (medium classes), becoming failure regions (high classes).

6.3.1 The relationship between the trends of rainfall and slope gradients in three hazard classes in the future

Based on the results obtained in Chapter 5, this section will show the correlation between three hazard classes and rainfall conditions in Thapla district each five years from 2013 to 2099. Regression analysis is used to show the correlation in terms of linear regression. It can be seen that the trend of the four simulations is similar among all regressions between three hazard classes and rainfall values. The trend of the four simulations among all regressions between the high hazard classes and rainfall values is positive, while the trend of the four simulations among all regressions between the medium and low hazard classes and rainfall values is negative.

The correlation coefficient is presented nearly the same in four simulations: SDSMA2, SDSMB2, STARTA2 and STARTB2. Therefore, only simulation: SDSMA2 is shown for the relationship between three hazard classes: high, medium and low

and rainfall in Thapla district each ten years from 2013 to 2099. It explains that the increasing rainfall leads to the situation of instability (medium classes), becoming failure regions (high classes) and the situation of safety areas (low classes), becoming unstable (medium classes). As for discussion, the slope gradients: steep slopes, low slopes and flats in three hazard classes: high, medium and low are linked to each other. The correlation coefficient of three slope gradients: steep slopes, low slopes and flats in high hazard classes and rainfall is positive, while the correlation coefficient of three slope gradients: steep slopes, low slopes in medium hazard classes and rainfall is negative. The correlation coefficient of flats in medium hazard classes and rainfall is positive. In low hazard classes, the correlation coefficient of all three slope gradients: steep slopes, low slopes and flats is negative (Fig 6.2 – Fig 6.4).

The increasing rainfall leads to decreasing instability in both steep slope and low slope areas, becoming failure regions (high classes). So three slope gradients: steep slopes, low slopes and flats increase in high hazard classes. All three slope gradient areas decrease in low hazard classes, so the situation of safety areas (low classes) becomes unstable (medium classes). It leads to the increase of flat areas in medium hazard classes.

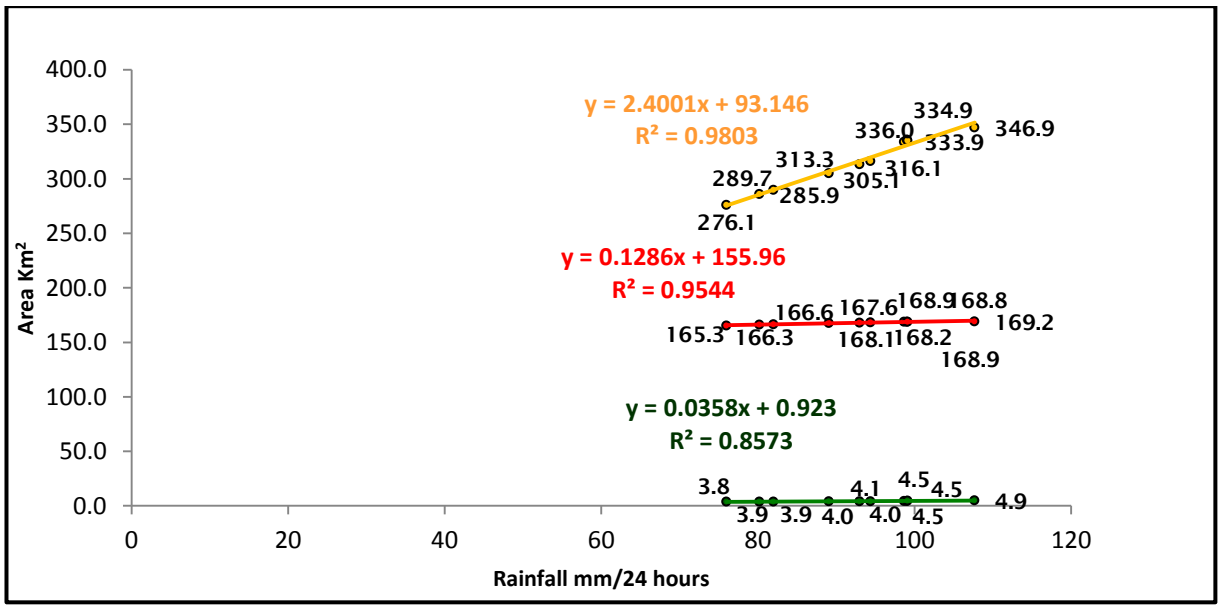

Figure 6.2 The correlation of three slope gradients: steep slopes, low slopes and flats in the high hazard classes

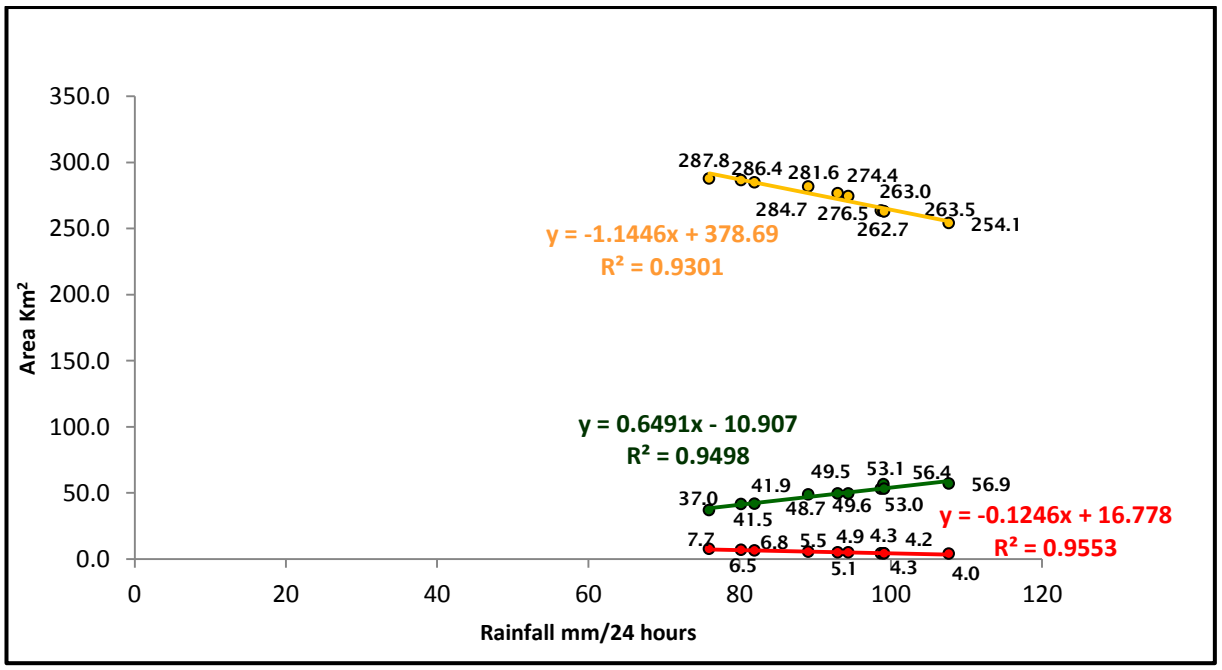

Figure 6.3 The correlation of three slope gradients: steep slopes, low slopes and flats in the medium hazard classes

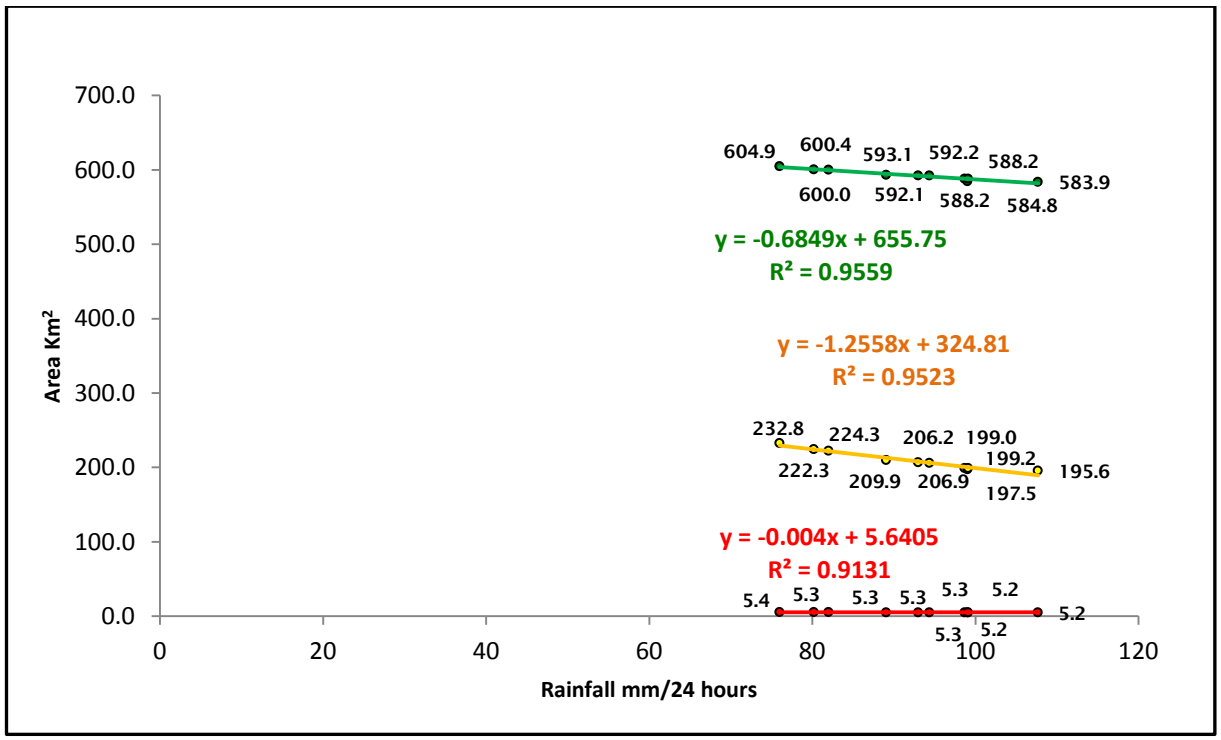

Figure 6.4 The correlation of three slope gradients: steep slopes, low slopes and flats in the low hazard classes

Finally, the quantitative analysis of SINMAP is presented in this chapter. The percentage of both the zonation of landslide risk and the slope gradients are presented in tambon Maephun in Laplea district and in tambon Namman in Thapla district:: 80.7% and 85.6% respectively. It means that both the zonation of landslide risk and the slope gradients are linked to each other. Both slope gradients and rainfall are dominant parameters. During prolonged rainfall (50 – 300 mm/24 hours), the high hazard class areas (failure region) directly increase in three slope gradients: steep slopes, low slopes and flats, especially in steep slope areas, while the low hazard class areas (safety areas) also decrease all three slope gradients. The dimensionless cohesion is high sensitivity because the increase of dimensionless cohesion value (root strength) from three ranges of dimensionless cohesion: 0 – 0.125, 0.125 – 0.5 and 0.5 – 1.0 Kpa leads to the decrease of failure region in three slope gradients: steep slopes, low slopes and flats (Table 6.7). The rainfall trend will increase in the future simulation both SDSM and START. Although the zonation of landslide risk under the present-day conditions and in the future simulation is nearly the same, the high class areas increase all three slope gradient areas: steep slopes, low slopes and flats respectively. However, both SINMAP parameters and the zonation of landslide risks are important for the landslide risk assessment and land management in the future.

CHAPTER 7 CONCLUSION

Climate conditions in Thailand are influenced by both southwest and northeast monsoons. The southwest monsoon brings heat steam from the Gulf of Thailand and Indian Ocean that becomes the rainfall in the rainy season. The slopes of hilly terrain and mountains, which are unstable (in physical terms), are found in Uttaradit province. The elevation of slope angles ranges from approximately 1 to 1749 metres and from 0^{o} – 65^{o}. Extrusive and Mafic Igneous rocks and Predominantly Metamorphic rock and the variable soil textures range from sand to silt to clay. Deforestation and clearance for agriculture also found in this province. The most damaging landslides in Thailand are always about 0.5-3 metres of soil depth in a shallow landslide (Tepparnich et al., 2010). The translational slide of landslide form is recorded from past landslides in Uttaradit province in 2006, especially in the clearance of agricultural zones. During heavy rainfall, the increase of the groundwater level leads to erosion or slippage on slopes because the internal pressure of the soils is high and the mass increases as water runs into the air space. The mechanism of slope failure is determined by using a simple infiltration model and slope stability equation, including the characteristics of soil and drainage conditions at the bottom of hilly slopes (Jotisankasa et al., 2008). The landslide type is related to the slope failure model. This research describes the linkage between the changes in rainfall patterns due to climate change on the landslide model, showing the risk areas in the future.

The SINMAP model is selected in this study area, since the translational slide form and root strength are applied by SINMAP software. The calibration and the sensitivity are used to setup the SINMAP model, including geotechnical data. The change in rainfall conditions in each district in Uttaradit province is described for the landslide risk both under present-day conditions and in the future simulation. Thus, the risk areas under present-day conditions and in the future simulation are presented by the landslide hazard mapping.

Furthermore, all landslide parameters of the SINMAP model are important for the simulation of landslide occurrences, corresponding with four parameters: dimensionless cohesion, permeability, slope gradients and rainfall. All parameters are linked with only one metre of soil deep. There are two dominant parameters: slope gradients and rainfall, including four important parameters:

dimensionless cohesion, angle of friction, permeability and soil depth, which affect the zonation of landslide risk, especially dimensionless cohesion (shear & root strength). As the result, the increase of root strength can reduce the failure regions (Chapter 6, Section 6.1.2). The high values of dimensionless cohesion are important in reducing failure regions in hilly terrains.

In terms of hydrological (rainfall values) simulation under climate change in the future, both SDSM and START downscaling techniques are used for this research. The annual modelled rainfall will be increased to approximately 300-500 mm. This result is the same direction as the IPCC (2012). So, the increase of rainfall is presented in the future simulation. The change in rainfall condition in each district in Uttaradit province is used to analyse the landslide risk both under present-day conditions and in the future simulation. Both SDSM and START show the rise of the high class areas are in the same direction. So, the increase of rainfall directly affects the failure regions in the future.

The correlation between the increase of rainfall values and all three slope gradients: steep slopes, low slopes and flats in three hazard classes: high, medium and low have a good correlation. The increasing rainfall leads to the decrease of instability (medium classes) in both steep and low slope areas, increasing failure regions (high classes) in all three slope gradient areas. The safety areas (low classes) decrease, increasing instability (medium classes) in flat areas. All three slope gradient areas in the low hazard classes will decrease. The zonation of landslide risk between under the present-day conditions and in the future simulation is nearly the same, while the instability becomes the failure region, especially in steep slope.

The qualitative of landslide risk assessment is used to evaluate the potential of landslide management (Lee and Moore et al, 2014). In this study, the zonation of landslide risk is presented in the hilly and mountainous terrains in each district in Uttaradit province. The zonation of landslide risk (km^2) in three slope gradients: steep slopes, low slopes and flats are found in all nine districts in Uttaradit province. Therefore, the potential problem of landslide risk is identified by the slope gradients and shown by map (km^2) (Section 5.1.3, Chapter 5). As can be seen, land cover/land use has been considered for mountainous and hilly terrain areas for landslide risk assessment.

The zonation of landslide risk in the future has been predicted for Uttaradit province. This is useful for land use planning, not only in Thailand but in other countries at risk. Because there has been a lot of deforestation for agriculture in the mountain areas. Deep tree roots reduce landslides. It would be good for future research to know the real time of landslides after heavy rainfall, so that the people living around the mountains can be forewarned, therefore able to escape in time.

As is seen due to the limitation of SINMAP, the SINMAP model can calculate only hazard class areas in terms of slope stability index, but cannot calculate the real-time of landslides after heavy rainfall occurs. As for future research, it would be good to have calculations for the real-time of landslide occurrences. Therefore, landslides will be predicted after heavy rainfall. As for the SDSM version 4.2, this version may have an error because it cannot specify latitudes and longitudes, when downscaled in local areas. Thus, new version of SDSM should be downscaled in latitudes and longitudes in local areas. This may reduce errors in prediction.

LIST OF REFERENCES

Acharya, G., et al. (2006). "Assessing landslide hazard in GIS: a case study from Rasuwa, Nepal." Bulletin of Engineering Geology and the Environment 65(1): 99-107.

Ali, A., et al. (2014). "Simplified quantitative risk assessment of rainfall-induced landslides modelled by infinite slopes." Engineering Geology 179: 102-116.

Amtayakul, P. (2006) "Estimating the monthly effective rainfall using dependable rainfall at 80 % in Thailand." Technical Document No. 551.577-21-01-2006, pp. 60-63.

Annual Book of ASTM Standards, Section 4, Construction, Soil and Rock(I): D420-D4914, Vol. 04.08, 1997.

Archer, D. and S. Rahmstorf (2010). The climate crisis: An introductory guide to climate change, Cambridge University Press.

Artlert, K. and C. Chaleeraktrakoon (2013). "Modeling and analysis of rainfall processes in the context of climate change for Mekong, Chi, and Mun River Basins (Thailand)." Journal of Hydro-environment Research 7(1): 2-17.

Ashrit, R., et al. (2003). "Response of the Indian monsoon and ENSO-monsoon teleconnection to enhanced greenhouse effect in the CNRM coupled model." Japan 81(4): 779-803.

Bellugi, D., et al. (2011). "Spatially explicit shallow landslide susceptibility mapping over large areas."Journal of Engineering Geology and Environment, pp. 399-407.

Beven, K. and M. J. Kirkby (1979). "A physically based, variable contributing area model of basin hydrology/Un modèle à base physique de zone d'appel variable de l'hydrologie du bassin versant." Hydrological Sciences Journal 24(1): 43-69.

Bhalme, H. and S. Jadhav (1984). "The southern oscillation and its relation to the monsoon rainfall." Journal of climatology 4(5): 509-520.

Bryant, E. (1997). Climate process and change, Cambridge University Press.

Bui, D. T., et al. (2012). "Spatial prediction of landslide hazards in Hoa Binh province (Vietnam): a comparative assessment of the efficacy of evidential belief functions and fuzzy logic models." Catena 96: 28-40.

Burton, A., and Bathurst, J. C. (1998) Physically based modelling of shallow landslide sediment yield at a catchment scale. Environment Geology, 35(2-3), 89-99.

Cervi, F., et al. (2010). "Comparing predictive capability of statistical and deterministic methods for landslide susceptibility mapping: a case study in the northern Apennines (Reggio Emilia Province, Italy)." Landslides 7(4): 433-444.

Collins, B. D. and D. Znidarcic (2004). "Stability analyses of rainfall induced landslides." Journal of Geotechnical and Geoenvironmental Engineering 130(4): 362-372.

Collins, M., et al. (2001). "The internal climate variability of HadCM3, a version of the Hadley Centre coupled model without flux adjustments." Climate Dynamics 17(1): 61-81.

Cooper, M., et al. (1998). "The Selborne cutting stability experiment." Géotechnique 48(1): 83-101.

Coppin, N. J. and I. G. Richards (1990). Use of vegetation in civil engineering, Construction Industry Research and Information Association London.

Costa-Cabral, M. C. and S. J. Burges (1994). "Digital elevation model networks (DEMON): A model of flow over hill slopes for computation of contributing and dispersal areas." Water resources research 30(6): 1681-1692.

Crozier, M. and R. Eyles (1980). Assessing the probability of rapid mass movement. Third Australia-New Zealand conference on Geomechanics: Wellington, May 12-16, 1980, Institution of Professional Engineers New Zealand.

Darby, S. E., Leyland, J., Kummu, M., Rasanen, T. A., and Lauri, H. Decoding the drivers of bank erosion on the Mekong river: The roles of the Asian monsoon, tropical storms, and snowmelt, Water Resour. Res., 49, 2146-2163, 2013.

DeGroot, D. J. and G. B. Baecher (1993). "Estimating autocovariance of in-situ soil properties." Journal of Geotechnical Engineering 119(1): 147-166.

De Vleeschauwer, C. and F. De Smedt (2002). Modeling slope stability using GIS on a regional scale. Proceedings of the first Geological Belgica International. Meeting, Leuven, 11-15 September 2002. Aardkundige Mededelingen, 12:253-256.

Dietrich, W. E., et al. (1995). "A process-based model for colluvial soil depth and shallow landsliding using digital elevation data." Hydrological processes 9(3-4): 383-400.

Dietrich, W. E., et al. (1998). "A validation study of the shallow slope stability model, SHALSTAB, in forested lands of Northern California." Stillwater Ecosystem, Watershed & Riverine Sciences. Berkeley, CA.

DMR (Department of Mineral Resources) Thailand (2004) Landslide Risk map of Thailand.

DMR (Department of Mineral Resources) Thailand (2006) Landslide scar data base in Uttaradit province.

DMR (Department of Mineral Resources) Thailand (2011a) Landslide Risk Assessment and local community in landslide areas in Uttaradit provinces, Thailand (in Thai).

DMR (Department of Mineral Resources) Thailand (2011b) Landslide Risk Assessment and local community in landslide areas in Chiang Rai provinces, Thailand (in Thai).

DMR (Department of Mineral Resources) Thailand (2011c) Landslide Risk Assessment and local community in landslide areas in Prea provinces, Thailand (in Thai).

DMR (Department of Mineral Resources) Thailand (2011d) Landslide Risk Assessment and local community in landslide areas in Nan provinces, Thailand (in Thai).

DMR (Department of Mineral Resources) Thailand (2011e) Landslide Risk Assessment and local community in landslide areas in Suratthani provinces, Thailand (in Thai).

DMR (Department of Mineral Resources) Thailand (2011f) Landslide Risk Assessment and local community in landslide areas in Nakornsrithammarach provinces, Thailand (in Thai).

DMR (Department of Mineral Resources) Thailand (2011d) Landslide Risk Assessment and local community in landslide areas in Chumporn provinces, Thailand (in Thai).

DMR (Department of Mineral Resources) Thailand (2012) The statistical threshold value of rainfall with landslide occurrences, Thailand (in Thai).

DWR (Department of Water Resources) Thailand (2010) The risk factor and local community in landslide areas in Loei and Uttaradit provinces, Thailand (in Thai).

DWR (Department of Water Resources) Thailand (2014) The possibility and frequency of landslide occurrences on climate change in the northern part of Thailand, Thailand (in Thai).

Fairfield, J. and P. Leymarie (1991). "Drainage networks from grid digital elevation models." Water resources research 27(5): 709-717.

Fontes, R., Ramos, M and Redivo, L. (2003) 'Application of the SHALSTAB Model for Mapping Susceptible Landslide Areas in Mine Zone', pp.2444-2446.

Fowze, J., et al. (2012). "Rain-triggered landslide hazards and mitigation measures in Thailand: From research to practice." Geotextiles and geomembranes 30: 50-64.

GERD (Geotechnical Engineering Research and Development Centre) Thailand (2006) Landslide data base of Thailand, Thailand (in Thai).

GERD (Geotechnical Engineering Research and Development Centre) Thailand (2012) The development of early warning system in the northern and the southern part of Thailand, Thailand (in Thai).

GERD (Geotechnical Engineering Research and Development Centre) Thailand (2013) Geological data in Thailand, Thailand (in Thai).

Gui, S., et al. (2000). "Probabilistic slope stability analysis with stochastic soil hydraulic conductivity." Journal of Geotechnical and Geoenvironmental Engineering 126(1): 1-9.

Guimarães, R. F., et al. (2003). Application of the SHALSTAB model for mapping susceptible landslide areas in mine zone (Quadrila´ tero Ferri´ fero in southeast Brazil). Geoscience and Remote Sensing Symposium, 2003. IGARSS'03. Proceedings. 2003 IEEE International, IEEE.

Hammond, C., et al. (1992). "Level I stability analysis (LISA) documentation for version 2.0." General technical report INT; 285.

Head, K. 1994. Vol. 2: Permeability, shear strength and compressibility tests, London: Pentech Press.

Hearn, G. and J. Griffiths (2001). "Landslide hazard mapping and risk assessment." ENGINEERING GEOLOGY SPECIAL PUBLICATION: 43-52.

Houghton, J. (2009) Global Warming. New York: Cambridge University Press. pp 139-140.

IPCC (2007) Climate Change 2007: The Physical Science Basis. Contribution of working Group I to the Fourth Assessment Report of the Intergovernmental Panel on Climate Change [Solomon, S. Qin, D. Manning, M. Chen, Z. Marquis, M. Averyt, K.B. Tignor, M. and Miller, H.L. (eds.)]. Cambridge University Press, Cambridge, United Kingdom and New York, NY, USA, pp.608-631.

IPCC (2012) Managing the Risks of Extreme Event and Disasters to Advance Climate Change Adaptation. http://ipcc –wg2.gov/SREX/report (Accessed 24/9/2013).

Jenson, S. K. and J. O. Domingue (1988). "Extracting topographic structure from digital elevation data for geographic information system analysis." Photogrammetric engineering and remote sensing 54(11): 1593-1600.

Jotisankasa, A. and H. Vathananukij (2008). Investigation of soil moisture characteristics of landslide-prone slopes in Thailand. International Conference on Management of Landslide Hazard in the Asia-Pacific Region 11th-15th November.

Jotisankasa, A. & Sawangsuriya, A. (2008) Application of unsaturated soil mechanics to slope stability, Proceedings of the 13th National Convention on Civil Engineering, Thailand.

Ju, J. and J. Slingo (1995). "The Asian summer monsoon and ENSO." Quarterly Journal of the Royal Meteorological Society 121(525): 1133-1168.

Jutakorn, J. (2010). "El Niño and La Niña phenomenon effected on southwest monsoon in Thailand. Meteorological department." Weather report (551.557-21).

Kalnay, E., et al. (1996). "The NCEP/NCAR 40-year reanalysis project." Bulletin of the American meteorological Society 77(3): 437-471.

Kangsasitiam, M. (2004) Soil mechanic pp72-73. (in Thai).

Kayastha, P. (2006) Slope stability analysis using GIS on a regional scale. Unpublished M. Sc. thesis in Physical Land Resources, Vrije Universiteit Brussels.

Kripalani, R., et al. (1995). "Variability of the summer monsoon rainfall over Thailand—comparison with features over India." International journal of climatology 15(6): 657-672.

Kripalani, R., et al. (2007). "South Asian summer monsoon precipitation variability: coupled climate model simulations and projections under IPCC AR4." Theoretical and Applied Climatology 90(3-4): 133-159.

Kunlong, Y., et al. (2007). "Regional landslide hazard warning and risk assessment." Earth Science Frontiers 14(6): 85-93.

Lal, M. and H. Harasawa (2001). "Future climate change scenarios for Asia as inferred from selected coupled atmosphere-ocean global climate models." Journal of the Meteorological Society of Japan 79(1): 219-227.

Lan, H., et al. (2004). "Landslide hazard spatial analysis and prediction using GIS in the Xiaojiang watershed, Yunnan, China." Engineering Geology 76(1): 109-128.

LDD (Land Development Department) Thailand (2012) Characteristics and Properties of Established Soil Series in the North and Central Highland Regions of Thailand, Report by Department of Land Department, Thailand (in Thai).

Lee, E., et al. (2007). "Ventnor Undercliff: development of landslide scenarios and quantitative risk assessment." Landslides and Climate Change: Challenges and Solutions. Balkema, Rotterdam: 323-334.

Limsakul, A., et al. (2010). "Asian summer monsoon and its associated rainfall variability in Thailand." Environment Asia 3(2): 79-89.

Li, W. C., et al. (2013). "Combined roles of saturated permeability and rainfall characteristics on surficial failure of homogeneous soil slope." Engineering Geology 153: 105-113.

Maijandee, S., Kreasuwun, J., Komonjinda, S., Promnopas, W. (2014) Effects of Climate Change on Future Extreme Rainfall Indices over Thailand. Global NEST, 16, 306-315.

Michael, D. and Dixon, P.E., (1998) Landslide Computer Modeling Potential, [On-line]. Available at: http://www.fs.fed.us/t-d/pubs/pdfpubs/pdf03713804/pdf03713804dpi72.pdf/ (Accessed on 22.02.2015)

Montgomery, D. R. and W. E. Dietrich (1989). "Source areas, drainage density, and channel initiation." Water resources research 25(8): 1907-1918.

Montgomery, D. R. and W. E. Dietrich (1994). "A physically based model for the topographic control on shallow landsliding." Water resources research 30(4): 1153-1171.

Nakicenovic, N., et al. (2000). Special report on emissions scenarios: a special report of Working Group III of the Intergovernmental Panel on Climate Change, Pacific Northwest National Laboratory, Richland, WA (US), Environmental Molecular Sciences Laboratory (US).

Neelin, D. (2009) Rainfall in the climate system: change under global warming, and challenges for climate modeller, Mathematics and Climate, [On-line]. Available at: www.mathaware.org/mam/09/essays/Neelin_rain.pdf (Accessed on 22.03.2012)

Nilaweera, N. (1994). "Effects of tree roots on slope stability: the case of Khao Luang Mountain area, southern Thailand." Doctor of technical science dissertation. Asian Inst Tech, Bangkok, Thailand: 93-92.

Nounmusig, W., et al. (2006). Effects of ENSO on precipitation over northeast Thailand during rainy season 1997-1999. The 2nd Joint International Conference on" Sustainable Energy and Enviroment.

O'Callaghan, J. F. and D. M. Mark (1984). "The extraction of drainage networks from digital elevation data." Computer vision, graphics, and image processing 28(3): 323-344.

Ohtsu, H., Koga, H., Chaleiwchalard, N. & Soralump, S. (2012) A Study on Landslide Early Warning System Considering the Effect of Antecedent Rainfall on Slope Stability.

Olivares, L. and L. Picarelli (2003). "Shallow flowslides triggered by intense rainfalls on natural slopes covered by loose unsaturated pyroclastic soils." Géotechnique 53(2): 283-287.

Pack, R., et al. (1998). The SINMAP approach to terrain stability mapping. 8th congress of the international association of engineering geology, Vancouver, British Columbia, Canada.

Pack, R., et al. (1999). "SINMAP 2.0–A Stability Index Approach to Terrain Stability Hazard Mapping, User's Manual. Produced in ArcView Avenue and C++ for Forest Renewal BC under Research Contract No: PA97537-0RE, ht tp." digitalcommons. usu. edu/cgi/viewcontent. cgi.

Peck, R. B. and K. Terzaghi (1948). Soil mechanics in engineering practice.

Petley, D. Saturday, 13 February 2010. An analysis of fatal landslides in the Asia-Pacific region for 2006 to 2008 The Landslide Blog [Online]. Available at: http://www.landslideblog.org/2010/02/analysis-of-fatal-landslides-in-asia.html 2010].

Prakarnrat, S., Amatayakul, P. (2008) Probability and Return periods of monthly rainfall amount for Thailand, Technical Document No. 551.577.3-01-2008 , pp. 1-132.

Quinn, P., et al. (1991). "The prediction of hill slope flow paths for distributed hydrological modelling using digital terrain models." Hydrological processes 5(1): 59-79.

Ray, R. L., et al. (2010). "Impacts of unsaturated zone soil moisture and groundwater table on slope instability." Journal of Geotechnical and Geoenvironmental Engineering 136(10): 1448-1458.

Rodwell, M. J. and B. J. Hoskins (1995). "A model of the Asian summer monsoon. Part II: Cross-equatorial flow and PV behavior." Journal of the atmospheric sciences 52(9): 1341-1356.

Roger, G. and Richard, J. (1987) Atmosphere, Weather & Climate. 5th edn. Great Britain: Richard Clay.

Sarthi, P. P., et al. (2012). "Possible changes in the characteristics of Indian Summer Monsoon under warmer climate." Global and Planetary Change 92: 17-29.

Sidle, R. C. and H. Ochiai (2006). Landslides: processes, prediction, and land use, American Geophysical Union.

Singhrattna, N., et al. (2005). "Interannual and interdecadal variability of Thailand summer monsoon season." Journal of Climate 18(11): 1697-1708.

Soralump, S. (2007). Corporation of geotechnical engineering data for landslide hazard map in Thailand. EIT-JSCE Joint seminar on Rock Engineering, Bangkok, Thailand, Citeseer.

Soralump, S. and W. Chotikasathien (2007). Integration of geotechnical engineering and rainfall data into landslide hazard map in Thailand. Proceedings of GEOTHAI'07 international conference on geology of Thailand: towards sustainable development and sufficiency economy.

Soralump, S. and A. Jotisankasa (2008). Mitigation of Landslide Hazard in Thailand. Expert Symposium on Climate Change: Modelling, Impacts & Adaptations. Singapore.

Soralump, S. and W. Torwiwat (2009). Shear strength behavior of residual soil in Thailand subjected by changing in moisture content for supporting the landslide warning measure. 14th Civil Engineering Conference, Suranari.

Soralump, S. and Thowiwat, W. (2010) Shear Strength-Moisture Behaviour of Residual Soils of Landslide Sensitive Rock Group in Thailand, GEOTHAI 2010.

Srinil, S (2001) Soil Laboratory Testing, King Mongkut's Institute of Technology Ladkrabang (KMITL), Thailand (in Thai).

START, (Southeast Asia START Regional Centre) (2010) Preparation of Climate Change Scenarios for Climate Change Impact Assessment in Thailand Southeast Asia Regional Thai Centre.

START (Southeast Asia START Regional Centre) (2012) [On-line]. Available at : http://climatechange.jgsee.org/v2 (Accessed on 30.06.2012).

Tarboton, D. G. (1997). "A new method for the determination of flow directions and upslope areas in grid digital elevation models." Water resources research 33(2): 309-319.

Teerarungsigul, S., et al. (2007). Landslide prediction model using remote sensing, GIS and field geology: A case study of Wang Chin District, Phrae province, Northern Thailand. Proc. 2007 International Conference on Geology of Thailand: Towards Sustainable Development and Sufficiency Economy.

Tepparnich, J., Jotisankasa, A. (2010) Behaviour of Soil Slope and Shear Strength Properties in The landslide-prone area of Laplae, Uttaradit. [On-line]. Available at: http://www.gerd.eng.ku.ac.th/Paper/Paper_Other/NCCE15/GTE022.pdf (Accessed on 30.07.2015).

Timmermann, A., et al. (2004). "Intensification of the annual cycle in the tropical Pacific due to greenhouse warming." Geophysical Research Letters 31(12).

TMD (Thai Meteorological Department) (2006) Annual Tropical Cyclone Report 2006, Weather Report No. 551.515.2 – 02 –2007.

TMD (Thai Meteorological Department) (2008) Annual Tropical Cyclone Report 2006, Weather Report No. 551.515.2 – 02 -2009.

TMD (Thai Meteorological Department) (2007a) [On-line]. Available at: http://www.tmd.go.th/info/info.php?FileID=51 (Accessed on 10.02. 2012)

TMD (Thai Meteorological Department) (2007b) Annual Tropical Cyclone Report 2006, Weather Report No. 551.515.2 – 02 -2008.

TMD (Thai Meteorological Department) (2008) Tropical Cyclone Analysis Which Moved to Northern Thailand, No. 551.515.2 – 01-2008.

TMD (Thai Meteorological Department) (2009) Annual Tropical Cyclone Report 2009, Weather Report No. 551.515.2 – 02-2010.

TMD (Thai Meteorological Department) (2010) Annual Tropical Cyclone Report 2010, Weather Report No. 551.515.2 – 01-2011.

TMD (Thai Meteorological Department) (2011a) [On-line]. Available at : http://www.tmd.go.th/programs%5Cuploads%5Cphenomena%5C%C5%D2%B9%D5%AD%D2(%A1%C3%A1%AF%D2%A4%C1)-2011.pdf (Accessed on 1.04. 2012).

TMD (Thai Meteorological Department) (2011b) Annual Tropical Cyclone Report 2011, Weather Report No. 551.515.2 – 01-2012.

TMD (Thai Meteorological Department) (2011c) Rainfall and severe flooding over Thailand in 2011. Climatological Center [On-line]. Available at: http://www.tmd.go.th/en/event/NaturalDisasters-2011.pdf (Accessed on 23.02. 2012)

TMD (Thai Meteorological Department) (2011d) Rainfall and severe flooding over Thailand in 2011. Climatological Center, [On-line]. Available at: http://www.tmd.go.th/en/event/flood_in_2011.pdf (Accessed on 28.01. 2012)

TMD (Thai Meteorological Department) (2011e) [On-line]. Available at: http://www.tmd.go.th/info/info.php?FileID=51 (Accessed on 29.01. 2012)

TMD (Thai Meteorological Department) (2012a) [On-line]. Available at: http://www.tmd.go.th/info/info.php (Accessed on 25.02. 2012)

TMD (Thai Meteorological Department) (2012b) The rainfall and rain stations data base in Thailand.

TMD (Thai Meteorological Department) (2012c) The tropical cyclone data base in Thailand.

TMD (Thai Meteorological Department) (2012d) The situation of ENSO in 2012 in Thailand.

TMD (Thai Meteorological Department) (2013) The rainfall amount in rainy season from 2000 to 2013.

Tsaparas, I., et al. (2002). "Controlling parameters for rainfall-induced landslides." Computers and geotechnics 29(1): 1-27.

Turner, A. G. and H. Annamalai (2012). "Climate change and the South Asian summer monsoon." Nature Climate Change 2(8): 587-595.

USGS, (2004) Landslide Types and Processes. [On-line]. Available at: http://pubs.usgs.gov/fs/2004/3072/fs-2004-3072.html (Accessed on 25.06. 2012).

Utah State University, formerly of Terratech Consulting Ltd. (2005) SINMAP user's manual. [On-line]. Available at: http://www.engineering.usu.edu/dtarb/sinmap.html (Accessed on 1.09. 2012).

Vecchi, G. A., et al. (2006). "Weakening of tropical Pacific atmospheric circulation due to anthropogenic forcing." Nature 441(7089): 73-76.

Veder, C. (1981) Landslides and their stabilization, Springer-Verlag.

Wangwongchai, A., et al. (2005). "A case study on a strong tropical disturbance and record heavy rainfall in Hat Yai, Thailand during the winter monsoon." Advances in Atmospheric Sciences 22(3): 436-450.

Webster, P. J., et al. (1998). "Monsoons: Processes, predictability, and the prospects for prediction." Journal of Geophysical Research: Oceans 103(C7): 14451-14510.

Westen, C. v. and M. Terlien (1996). "An approach towards deterministic landslide hazard analysis in GIS. A case study from Manizales (Colombia)." Earth Surface Processes and Landforms 21(9): 853-868.

Wikarmpapraharn, C. and E. Kositsakulchai (2010). "Relationship between ENSO and rainfall in the Central Plain of Thailand." Kasetsart Journal (Natural Science) 44: 744-755.

Wilby, R. and C. Dawson (2007). SDSM 4.2–A decision support tool for the assessment of regional climate change impacts, User Manual. Department of Geography, Lancaster University, UK, ed.

Witthawatchutikul, P., Panuthai, S., Thitirojanawat, P. (2011) Simulating the 2011 Severe Flooding in Thailand.

Witt, A. C. (2005). "Using a GIS (Geographic Information System) to model slope instability and debris flow hazards in the French Broad River watershed, North Carolina."

Wu, W. and R. C. Sidle (1995). "A distributed slope stability model for steep forested basins." Water resources research 31(8): 2097-2110.

Yilmaz, I. (2009). "Landslide susceptibility mapping using frequency ratio, logistic regression, artificial neural networks and their comparison: a case study from Kat landslides (Tokat—Turkey)." Computers & Geosciences 35(6): 1125-1138.

Zhang, G., et al. (2011). "Real-time warning system of regional landslides supported by WEBGIS and its application in Zhejiang Province, China." Procedia Earth and Planetary Science 2: 247-254.